CONSTITUTIVE MODELLING OF TIME-DEPENDENT STRESS-STRAIN BEHAVIOUR OF SOILS

BY

JIAN-HUA YIN

A THESIS

SUBMITTED TO THE FACULTY OF GRADUATE STUTIES

IN PAITIAL FULFILLMENT OF THE REQUIREMENTS FOR THE DEGREE OF

DOCTOR OF PHILOSOPHY

DEPARTMENT OF CIVIL ENGINEERING

THE UNIVERSITY OF MANITOBA

WINNIPEG, MANITOBA, CANADA

MARCH 9, 1990

ISBN 0-315-63260-7

CONSTITUTIVE MODELLING OF TIME-DEPENDENT STRESS-STRAIN BEHAVIOUR OF SOILS

BY

JIAN-HUA YIN

A thesis submitted to the Faculty of Graduate Studies of the University of Manitoba in partial fulfillment of the requirements of the degree of

DOCTOR OF PHILOSOPHY

ABSTRACT

As is commonly known, the stress-strain behaviour in some soils such as clays, frozen soils and ice is non-linear, irreversible, anisotropic and time-dependent. This thesis develops three types of models to describe (1) time-independent stress-strain behaviour in triaxial stress states (and general stress states); (2) time-dependent stress-strain behaviour in 1-D straining; and (3) time-dependent stress-strain behaviour in triaxial stress states (and general stress states).

This thesis first presents a three-modulus hypoelasticity model for time-independent behaviour. Two new methods are suggested for determining the three moduli in the model using simple conventional triaxial tests. The model is calibrated for a sand-bentonite mixture and a medium-stiff plastic Paris clay using isotropic consolidation tests and CI$\bar{U}$ tests and for a medium dense Wuhan sand using isotropic consolidation tests and CID tests. The calibrated models are then used to predict the behaviour of the soils in different types of tests (constant-p' compression tests and a constant stress ratio σ'_3/σ'_1 test). The predicted values are compared with the measured results for the three different soils. Validation of the model is then examined.

A new Elastic Visco-Plastic (EVP) model is developed for time-dependent behaviour of soils in 1-D straining based mainly on Bjerrum's work. A number of important new concepts, such as "equivalent times", "reference time line", "instant time line" are introduced. A general

$\sigma'_z - \dot{\sigma}'_z - \varepsilon_z - \dot{\varepsilon}_z$ relationship is then derived using these concepts. New methods for determining all parameters in the model are suggested. Two particular constitutive models are obtained from the general relationship using logarithmic functions and power functions. The two models are calibrated and validated using various types of tests and soils.

Based on the work of hypoelasticity models and 1-D EVP models, a new framework of 3-D EVP models is developed. Some concepts such as "flow surfaces", "visco-plastic potential", "consistency conditions" and "evolution law" are used in the framework. Two 3-D flow functions are developed for initially isotropic and anisotropic soils. Non-linear strength envelopes may be incorporated in the flow functions. New scaling and calibration methods are proposed for the 3-D EVP models. Two specific models from the framework are constructed and applied to a sand-bentonite mixture and a frozen sand. The two models are calibrated using some tests and are verfied using different tests.

Uncertainties and limitations of the three types of models are discussed. Suggestions for further development and refinement of these models are also presented in this thesis.

ACKNOWLEDGEMENTS

I am deeply grateful to my advisor Professor James Graham D.Sc. for his constant guidance, encouragement and constructive suggestions through all phases of my work on the project.

My special thanks are extended to my colleagues in the research group of Professor Graham at the University of Manitoba, Messrs James M. Oswell, Brain Lingnau, Farbod Saadat, Mark Jamieson, Alan W.-L. Wan, Darren Yarechewski and Miss Gayle Homenick for sharing our experiences. Many thanks are also due to Mr. Narong Piamsalee and Ms. Ingrid Trestrail for their technical assistance during the experimental program and preparation of the thesis.

Helpful discussions with Professor Donald H. Shields, Dr. N. Rajapakse, University of Manitoba, Dr. Viriyawan Murti, University of New South Wales, Australia, and Dr. Malcolm Gray, Dr. Steven Cheung and Mr. David Dixon, Atomic Energy of Canada Limited, Pinawa are gratefully acknowledged. I sincerely wish to thank Professor L. Domaschuk for his suggestions in the modelling of a frozen sand in Chapter 10 of the thesis, and external examiner Dr. S. Pietruszczak for his helpful comments and suggestions on the theoretical work of the modelling in the thesis.

Finally I wish to express my gratitude to my wife Jun Sun and my mother Fengyi Li for their understanding, encouragement and support during the course of the program.

TABLE OF CONTENTS

LIST OF SYMBOLS

C_c; C_r	compression index (V, log stress); reload index
$C_{\alpha e}$, $C_{\alpha \varepsilon}$	creep coefficient (V, log t), (ε, log t)
CEL	creep equilibrium line
CID	isotropicly consolidated drained compression tests
CI$\bar{U}$	isotropicly consolidated undrained compression tests
CSL	critical state line
CRSN	constant rate of strain
CRSS	constant rate of stress
D	apparent shear modulus
e	void ratio
E	Young's modulus
F	yield function or flow function
G_s	specific gravity of soil particle
J_2	the second deviator stress invariant
K, G, J	bulk modulus, shear modulus, coupling modulus
m, n	parameters in flow functions
M	stress ratio $(q/p')_f$ at failure
MSL	multi-stage loading
p, q	mean stress, deviator stress
Q	plastic potential or visco-plastic potential
S	scaling function
SEL	swelling equilibrium line
S_r	degree of saturation
t	time
t_e	equivalent time
u, u_b, Δu	porewater pressure, back porewater pressure, excess porewater pressure
V	specific volume occupied by unit volume of solids
V_c	clay specific volume
w	water content

Greek letters:

σ', ε	effective stress, strain

λ, κ, ψ	compression index (V, ln stress), reload index, creep coefficient (V, ln t)
ϕ	friction angle
θ	the Lode angle
ν	poisson's ratio
β	parameter in flow functions
γ	unit weight
γ_d	dry density
δ, Δ	incremental
δ_{ij}	the Kronecker delta
η	stress ratio q/p'

Superscripts:

·, e, ep, p	rate, elastic, elastic-plastic, plastic
m, n	exponential parameters
sp, tp	time-independent plastic, time-dependent plastic
ve, vp	visco-elastic, visco-palstic

Subscripts:

c, v, z	preconsolidation (or compression, critical, clay), volumetric, vertical
con, cons	consolidation
crit	critical
f	failure
iso	isotropic
m, n	on p'-axis, on neutral line
o, i, e,	reference, initial, equivalent (or extension)
s	shear

LIST OF TABLES

LIST OF FIGURES

Chapter 1

INTRODUCTION

As an introduction to the work in the rest of this thesis, some typical aspects of time and strain effects on the deformation of soils as observed in both laboratory and field will be examined. Then the role of constitutive modelling of time-dependent stress-strain behavior is discussed.

1.1 Time-Dependent Stress-Strain Behavior Observed in Laboratory

The time-dependent stress-strain behavior of soils has been studied intensively in laboratory tests. This section shows some features of the influence of times and strain rates on stress-strain behavior of soils in oedometer tests and triaxial shear tests.

1.1.1 Time and strain rate effects in 1-D straining

In oedometer tests, no lateral strains are permitted and the deformations are in the vertical direction only. Here four types of tests are discussed.

Single-stage loading tests: The vertical pressure is applied suddenly to a specimen. The data of vertical strain vs. time (ε_z vs. t) can be measured, (in some advanced oedometers, the excess porewater pressure vs. time (u vs. t) can also be measured,) (see Fig.1.1 from Brerre and Iversen 1972). After primary consolidation of clays, the excess porewater pressure is dissipated; the total vertical stress σ_z is equal to vertical effective stress σ'_z, and yet continuing compression is observed. The part of compression occurring after the primary consolidation is called "secondary compression". The deformation of the soil "skeleton", that is, the physical framework of mineral particles, under constant vertical effective stress σ'_z consists of a time-independent part (also called instant compression) and a time-dependent part (also called creep deformation or delayed compression). Creep deformation of soil skeleton actually occurs during the whole consolidation process, that is, both before and after the primary consolidation. Because time-dependent deformations due to the dissipation of excess porewater pressure are coupled with time-dependent deformations due to the viscous nature of the soil skeleton, it is difficult to distinguish them in the period of primary consolidation and to define the instant compression uniquely, (see Fig.1.1).

Multi-stage loading tests: In this type of test, the vertical pressure is applied in steps. Each vertical pressure is kept constant for a pre-determined time, and curves similar to those in Fig.1.1 can be

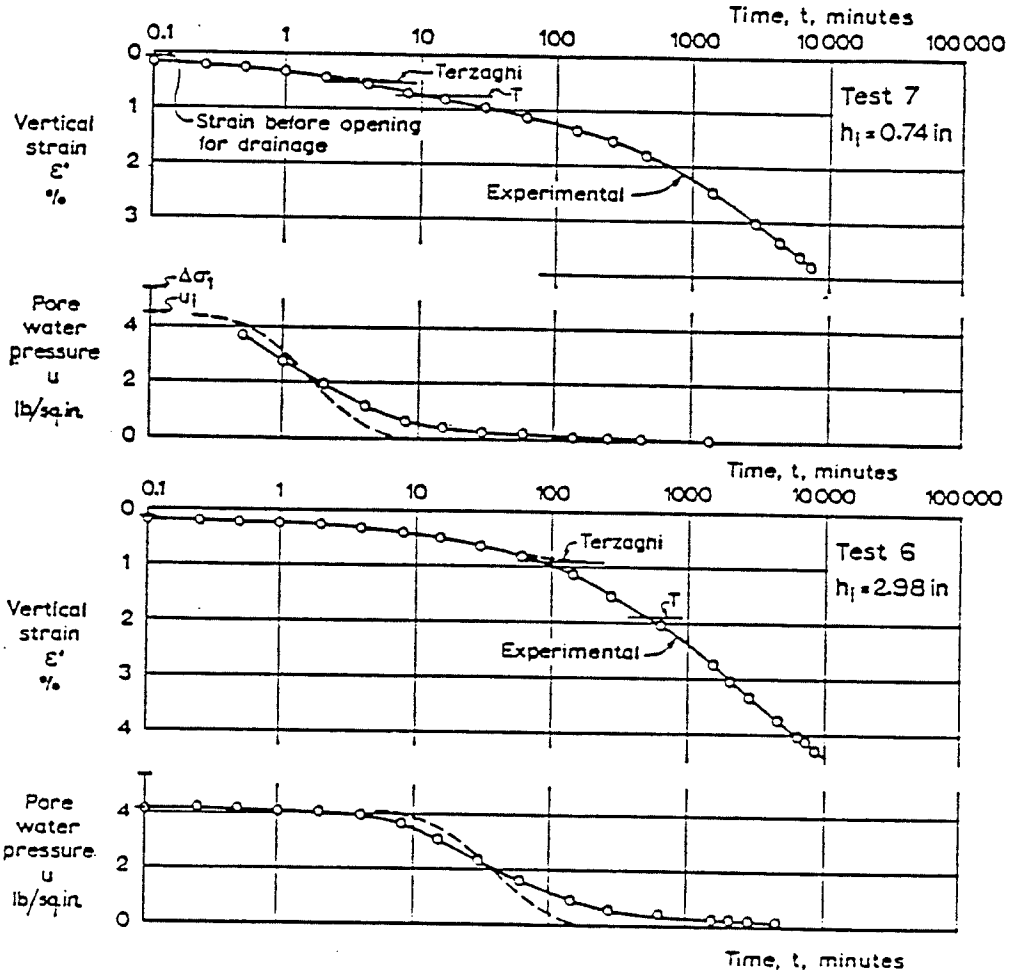

Fig.1.1 Consolidation tests - strains, excess porewater pressures and creep (after Berre and Iversen 1972)

measured, (Fig.1.2, Bjerrum 1967a). When an additional load is applied after a period of delayed compression, an apparent preconsolidation pressure p_c, (also called critical pressure by Bjerrum 1967a) is found. Using multi-stage tests, the relationship between void ratio and vertical effective pressure (related to ε_z vs. σ'_z) can be measured. It is found that this relationship is not unique but depends on the time duration of each loading increment, (see Fig.1.2).

Constant rate of strain (CRSN) tests: In a CRSN test, the specimen is deformed at a constant rate of vertical compression. The vertical pressure, vertical deformation and porewater pressure at the undrained bottom of the specimen can be measured directly. The effective vertical stress is estimated by $\sigma'_z = \sigma_z - \frac{2}{3} u$, where σ_z is total vertical stress and u is the porewater pressure at the bottom. It is found that the curves of σ'_z vs. ε_z and preconsolidation pressure for most clay soils depend on the strain rates, (Fig.1.3, Sallfors 1975).

Relaxation tests: In this type of test, when a certain strain ε_z is reached by any type of loading, the strain is held constant. That is, the strain rate $\dot{\varepsilon}_z = 0$. When this is so, the vertical effective stress is observed to decrease with time (Fig.1.4, Yin and Graham 1989a). This phenomenon is called stress relaxation.

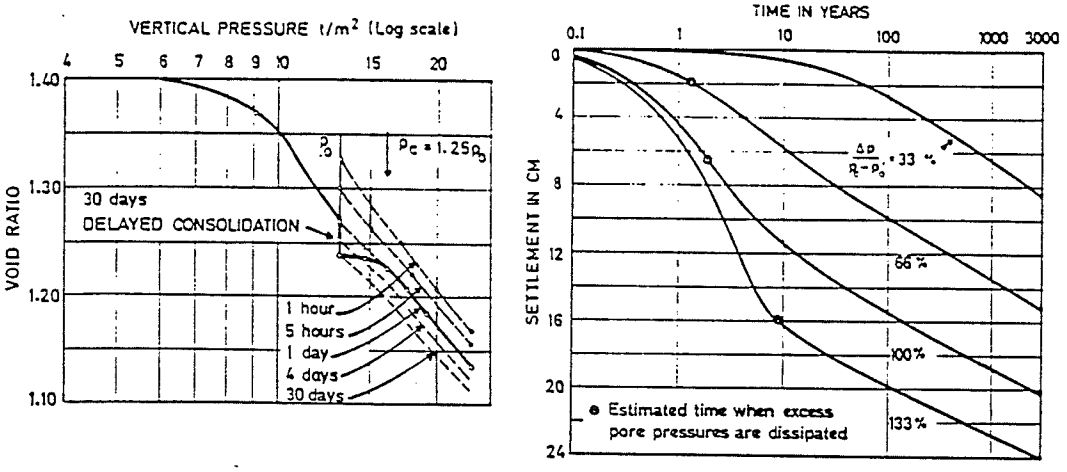

Fig.1.2 Multi-stage consolidation test - void ratio, settlements, time lines, critical pressure p_c and creep (after Bjerrum 1967a)

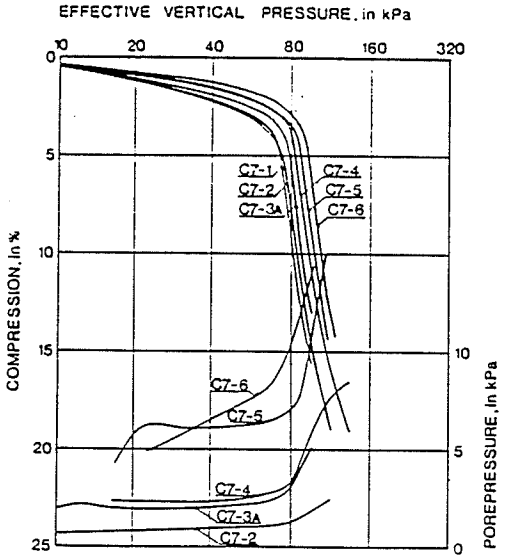

Legend

Test	Depth m	Rate of def. mm/min
C7-1	7	0,0006
C7-2	7	0,0012
C7-3A	7	0,0024
C7-4	7	0,0040
C7-5	7	0,0090
C7-6	7	0,0200

Fig.1.3 Tests of constant rate of strain (CRSN) - ε_z vs. σ'_z and u vs. σ'_z at different strain rates $\dot{\varepsilon}_z$ (after Sallfors 1975)

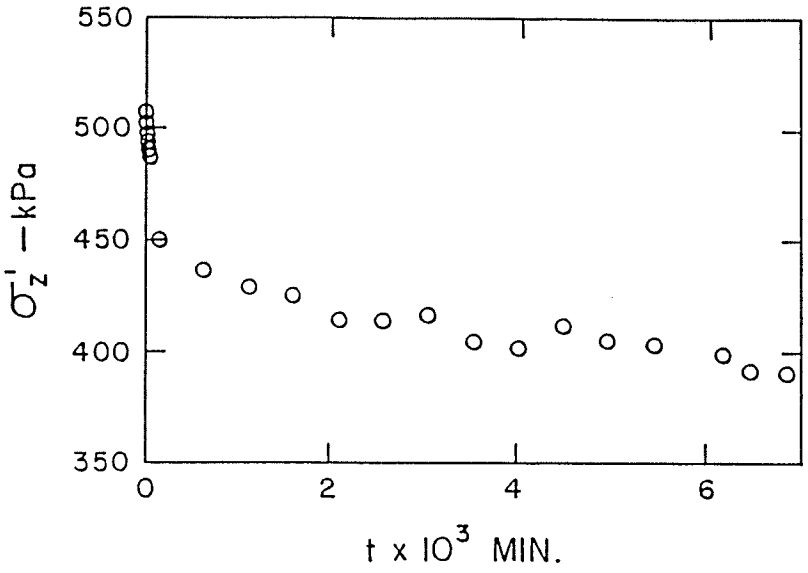

Fig.1.4 Relaxation in an oedometer test - σ'_z vs. time (after Yin and Graham 1989a)

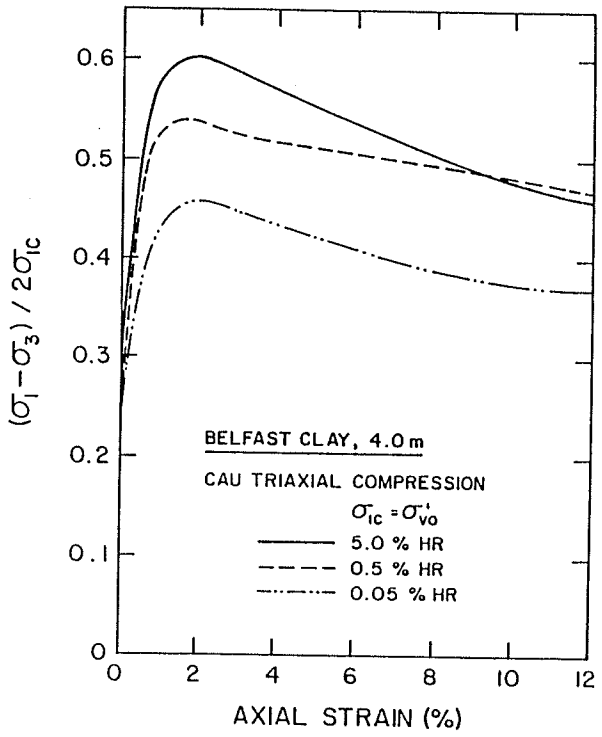

Fig.1.5 Triaxial compression tests - $(\sigma_1 - \sigma_3)/(2\sigma_{1c})$ vs. ε_1 at different strain rates $\dot{\varepsilon}_1$ (after Graham et al. 1983)

1.1.2 Time and strain rate effects in triaxial stress states

Much soil testing is done under "triaxial" stress states in which cylindrical specimens are first loaded by all-round (hydrostatic) pressure in a cell, and then the axial stress is increased (or decreased). The test equipment permits various combinations of measuring volume changes or porewater pressure changes during shearing. The results of triaxial tests also show evidence of time and strain rate effects on the stress-strain behavior of clays.

Constant rate of strain (CRSN) tests: A specimen is sheared at a chosen constant rate of vertical movement usually under undrained conditions. The observed curves of deviator stress vs. axial strain (q vs. ε_1) and excess porewater pressure vs. axial strain (u vs. ε_1) depend on the strain rates used (Fig. 1.5, Graham et al 1983). Higher strain rates result in larger deviator stresses and porewater pressures. The undrained shearing strength depends on the strain rates, (Fig. 1.5, Graham et al 1983).

Step-changed constant rate of strain tests: When the axial strain rate is changed by steps, it is clearer to see that the strain rate affects the relationships q vs. ε_1 and u vs. ε_1 (Fig. 1.6, Graham et al 1983).

Relaxation tests: In this procedure, when specimens are sheared up to a certain axial strain and then the driving motor of the triaxial apparatus is shut off, the axial strain remains almost constant, but

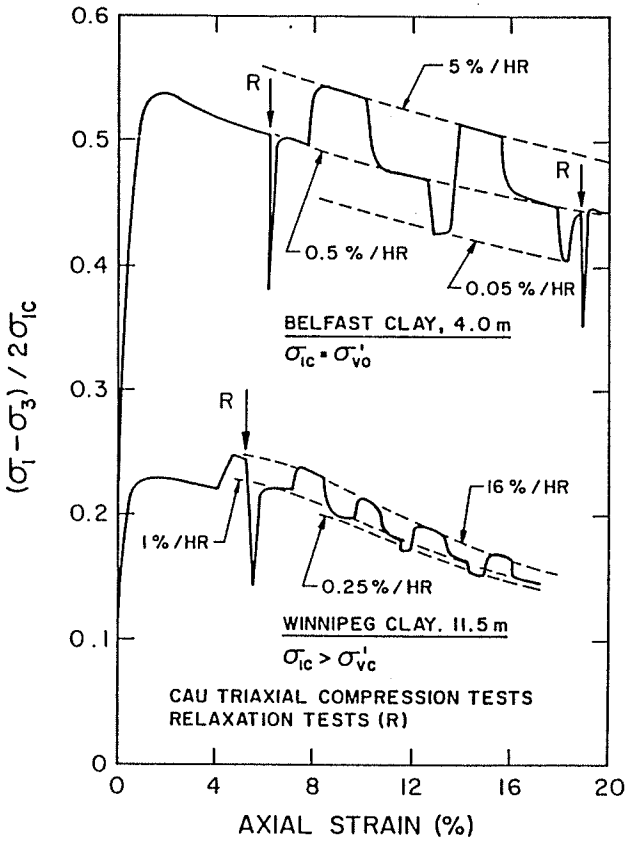

Fig.1.6 Triaxial compression and relaxation tests - $(\sigma_1 - \sigma_3)/(2\sigma_{1c})$ vs. ε_1 using step-changed strain rate $\dot{\varepsilon}_1$ (after Graham et al. 1983)

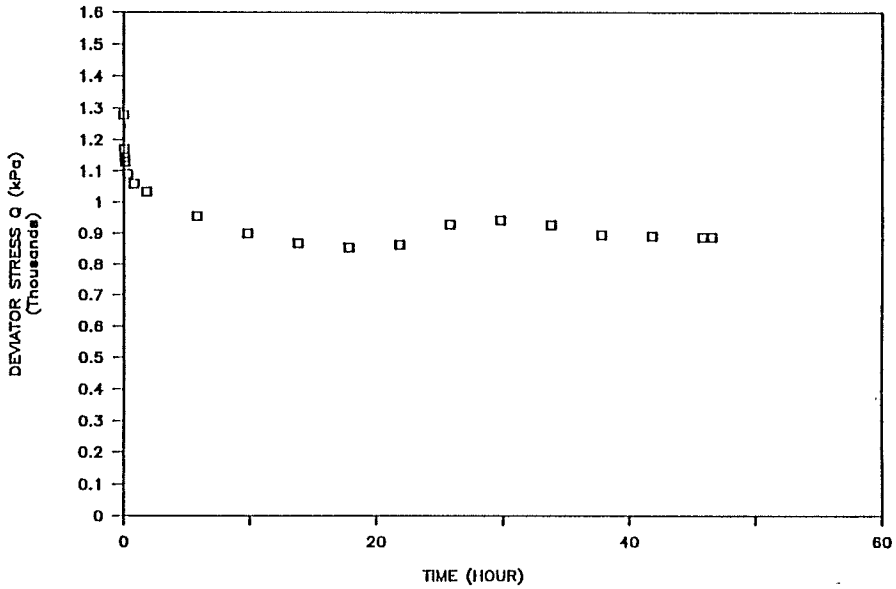

Fig.1.7 Triaxial relaxation test - $(\sigma_1 - \sigma_3)$ vs. time

it is found that the deviator stress decreases with time (Figs.1.6 and 1.7).

Undrained multi-stage q creep tests: This type of tests is a combination of relaxation and creep. When running a test, the volumetric strain ε_v and the cell pressure σ_3 are kept constant, while the axial stress σ_1 (i.e. deviator stress q) is increased incrementally by steps. At each step, the deviator stress q is kept constant for a fixed period of time. It is found that the effective mean stress p' decreases with time, while the corresponding porewater pressure increases with time see Fig.1.8. Shear strains increase also with time with the rate of shear strain depending on the deviator stress. At lower deviator stresses, the rate decreases with time, whereas at high deviator stresses leading to failure, the rate increases (Fig.1.8).

1.1.3 Other characteristics of stress-strain behavior

The previous two sections outlined the effects of time and strain rate on the stress-strain behavior of clay soils. As is commonly known, the stress-strain behavior of clays is non-linear, irreversible and dependent on loading history (or stress paths for time-independent materials). In some soils, the behavior is initially isotopic and becomes anisotropic after shearing. However in most natural soils, the behavior is inherently anisotropic (Graham and Houlsby 1983, Graham et al 1989).

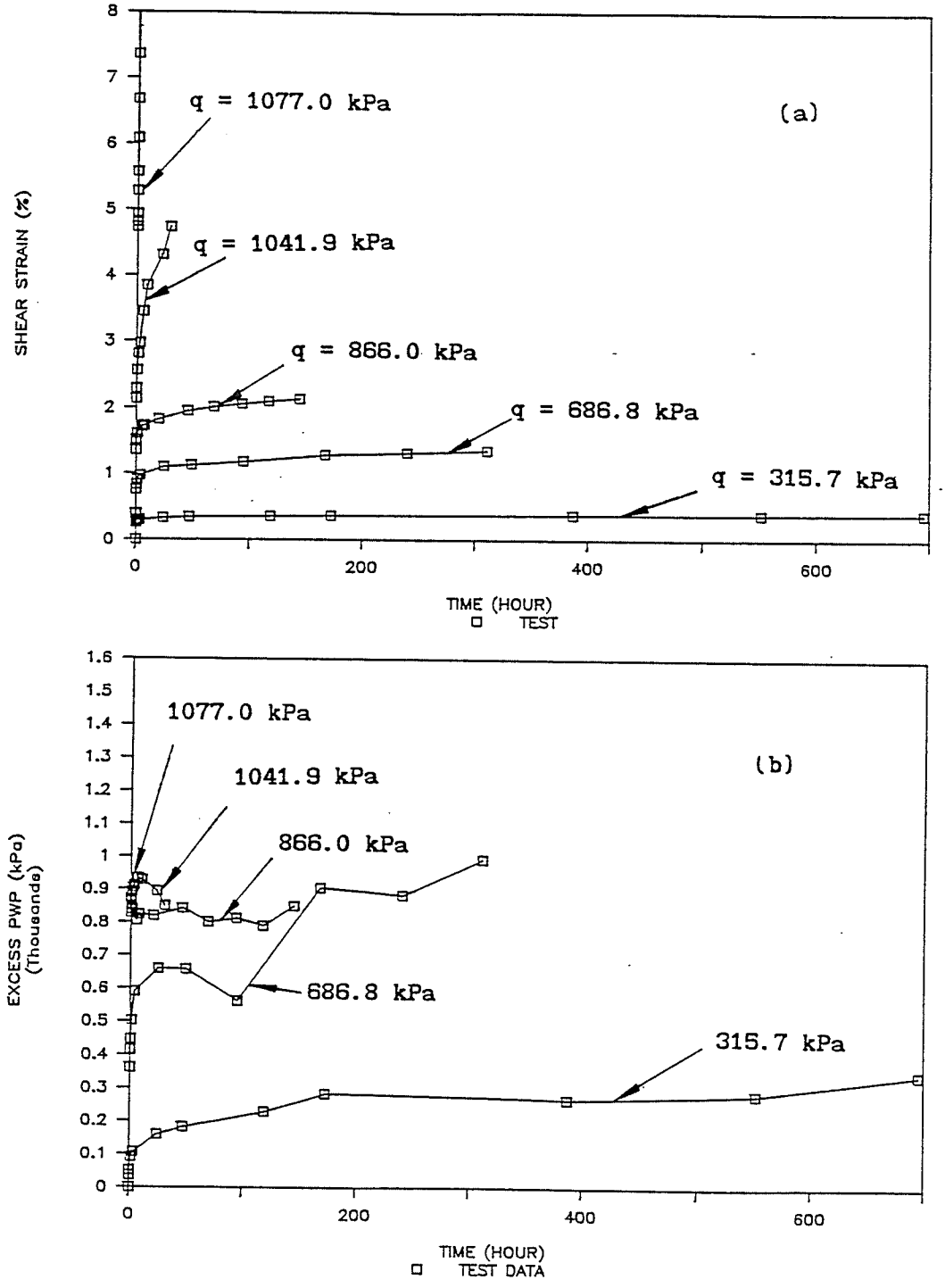

Fig.1.8 Undrained multi-stage q creep shear test
(a) ε_s, t-relationship, (b) Δu, t-relationship

1.2 Time-Dependent Deformation Observed in the field

The Tower of Pisa: The construction of the Tower began in 1173 (Kérisel 1985). Since then the Tower has leant in a variety of directions, successively to the east, the north, the west. and finally the south, while at the same time it lowered itself 3 m into the ground, (Fig. 1.9, Kérisel 1985).

Croce et al (1981) reported the results of observations made on the Tower and on surrounding monuments during the last decades. Fig. 1.10 shows the Tower inclination measurements. In Fig. 1.10a, the values of θ was measured by Pizzetti's method from 1911 to 1934 (dotted line). After 1934, the Tower rotation has been measured accurately with a pendulum, referred to two vertical plans, one of which coincides with the 1934 plan of maximum inclination and forms an angle of only $2^{o}26'$ with the N-S direction. The two components of the Tower rotation are indicated as α_{NS} and α_{EW} in Fig. 1.10.

Settlement of Konnerud gate 16: Bjerrum (1967a) reported a case study on Konnerud gate 16 which was representative of four identical four-storey apartment blocks built between 1950 and 1956 in Drammen, Norway. The measured settlement curve is shown in Fig. 1.11. Piezometers installed in 1964 indicated that the excess porewater pressures had dissipated ten years after the load was applied. The

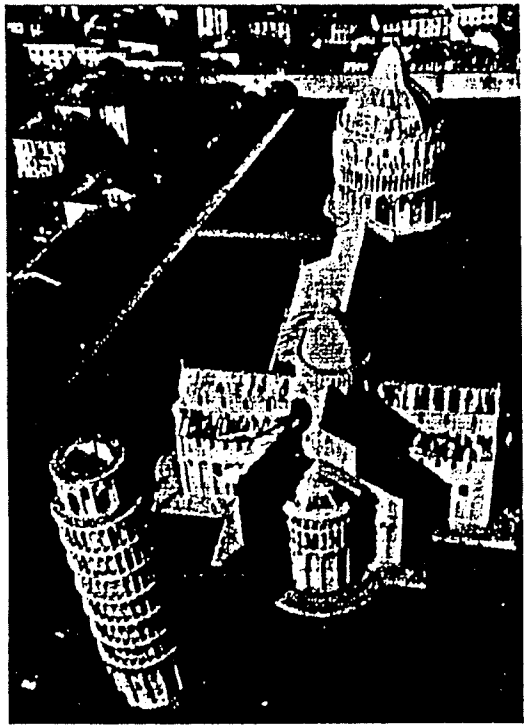

Fig.1.9 The Tower of Pisa

(after Kerisel 1985)

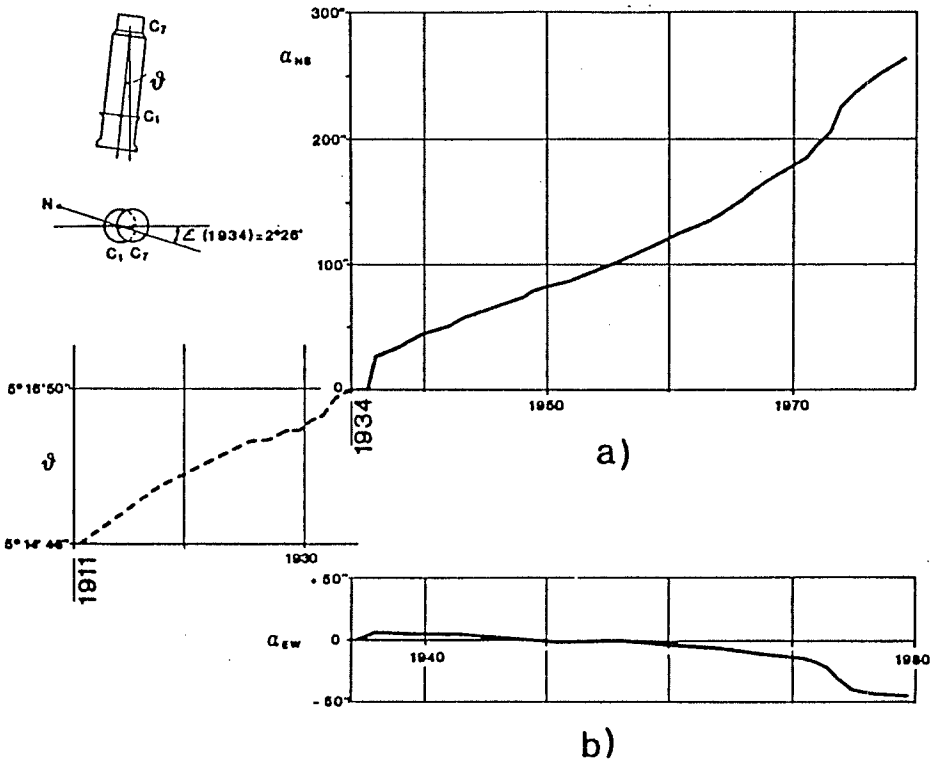

Fig.1.10 The Tower inclination measurements

(after Croce et al. 1981)

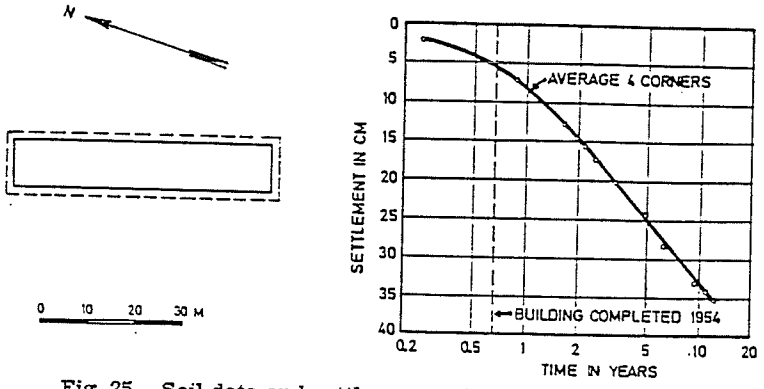

Fig. 25. Soil data and settlements of Konnerud gate 16

Fig.1.11 Settlement of Konnerud gate 16 (after Bjerrum 1967a)

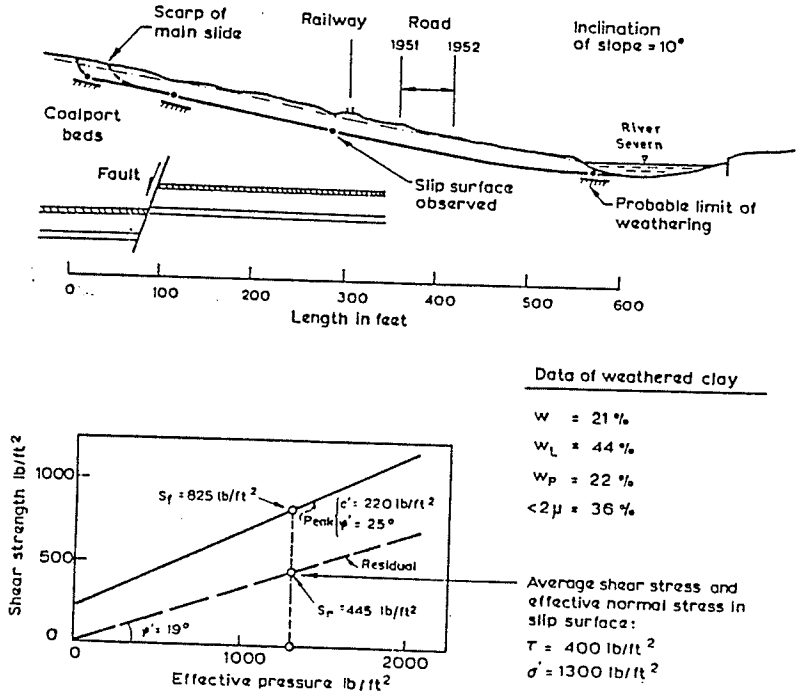

Fig.1.12 Progressive failure of Jackfield landslide (Skempton 1964) (after Bjerrum 1967b)

settlements in subsequent years had thus occurred at constant effective stresses and could therefore only be explained by delayed consolidation (creep) of the plastic clay.

Progressive failure in slopes: Fig. 1.12 shows progressive failure of a slope at Jackfield, England (Skempton 1964). Movement of the slope started in 1950. By 1952, a landslide occurred, destroying several houses and causing major dislocations in a railway and road. It was found that when this landslide took place, the strength of the clay was closely equal to its residual strength.

It was found that progressive slope failure occurred mostly in overconsolidated plastic clay and clay shales (Bjerrum 1967b). In the development of failure, the strength in the soil is transferred from its peak value to its residual value. The reduction in strength is time-dependent and partly due to the viscous nature of the soil (Bjerrum 1967b).

1.3 The Role of Constitutive Modelling

As shown in the proceding section, because of the viscous nature of soils, a slope may fail gradually and settlements of a foundation may continue over a long period, increasing the risk to buildings on the foundation. In order to (1) design a geotechnical structure which is safe, of good performance and economic, (2) analyze a failed structure

or (3) predict the performance of a existing structure in the future, we need to understand and model the time-dependent behavior of soils and to use this model to analyze the stability and deformations of soil masses. The traditional approach in geotechnical engineering has been to treat the stability and deformation separately, using linear elasticity to calculate the deformation and rigid-plasticity to analyze the stability. As shown in Section 1.1, behavior of real soils is non-linear, inelastic, anisotropic and time-dependent. With the development of numerical analysis techniques and the availability of large digital computers and powerful personal microcomputers, it is now possible to solve problems in practice using more complex (and more realistic) stress-strain behavior and geometry. The key to analyzing the stress, deformation and failure of structures that rest on or use geotechnical material, whose behavior may be time-dependent, is to use a constitutive model which best represents the real time-dependent stress-strain behavior of the material.

The role of constitutive modelling of time-dependent stress-strain behavior of soils (including frozen soils and ice used for geotechnical structures) is as follows:

(1). Constitutive equations can be combined with other equations in continuum mechanics to solve boundary value (or mixtured) problems, that is, to analyze the development of stresses, porewater pressures, deformations, and failure zones. Results from these analyses can be used directly, for example, for the design of a new earth structure, for performance checking of an

existing structure, and for finding the causes for a failed structure.

(2). Constitutive equations can be used to predict time-dependent stress-strain behavior in laboratory tests. Results in this calculation may be used indirectly for the analyses of earth structures.

(3). The establishment of a constitutive model is based on fundamental physical laws, assumptions, observations and qualitative understanding of soil behavior in laboratory tests. At times, the observations made in laboratory testing may not reflect completely the entire spectrum of soil behavior. Phenomena observed in the laboratory may seem unrelated. For example, a clay may exhibit strain rate effects in strain controlled tests, but exhibit time effects in creep tests and relaxation tests. A constitutive model may provide us some understanding of interrelationships between these phenomena.

1.4 Organization of the Thesis

This thesis consists of eleven chapters.

Chapter 1: Introduction.

Chapter 2: This chapter gives a critical review of the literature in the field of constitutive modelling with emphasis on hypoelastic models

and the modelling of the time-dependent stress-strain behavior. After this review, the detailed objectives of the thesis are presented.

Chapter 3: In this chapter, the framework of a new three-modulus hypoelastic model is described. Two methods are suggested for determining the moduli.

Chapter 4: Applications of the general framework of the new model in Chapter 3 to three different soils are presented in this Chapter. The work includes formulation, calibration and verification of the model.

Chapter 5: This chapter develops a new general Elastic Visco-Plastic (EVP) model for time-dependent stress-strain behavior of soils in 1-D straining. An important concept called "equivalent time" is introduced.

Chapter 6: The general formulation of the new EVP model in Chapter 5 is developed for a specific case using the logarithmic functions commonly used in practice. The model is then calibrated and examined using the test data from three different soils.

Chapter 7: Here, the general formulation of the new EVP model in Chapter 5 is specified using power functions which are better fitted to test data than logarithmic functions in some soils. Calibration and validation of the model for two soils are presented.

Chapter 8: This chapter is further development of work in the previous chapters. Here, a new general framework is suggested for 3-D Elastic Visco-Plastic (EVP) straining. Methods for calibrating the new model

are presented.

Chapter 9: In this chapter, the new 3-D EVP model in Chapter is applied for the first time to describe the time-dependent stress-strain behavior of a sand-bentonite buffer material proposed for the Canadian Nuclear Fuel Waste Management Program.

Chapter 10: Here, the new 3-D EVP model is applied to a frozen sand that has been the subject of recent doctoral studies supervised by Dr. L. Domaschuk at the University of Manitoba.

Chapter 11: This chapter summarizes the conclusions of the thesis and presents suggestions for further research.

Detailed information and reference material required for some chapters are all presented in Appendices. A full list of published references is given at the end of the thesis.

Chapter 2

CONSTITUTIVE MODELLING

—— a critical review and objectives of the research

This chapter first reviews some representative constitutive models in the literature. Features, limitations and problems associated with these models are discussed. After this review, the objectives of the research described in the thesis are presented.

2.1 Modelling of Time-independent Behavior

Chapter 1 showed that the stress-strain behavior of most soils is time-dependent. In some theoretical models of soil behavior, time-dependent strains are decomposed into two parts comprising time-independent strains and time-dependent strains. For example in Elastic Visco-Plastic (EVP) models, the total strain rate consists of elastic (time-independent) strain rate and visco-plastic strain rate. In some soils like sand, the stress-strain behavior is essentially time-independent but may be non-linear and non-reversible. We may treat time-independent behavior as a particular case of time-dependent behavior when the viscosity is zero. Separate and distinct models may be required to define the complexity of time-independent behavior.

Many constitutive models have been developed in the past for time-independent behavior. This section discusses only hypoelastic models and elastic-plastic (Cam-Clay) models. The framework of hypoelastic models will be used to calculate the time-independent part of strains of soils in the elastic visco-plastic (EVP) models to be developed later in the thesis. The EVP models will be related to the Cam-Clay models that are representive of the current range of elastic-plastic models.

2.1.1 Hypoelasticity models

This type of model is characterized by the following constitutive relationship (Truesdell 1955, Truesdell 1965, Coon and Evans 1971):

$$[2.1] \quad F_{ij}(\sigma'_{kl},\ \dot{\sigma}'_{mn},\ \varepsilon_{pq},\ \dot{\varepsilon}_{st}) = 0$$

In this equation, the tensor function F_{ij} is homogeneous in time. This means that time occurs to the same order in all terms of Eqn.[2.1] and therefore, may be eliminated. Thus Eqn.[2.1] is actually a relationship among infinitesimal increments, $d\sigma'_{mn}$, $d\varepsilon_{st}$ and stresses and strains for time-independent stress-strain behavior. This model describes the mechanical behavior of a class of materials in which the final total strains depend on both the current stress state and the stress paths used to reach that state, but not on time or strain rate.

Coon and Evans (1971) presented four special cases of the general expression [2.1]:

$$[2.2a] \quad d\sigma'_{ij} = A_{ijkl}(\sigma'_{ij})\, d\varepsilon_{ij}$$

$$[2.2b] \quad d\sigma'_{ij} = B_{ijkl}(\varepsilon_{ij})\, d\varepsilon_{ij}$$

$$[2.2c] \quad d\varepsilon_{ij} = C_{ijkl}(\varepsilon_{ij})\, d\sigma'_{ij}$$

$$[2.2d] \quad d\varepsilon_{ij} = D_{ijkl}(\sigma'_{ij})\, d\sigma'_{ij}$$

It is seen that the behavior described by Eqn.[2.2] is infinitesimally (or incrementally) reversible. This justifies the use of the suffix "elastic" in the term hypoelastic used by Truesdell (1955) to describe the constitutive equation [2.2a] (Saleeb and Chen 1981). Based on [2.2], two different approaches have been used to develop some special hypoelastic models. One approach is to express the functions A_{ijkl}, D_{ijkl} in a stress tensor series and B_{ijkl}, C_{ijkl} in a strain tensor series. Another approach is to make a further assumption on these functions to reduce the number of A_{ijkl}, D_{ijkl}, C_{ijkl}, D_{ijkl}. The reduced parameters can then be obtained by differentiating curves fitted to test data in laboratory.

In the first approach, Coon and Evans (1971), for instance, presented a first order form for Eqn.[2.2a]:

$$[2.3] \quad \Delta\sigma'_{ij} = a_{ijkl}\, \Delta\varepsilon_{kl} + a_{ijklmn}\sigma'_{mn}\Delta\varepsilon_{kl}$$

in which the $36a_{ijkl}$ and $216a_{ijklmn}$ are material constants which can

not be determined using conventional tests. When $a_{ijklmn} = 0$, Eqn.[2.3] is zero order hypoelasticity and is equivalent to anisotropic elasticity of a Cauchy-type material model. Eqn.[2.3] can be considerably simplified with the added restriction of material isotropy (Truesdell 1965, Coon and Evans 1971).

Falling into the second approach are models such as the "hyperbolic" E,ν model (Kondner 1963, Konder and Zelasko 63, Duncan and Chang 1970) and the K,G model (Domaschuk and Wade 1969, Domaschuk and Valliappan 1975). There are only two "moduli" in both these models though it should be pointed out that they are not constants but functions depending on stress level, strain, stress history, etc. In the E,ν model, conventional triaxial shear tests with constant confining pressures are used to determine the modulus functions E and ν. If the model is used in effective stress analyses, drained CID tests are required; if the model is used in total stress analyses, then only undrained CI$\bar{U}$ tests are required. A hyperbolic function is best fitted to the relationships of $(\sigma_1 - \sigma_3)$ vs. ε_1 at different confining stresses σ_1 (Kondner 1963). The modulus E_t for first-loading is expressed as $E_t = d(\sigma_1 - \sigma_3)/d\varepsilon_1$ at different confining stress σ_3. The modulus E_t can then be obtained by differentiating the fitting functions, it is a function of $(\sigma_1 - \sigma_3)$ and stress σ'_3 in CID tests and a function of $(\sigma_1 - \sigma_3)$ and σ_3 in CI$\bar{U}$ tests. The modulus ν_t for first-loading is $\nu_t = -d\varepsilon_3/d\varepsilon_1$. A mathematical function is fitted to the data of (ε_3 vs. ε_1) at different confining stresses σ_3. In CI$\bar{U}$ tests, ν_t is 0.5. In CID tests, ν_t is a function of $(\sigma_1 - \sigma_3)$ and σ'_3.

In a similar way, moduli E_{ur} and ν_{ur} can be determined for unloading-reloading.

In the K,G model, the bulk modulus K is defined as $K = dp'/d\varepsilon_v$, and the shear modulus is $G = dS_d/d\varepsilon_d$, where the resultant deviatoric stress $S_d = (\sqrt{2}/\sqrt{3})\ (\sigma_1 - \sigma_3)$ and resultant deviatoric strain $\varepsilon_d = (2\sqrt{2}/\sqrt{3})\ (\varepsilon_1 - \varepsilon_3)$ in triaxial stress states (Domaschuk and Wade, 1969). A mathematical function is chosen to fit the data of p' vs. ε_v from isotropic consolidation tests. The modulus function K is then obtained by differentiating the fitting function. A series of constant effective mean stress triaxial compression tests were used to find the shear modulus G (Domaschuk and Wade 1969, Domaschuk and Valliappan 1975). A hyperbolic function was used to fit the test data of S_d vs. ε_d. The modulus function G is then given by the tangent values of the fitting function. It was found that the modulus K depends on the effective mean stress p' and relative density D_r. The modulus G depends on the effective mean stress p', the resultant deviatoric stress S_d and the relative density D_r.

A limitation of the E,ν model and K,G model is that they can not account for volumetric strains produced by shear strains and shear strains produced by effective mean stresses. Such anisotropic behavior is known to be common in natural soils because of their mode of deposition. Graham and Houlsby (1983) suggested a simplified model for anisotropic behavior before yielding. Three moduli are used in the model, the bulk modulus K, shear modulus G and a cross modulus J which

expresses the relationships between mean stress and shear strain and between shear stress and volumetric strain. A least squares solution was used to evaluate these parameters from triaxial tests on Lake Agassiz clay from Winnipeg, Canada. They found that the ratios K/σ'_{vc}, G/σ'_{vc}, and J/σ'_{vc} were constant, where σ'_{vc} is the preconsolidation pressure in the soil.

Yin and Yuan (1985a,b) suggested a hypoelastic model to account for non-linearity and dilatancy in a medium sand. However this model can not consider the shear strains contributed by effective mean stresses. The matrix form of this model is not symmetric. Models with more than three moduli have been suggested (Darve et al 1986, Darve et al 1989). Darve et al (1986) developed a second order model which can account for non-linearity, irreversibility and stress path dependence. This model has eighteen independent moduli, half of which are determined from drained compression shear tests, and the other half from drained extension shear tests.

2.1.2 Cam-Clay Model

The Cam-Clay model will be discussed as an example of elastic plastic models. The original Cam-Clay model and its development, modified Cam-Clay, have been widely used in numerical modelling of stress-strain behavior of soils. Some elastic visco-plastic models use concepts from the Cam-Clay model family.

An important feature used in the Cam-Clay model is a unique State Boundary Surface (SBS) in p',q,e-space which was first proposed by Roscoe et al. (1958). In all shear tests, the final failure state points lie on a Critical State Line (CSL) on the SBS. On the CSL, $\partial p'/\partial \varepsilon_s = \partial q/\partial \varepsilon_s = \partial \varepsilon_v/\partial \varepsilon_s = 0$. The CSL is represented in p',q-space by $q_{cs}/p'_{cs} = \eta_{cs} = M$. A feature of the original Cam-Clay model is the formulation of an energy dissipation expression based on three assumptions (Roscoe et al 1963).

$$[2.4] \quad p'd\varepsilon_v + qd\varepsilon_s = \frac{\kappa}{1+e}\, dp' + Mp'd\varepsilon_s$$

Using the Associated Flow Rule, from Eqn.[2.4] we have:

$$[2.5] \quad \frac{dq}{dp'} - \frac{q}{p'} + M = 0$$

By integrating, [2.5] becomes:

$$[2.6] \quad \frac{q}{Mp'} + \ln(p'/p'_o) = 0$$

where p'_o is the point on the p'-axis intercepted by curve [2.6]. Eqn.[2.6] is the yield surface in p',q-space. This yield surface looks like a bullet shape with a discontinuity at the "nose" on the p'-axis. It has been found that the constitutive equations using this yield surface (Eqn.[2.6]) overpredict shear strains at small shear stress levels.

Burland (1969) and Roscoe and Burland (1969) suggested a modified version of the Cam-Clay model that uses a different energy dissipation

expression for Eqn.[2.4]. The yield surface resulting from the modified energy dissipation expression is an ellipse:

$$[2.7] \quad p'^2 - p'_o p' + q^2/M^2 = 0$$

whose size depends on the isotropic consolidation pressure p'_o and $M = (q/p')_f$ which is a function of the clay mineralogy. It can be summarized that in the modified Cam-Clay:

(1). the elastic behavior is isotropic;

(2). the yield surface is elliptical, i.e. Eqn.[2.7];

(3). the flow rule is associated flow rule;

(4). the hardening law is that the plastic volumetric strain ε_v^p on the yield surface is constant, i.e. represented by $d\varepsilon_v^p = \frac{\lambda - \kappa}{V} dp'_o/p'_o$;

(5). the consistency condition is that the current stress point is kept on the yield surface in yielding.

It has been subsequently found in most natural soils that (1) yield loci are not elliptical; (2) traces of yield loci in e,ln(p')-space are not straight lines but have "hook" shapes; (3) behavior before yielding is not isotropic (Graham et al. 1988, Graham et al. 1983). Typical data are shown in Fig.2.1. Graham and Houlsby (1983) developed a simplified transverse anisotropic model to describe anisotropic elastic behavior inside the yield loci. More recently, it was found (Wood and Graham 1987, Graham et al. 1989) that the state boundary surface (SBS) in anisotropic soils has approximately the same elliptical shape as the SBS in the modified Cam-Clay. Anisotropic elasticity and normalized elliptical yield loci can be used to reproduce the asymmetric yield surfaces in p',q-space and the "hooked" traces of the yield loci in

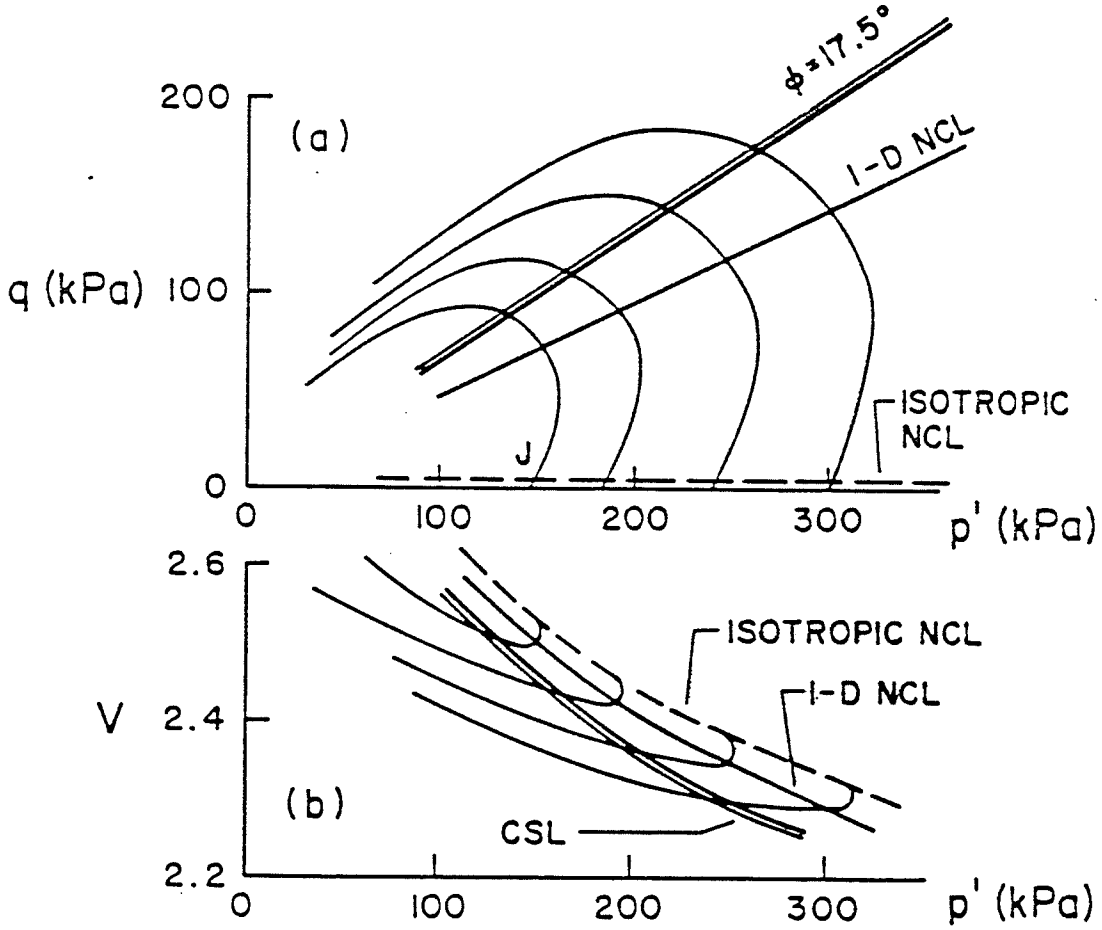

Fig.2.1 Asymmetric yield loci in q,p'-space and corresponding "hooked" traces in V,p'-space for natural plastic clay from from Winnipeg (after Graham et al. 1983)

e, ln(p')-space (Graham et al. 1989).

2.2 Modelling of Time-Dependent Behavior in 1-D Straining and 1-D Stressing

As shown in Chapter 1, the stress-strain behavior in some soils, such as clays, frozen soils and ice, is time or strain rate dependent. This was not considered by the models in the proceding section. In past decades, a number of models have been developed for time-dependent straining. These may be roughly divided into three categories according to the approach they used. The first is based on the rheological analogy. The second is empirical. The third uses elastic visco-plasticity. According to the dimensions of the models, we may divide them into those which describe 1-D straining (and 1-D stressing) and 3-D (or axisymmetric) stressing. Since the procedure used in this research starts with 1-D models and develops towards 3-D models, it is appropriate to review some representative models according to the dimensions of the models. This section reviews models for 1-D straining and 1-D stressing.

2.2.1 Bjerrum's time line model (1967a)

In Bjerrum's model (1967a), the total compression is divided into 'instant compression' and 'delayed compression'. The delayed compression can be described by a system of time lines or curves in an

e,log(p)-space (Fig.2.2) in which the outermost line (lowest e for a given pressure) is the instant time line. Bjerrum believed that these time lines represent a unique relationship between void ratio (related to vertical strains ε_z), pressure (in particular, the vertical effective stress σ'_z) and time. This means, in his terms, "that to any given value of the overburden pressure and void ratio there corresponds an equivalent time of sustained loading and a certain rate of delayed consolidation, independent of the way in which the clay has reached these values." Bjerrum believed that the usual separation of compression into primary and secondary compression is arbitrary, and that this division is unsuited to describe the behavior of the soil structure with respect to effective stresses. The principle for computing settlements using these ideas is shown in Fig.2.2 where p_c was called 'critical pressure' by Bjerrum. The pressure p_c results from creep under the previous pressure, that is aging and delayed compression. The p-stress in Figs.2.3 and 2.3 are vertical effective stresses and in the remaining Chapters will be called σ'_z. The symbol "p" will then be reserved for mean stresses.

Garlanger (1972) developed a mathematical equation for Bjerrum's time line model. For a pressure p above the critical pressure p_c, the compression at any time t can be calculated from:

$$[2.8] \quad \Delta e = C_r \log \frac{p_c}{p_o} + C_c \log \frac{p}{p_c} + C_\alpha \log \frac{t + t_i}{t_i}$$

where Δe is the change in void ratio, C_r is the slope on an e-log(p) diagram of the compression line from p_o to p_c, C_c is the slope of the

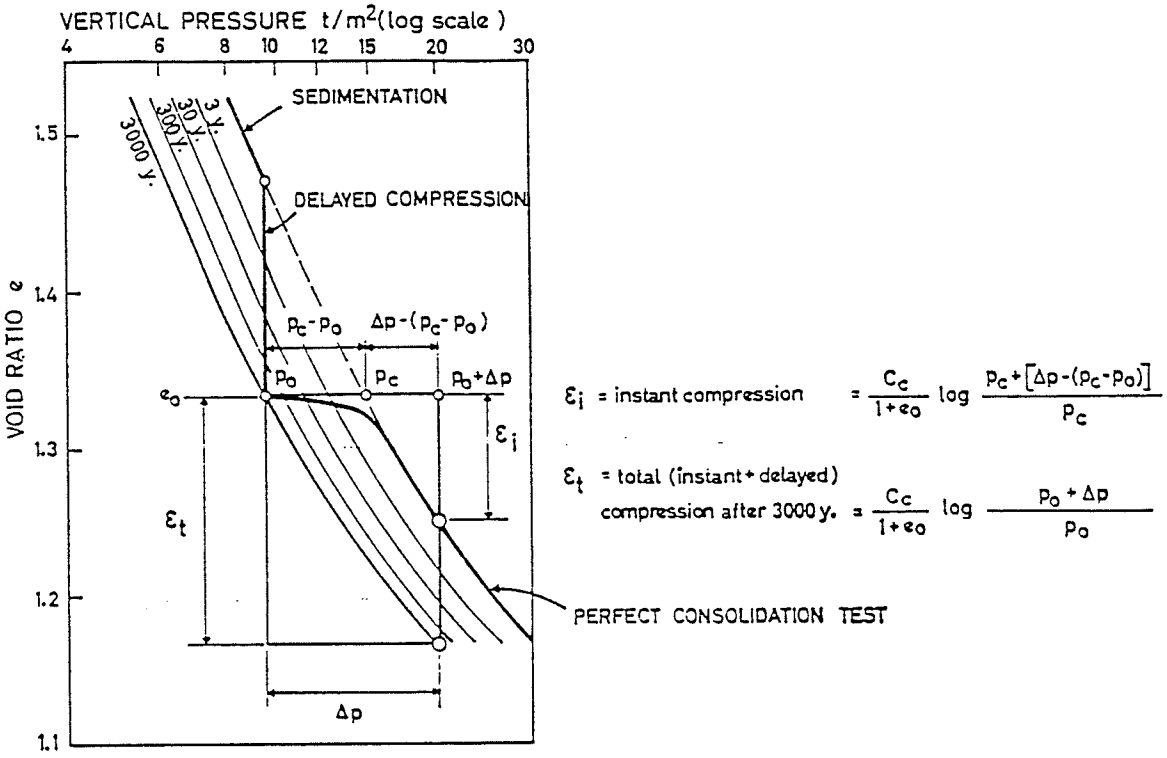

Fig.2.2 Principle of settlement calculation in the time line model (after Bjerrum 1967a)

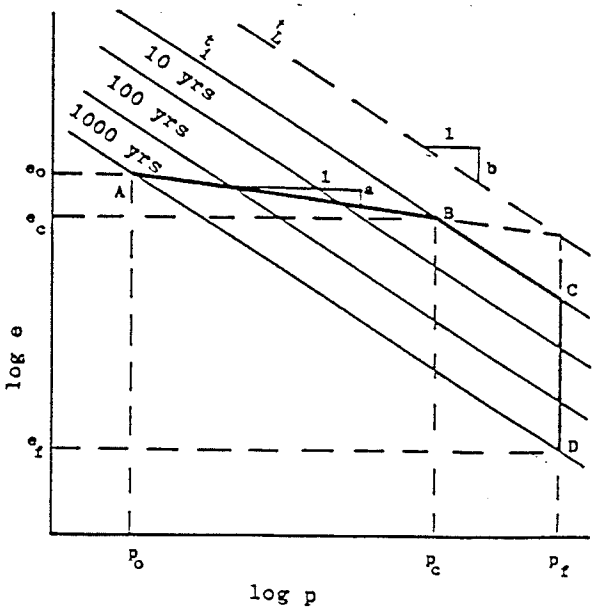

Fig.2.3 Instant time line, limit time line and other time lines in log(e),log(p)-space (after Christie and Tanks 1985)

instant line, C_α is the slope of the e-log(time) curve, and t_i is the time given to the instant line which is the same as that defined by Bjerrum (1967a).

The equation that governs the consolidation of a saturated clay undergoing one-dimensional compression and drainage is:

$$[2.9] \quad \frac{\partial e}{\partial t} = \frac{k(1 + e_o)}{\gamma_w} \frac{\partial^2 u}{\partial z^2}$$

Garlander applied his mathematical model Eqn.[2.8] into Eqn.[2.9] by simply differentiating [2.8] with respect to natural time t to get $\frac{\partial e}{\partial t}$ in Eqn.[2.8]. The reason for the emphasis of the underlining will be seen later.

Christie and Tanks (1985) argued that the 'instant time line' used by Bjerrum (1967) and Garlanger (1972) was ambiguous. They defined instant compressibility by a single coefficient and proposed a limit time line passing through the point L which is obtained by extending AB in Fig.2.3 to meet the ordinate at the final value of the effective stress. The time associated with this line, t_L, is obtained by extrapolation of the log(e)-log(t) data. They still used Bjerrum's method to find other time lines, that is these lines were obtained by drawing lines through points representing equal durations of applied pressure. The results from their experimental program "confirmed Bjerrum's statement that the time lines represent a unique relationship between e, p, and t, independent of the way in which the clay has reached these values." For example, the 1-day time line could be

obtained either by applying pressure increments at intervals of 24 hours or by the other loading sequence such as singe-stage loading. Christie and Tanks (1985) then used the same procedure as Garlanger (1972) to apply their model to solve the consolidation problem.

Comments:

The contributions in Bjerrum's model (1967a) are:

(1). He divided the total creep strain into "instant" strain and "delayed" strain which occurs during whole consolidation process.

(2). He first presented the "equivalent time" concept. He found that the "equivalent time" and the creep rate depend on the vertical stress and void ratio, but are independent of loading history.

The limitations of the model are:

(1). His instant time line is incorrect. This line is in conflict with observations in high constant rate of strain tests.

(2). He did not give a method for finding the equivalent time.

(3). The time lines are obtained directly from single-stage consolidation tests.

(4). He did not develop general equations for step-wise loading and continuous loading.

Garlanger worked at developing Bjerrum's model. In his work (1972), he suggested Eqn.[2.8] for general loading. However, the real time t was used in this equation. The use of real time t is in conflict with the uniqueness of the time lines in Bjerrum's model and the idea of

"equivalent time". Garlanger also used the incorrect instant time line used by Bjerrum (1967a).

Christie and Tanks (1985) correctly used one parameter to describe the instant compression and removed the instant time line used by Bjerrum (1967a) and Garlanger (1972). However they still had not developed general equations for any step-changed loading and continuous loading.

2.2.2 The model using C_α/C_c

Mesri and his co-workers have suggested a model which uses the ratio of secondary consolidation coefficient C_α to compression index C_c, that is C_α/C_c (Mesri and Godlewski 1977 and 1979, Mesri and Choi 1985a and 1985b, Mesri and Castro 1987). They found that the ratio C_α/C_c is in the range of 0.02-0.10 for most clays (Mesri and Godlewski 1977). During 1-D consolidation, the void ratio at any depth Z is a function of effective stress and time (Mesri and Choi 1985a):

$$[2.10] \quad e = f(\sigma'_v,\ t)$$

Using their notation, the rate of decrease in void ratio with time is:

$$[2.11] \quad \frac{de}{dt} = \left(\frac{\partial e}{\partial \sigma'_v}\right)_t \frac{d\sigma'_v}{dt} + \left(\frac{\partial e}{\partial t}\right)_{\sigma'_v}$$

Then the change in void ratio in [2.11] is the sum of the primary compression $(\Delta e)_p$ and secondary compression $(\Delta e)_s$:

$$[2.12] \quad \Delta e = (\Delta e)_p + (\Delta e)_s$$

$$[2.13] \quad (\Delta e)_p = \int_0^{t_p} [(\frac{\partial e}{\partial \sigma'_v})_t \frac{d\sigma'_v}{dt} + (\frac{\partial e}{\partial t})_{\sigma'_v}] \, dt$$

$$[2.14] \quad (\Delta e)_s = \int_{t_p}^{t} (\frac{\partial e}{\partial t})_{\sigma'_v} \, dt = \int_{t_p}^{t} - \frac{0.434 \, C_\alpha}{t} \, dt$$

Mesri and Choi (1985a) thought that "the end-of-primary void ratio-effective stress relationship, (i.e. Eqn.[2.13]), is practically independent of the duration of the primary consolidation stage." "Thus, the e-log(σ'_v) curve determined from the standard oedometer test can be used directly to compute primary settlement of the clay layers in the field." The calculation of the secondary compression $(\Delta e)_s$ in Eqn.[2.14] was related to the secondary coefficient C_α.

Using the concept of C_α/C_c, the preconsolidation pressure p'_c resulted from aging is (Mesri and Choi, 1979, 1980, 1984):

$$[2.15] \quad \frac{p'_c}{p'_i} = (\frac{t}{t_p})^{(C_\alpha/C_c)/(1- C_r/C_\alpha)}$$

Mesri and Castro (1987) put [2.15] into an expression for the static pressure coefficient K_o proposed by Mayne and Kulhawy (1982):

$$[2.16] \quad K_o = (1 - \sin\phi') \, (\frac{t}{t_p})^{(C_\alpha/C_c)/(1- C_r/C_\alpha) \, / \, \sin\phi'}$$

for calculating the time-dependent K_o.

Comments:

The range of the ratio C_α/C_c found by Mesri and his co-worker is valuable. The equations for calculating p'_c, K_o and settlement are valid under certain conditions in which the correct time t must be used in the equations. What kind of time t should be used in Eqns.[2.15],[2.16] for cases of stepwise loading or continuous loading is not explained. Eqns.[2.10],[2.11] are not fundamental constitutive equations. They simply state that the void ratio e depends only on the current state point (σ'_v, t), not on the loading history of how the soil reaches this point.

2.2.3 Stress-strain-strain rate relationship

Leroueil et al. (1985) found that the viscous behavior of clays is controlled by a unique stress-strain-strain rate relationship, σ'_v-ε_v-$\dot{\varepsilon}_v$. This relationship is simply described by two curves, σ'_p vs. $\dot{\varepsilon}_v$ and (σ'_v/σ'_p) vs. ε_v, where σ'_p is the 1-D preconsolidation pressure (Leroueil 1988).

In developing the work of Leroueil et al (1985), Kabbaj et al (1986) argued that the model by Leroueil et al (1985) "represents the behavior of clay in oedometer tests in which the strain is always increasing. It should be noted that, when defined in terms of total strains, it presents some shortcomings. In particular, the model cannot represent correctly the behavior observed in relaxation tests in which there is a

decrease of the effective stress under constant strain. Such a decrease is most likely associated with the combined effects of elastic and plastic strains." Kabbaj et al. (1986) then modified this model into two independent relationships, i.e. $\sigma'_v - \varepsilon_v^p - \dot{\varepsilon}_v^p$ and $\varepsilon_v^e = \kappa/(1+e_o)\ \ln(\sigma'_v/\sigma'_{vo})$.

Comments:

The model suggested by Leroueil et al (1985) and Leroueil (1988) was mainly based on the tests at constant rate of strain (CRSN). Thus, as found by Kabbaj et al (1986), this model can only be applied to calculate strains for this type of test, and can not be applied to other types of tests such as relaxation tests. The modified model proposed by Kabbaj et al (1986) introduced the concept of elastic visco-plastic mechanics. However, in establishing the relationship $\sigma'_v - \varepsilon_v^p - \dot{\varepsilon}_v^p$, they utilized results that will be seen later to belong to the 3-D elastic visco-plastic model by Adachi and Oka (1982). The limitations of this type of model will be discussed in Section 2.3.1.

2.2.4 Rheological models in 1-D stressing

In linear rheological models, there is a linear relationship between the stress, σ, strain, ε, and their successive derivatives with respect to time (Suklje, 1969):

$$[2.17] \quad E_o\varepsilon + E_1\dot{\varepsilon} + E_2\ddot{\varepsilon} + \ldots = S_o\sigma + S_1\dot{\sigma} + S_2\ddot{\sigma} + \ldots$$

where E_o, E_1, ... and S_o, S_1, ... are constant. Important linear models are the generalized Kelvin-Voigt model and the generalized Maxwell model.

Cernocky and Krempl (1979) presented a first order uniaxial non-linear model to consider rate effects, creep and relaxation:

[2.18] $m(\sigma, \varepsilon)\ \dot{\varepsilon} + g(\varepsilon) = \sigma + k(\sigma, \varepsilon)\ \dot{\sigma}$

where m and k are functions of stress σ and strain ε, g is a function of strain ε.

2.3 Modelling of Time-Dependent Behavior in 3-D stress states

In this section we discuss three types of models. The first one is Perzyna's elastic-viscoplastic model (1963, 1966), which is also called an over-stress model. The second type is flow surface models. The third type may be called elastic-plastic-viscous models.

2.3.1 Development of Perzyna's model (1963, 1966)

A number of elastic visco-plastic models have been developed from the model proposed by Perzyna (1963, 1966). The basic assumptions in this type of model are:

(1). Total strain rates are the sum of time-independent elastic strain

rates and time-dependent viscoplastic strain rates:

$$[2.19] \quad \dot{\varepsilon}_{ij} = \dot{\varepsilon}^{e}_{ij} + \dot{\varepsilon}^{vp}_{ij}$$

(2). A separate elastic constitutive law is required to relate the strain rates $\dot{\varepsilon}^{e}_{ij}$ to stress rates $\dot{\sigma}_{ij}$:

$$[2.20] \quad \dot{\varepsilon}^{e}_{ij} = C_{ijkl}\dot{\sigma}_{kl}$$

(3). Viscoplastic strain rates are calculated from the following flow rule:

$$[2.21] \quad \dot{\varepsilon}^{vp}_{ij} = \gamma \, \langle \phi(F) \rangle \, \frac{\partial Q}{\partial \sigma_{ij}}$$

where γ is referred to as the fluidity parameter with units of inverse time, F is yield function, and Q is plasticity potential. If $Q \equiv F$, Eqn.[2.21] is an associative flow law, if $Q \neq F$, it is a non-associative situation. The parameter ϕ is scalar function where:

$$[2.22] \quad \begin{aligned} \langle \phi(F) \rangle &= \phi(F) \quad \text{for } F > 0 \\ \langle \phi(F) \rangle &= 0 \quad \text{for } F \leq 0 \end{aligned}$$

Zienkiewicz and Cormeau (1974) used the following scalar function ϕ:

$$[2.23] \quad \phi = \left(\frac{F}{F_o}\right)^n$$

where the yield function F was chosen to be a Drucker-Prager yield surface (Drucker and Prager 1952) or Mohr-Coulomb yield surface (Nayak and Zienkiewicz 1972). F_o in [2.23] denotes any convenient reference value of F to render the expression dimensionless.

Katona (1984) incorporated a cap model into Perzyna's elasto-viscoplastic theory. The two popular forms of scalar function ϕ are Eqn.[2.23] and Eqn.[2.24]:

$$[2.24] \quad \phi = \exp\left(\frac{F}{F_o}\right)^n - 1$$

The yield function F consists of three regions; namely a cap region, a failure region and a tension cutoff region. F is a function of stresses σ_{ij}, and a strain hardening parameter k, which in turn is defined by some hardening function of the viscoplastic strain history, that is, $k = k(\varepsilon_{ij}^{vp})$. "For a given value of k, all states of stress that satisfy F = 0 forms the current 'static' yield surface in a six-dimensional stress space (i.e., classical plasticity yield surface)." Katona (1984) assumed the strain hardening parameter k was:

$$[2.25] \quad k = X(\bar{\varepsilon}) = \frac{1}{D_o} \ln\left(\frac{\bar{\varepsilon}}{W} + 1\right)$$

where W and D_o are positive material hardening constants; and the hardening argument, $\bar{\varepsilon}$, is given by:

$$[2.26] \quad \bar{\varepsilon} = \bar{\varepsilon}_o + \int_0^t \min(\dot{\varepsilon}_{11}^{vp} + \dot{\varepsilon}_{22}^{vp} + \dot{\varepsilon}_{33}^{vp})\, dt$$

Desai and Zhang (1987) and Vulliet and Desai (1989) used the generalized yield function proposed by Desai and co-workers for the yield function F in Eqns.[2.23],[2.24]. The yield function is (Desai 1980, Desai et al. 1986):

$$[2.27] \quad F = J_{2D} - (-\alpha J_1^n + \bar{\gamma} J_1^2)\, F_s$$

where J_{2D} is the second invariant of the deviatoric stress tensor, S_{ij}. J_1 is the first invariant of the stress tensor, σ_{ij}. F_s is a shape function which controls the shape of the yield surface on π-plane (Desai 1980, Desai et al. 1986). The parameter n is a material constant controlling the shape of the yield surface in J_{2D}, J_1-space. The material constant $\bar{\gamma}$ is related to $M_c^2 = J_{2D}/J_1^2$ which defines a zero volume change line by $M_c^2 = 2\bar{\gamma}/n - \alpha$. The parameter α in [2.27] is a growth or hardening function which may be expressed as:

$$[2.28] \quad \alpha = \frac{a}{(\xi_{vp})^{\eta}}$$

where a and η are hardening constants and ξ_{vp} is the trajectory of viscoplastic strain given by:

$$[2.29] \quad \xi_{vp} = \int (d\varepsilon_{vp}^T \, d\varepsilon_{vp})^{1/2}$$

Adachi and Oka (1982) presented an elasto-viscoplastic constitutive relationship based on Perzyna's elasto-viscoplastic theory and the original critical state energy theory (Roscoe et al. 1963). In their model, the scalar function ϕ in Eqn.[2.23] is:

$$[2.30] \quad \gamma \, \phi(F) = c_o \exp[m' \ln(\sigma'^{(d)}_{my} \, / \, \sigma'^{(s)}_{my})]$$

in which c_o and m' are parameters related to the time-dependent properties of materials. The stress $\sigma'^{(s)}_{my}$ in [2.30] is related to the strain hardening parameter k_s, representing strain hardening effects in the change of stress state from $\sigma'_m = 0$ to $\sigma'_m = \sigma'_{my}$. The stress $\sigma'^{(s)}_{my}$ controls the position of the static yield surface:

$$[2.31] \quad f_s = \sqrt{2J_2^{(s)}}\,/(M\sigma'^{(s)}_m) + \ln\sigma'^{(s)}_m = \ln\sigma'^{(s)}_{my} = k_s$$

This yield surface is the same as Eqn.[2.6] derived from the original critical state energy theory (Roscoe et al. 1963). In [2.30] $\sigma'^{(d)}_{my}$ is related to the strain hardening parameter, k_d, which represents both strain hardening and rate effects. The stress $\sigma'^{(d)}_{my}$ controls the position of the dynamic yield surface:

$$[2.32] \quad f_d = \sqrt{2J_2}/(M\sigma'_m) + \ln\sigma'_m = \ln\sigma'_{my} = k_d$$

The function F in [2.23] was defined as:

$$[2.33] \quad F = f_d/k_s - 1$$

Thus [2.30] becomes:

$$[2.34] \quad \gamma\,\phi(F) = c_o \exp(m'F\,k_s)$$

where k_s is related to inelastic volume strain through $\ln\sigma'^{(s)}_{my}$:

$$[2.35] \quad \varepsilon^p_v - \varepsilon^p_{vi} = \frac{\lambda - \kappa}{1+e} \ln[\sigma'^{(s)}_{my}/\sigma'^{(s)}_{myi}]$$

Comments:

Perzyna's elasto-viscoplastic theory provides some understanding of the modelling of the time-dependent stress-strain behavior in three dimensions. The question arises why the scalar function ϕ should be a function of the yield function F. The mathematical forms of ϕ (Eqns.[2.23], [2.24] and [2.34]) are much different from one another. The determination of model parameters are difficult and not clear.

2.3.2 Flow Surface Models

Matsui and Abe (1985, 1986) presented a flow surface model based on the pioneer work of Nahhdi and Murch (1963), Olszak and Perzyna (1964, 1966) and Sekiguchi (1984). In their model, the total strain rates are divided into elastic strain rates and viscoplastic strain rates as in Eqn.[2.23]. The time-dependent yield surface in the model is called the flow surface (or loading surface) which is similar to the dynamic yield surface in Perzyna's approach in the preceding section. The flow surface F was assumed to be:

$$[2.36] \quad F = F(\sigma_{ij},\ \varepsilon^{vp}_{ij},\ k,\ \eta) = 0$$

where k is the strain hardening parameter, and η is a parameter which is a function of time. When F equals zero, both elastic and viscoplastic strains occur. When F is negative, only elastic strains occur. Assuming that the flow surface is convex and that the direction of the viscoplastic strain rate vector coincides with the direction of the outer normal vector to the flow surface at the stress point:

$$[2.37] \quad \dot{\varepsilon}^{vp}_{ij} = \lambda \frac{\partial F}{\partial \sigma_{ij}}$$

in which λ is a positive scalar parameter, which is determined by the following equation of the consistency condition:

$$[2.38] \quad \dot{F} = \frac{\partial F}{\partial \sigma_{ij}} \dot{\sigma}_{ij} + \frac{\partial F}{\partial \varepsilon^{vp}_{ij}} \dot{\varepsilon}^{vp}_{ij} + \frac{\partial F}{\partial k} \dot{k} + \frac{\partial F}{\partial \eta} \dot{\eta} = 0$$

In their latest paper (Matsui et al. 1989), it is assumed that the flow

surface is:

$$[2.39] \quad F = \mu \ln\{\frac{1}{\delta}\,[(1-\exp(-\frac{\delta}{\mu}\,\dot{v}_r^v\,t))\,\exp(\frac{f}{\mu}) + \delta\,\exp(-\frac{\delta}{\mu}\,\dot{v}_r^v\,t)]\} - v^{vp} = 0$$

where δ, μ, $\dot{v}_r^v$ are the viscoplastic material parameters, v^{vp} the viscoplastic volumetric strain, and t the elapsed time. The scalar function f in [2.39] is the volumetric strain in the reference state which is a function of stress. Using Eqns.[2.23], [2.24] and [2.39], [2.38], [2.39], the resulting constitutive equations are (Matsui et al. 1989):

$$[2.40] \quad \dot{\varepsilon}_{ij} = C_{ijkl}\dot{\sigma}_{kl} + [(\frac{\partial F}{\partial \sigma_{mn}}\,\dot{\sigma}_{mn} + \frac{\partial F}{\partial t}) \,/\, \frac{\partial F}{\partial p}]\,\frac{\partial F}{\partial \sigma_{ij}}$$

Comments:

The feature of flow surface models is that the models employ a flow function which is a non-stationary loading function, and is used as the viscoplastic potential. A consistency condition is used to find the scalar function in the flow rule. The problem is how to find the flow function Eqn.[2.36]. Although Matsui and Abe (1985, 1986) assumed a more basic equation to derive the flow function [2.39], the theoretical and experimental basis for the flow function is not clear, nor is the determination of the material parameters for the model.

2.3.3 Elastic-plastic-viscous models

Borja and Kavazanjian (1985) suggested an elastic-plastic-viscous model

based on Bjerrum's model for 1-D straining (1967a), and the modified Cam-Clay model. This approach was developed by Liang et al (1987) using the concepts of the boundary surface plasticity. In the model (Borja and Kavazanjian 1985), the strain rate tensor $\dot{\varepsilon}_{ij}$ is decomposed into:

$$[2.41] \quad \dot{\varepsilon}_{ij} = \dot{\varepsilon}^{e}_{ij} + \dot{\varepsilon}^{p}_{ij} + \dot{\varepsilon}^{t}_{ij}$$

where elastic strain rates $\dot{\varepsilon}^{e}_{ij}$ are calculated using Eqn.[2.24], time-independent plastic strain rates $\dot{\varepsilon}^{p}_{ij}$ are calculated using the same procedure as in the modified Can-Clay model:

$$[2.42] \quad \dot{\varepsilon}^{p}_{ij} = \phi \frac{\partial F}{\partial \sigma_{ij}}$$

and the yield function F is Eqn.[2.7]. However the stress parameter p_o in the equation was assumed to depend on the plastic volume strain ε^{p}_{v} due to strain hardening, and on the time t_v due to aging:

$$[2.43] \quad p_o = p_o(\varepsilon^{p}_{v},\ t_v)$$

The scalar factor ϕ is determined by using the consistency condition:

$$[2.44] \quad \dot{F} = \frac{\partial F}{\partial \sigma_{ij}} \dot{\sigma}_{ij} + \frac{\partial F}{\partial p_o} \dot{p}_o = 0$$

Time-dependent creep strain rates, $\dot{\varepsilon}^{t}_{ij}$, in [2.43] are calculated from the following rule:

$$[2.45] \quad \dot{\varepsilon}^{t}_{ij} = \varphi \frac{\partial F}{\partial \sigma_{ij}}$$

where F is the same as in [2.42]. The scalar function φ is determined with a volumetric scaling method or a deviatoric scaling method. In

the volumetric scaling method, φ is related the rate of secondary compression by ψ:

$$[2.46] \quad \varphi = \frac{\psi}{(1 + e)\ t_v\ (2p - p_o)}$$

where ψ is secondary coefficient, and t_v is the time in volumetric creep.

Comments:

The feature of the elastic-plastic-viscous model is that total strain rates are decomposed into elastic strain rates, time-independent plastic strain rates and time-dependent creep strain rates. The question is how to separate the plastic strain rates from the creep strain rates. The determination of φ is related to the time t_v. How to account for the time t_v is not clear. The instant time line used in the model is the same as that defined in Bjerrum's model. As pointed in Section 2.2.1, this instant time line is incorrect.

2.4 Objectives of the Research

In the past, many models have been suggested and developed for time-independent or time-dependent behavior, for one- dimensional cases or three-dimensional stress states. As reviewed and commented on the preceding sections, each of these models has some advantages and some limitations. This thesis will utilize the work in the existing literature, overcome some limitations in the mentioned models, and

develop a new constitutive model for the time-dependent stress-strain behavior of soils. To achieve this goal, the detailed objectives in this research are listed as follows:

1. Develop a new three-modulus hypoelasticity model for time-independent behavior:

(1). The hypoelasticity model can be used to calculate the time-independent part of the total strains in time-dependent soils, or to describe the stress-strain behavior of time-independent soils.

(2). The model can account for some principal characteristics of soil behavior, such as non-linearity, anisotropy, and the couplings of p'-ε_s and q-ε_v.

(3). Suggest new methods for determining the three moduli in the model using simple conventional triaxial tests.

(4). Calibrate and verify the model using different types of tests.

2. Develop a new Elastic Visco-Plastic (EVP) model for the time-dependent behavior of soils in 1-D straining:

(1). Develop a new theoretical framework of EVP models for 1-D straining based mainly on Bjerrum's work (1967a).

(2). The EVP models can account for non-linearity, irreversibility, creep, relaxation, strain rate effects etc. in 1-D straining.

(3). Suggest some new methods for determining all parameters in the

model using simple oedometer tests.

(4). The models should be calibrated and validated using various types of tests and soils.

3. Develop a new Elastic Visco-Plastic (EVP) model for the time-dependent behavior of soils in general 3-D stress states:

(1). Based on the work of hypoelasticity models and 1-D EVP models, the framework of 3-D EVP models is developed.

(2). The 3-D EVP models should be capable of describing non-linearity, irreversibility, anisotropy, creep, relaxation and strain rate effects in more general three dimensional stress states.

(3). Suggest some new methods to find the model parameters using simple triaxial tests.

(4). The models should be constructed, calibrated for different soils, and verified using different tests.

It will be helpful to clarify how the new material in this thesis relates to previously published work by other authors. One, the new three-modulus hypoelastic model in Chapters 3,4 takes account of additional features of soil behavior compared with existing two-modulus models. It must therefore be considered conceptually superior to the earler models. Two, the 1-D EVP model in Chapters 5,6,7 presents, for the first time in the geotechnical literature, a general mathematical model that describes the σ'_z-$\dot{\sigma}'_z$-ε_z-$\dot{\varepsilon}_z$ relationships in clay soils. This

single model can be used to predict behavior in incremental loading, constant rate of strain, creep and relaxation tests. Three, the EVP model is also developed for axi-symmetric stressing. This allows complex test procedures such as speed changing, relaxation, and loading history dependency to be predicted by using a single mathematical model.

The approach adopted in the thesis has been to concentrate on the mathematical modelling and to introduce validation where experimental data are available. This inevitably means that further research will be required to examine (a) the broader applicability of the assumptions used in the modelling, and (b) restrictions on when the models can be used successfully.

Chapter 3

HYPOELASTICITY MODELS

3.1 Introduction

In some soils such as sandy soils and some inactive clays, strain rate effects are small and may be ignored. Only time-independent stress-strain behavior needs modelling for engineering applications. However in most clay soils, strain rate and time effects are very significant (Graham et al. 1983). However, even in these cases, total strains may be divided in principle into two parts, time-dependent strains and time-independent strains. When this is done, a constitutive law is required to calculate each part separately. In this Chapter, we will deal with only the time-independent part, and time dependency will be dealt with later. The main characteristics of time-independent stress-strain behavior are irreversibility, non-linearity, anisotropy, expansion or compression during shear, and the shear strains which can accompany changes in mean stress. Here we will develop a new procedure for hypoelastic (that is, non-linear differential elasticity) modelling.

Eringen (1962) and Saleeb and Chen (1981) have reviewed the techniques that are commonly used for constitutive modelling of the time-independent behavior. The simplest models are based on linear or

non-linear elasticity. However, most soils exhibit non-recoverable straining in at least part of their stress range. This has led to the development of elastic-plastic models such as the Cam-clay family (Roscoe and Burland 1968) in which strains depend, in general, on both the stress-path and the stress history of the clay. These models also include the tendency to volume change that usually accompanies shearing in clays. This is commonly known as "dilatancy" and may be compressive or expansive in nature. The applicability of elasto-plasticity to natural clays has been reviewed by Wroth and Houlsby (1985) and Graham et al. (1989).

Another approach is to use hypoelasticity (Truesdell 1955; Truesdell 1965; Coon and Evans 1971) which assumes a general incremental constitutive relationship for time-independent materials:

$$[3.1] \quad F_{ij}(\sigma'_{kl}, \dot{\sigma}'_{mn}, \varepsilon_{pq}, \dot{\varepsilon}_{st}) = 0$$

provided that this equation is homogeneous in time, i.e. time occurs to the same order in all terms of the equation and therefore, may be eliminated. This approach emphasizes the non-linear nature of soil response to loading but does not readily include some of the discontinuous behaviour (for example, porewater pressure generation or dissipation) that is well handled by elasto-plasticity. Hypoelasticity has drawn some criticism for its lack of incremental continuity of response along certain load paths (Mroz, 1980).

Coon and Evans (1971) suggested four reduced forms of [3.1]. One of the reduced forms is:

$$[3.2] \quad d\varepsilon_{ij} = C_{ijkl}(\sigma'_{mn})\, d\sigma'_{kl}$$

Here C_{ijkl} are complementary constitutive tensors (or moduli) which are stress level dependent. Eqn.[3.2] gives a general linear relationship between incremental strains and incremental stresses which may then be integrated to determine a required stress-strain relationship.

Two different types of hypoelasticity models have been developed from the general framework given by [3.2]. One type expresses C_{ijkl} in a stress tensor series (Coon and Evans 1971; Yin 1984). Obtaining the resulting material constants is difficult, and sometimes impossible. The second type makes a further assumption to reduce the required number of stress level dependent parameters C_{ijkl} in [3.2]. This set of parameters can be determined by differentiating curves fitted to experimentally observed stress-strain data. Examples of this type are the E,υ model of Duncan and Chang (1970); the K,G model of Domaschuk and Valliappan (1975); the three modulus model of Yin and Yuan (1985a,b); and models with more than three moduli, for example by Darve et al. (1986).

The new model presented in this chapter uses three stress dependent modulus functions that will be referred to subsequently as "moduli". These are (1) the bulk modulus K, (2) the shear modulus G, and (3) a coupling modulus J. The model incorporates non-reversibility, nonlinearity, dilatancy, and the related phenomenon which produces shear strains from mean stress changes. The three moduli can be determined from routine undrained CI$\bar{\text{U}}$ triaxial tests or drained CID

tests.

3.2 Framework of Hypoelasticity Models

One reduced form from [3.1] for the time-independent behavior is:

$$[3.3] \quad d\varepsilon_{ij} = C_{ijkl}(\sigma'_{mn}, \varepsilon_{pq})\, d\sigma'_{kl}$$

This expression is more general than [3.2]. Moduli C_{ijkl} in [3.3] may depend on both effective stresses and strains. The KGJ model to be discussed in this Chapter and Chapter 4 is based on further reduction of [3.3]. In the KGJ model, the moduli G and J depend on both stresses and volumetric strains.

Graham and Houlsby (1983) suggested a constitutive relationship:

$$[3.4] \quad \begin{cases} dp' = \bar{K}\, d\varepsilon_v + \bar{J}\, d\varepsilon_s \\ dq = \bar{J}\, d\varepsilon_v + 3\bar{G}\, d\varepsilon_s \end{cases}$$

for modelling anisotropic elastic straining, where in triaxial stress conditions, volumetric strain $\varepsilon_v = \varepsilon_1 + 2\varepsilon_3$; deviator strain $\varepsilon_s = \frac{2}{3}(\varepsilon_1 - \varepsilon_3)$; effective mean stress $p' = \frac{1}{3}(\sigma'_1 + 2\sigma'_3)$; and deviator stress $q = \sigma_1 - \sigma_3$.

Yin and Yuan (1985a,b) presented a hypoelastic model which can account for non-linearity and dilatancy in a medium sand:

$$[3.5] \quad \begin{cases} d\varepsilon_v = \frac{1}{K_1}\, dp' + \frac{1}{K_2}\, dq \\ d\varepsilon_s = \frac{1}{3G}\, dq \end{cases}$$

where K_1 is a bulk modulus, K_2 a shear dilatancy modulus and G a shear modulus. Note that this equation is written in compliance form rather than the stiffness form in [3.4]. It can be seen at once that the general matrix of the model in [3.5] is not symmetric. The model does not therefore incorporate shear strains generated by changes in mean effective stress p', for example in clays with inherent anisotropy.

In this chapter, a new formulation that includes p'-generated shear strains is suggested.

$$[3.6] \quad \begin{cases} d\varepsilon_v = \frac{1}{K}\, dp' + \frac{1}{J}\, dq \\ d\varepsilon_s = \frac{1}{J}\, dp' + \frac{1}{3G}\, dq \end{cases}$$

Here, the bulk modulus K represents the volumetric stiffness of the clay with respect to dp' ($K > 0$). The shear modulus G controls shear deformations with respect to dq ($G > 0$). The coupling modulus J accounts for the volumetric strain produced by an increment dq in deviator (shear) stress, and also the shear strain produced by an increment dp' in mean effective stress. The formulation assumes that the $dp', d\varepsilon_s$-coupling and the $dq, d\varepsilon_v$-coupling are controlled by the same J-modulus. Positive dilatancy, that is, expansion during shearing, is associated with $J < 0$. Compression during shearing produces $J > 0$. If there is no dilatancy or no anisotropy, $J = \infty$, and [3.6] has the same form as the K,G model described by Domaschuk and Valliapan (1975). The moduli K,G,J may depend on both stresses and strains.

The elastic model in [3.4] had $\bar{J} = 0$ for isotropy. Note that the hypoelastic moduli in [3.6] are not directly comparable to the elastic moduli in [3.4] but can be related to them by inversion. For example, J in [3.6] is equal to $-\bar{J}/(3\bar{K}\bar{G}-\bar{J}^2)$ from [3.4]. The difference is due to the forms chosen for [3.4] and [3.6]. It is also known that the moduli $\bar{K},\bar{G},\bar{J}$ in [3.4] are constant for a given preconsolidation pressure. While modulus functions K,G,J in [3.6] depend on both stresses and strains.

When the current total unit strain energy is lower than any previous higher strain energy level (for example, during unloading or reloading), the same form as [3.6] is used but the moduli K, G and J are replaced by K^e, G^e and J^e. Appropriate moduli (K,G and J, or K^e,$G^e$and J^e) are chosen depending on whether the stress changes are for first-time "loading" or for "unloading/reloading" expressed in terms of unit strain energy. The distinction between "first loading" and "unloading/reloading" has also been made on the basis of previous higher values of p' or q (Yin et al. 1988), but the energy criterion used in this chapter is considered superior (see also Mroz 1980, Duncan 1981).

It should be pointed out that when the modulus functions K,G,J are used for first loading and the moduli K^e,G^e,J^e are used for unloading/reloading, deformations may not be reversible for an even infinitesimal stress cycle. This means that this type of models with unloading/reloading moduli is different from the originally defined

hypoelasticity, in which the deformation is reversible in a infinitesimal stress cycle. In complicated unloading/reloading cases, the use of the model with K^e, G^e, J^e should be restricted within the strength envelope so that the stress trajectories which are not accessible for geological material can be avoided. For a neutral loading path, there may be an abrupt change in the material behavior, and the responce is not unique, energy may be continuously extracted from a sample when subjecting it to a closed stress cycle (Zytynski et al. 1978).

Eqn. [3.6] can also be extended for a general 3-D stress state in tensor form:

$$[3.7] \quad d\varepsilon_{ij} = [(\frac{1}{9K} - \frac{1}{3qJ}\sigma'_{mn} - \frac{1}{6G})\delta_{ij}\delta_{kl} + \frac{1}{2qJ}\sigma'_{kl}\delta_{ij} + \frac{1}{2qJ}\sigma'_{ij}\delta_{kl} + \frac{1}{4G}(\delta_{ik}\delta_{jl} + \delta_{il}\delta_{jk})]\, d\sigma'_{kl}$$

where the deviator stress $q = \sqrt{3J_2}$, J_2 is the second deviator stress invariant, $J_2 = 1/2\ S_{ij}S_{ij}$, and δ is the Kronecker delta ($\delta_{ij} = 1$ if $i = j$ or $\delta_{ij} = 0$ if $i \neq j$). Equation [3.7] can be written in matrix form

for finite element applications:

$$[3.8]\quad \begin{Bmatrix} d\varepsilon_{11} \\ d\varepsilon_{22} \\ d\varepsilon_{33} \\ d\varepsilon_{12} \\ d\varepsilon_{23} \\ d\varepsilon_{31} \end{Bmatrix} = \begin{bmatrix} a_1+2b_1 & a_2+b_1+b_2 & a_2+b_1+b_3 & c_1 & c_2 & c_3 \\ a_2+b_1+b_2 & a_1+2b_2 & a_2+b_2+b_3 & c_1 & c_2 & c_3 \\ a_2+b_1+b_3 & a_2+b_2+b_3 & a_1+2b_3 & c_1 & c_2 & c_3 \\ c_1/2 & c_2/2 & c_3/2 & \frac{1}{2G} & 0 & 0 \\ c_1/2 & c_2/2 & c_3/2 & 0 & \frac{1}{2G} & 0 \\ c_1/2 & c_2/2 & c_3/2 & 0 & 0 & \frac{1}{2G} \end{bmatrix} \begin{Bmatrix} d\sigma'_{11} \\ d\sigma'_{22} \\ d\sigma'_{33} \\ d\sigma'_{12} \\ d\sigma'_{23} \\ d\sigma'_{31} \end{Bmatrix}$$

where $a_1 = \frac{1}{9K} + \frac{1}{3G}$; $a_2 = \frac{1}{9K} - \frac{1}{6G}$; $b_1 = (2\sigma'_{11}-\sigma'_{22}-\sigma'_{33})/(6qJ)$

$b_2 = (2\sigma'_{22}-\sigma'_{11}-\sigma'_{33})/(6qJ)$; $b_3 = (2\sigma'_{33}-\sigma'_{11}-\sigma'_{22})/(6qJ)$

$c_1 = \sigma'_{12}/(qJ)$; $c_2 = \sigma'_{23}/(qJ)$; $c_3 = \sigma'_{31}/(qJ)$

Under triaxial stress conditions in which shear stresses are zero and the principal stress $\sigma'_2 = \sigma'_3$, [3.8] can be written in the same form as [3.6]. If $J = \infty$, and there is no cross-coupling, [3.8] has the same form as the isotropic K,G model. Note that the matrix in [3.8] is not symmetric.

3.3 Methods for Determining K, G, J Moduli

For a model to be useful, the required tests for calibrating the model must be relatively simple to perform and the data should be consistently reliable. For example, Duncan and Chang (1970) used CID

data to find E and υ as functions of q and σ'_3, while Domaschuk and Valliapan (1975) used isotropic consolidation to find K, and constant-p' tests to find G as a function of q and p'.

Conventional CID tests or incremental constant p' tests on clays last a long time, and in the latter case, are relatively difficult to run. When a load increment is applied, the porewater pressure inside the specimen changes, and the real effective stress path deviates from the target one. Despite requiring additional instrumentation, CI$\bar{U}$ tests are in some ways easier to run and more reliable than CID tests. No water flows into or away from the specimen, and apart from some end effects or localized effects in expansive strain-softening specimens, effective stresses can often be considered substantially constant throughout the specimens. In this case the specimen can be treated as an infinitesimal element for finding differential relationships for stress-strain behaviour. Two methods for determining the K,G,J moduli functions will be described below.

3.3.1 Method one: using isotropic consolidation tests and CI$\bar{U}$ tests

In this method, isotropic consolidation is used to find the bulk modulus K, while undrained CI$\bar{U}$ tests are used to find the shear modulus G and the coupling modulus J. Unload-reload cycles are incorporated into these tests to determine the elastic moduli K^e, G^e and J^e.

3.3.1.1 Bulk modulus K

Isotropic consolidation provides data relating effective mean stresses p' and volumetric strains ε_v. Fitting appropriate mathematical functions to these data produces equations $\varepsilon_v = f_1(p')$ for loading and $\varepsilon_v = f_1^e(p')$ for unloading-reloading. The bulk modulus K is then found from the first equation in [3.6] with dq = 0:

$$[3.9] \quad K = \frac{dp'}{d\varepsilon_v}$$

and K^e is obtained in a similar way from unload/reload data. The moduli K and K^e are functions only of p'.

3.3.1.2 Coupling modulus J

In CI$\bar{U}$ tests the total confining stress σ_3 is constant and the total vertical stress σ_1 increases (dq > 0). Mean effective stresses increase in specimens that are expansive in shear (dp' > 0), and decrease when the specimens are compressive (dp' < 0). Two independent relationships, q vs. p' and q vs. ε_s can be measured directly. The first relationship is used to determine the coupling modulus J.

In undrained shear, the volumetric strain is constant, $d\varepsilon_v = 0$. So from the first equation in [3.6]:

$$[3.10] \quad \frac{J}{K} = -\frac{dq}{dp'}$$

where p' = p - u; K has already been determined from isotropic

consolidation tests; and u, p and q are measured during the test. The q,p' data may be normalized by a factor which is kept constant during this type of tests. For example, the q,p' data of CI$\bar{U}$ tests can be normalized by consolidation pressures, which is then related the volumetric strains that are constant during testing. Eqn.[3.10] means that -J/K can be obtained by differentiating a curve fitted to the normalized q vs. p' test data. In this form, [3.10] is valid for first loading. An unload-reload cycle in the CI$\bar{U}$ test allows J^e to be determined using similar procedures.

3.3.1.3 Shear modulus G

Measured q - ε_s relationships can be used to determine G and G^e. Using [3.10] with the second equation in [3.6], we have:

$$[3.11] \quad 3D = \frac{dq}{d\varepsilon_s} = \frac{3GJ^2}{J^2-3GK}$$

where 3D is introduced for convenience to denote the local slope of q vs. ε_s, called the apparent shear modulus. From [3.11]:

$$[3.12] \quad G = \frac{DJ^2}{J^2+3DK}$$

If the soil is neither expanding or compressing in shear, then J = ∞, and the shear modulus G equals the apparent shear modulus D. Again, G is a function of p' and q, and varies with the total ε_v produced by p'_{cons}.

In a general case, K, K^e, J and J^e have already been determined at this stage. The q, ε_s data can be normalized by the same factor as used for q,p' data. Then an appropriate mathematical function is fitted to the data, and is differentiated to provide D. The shear modulus G is then obtained from [3.12]. As in previous cases, unloading-reloading $CI\bar{U}$ data allow determination of the elastic shear moduli D^e and G^e.

Details of this method will be described in Section 4.1 of Chapter 4 using the results from triaxial tests on 50-50 mixtures by dry mass of bentonite and sand proposed for nuclear fuel waste management in Canada.

3.3.2 Method two: using isotropic consolidation tests and CID tests

This method also uses isotropic consolidation tests to find the bulk modulus K. The difference in this method is that drained CID tests (and not $CI\bar{U}$ tests) are then used to find the moduli J and G. The application of this method will be presented in Section 4.2 of Chapter 4 using test data on a medium dense sand from Wuhan, China.

3.3.2.1 Coupling modulus J

In CID tests, two independent relationships were obtained, namely volumetric strain vs. deviator stress, ε_v - q, and shear strain vs. deviator stress, ε_s - q. The first of these relationships can be used

to find the coupling modulus J.

The ε_v,q data may be normalized by a factor which is kept constant. In CID tests, the confining pressure σ'_3 is constant, a function of which can be used for the normalization. We define $dq/d\varepsilon_v$ as J_e which is differentiation of q,ε_v. From the first equation in [3.6], we can find the relation between J_e and J:

$$[3.13] \quad J = \frac{\eta K J_e}{\eta K - J_e}$$

where $\eta = dq/dp' = 3$ for CID tests. We can obtain K from isotropic tests and we have J_e by differentiating the function fitted to ε_v,q data. Eqn.[3.13] allows calculation of J.

3.3.2.2 Shear modulus G

If we define a equivalent shear modulus G_e which is equal to $(dq/d\varepsilon_s)/3$, then from the second equation in [3.6], we have:

$$[3.14] \quad G = \frac{\eta G_e J}{\eta J - 3G_e}$$

where, again, $\eta = dq/dp'$. Therefore if we know G_e in [3.14] we can find the shear modulus G. The ε_s,q data are normalized by the same factor as used for ε_v,q data. A appropriate function is used to fit these data. By differentiating we can obtain G_e.

Using the same procedure, and from the data of unloading/reloading in

CID tests, we can find J^e and G^e.

The first method is suitable to soils with either low permeability or high permeability. However the second method is only suitable to the high permeable soils since it is very difficult to obtain reliable data from drained CID tests on low permeable soils.

Chapter 4

APPLICATIONS OF THE KGJ MODEL

4.1 Method 1: Calibration for Buffer Materials and Paris Clay

The framework of the KGJ model (Eqns.[3.6] and [3.7] or [3.8]) presented in Chapter 3 is itself a assumption. Validation of the model needs to be established using data from a variety of soils and test conditions. In this section, undrained test results from two sand-bentonite buffer materials and a Paris clay are used to calibrate the KGJ model. The subsequent section uses drained test data from Wuhan sand. In each case, predictions from the model are compared with measured results which had not been previously used in the calibration.

4.1.1 Buffer materials and testing

The dominant constituent of the "buffer" is sodium-based bentonite with liquid limit 250% and plasticity index 200% (Graham et al. 1989). It controls the swelling, strength and hydraulic conductivity of the mixture. The composition of the bentonite was reported by Dixon and Woodcock (1986) and Quigley (1984). The sand component is a uniformly graded mixture of sub-rounded fine to medium crushed quartz (Gray et al. 1984).

In a larger program at the University of Manitoba associated with the Canadian Nuclear Fuel Waste Management Program, test specimens, 50 mm diameter and 100 mm high, were formed by static compaction of mixtures of dry sand, bentonite and distilled water to 85% or 95% ASTM Modified Density. Details of the densities, water contents and saturations after compaction are given in Table 4.1 (Saadat, 1989). Dixon and Woodcock (1986) and Graham et al. (1989) showed that the buffer properties are dominated by the clay component and can be related to the density or specific volume of the clay-water phase. The sand acts mostly as an inert filler but is effective in increasing the thermal conductivity and reducing shrinkage in the buffer. The triaxial test arrangements included spiral filter drains, double membranes separated by silicone oil, drainage from the bottom of the specimen, and deaired cell water. Three series of tests were done at confining pressures up to 10 MPa - (1) isotropic consolidation; (2) undrained triaxial compression with porewater pressure measurement; and (3) drained incremental shear loading at constant p'. Application of 0.2 to 0.5 MPa back pressure generally produced B-values of 0.98 - 1.00, indicating acceptable saturation. The majority of the specimens in this program have been sheared in undrained triaxial compression and will be used to evaluate the K,G,J model. The model will then be compared with results from the constant-p' tests.

Table 4.1 Consistency of Specimens after Compaction

	ASTM Modified Dry Density	
	85%	95%
Dry density, Mg/m^3	1.50 ± 0.02	1.66 ± 0.01
Moisture content, %	28.4 ± 0.9	22.5 ± 0.2
Saturation, %	98 ± 1.5	97 ± 0.9
Clay specific volume	2.58 ± 0.04	2.24 ± 0.01

Full details of the testing program have been given by Graham et al. (1989). Some comments need to be made about the applicability of the effective stress principle to the bentonite in the mixture. It is assumed here that the properties of the buffer can be related to the tensor difference between externally applied pressures and porewater pressures measured on externally mounted pressure transducers. More detailed discussion of this important assumption has been given by Graham et al. (1988b, 1989).

4.1.2 Evaluation of K, G, J moduli using method one

The permeability of the buffer materials is very low. The hydraulic conductivity is 10^{-12} to 10^{-13} m/s for high density buffer (γ_d = 1.67 Mg/m^3) (Dixon and Gray 1985). This means, for example, that there was still 709 kPa of excess porewater pressure left in test T1001 after 76 days of isotropic consolidation (cell pressure was 3500 kPa, back pressure was 500 kPa). The excess porewater pressure in test T1002 was

89 kPa after 84.75 days of isotropic consolidation (cell pressure was 3500 kPa, back pressure was 500 kPa). (More details can be found in Chapter 9.) As a result, drained shear tests in the buffer would take a very long time, and the data obtained may be difficult to interpret. However, undrained shear tests are relatively easier to run, and the test data appear more reliable. It is therefore appropriate to use the first method discussed in Chapter 3 (that is, using CIŪ tests) to calibrate the KGJ model for buffer.

4.1.2.1 Mean pressure-volume change relationship for K and K^e

Fig.4.1 shows p', ε_v relationships from isotropic consolidation tests on sand-bentonite buffer materials with two different dry densities, γ_d = 1.50 Mg/m^3 and γ_d = 1.66 Mg/m^3. These data can be represented (see Fig.4.2), by:

$$[4.1] \quad V_c = -\lambda_c \ln(p'_{cons}) + V_{co}$$

where the clay specific volume V_c is the volume of clay and water occupied by unit volume of clay solids. The relation between V and V_c (that is, between the specific volume V for the sand-clay-water mixture and the clay specific volume V_c in the clay-water phase) is $V = 0.491V_c + 0.509$ (Graham et al. 1989). This produces from [4.1]:

$$[4.2] \quad V = -\lambda \ln(p'_{cons}) + V_o$$

and the corresponding relationship between ε_v and p' is:

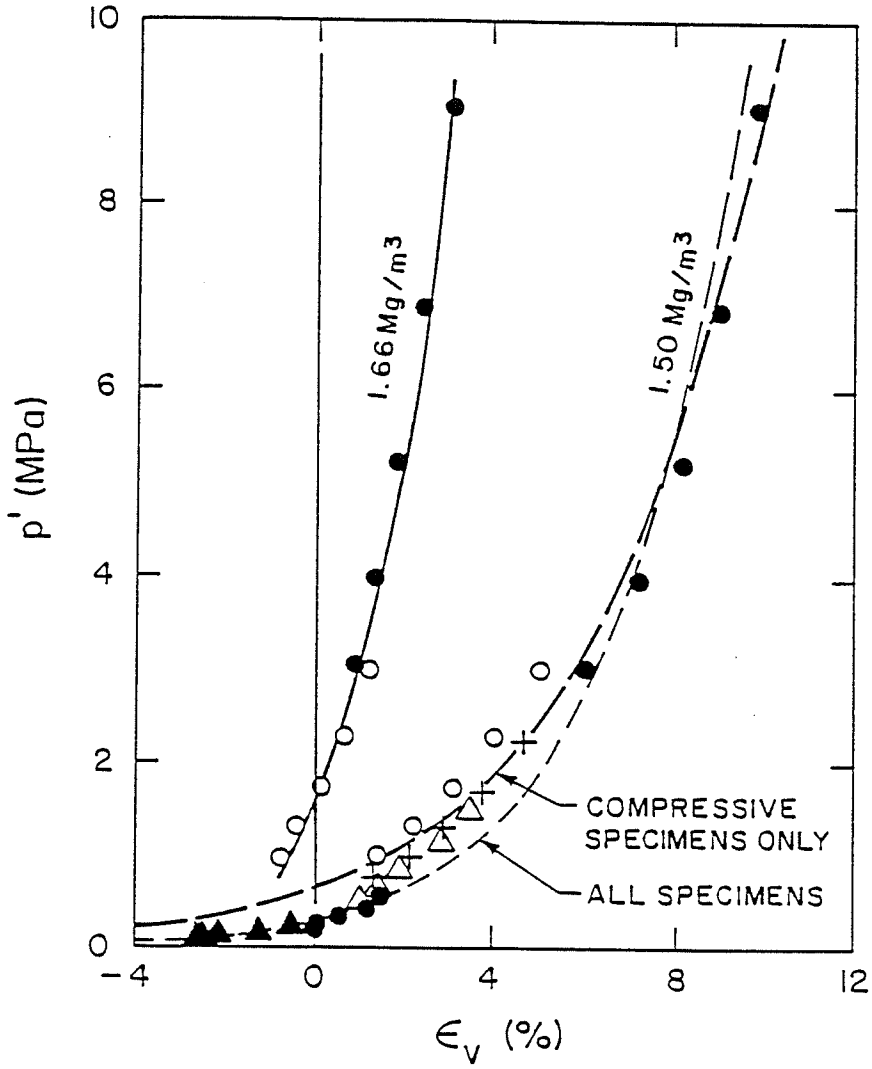

Fig.4.1 Incremental 3-day p', ε_v-relationships - isotropic consolidation (after Graham et al. 1989)

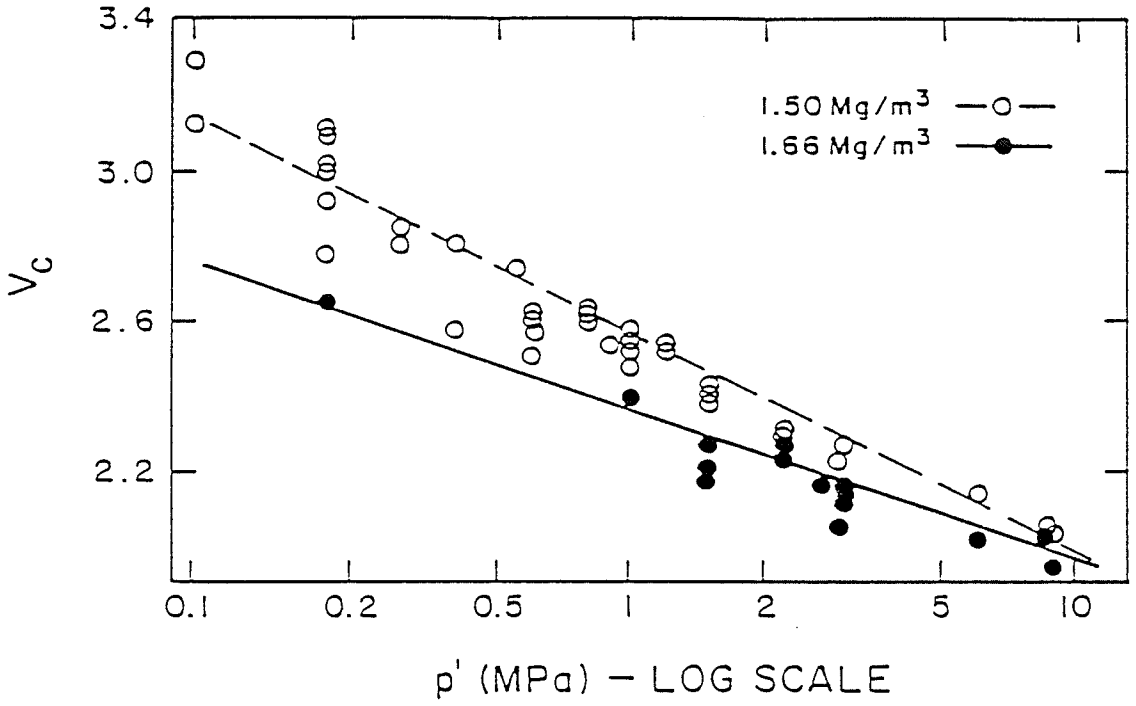

Fig.4.2 End-of-consolidation log(p'),V_c-relationships - isotropic consolidation (after Graham et al. 1989)

[4.3] $\varepsilon_v = \lambda/V_i \ \ln(p'_{cons}) + \varepsilon_{vo}$

where $V_i = 1 + e_o$, the initial specific volume before straining.

Fig.4.1 was drawn using strains accumulated in the first three days of each increment (Mesri and Godlewski 1977; Graham et al. 1983) for both densities of buffer. In Fig.4.1 the 1.50 Mg/m^3 buffer swells when the confining pressure is less than 0.7 MPa. The corresponding pressure for 1.66 Mg/m^3 buffer is 1.7 MPa (Saadat 1989).

The behaviour of buffer is strongly time-dependent (Graham et al. 1989) and test durations up to 60 days were at times required to reduce volumetric straining rates to 0.1% /day, a rate that was taken to indicate "end-of-consolidation". Fig.4.2 shows "end-of- consolidation" (EOC) relationships rather than the "3-day" results shown in Fig.4.1. The lines in Fig.4.2 have been drawn through data from specimens that were compressive (that is, they showed increasing porewater pressures) during subsequent undrained shearing. Fig.4.2 includes data from a limited number of specimens with different initial densities. Those with densities 1.58 Mg/m^3 (90% ASTM Modified Density) or less, have been included with the 1.50 Mg/m^3 data. The remainder have been included with the 1.66 Mg/m^3 data. Table 4.2 shows the EOC parameters in [4.3] that result from this data. The compression index λ is larger than the corresponding value measured from the "3-day" data in Fig.4.1. This suggests the specimens were not fully equilibrated at the earlier stage (Graham et al. 1989).

Saadat (1989) showed however that specimens were about 95% consolidated at EOC. Multiple regression analysis on tests with different consolidation times suggests that the durations of the tests were sufficiently long that the effects of time on the EOC relationships in Fig.4.2 should be small. The long-term swelling pressure of the buffer at 85% ASTM modified density is estimated at 1.0 MPa from the EOC data rather than 0.7 MPa from 3-day data (Saadat 1989).

The elastic bulk compressibility of the buffer is determined through an isotropic swell-compression cycle represented mathematically by:

$$[4.4] \quad \varepsilon_v = \kappa/V_i \ \ln(p'_{cons}) + \varepsilon^e_{vo}$$

The data show $\kappa/V_i = 0.0105$ ($R^2 = 0.95$) and $\kappa/V_i = 0.0125$ for 3-day and 5-day strains respectively in 1.50 Mg/m^3 buffer (Saadat 1989). Because strains and strain rates are small in the elastic range, it is reasonable to use short duration data.

Applying [3.9] and differentiating [4.3] and [4.4], the bulk moduli K and K^e are:

$$[4.5] \quad \begin{cases} K = p'/(\lambda/V) \\ K^e = p'/(\kappa/V) \end{cases}$$

The introduction of p' in [4.5] instead of p'_{cons} in [4.3] and [4.4] involves an important assumption that the volumetric strain induced by p' is independent of q. Using Table 4.2 and the EOC data in Fig.4.2 for 1.50 Mg/m^3 buffer produces $K/p' = 13.7$. The 5-day unload/reload data suggest in [4.4] that $K^e/p' = 80.0$, ($K/K^e = 5.8$).

Table 4.2 Curve-fitting Parameters in KGJ Model

Soil	K-modulus			J-modulus			G-modulus		
	λ/V_i	ε_{vo}	R^2	A	n	R^2	E	F	R^2
1	.073	-0.003	0.92	1.32	0.81	0.81	0.0086	2.15	0.96
2	.052	-0.039	0.95	1.25	0.65	0.64	0.0108	1.83	0.99
3	.029	-0.172	0.98	-8.93	1	0.98	0.0039	0.92	-

Soil: 1. Sand-bentonite buffer γ_d = 1.50 Mg/m^3 (Graham et al. 1988)
2. Sand-bentonite buffer γ_d = 1.66 Mg/m^3 (Graham et al. 1988)
3. Paris clay, France (Azizi, 1987)

4.1.2.2 Effective mean stress-deviator stress relationship for J and J^e

Figs.4.3a,b show data from compressive $C\bar{I}U$ specimens with initial densities 1.50 Mg/m^3 and 1.66 Mg/m^3 respectively. The stress paths incline leftwards at the beginning of shearing indicating anisotropy. The p',q data have been normalized by p'_{cons} in the range 0.8 - 3.0 MPa. They normalize into reasonably restricted zones in the Figures and this has been taken to support the use of "effective stresses" to describe the tests. A power law [4.6] has been used to describe the best-fit normalized stress paths:

$$[4.6] \quad q/p'_{cons} = A\left(1 - \frac{p'}{p'_{cons}}\right)^n$$

Values of A, n and R^2 are given in Table 4.2. The R^2 coefficient

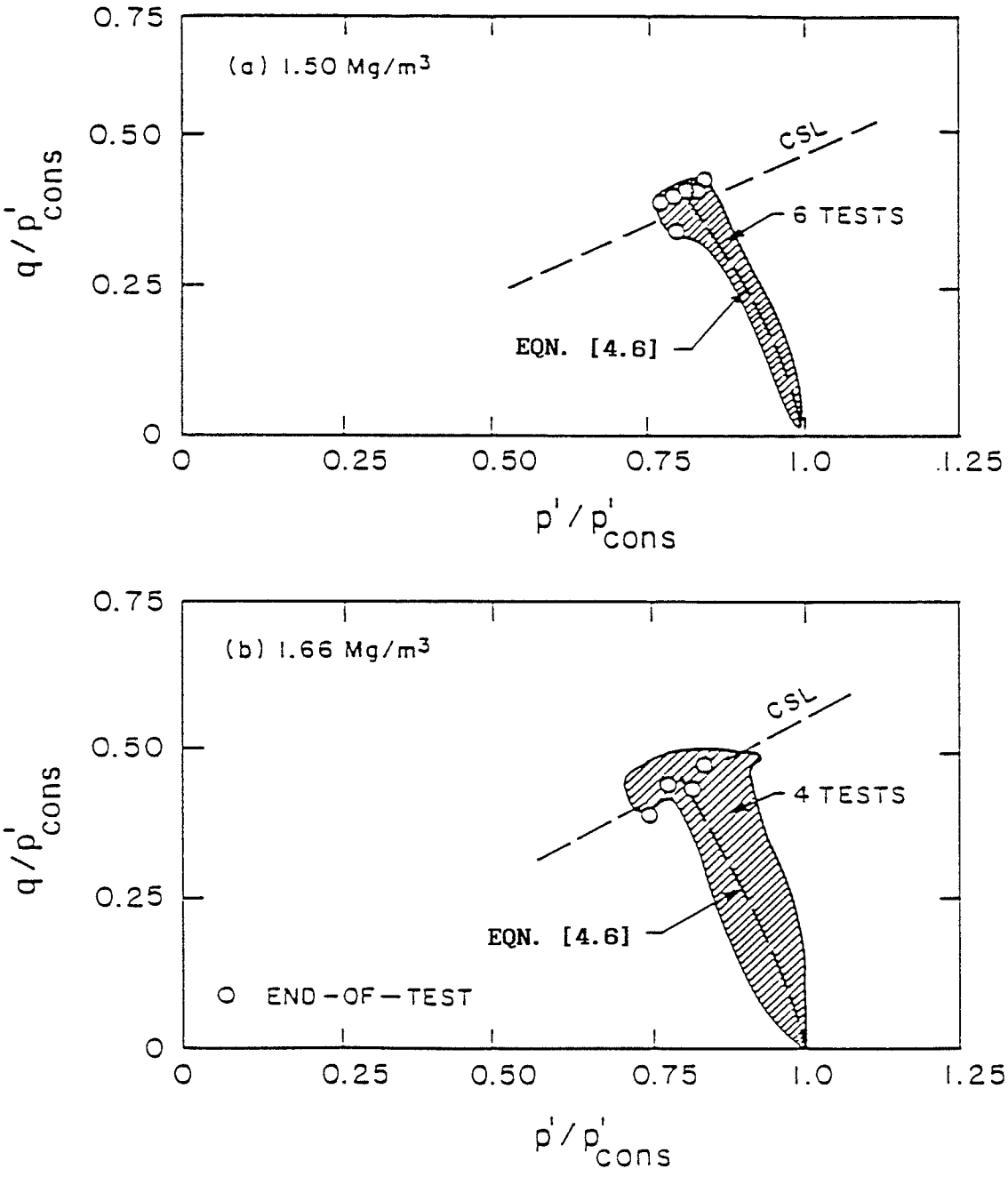

Fig.4.3 Normalized q/p'_{cons}, p'/p'_{cons}-relationships - CIŪ tests

reflects variability of the normalized stress paths due to differences in initial density, fabric structure and consolidation duration.

Using [3.10] and differentiating [4.6] with respect to p', the coupling modulus can be written:

$$[4.7] \quad J/K^e = nA^{1/n} \, (q/p'_{cons})^{(n-1)/n}$$

$$= c \, (p'_{cons}/q)^d$$

where $c = nA^{1/n} = 1.05$, $d = (1-n)/n = 0.41$. Using the value $K^e/p'_{cons} = 80$ obtained in the previous section from [4.5], the coupling modulus for buffer with 1.50 Mg/m^3 initial dry density is:

$$[4.8] \quad J = 1.05 \times 80p' \, (0.962 \exp(13.72\varepsilon_v)/q)^{0.41}$$

It can be seen that J and J^e are functions of p' and q, and vary with the volumetric strain ε_v from the beginning of the test due to consolidation under p'_{cons}. When q = 0, the coupling modulus $J = \infty$, implying that the initial behaviour in shear is isotropic. This deviates from the observed average behaviour in Fig.4.3 which is initially anisotropic, probably because the specimens were formed by compaction in rigid molds..

4.1.2.3 Undrained shear stress-strain relationship for G and G^e

Fig.4.4 shows reasonably consistent results from compressive specimens with initial densities 1.50 Mg/m^3 and 1.66 Mg/m^3 and effective

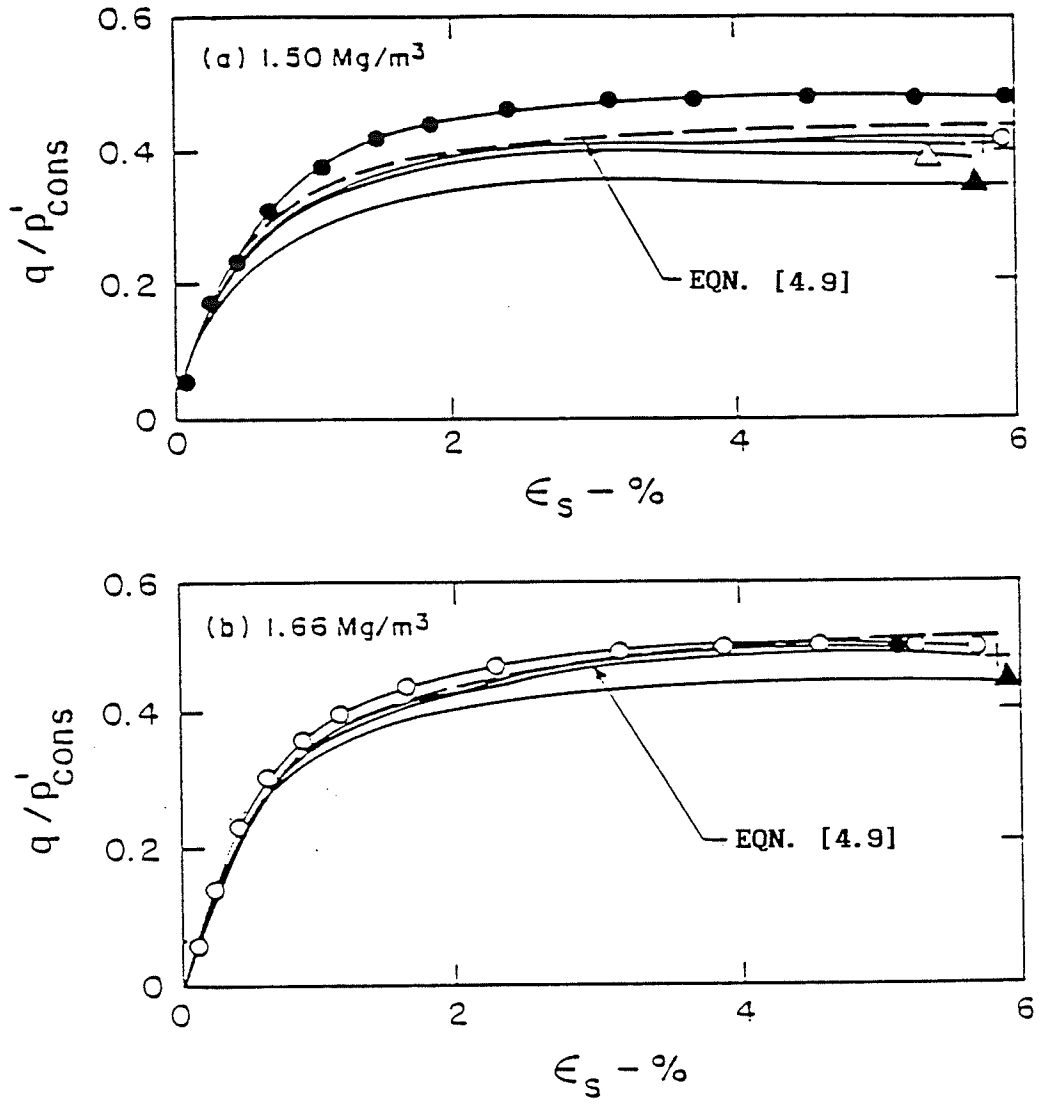

Fig. 4.4 Normalized q/p'_{cons}, ε_s-relationships - CIŪ tests

confining pressures in the range 0.8 - 3.0 MPa. The q-data have again been normalized by p'_{cons}. Peak shear stresses were generally reached at about 4% shear strain and the shearing resistance only decreases by a small amount (average 4%) with further straining. The shear stress-strain relationship has been modelled using a best-fit hyperbolic function (Duncan and Chang 1970, Domaschuk and Valliappan 1975):

$$[4.9] \quad q/p'_{cons} = \frac{\varepsilon_s}{E + F\varepsilon_s}$$

Values of E, F and R^2 are shown in Table 4.2. Using [3.11] and differentiating [4.9]:

$$[4.10] \quad 3D = \frac{p'_{cons}}{E}\left(1 - F\,\frac{q}{p'_{cons}}\right)^2$$

Then replace p'_{cons} with ε_v from [4.3]:

$$[4.11] \quad 3D = 111.86 \exp(13.72\varepsilon_v)\,[1 - 2.235\, q \exp(-13.72\varepsilon_v)]^2$$

for buffer with 1.5 Mg/m^3 initial dry density. This shows D to be a function of q and the strains ε_v produced by p'_{cons}. The parameter D represents an equivalent shear modulus G_{eq} (Graham and Houlsby 1983) for an idealized isotropic elastic material. Using $K^e = 80p'$ from [4.5], J obtained from [4.8], and D obtained from [4.11], the shear modulus G can be found from [3.12] as a function of p', q and ε_v.

The elastic parameter D^e has been measured as $D^e/p'_{cons} = 37.5$ from the results of unload-reload cycles in an undrained shear test on 1.50 Mg/m^3 buffer. It is assumed here that the unload-reload behaviour is

isotropic elastic, so, from [3.12], $G^e = D^e$.

4.1.3 Calibration for Paris clay

The KGJ model [3.6] has also been calibrated for a medium-stiff plastic clay from Paris, France (Azizi, 1987). The same method as for buffer materials was used to find K,G,J moduli. The curve fitting functions for Paris clay were Eqns.[4.3],[4.6],[4.9]. Figs.4.5,4.6 and 4.7 show the best fittings. The parameters of K,G,J moduli for Paris clay are shown in Table 4.2.

4.2 Method 2: Calibration for Wuhan Sand

As a further development of the KGJ model and an example of the applications of Method 2 for drained tests in Chapter 3, the data on Wuhan sand are now used to calibrate the model.

4.2.1 Calibration using method two

The Wuhan sand as tested was medium dense with relative density I_D = 57% and dry density γ_d = 1.55 Mg/m^3. The coefficient of uniformity C_u (defined as D_{60}/D_{10}) is 2.13. As we know, sand has high permeability. During shearing, excess porewater pressures can quickly reach equilibrium. If a drained shearing test is run, the excess porewater

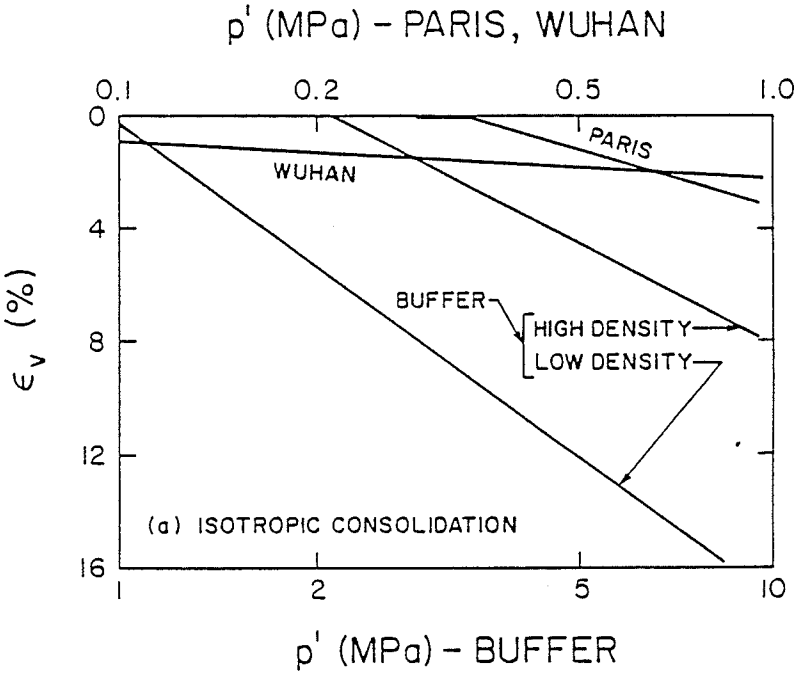

Fig.4.5 p',ε_v-relationships for Buffer, Paris clay and Wuhan sand - isotropic consolidation

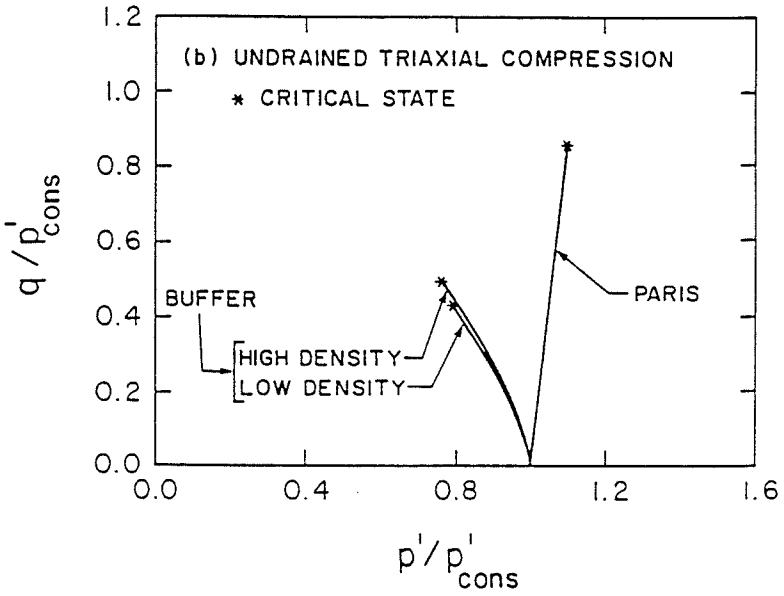

Fig.4.6 Normalized q/p'_{cons}, p'/p'_{cons}-relationships for Buffer and Paris clay - $CI\bar{U}$ tests

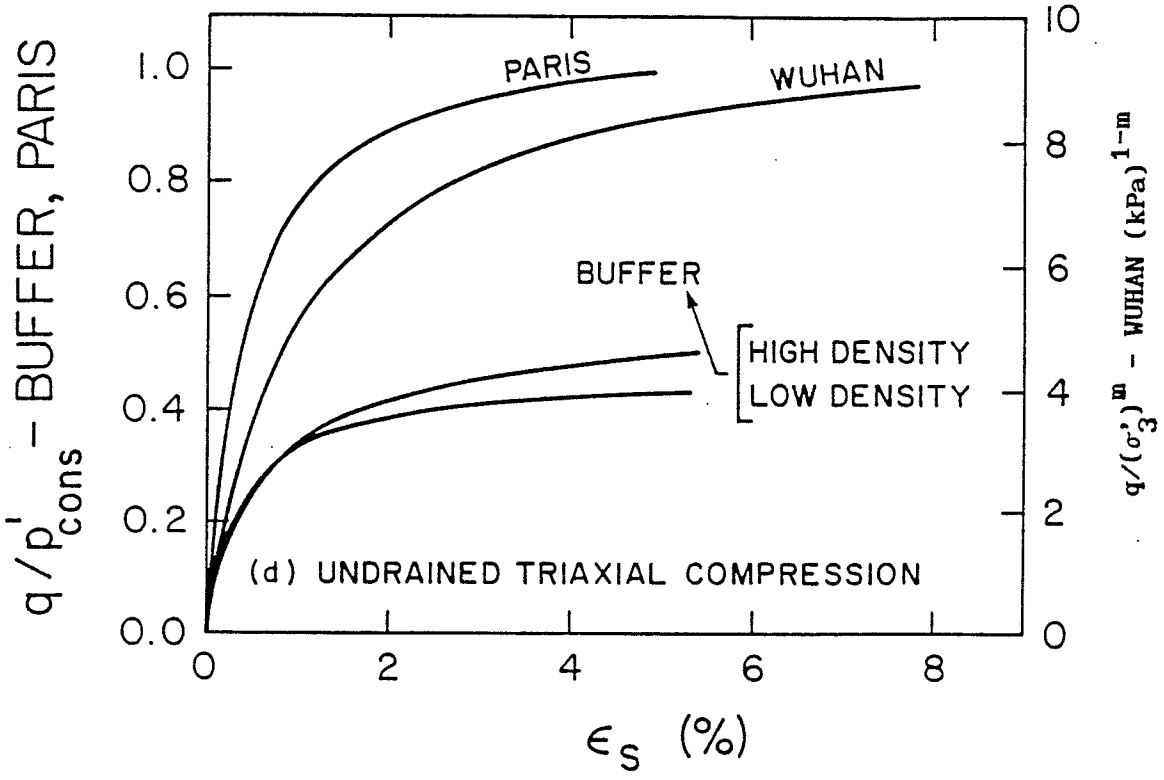

Fig.4.7 Normalized $q/p'_{cons}, \varepsilon_s$-relationships for Buffer, Paris clay and Wuhan sand - CIŪ tests

pressure is almost zero throughout the specimen. Data from drained tests on sand are therefore highly reliable. The following sections use the second method outlined in Chapter 3 to calibrate the KGJ model for Wuhan sand.

4.2.1.1 Determination of bulk modulus K

At this step, the method is the same as Method 1, using isotropic consolidation tests to find bulk modulus K. Fig.4.8 shows isotropic consolidation test data for Wuhan sand. The data have been fitted by a hyperbolic function:

$$[4.12] \qquad \varepsilon_v = \frac{p'_{cons}}{R + S\, p'_{cons}}$$

where R = 6867 kPa, S = 39.4. Differentiating [4.12] using [3.9], the bulk modulus K is:

$$[4.13] \qquad K = (6867 + 39.4\, p')^2 / 6867$$

4.2.1.2 Determination of coupling modulus J

Three drained CID tests were done with confining pressure 98.1 kPa, 196.2 kPa and 392.4 kPa respectively. Two independent relationships were obtained, namely volumetric strain vs. deviator stress, $\varepsilon_v - q$, and shear strain vs. deviator stress, $\varepsilon_s - q$. The first of these relationships can be used to find the coupling modulus J.

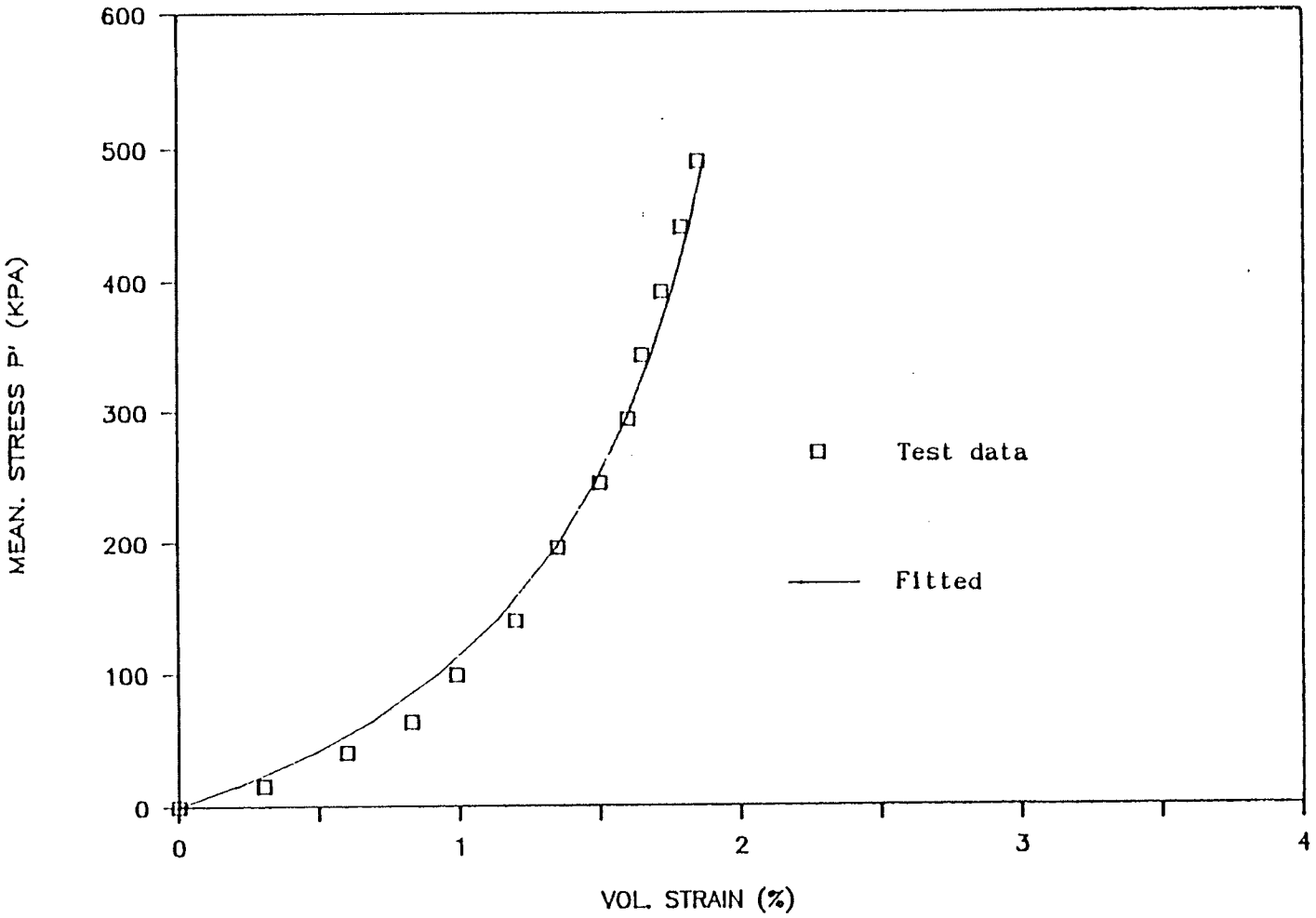

Fig.4.8 p',ε_v-relationships for Wuhan sand
- isotropic consolidation

The first approach to normalize the ε_v-q data was to use the confining pressure σ'_3 in the same way as in clays. It was found however that data normalized in this way were scattered, probably as a result of non-linearity of the strength envelope of the sand (Fig.4.10). However if $(\sigma'_3)^{0.85}$ was used in the normalization, a good relationship was obtained, in Fig.4.9, m = 0.85. The same $(\sigma'_3)^{0.85}$ will also be used to normalize ε_s - q data in the following section for the shear modulus G.

The following function provides a good curve fitting of the data in Fig.4.9:

$$[4.14] \qquad \varepsilon_v = T \frac{U(U - U_o)}{U - U_{ult}}$$

where $U = q/(\sigma'_3)^m$, m =0.85, T =0.0015, U_o = 7, U_{ult} = 10.

The "equivalent coupling modulus" J_e is, by differentiating [4.14]:

$$[4.15] \qquad J_e = \frac{dq}{d\varepsilon_v} = (\sigma'_3)^m \frac{(U - U_{ult})^2}{U^2 - 2UU_{ult} - U_o U_{ult}}$$

From Eqn.[3.13], we can find the coupling modulus J.

4.2.1.3 Determination of shear modulus G

Fig.4.11 shows the ε_s - q data normalized by $(\sigma'_3)^{0.85}$. A hyperbolic function was then used to fit these data:

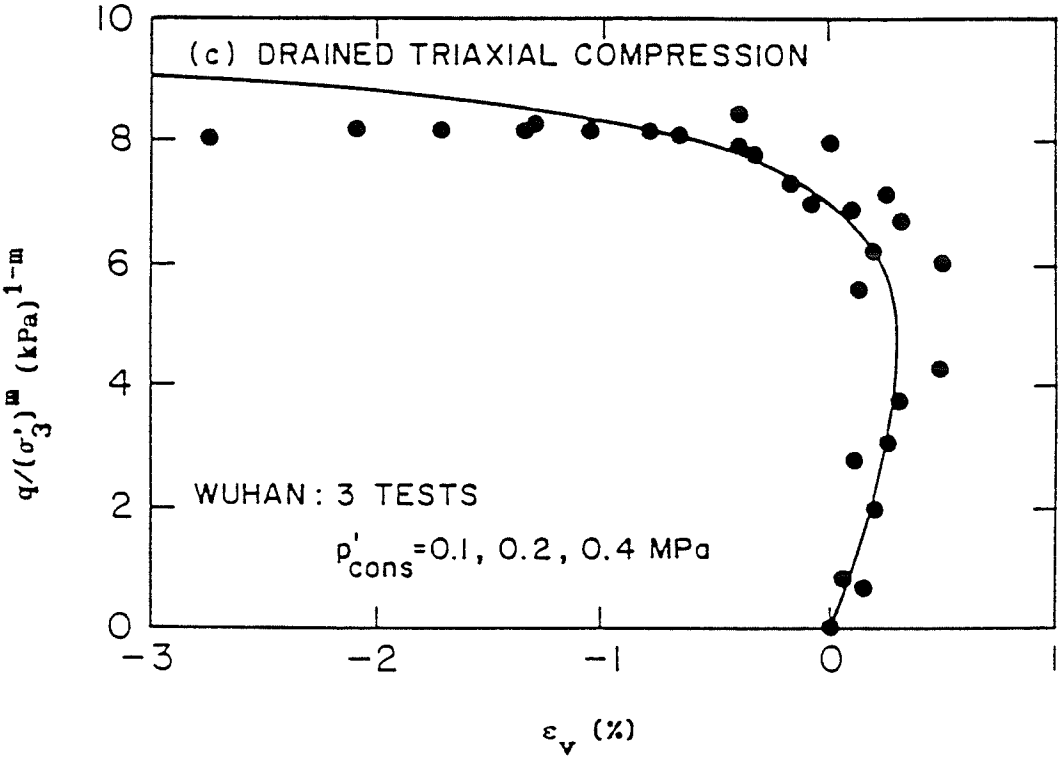

Fig.4.9 $q/(\sigma'_3)^m, \varepsilon_v$-relationships for Wuhan sand - CID tests

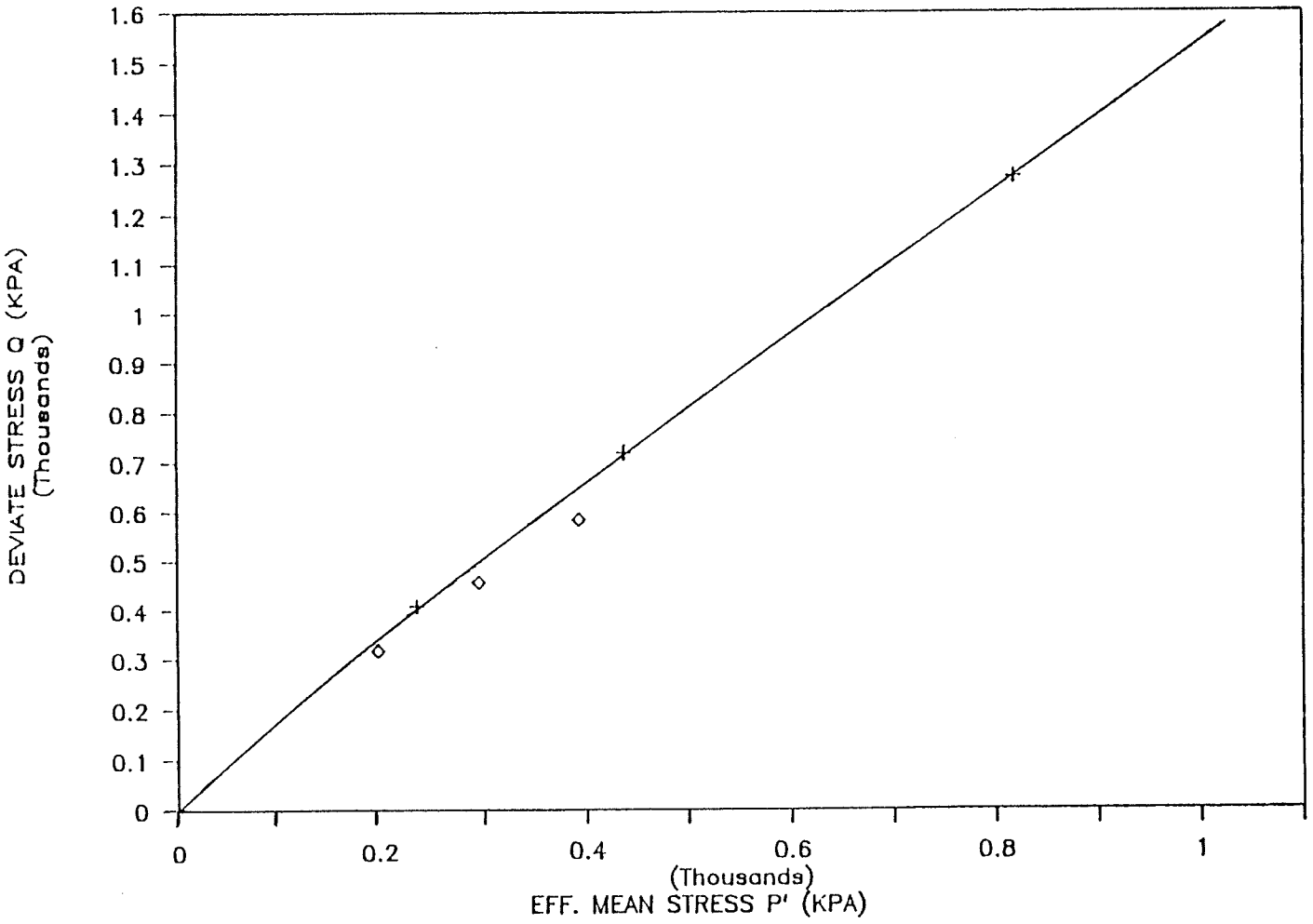

Fig.4.10 Curved strength envelope
- Wuhan sand

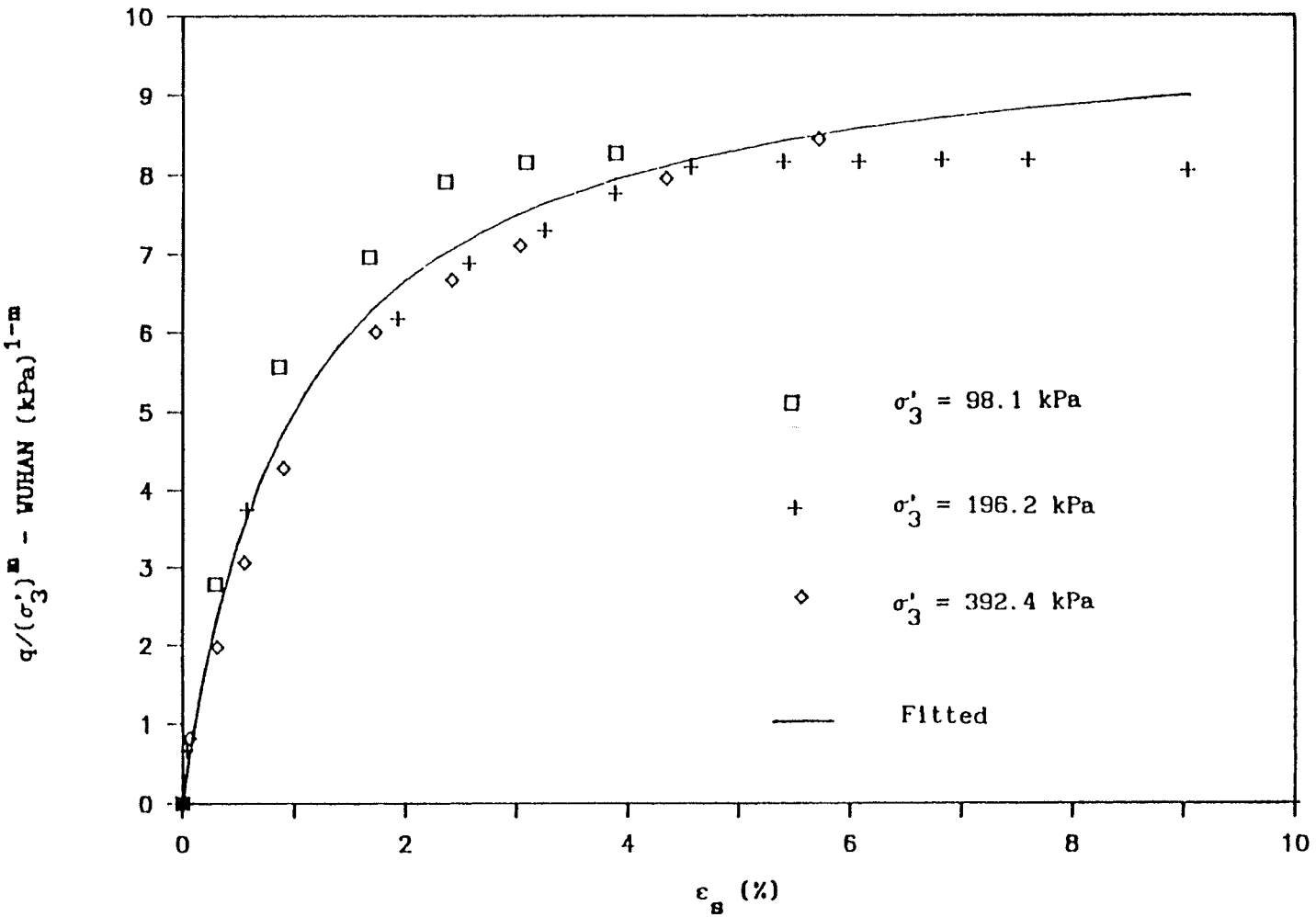

Fig.4.11 Normalized $q/(\sigma'_3)^m$, ε_s-relationships for Wuhan sand - CID tests

$$[4.16] \quad q/(\sigma'_3)^m = \frac{\varepsilon_s}{V + W\varepsilon_s}$$

where m = 0.85, V = 0.001 $(kPa)^{m-1}$, W = 0.10 $(kPa)^{m-1}$. Differentiating [4.16]:

$$[4.17] \quad G_e = \frac{1}{3}\frac{dq}{d\varepsilon_s} = (\sigma'_3)^m \frac{1}{V}\left[1 - W\, q/(\sigma'_3)^m\right]^2$$

The shear modulus G is then found using [3.14].

So far we have obtained all three moduli for Wuhan sand from a isotropic consolidation test and three drained shear tests.

As mentioned in the last section, normalizing by $(\sigma'_3)^m$ is related to the curved strength envelope of the sand. From [4.16], at failure, $q_f/(\sigma'_3)^m = R$, where R is a constant depending on the definition of failure. We know that in CID tests $p' = \sigma'_3 + q/3$. So the strength envelope implied by the nonlinear normalization with $(\sigma'_3)^m$ is:

$$[4.18] \quad p'_f = (q_f/R)^{1/m} + q_f/3$$

The curved strength envelope represented by [4.18] is shown in Fig. 4.10.

4.3 Validation of the KGJ Model

The model outlined in the previous sections is of course general in the sense that it can be applied to any soil and any stress path, if

suitable test data are available. Validation of the KGJ model can be examined by comparing the predicted and measured results for tests which had not been used in originally calibrating the model.

4.3.1 Prediction of constant p' tests on buffer

The values of λ/V_i, ε_{vo}, A, n, E and F in Table 4.2 calibrate the general model for buffer with two different initial densities. Now the calibrated model will be used to predict the results of drained tests with constant p' on buffer materials. These predicted results will be checked against experimentally measured values which were not used in forming the original model.

In drained constant p' tests, the required condition is dp' = 0. From [3.6], [4.7] and [4.5], using an "unloading/reloading" criterion for K^e when $p' < p'_{max}$:

$$[4.19] \quad \frac{p'}{\kappa/V_i}\, c\, [\exp(-\varepsilon_{vo} V_i/\lambda)\, \exp(\varepsilon_v\, V_i/\lambda)/q]^d\, d\varepsilon_v = dq$$

which on integration and combination with [4.3] gives:

$$[4.20] \quad \varepsilon_v = \frac{\lambda}{V_i} \ln(p') + \varepsilon_{vo} + \frac{\lambda}{V_i d} \ln\left[1 + \frac{\kappa d}{(1+d)\lambda c}\left(\frac{q}{p'},\right)^{1+d}\right]$$

The volumetric strain produced by shearing is then:

$$[4.21] \quad \Delta\varepsilon_v = \frac{\lambda}{V_i d} \ln\left[1 + \frac{\kappa d}{(1+d)\lambda c}\, \left(\frac{q}{p'},\right)^{1+d}\right]$$

which is a function of $\eta = (q/p')$. Substituting appropriate values for buffer parameters in [4.21]:

[4.22] $\Delta\varepsilon_v = 0.178 \ln[1 + 0.0475 (q/p')^{1.41}]$

Fig.4.12 shows the calculated relationship resulting from [4.22] between q/p' and $\Delta\varepsilon_v$, and also experimentally measured relationships from four constant-p' tests at different stress levels. Although there is some scatter in the data, the prediction looks promising considering the small volume strains that are typically encountered in these constant-p' tests and the relative insensitivity of volume change measurements.

It is also possible to predict q vs. ε_s relationships in constant-p' tests. From the second equation in [3.6] with dp' = 0:

[4.23] $dq = 3G(p', q, \varepsilon_v)d\varepsilon_s$

where G is expressed in terms of D and J from [4.11] and [4.8] with $K^e = 80p'$. An analytical solution cannot be obtained for Eqn.[4.23] and it has been solved with the fourth-order Runge-Kutta method in conjunction with [4.20]. Fig.4.13 compares predicted and measured results for q/p' vs. ε_s for two different densities of buffer. The predicted normalized curve for different constant-p' values is unique and agrees well with the test data, especially when it is remembered that the tests were performed by incremental loading and are known to be difficult to interpret.

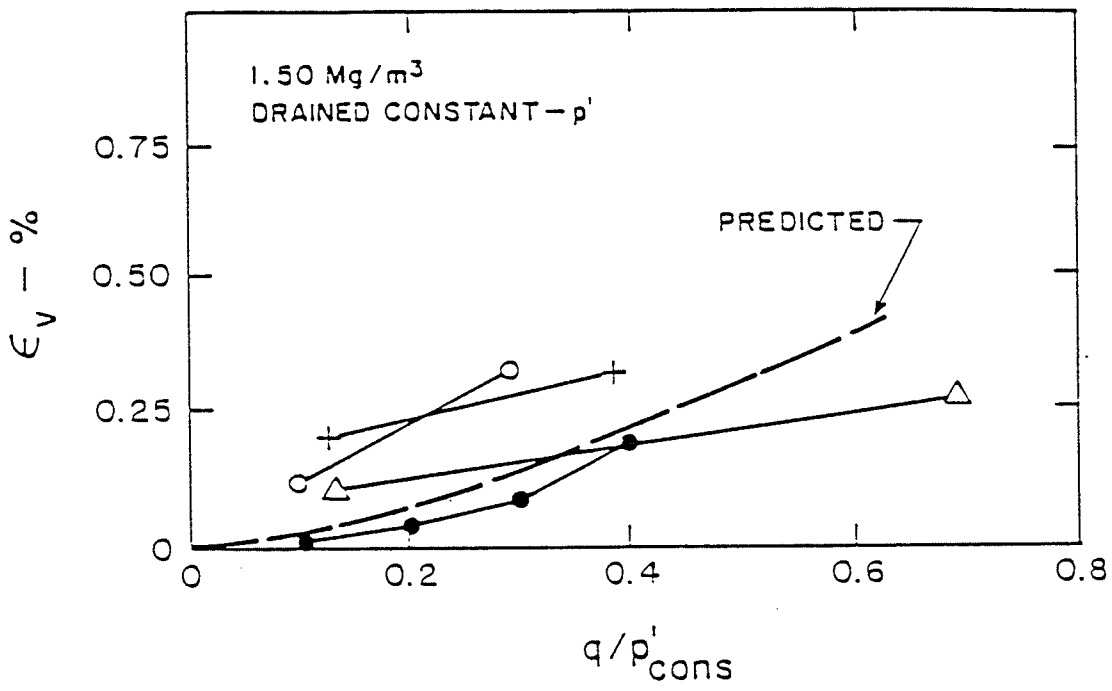

Fig.4.12 Comparisons of predicted and measured $\Delta\varepsilon_v, q/p'_{cons}$ curves in incremental constant-p' tests
- low density Buffer

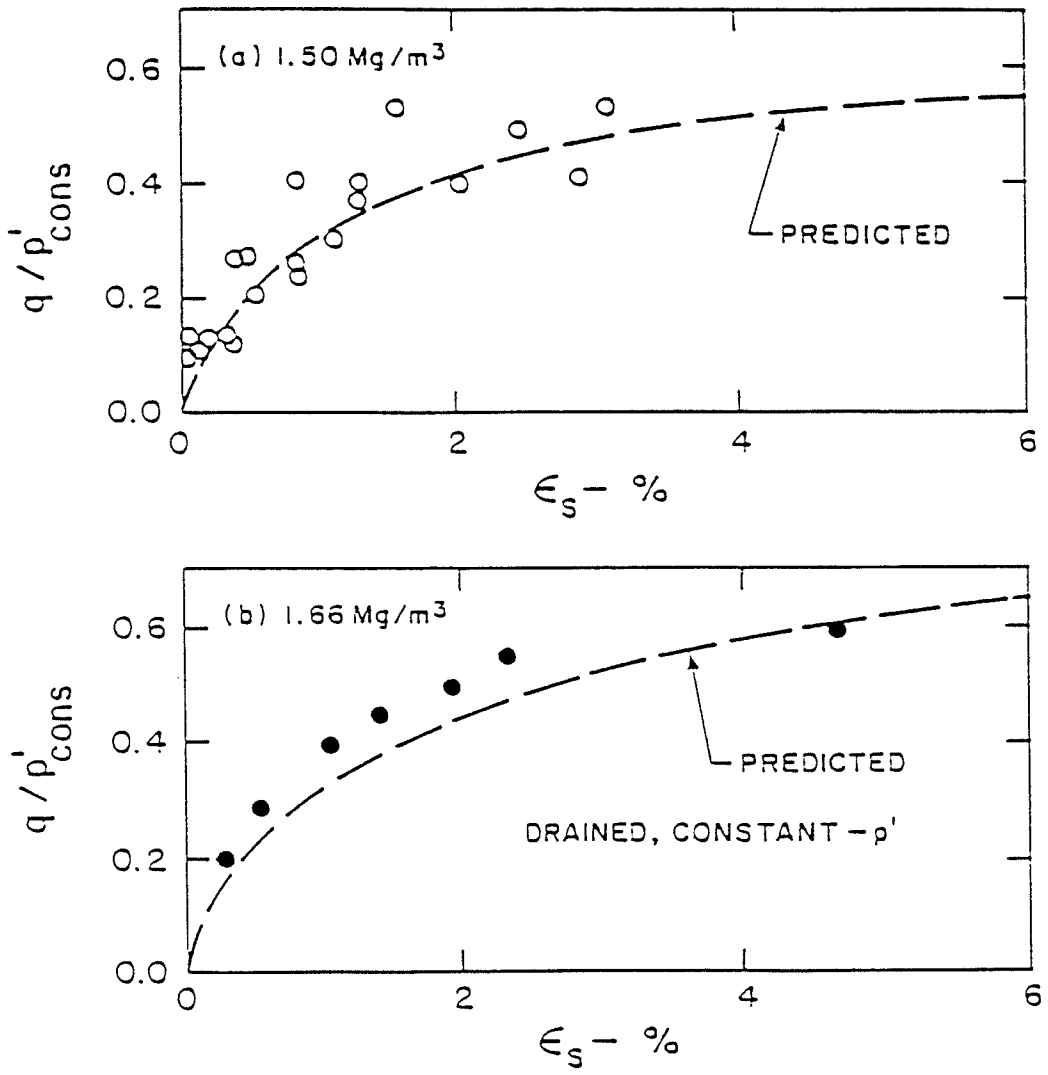

Fig.4.13 Comparisons of predicted and measured q/p'_{cons}, ε_s curves in incremental constant-p' tests
- low and high density Buffer

4.3.2 Prediction of a drained constant stress ratio test on Paris clay

Fig 4.14 compares predicted and measured results from a drained shear test on Paris clay with constant stress ratio $\sigma'_3/\sigma'_1 = 0.6$ (Azizi 1987). In this case some account of "elastic" straining has been built into the predictive model to account the ealy pre-yield straining observed in the testing program. The measured volume strains appear to be predicted reasonably well by the model. However the shear strains appear to be underpredicted.

4.3.3 Prediction of two constant p' tests on Wuhan sand

The program on Wuhan sand (Yin and Yuan 1985) also contained tests at constant mean effective stresses. The calibrated model for the sand has also been used to calculate the stress-strain curves for these tests which had not been used in the calibration. The predicted and measured results in Fig.4.15 are in good agreement for the two different confining pressures shown.

4.4 Discussions and Comments on KGJ Model

The model described in the preceding sections can be applied to a wide variety of soils and testing conditions. This is shown by its ability to determine the K, G, and J functions from either undrained tests in the sand-bentonite buffer materials and Paris clay, or from drained

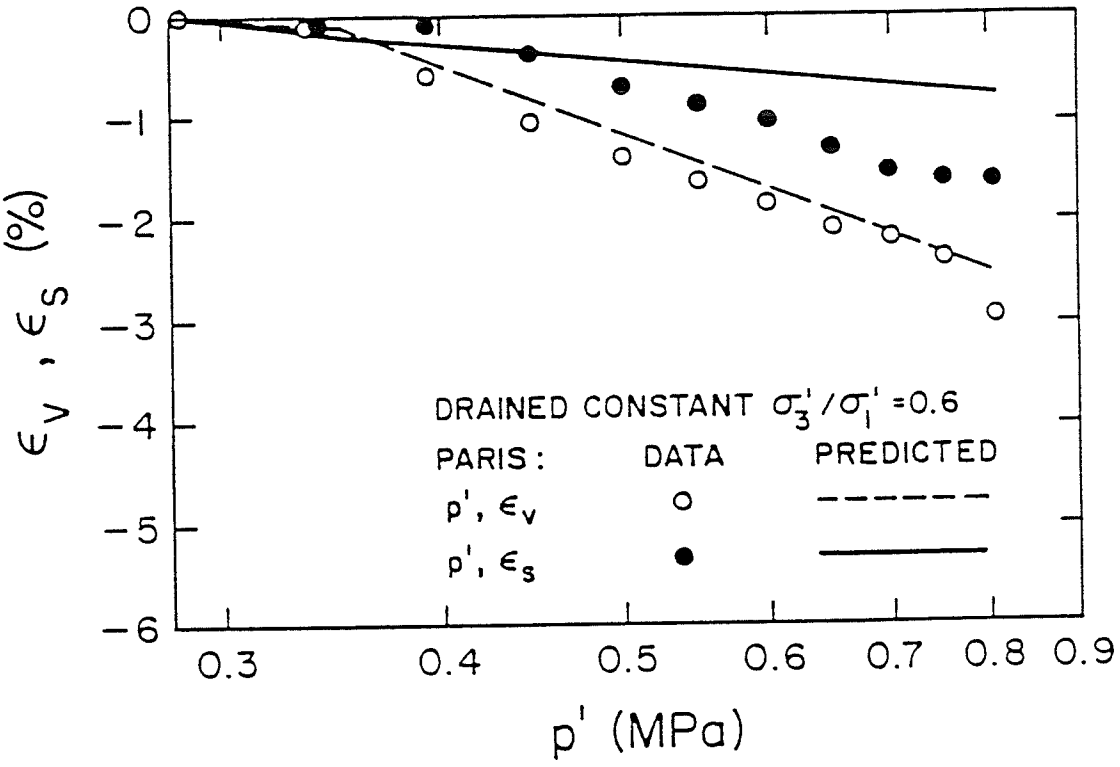

Fig.4.14 Measured and predicted p' vs. ε_s,ε_v results - Paris clay

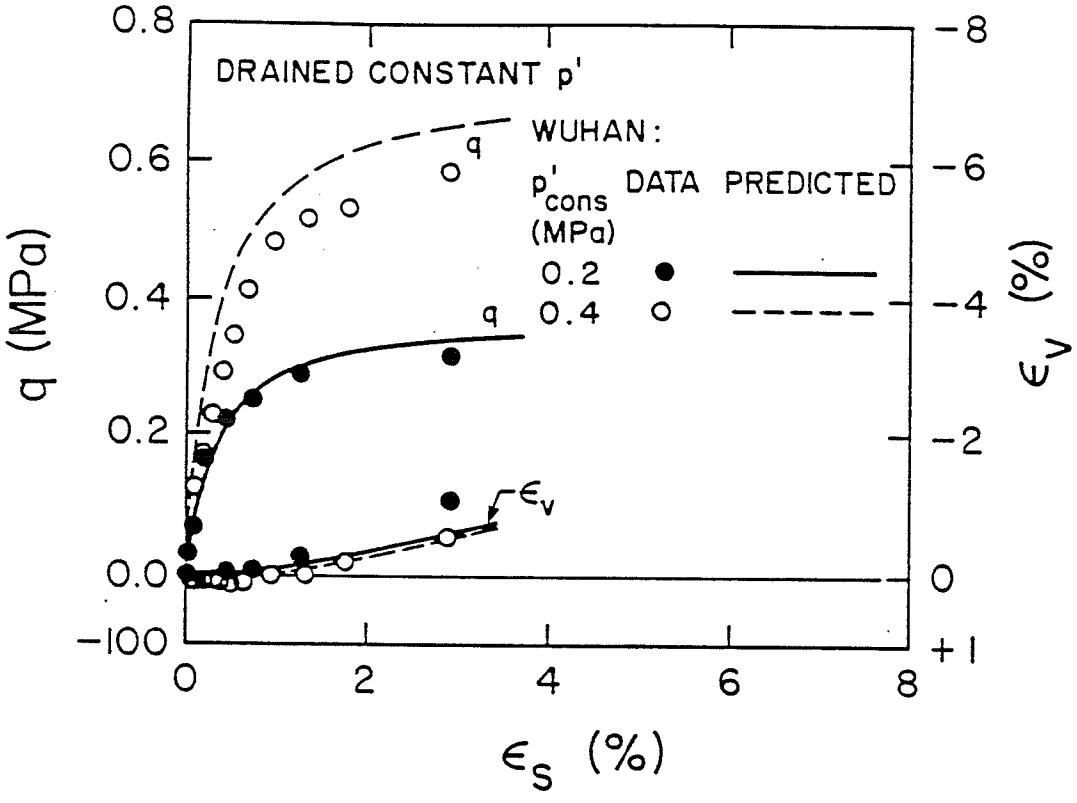

Fig.4.15 Measured and predicted q' vs. ε_s, ε_v results in constant-p' tests
- Wuhan sand

tests in Wuhan sand, and the promising predictions from the model shown in the previous section.

In terms of constructing the model, the principal uncertainties at this stage involve the assumption in [4.5] and [4.13] that K and K^e are independent of $\eta = q/p'$, and the relationship between J and J^e. One restriction of the model is that the data should be capable of being normalized into q/p'_{cons} vs. p'/p'_{cons} and q/p'_{cons} vs. ε_s or $q/(\sigma'_3)^m$ vs. ε_v and $q/(\sigma'_3)^m$ vs. ε_s relationships. Thus in clays, the modelling parameters (Table 4.2) will vary with overconsolidation ratio (OCR). In sands, normalization is only possible when specimens have the same "state parameter" ψ (Been and Jefferies 1985). Solutions based on elastic-plastic soil mechanics appear more suitable than hypoelasticity when different OCR's or ψ's have to be considered.

The stress states used for calibrating and verifying the model have only been triaxial (axisymmetric). The model needs to be developed and verified for more general stress states. However, with the restriction that it must be possible to normalize the data, the model can account for irreversible, nonlinear, shear-compressive or shear-expansive characteristics of soil behaviour, and the shear strains which can accompany changes in mean effective stress.

Chapter 5

1-D ELASTIC VISCO-PLASTIC MODELLING

5.1 Introduction

The stress-strain behaviour of many lightly overconsolidated clays is quite strongly time-dependent. For example, undrained shear strengths and preconsolidation pressures depend more strongly on the speed of testing than is commonly appreciated (Graham et al. 1983). This can affect the stress distribution, deformation and capacity of foundation soils beneath embankments, oil tanks, silos, etc., especially when the stresses are high enough to cause yielding.

In recent years, increased attention (Leroueil et al. 1985; Crawford 1986; Mesri and Castro 1987; Leroueil 1988) has been paid to the effects of time and strain rate on the effective stress-strain behaviour of the particle structure of clays. Most of this research fits rather simple functions (usually graphical functions) to data collected in the laboratory.

This Chapter develops an alternative approach using an important concept of "equivalent times" and three relationships for elastic, elastic-plastic and time-dependent straining. The resulting constitutive model predicts the behaviour of clay under step-wise loading, constant rate of straining, relaxation, and constant rate of

effective stress application.

5.2 Time and Strain Rate Effects and Modelling

The most common example of time dependent behaviour in clays is terminating creep (secondary consolidation) observed after the excess porewater pressures have completely dissipated. Creep displacements in clays are usually considered (Ladd et al. 1977) to vary linearly with log(time), and the coefficient of secondary consolidation is defined by alternative relationships $C_{\alpha e} = \Delta V/\log(t_i/t_o)$; $C_{\alpha\varepsilon} = \frac{\Delta V}{V}/\log(t_i/t_o)$; $\psi = \Delta V/\ln(t_i/t_o)$ where the specific volume $V = 1 + e$. One difficulty with these relationships involves deciding when creep movements actually begin , that is, the value of t_o (Crawford 1986). On one hand, Mesri and Choi (1985a,b) argue that compression strains at the "end of primary" (EOP) consolidation are "unique", that is creep only commences after excess porewater pressures have reduced to zero.

It is now frequently accepted that the compression index C_c and the preconsolidation pressure σ'_{zc} (commonly called σ'_{vc} or σ'_p) should be measured from stress-strain curves derived from EOP strains only. Mesri and Choi (1985a,b) defined the behaviour of the clay in terms of the e,log σ'_{vc} relationship at EOP, and the ratio $C_{\alpha e}/C_c$ which they consider constant for a given clay. (Graham et al. 1983 suggest that the $C_{\alpha e}/C_c$ ratio is strain dependent). However Kabbaj et al. (1988) showed that the laboratory EOP curve underestimates in situ settlements. This implies that the EOP stress-strain relationship is

not unique but depends on the duration of primary consolidation. If so, viscous deformation occurs during the whole consolidation process.

Alternatively, Wahls (1962), Mitchell (1976) and Crawford (1986) among others, have suggested that the separation of consolidation strains into primary and secondary stages is arbitrary. Adjustment of the internal structure of the clay involves time dependent deformations and it seems reasonable to include some elements of time dependency during primary consolidation. In a similar way, Bjerrum (1967a) argued that time dependent straining would occur at the same time as hydrodynamic consolidation. He divided the observed displacements into "instant compression" and "delayed compression", although he recognized that the instant compression strains would take place in finite time because of hydrodynamic consolidation, see Figs.5.1 and 5.2. He proposed that delayed consolidation could be described by parallel lines (in $V, \log \sigma'_z$)-space representing a series of equilibrium relationships after different durations of sustained loading.

The reductions in volume that occur during delayed compression lead to more stable clay microstructure. Thus during delayed compression or "aging", a clay develops increased strength and a reserve resistance against further compression, Fig.5.2, (Bjerrum 1967a). An apparent preconsolidation pressure is found when stresses are again increased after delayed compression at constant effective stress. This accounts for the small amounts of overconsolidation found in natural clays that have never experienced the usual causes of overconsolidation such as offloading, groundwater level changes, weathering, or cementation. The

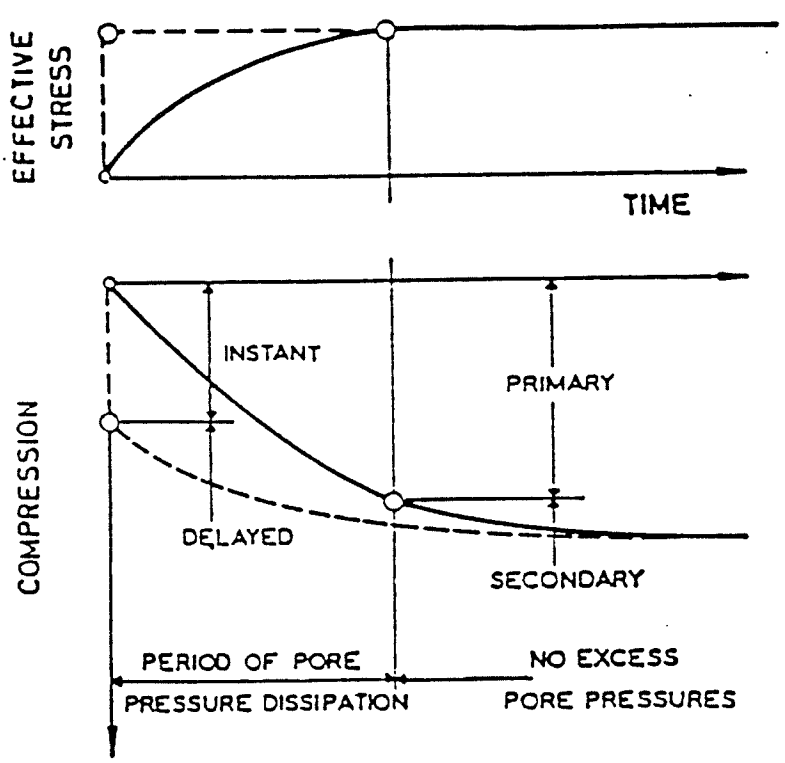

Fig.5.1 Definition of 'instant' and 'delayed' compression compared with 'primary' and 'secondary' compression (after Bjerrum 1967a)

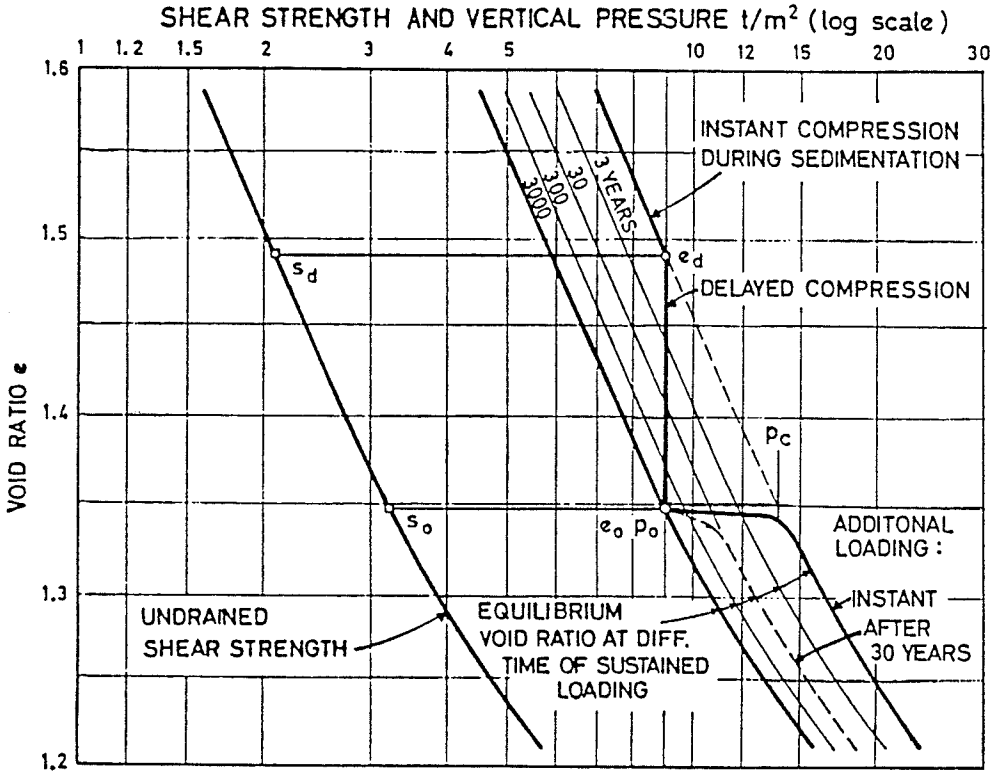

Fig.5.2 Compressibilty and shear strength of a clay exhibiting delayed consolidation (after Bjerrum 1967a)

preconsolidation pressure resulting from secondary compression can be predicted from the relationship $OCR = (t/t_p)^{C_\alpha/(C_c-C_r)}$ (Mesri and Choi 1984). They also derived a related expression in terms of straining rates. However the relationships are not fully general since they do not, for example, include the effects of relaxation or step-changes in straining rate.

To overcome this deficiency, Leroueil et al. (1985) used oedometer data from four clays from Canada and France to demonstrate that rheological behaviour of clays is controlled by a unique stress-strain-strain rate (σ'_z-ε_z-$\dot{\varepsilon}_z$) relationship. They presented the results in the form of a unique normalized curve of (σ'_z/σ'_{zc}) vs. ε_z plus a curved relationship between preconsolidation pressure σ'_{zc} and log (strain rate $\dot{\varepsilon}_z$) for each clay, see Figs.5.3 and 5.4.

In developing this work, Kabbaj et al. (1986) pointed out that the (σ'_z-ε_z-$\dot{\varepsilon}_z$) relationship can not represent relaxation tests in which the effective stresses decrease at constant strains. Such a decrease is most likely associated with the counteracting effects of elastic ε_z^e and plastic ε_z^p components of straining. Kabbaj et al. modified the (σ'_z-ε_z-$\dot{\varepsilon}_z$) model of Leroueil et al. 1985 by assuming unique σ'_z-ε_z^p-$\dot{\varepsilon}_z^p$ and $\varepsilon_z^e = \frac{\kappa}{V} \ln(\sigma'_z/\sigma'_{zo})$ relationships. The modified model was used to calculate time dependent deformations and porewater pressure distributions for different types of 1-D tests.

The models that have just been described all lack generality and for various mathematical reasons can not conveniently describe the full

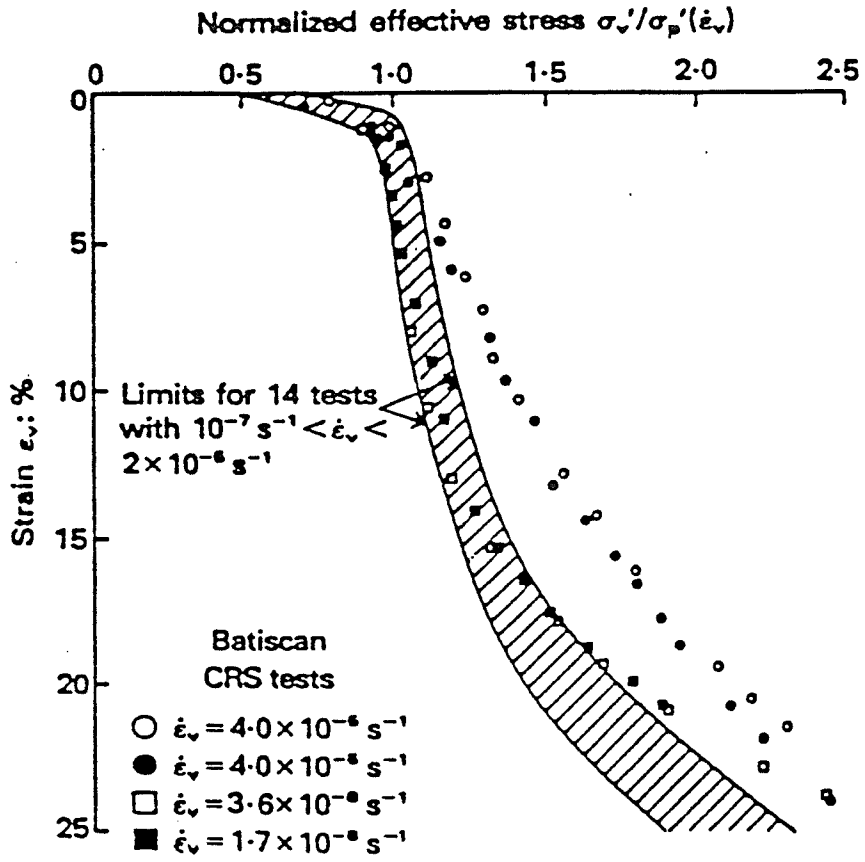

Fig.5.3 Normalized effective stress-strain relationship deduced from CRSN oedometer tests on Batiscan clay (after Leroueil et al. 1985)

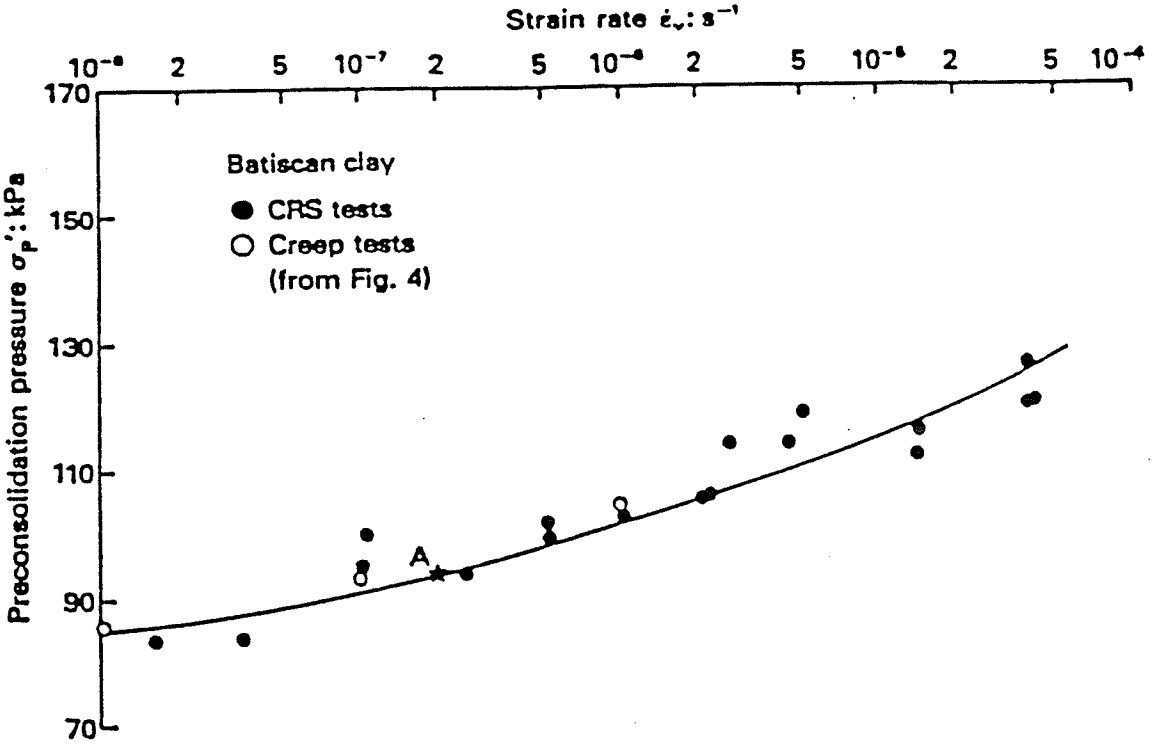

Fig.5.4 Variation in preconsolidation pressure with strain rate for Batiscan clay (after Leroueil et al. 1985)

range of procedures including multi-stage loading (MSL), relaxation and constant strain rate testing that are currently used in geotechnical laboratories. In a general sense, they can not describe relaxation or unloading-reloading tests because they lose their ability to model time effects if the strain rate is assumed zero. The best of these models (by Kabbaj et al. 1986) can describe relaxation tests but does not properly describe the viscous- elastic response that occurs during reloading.

In developing a constitutive model for the time dependent stress-strain behavior of soils in 1-D straining, we use the following points:

(1). Time dependent deformations occur during all consolidation process, before and after primary consolidation.

(2). Time and strain rate effects are related to the viscous nature of soils througth the constitutive relationships.

(3). The tests and procedure for determining the model parameters are simple.

(4). A general model should account for all aspects of the viscous behavior under general test conditions.

The 1-D elastic visco- plastic model suggested in this chapter is a mathematical extension of Bjerrum's work. It is a further development of the $\sigma'_z, \varepsilon_z, \dot{\varepsilon}_z$-model measured experimentally by Leroueil and his co-workers (Leroueil et al. 1985, Kabbaj et al. 1986), and the conceptual model outlined by Crawford (1988). An important concept of

"equivalent time" is used to model the differing creep behaviour of normally consolidated and overconsolidated specimens as a function of σ'_z, $\dot{\sigma}'_z$, ε_z, and $\dot{\varepsilon}_z$. This allows clay behaviour to be predicted in MSL tests, relaxation tests, and tests with constant rate of strain (CRSN) or constant rate of stress change (CRSS).

5.3 Time Lines and Equivalent Times

Bjerrum (1967a) proposed a series of parallel "time lines" in e,log(σ'_z)-space to represent (a) multistage loading (MSL) tests with different durations, (b) instant compression produced instantly after loading, (c) delayed compression at constant effective stress under engineered structures, and (d) "aging" in natural deposits (Fig.5.2). It can be seen in Fig.5.2 that the line of "instant compression" has almost the same slope as other time lines. This implies that there are elastic plastic deformations loading along this "instant compression" line.

Saturated clays are two-phase materials. When total stresses are suddenly applied, the effective stresses are only able to increase at the same rate as the porewater pressures decrease. Consequently the real strain-time relation for the soil skeleton can not be measured for primary consolidation, see Fig.5.1. Results of CRSN tests with high strain rates show that the observed compression lines are often far above the 24-hour line from stepped loading. This implies that the instant time line lies well above the 24-hour time line.

In the proposed model of this Chapter, the "time lines" are defined as the lines which have the same values of "equivalent time, t_e" not the same values of real duration times used in Bjerrum's definition, see Figs.5.2 and 5.5. The "equivalent time, t_e" at a state point is defined as the time which would be needed to creep from the reference time line to this point under the same effective stress. For example the equivalent time $t_{e3"}$ at point 3" in Fig.5.5 is the time which would be needed to creep from point 3' to 3". In fact, the specimen does not experience this loading history. Therefore according to this definition, the equivalent times are independent of loading history but depend on state points σ'_z, ε_z. It will be seen in Section 5.4 that equivalent times have a unique relationship with creep rates. Thus, creep rates depend on only the state points σ'_z, ε_z. In Fig.5.5, equivalent times are positive below the reference time line and negative above the line.

An important clarification in the proposed model is that "instant compression" is the time-independent deformation that occurs in zero time after loading. This instant deformation is treated as elastic deformation in the proposed model, Fig.5.5. The instant deformation line is determined from unloading/reloading tests. The slope of this line is completely different from the slopes of Bjerrum's time lines. That is, the "instant compression" line here is not one of Bjerrum's time lines which experience both elastic and plastic deformations.

Fig.5.5 shows that time-independent behaviour is restricted to elastic

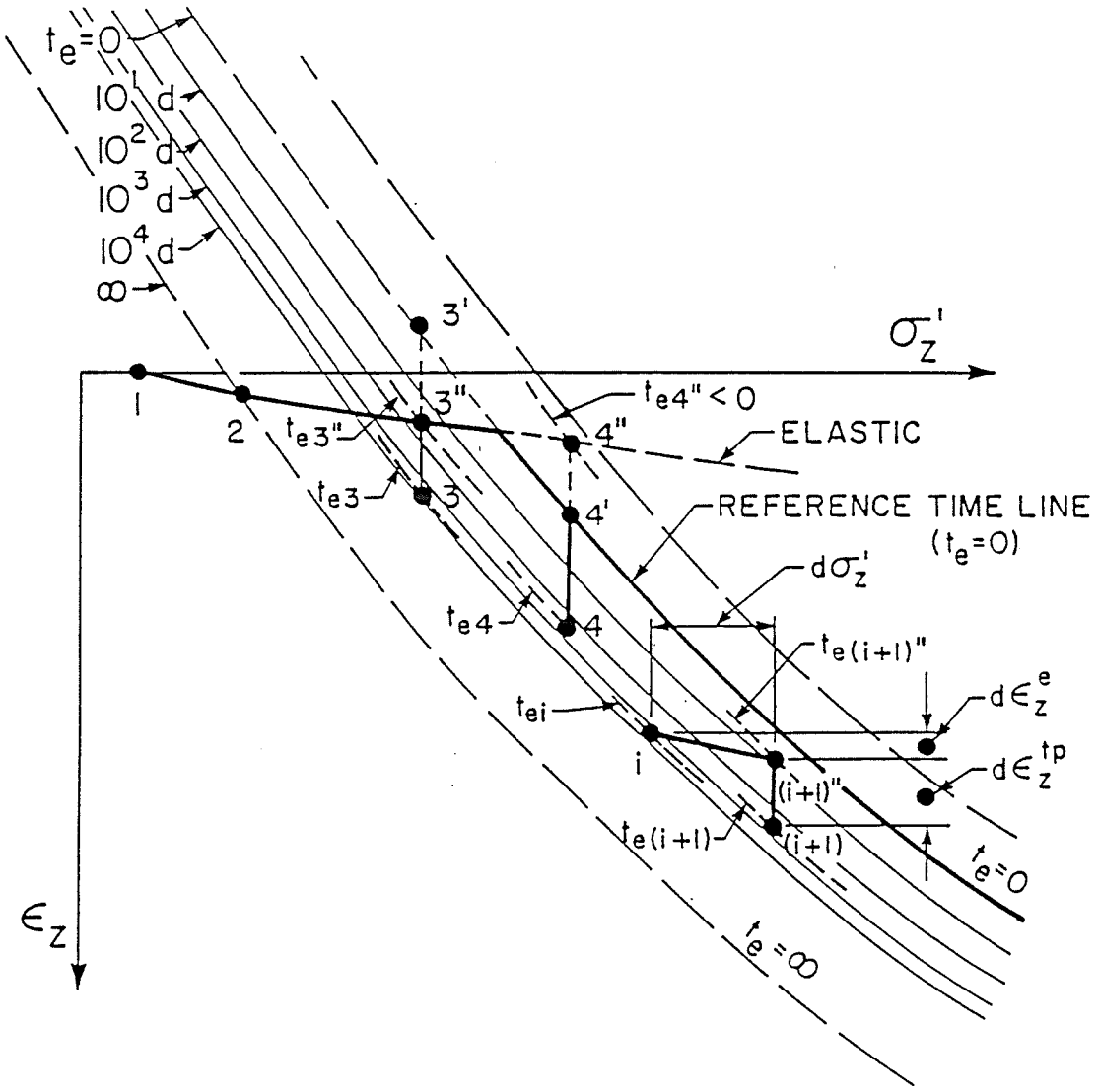

Fig.5.5 Definition of 'equivalent time', 'instant elastic line' and 'reference time line'

straining, that is, to 1-2-3"-4", or to (i)-(i+1)". It will be remembered that 4' represents the relationship between ε_z and σ'_z at some chosen time after loading. This could reasonably taken at the end of primary consolidation or at some other time which establishes a "reference time" for predicting creep strains. Here the "reference time line" is defined as the line on which a chosen "equivalent time" t_e is zero. Thus as the specimen creeps from 4' to 4, t_e goes from zero at 4' to t_{e4} at 4, and the straining rate decreases. If very rapid loading places the specimen in the range 4"-4' then very high creep rates are observed, starting with $t_{e4"} < 0$. The slower creep rates that are observed in the overconsolidated range 3"-3 start from $t_{e3"} > 0$, and end with t_{e3}. The increment $d\sigma'_z$ produces an elastic strain $d\varepsilon_z^e$ and creep strains $d\varepsilon_z^{tp}$ starting from $t_{e(i+1)"}$ and continuing to $t_{e(i+1)}$. This formulation means that the model assumes elastic visco- plastic (EVP) behaviour.

Details in determining the "instant compression line", "reference time line" and creep parameters will be explained in Chapter 6 and Chapter 7.

5.4 General Constitutive Relationships

The model assumes that strain changes ε_z in a soil element are made up of three strain components; one, ε_z^e due to "instantaneous" elastic straining only; the second, ε_z^{sp} due to time-independent plastic reaction of the soil skeleton to effective stress changes; and the

third, ε_z^{tp} due to time-dependent strains at constant effective stress. That is:

[5.1] $$\varepsilon_z = \varepsilon_z^e + \varepsilon_z^{sp} + \varepsilon_z^{tp}$$

where the functional relationships for ε_z^e, ε_z^{sp} and ε_z^{tp} are written:

(1). Elastic straining (elastic line in Fig.5.5)

[5.2] $$\varepsilon_z^e = f^e(\sigma'_z)$$

Elastic strains are recoverable by definition, and instantaneous. Instant strains are time-independent and may, or may not be recoverable.

(2). Elastic plastic straining (reference time line in Fig.5.5)

[5.3] $$\varepsilon_z^{ep} = \varepsilon_z^e + \varepsilon_z^{sp} = f^{ep}(\sigma'_z)$$

(3). Creep straining (time dependent straining)

[5.4] $$\varepsilon_z^{tp} = f^{tp}(t_e, \sigma'_z)$$

The relationships f^e, f^{ep} and f^{tp} are obtained by fitting appropriate functions to observed laboratory data. Thus in Fig.5.5, a specimen would move from 1 to 3 by first moving along the elastic line to 3" and then creeping at constant σ'_{z3} to 3. To move from 1 to 4, it would move first (under very rapid loading) to 4", before compressing with constant σ'_z to 4' and 4. In reality of course, hydrodynamic consolidation affects the behaviour, and the clay never actually attains the state at 4".

Using Eqns.[5.3] and [5.4], Eqn.[5.1] becomes:

$$[5.5] \quad \varepsilon_z = f^{ep}(\sigma'_z) + f^{tp}(t_e, \sigma'_z)$$

Eqn.[5.5] is a general equation for calculating total strains under stepped loading. From [5.5] we may solve for the equivalent time t_e as a function of state points σ'_z, ε_z. Applications of this equation will be presented in the next two Chapters.

Eqn.[5.5] is developed for stepped loading without considering in detail how the effective stresses actually increased. In practice, effective stresses vary continuously in laboratory tests and in field applications. Even in stepped loading tests such as the standard 24 hour odometer test (STD), multiple-stage loading (MSL), and single-stage loading (SSL), only the total stress is a constant and the effective stresses increase continuously as excess porewater pressures dissipate with time. In other laboratory tests such as the constant rate of strain test (CRSN), the controlled gradent test (CGT), the constant rate of loading test (CRL), and the continous load test (CL), the total and effective stresses both vary systematically. At full-scale, effective stresses beneath a geotechnical structure change as the external loads and the porewater pressures change.

Continous loading can be considered as a series of infinitesimally small incremental loads $d\sigma'_z$ in time dt. At any point i in Fig.5.5, to move from (i) to (i+1) under a stress change $d\sigma'_z$ in time dt, the clay first moves elastically to (i+1)" and then creeps to (i+1), so:

[5.6] $d\varepsilon_z = d\varepsilon_z^e + d\varepsilon_z^{tp} = (df^e/d\sigma'_z)d\sigma'_z + (\partial f^{tp}/\partial t_e)dt$

where $(\partial f^{tp}/\partial t_e)$ is the creep rate at the current point. It is known from [5.4] that the creep rate may depend on equivalent times and vertical effective stresses. That is, the creep rate depends only on the state points and not on the loading history. From [5.6]:

[5.7] $\dot{\varepsilon}_z = (df^e/d\sigma'_z)\,\dot{\sigma}'_z + (\partial f^{tp}/\partial t_e)$

Solving [5.5] and [5.7] using appropriate values of t_e provides a general σ'_z-$\dot{\sigma}'_z$-ε_z-$\dot{\varepsilon}_z$ relationship for any 1-D loading.

It will remembered that the reference time line is not unique but requires careful selection. Procedures for applying the model to real laboratory data will be prepared shortly. The proposed method uses a mathematical function to fit t,ε_z^{tp} data after excess porewater pressures have dissipated under a given vertical stress. The function may have two features - when $t_e \Rightarrow \infty$, $\varepsilon_z^{tp} \Rightarrow$ constant, and when $t_e = -t_o$, a constant determined from fitting the creep curve data, then $\dot{\varepsilon}_z^{tp} \Rightarrow \infty$. Procedures for identifying the reference time line will be explained in Chapters 6 and 7.

Chapter 6

1-D EVP MODELLING USING LOGARITHMIC FUNCTIONS

6.1 General $\sigma'_z - \varepsilon_z - t_e$ Relationship for Stepped Loading

Oedometer tests with multi-stepped loading (MSL) currently form the general basis on which consolidation behaviour is evaluated. More recently, CRSN tests have offered a faster way of determining the behaviour and have been correlated with experience from stepped loading tests (Sällfors 1975; Crawford 1986). Bjerrum's (1967a) representation of time-dependent behaviour and the evaluation by Mesri and Choi (1979) of apparent preconsolidation pressures were also derived from stepped loading tests.

In section 5.4 of Chapter 5, we have developed a general equation [5.5] for stepped loading. In this section, we will specify this equation by using logarithmic functions which are commonly used to fit oedometer test data in soil mechanics.

(1). Time-independent elastic straining is assumed linear in $\varepsilon_e, \ln(\sigma'_z)$-space ($\kappa$ - line in Fig.6.1):

$$[6.1] \quad \varepsilon_z^e = f^e(\sigma'_z) = \varepsilon_{zo}^e + \frac{\kappa}{V} \ln(\sigma'_z)$$

(2). Elastic plastic strains ε_z^{ep} can be obtained from the slope λ/V of

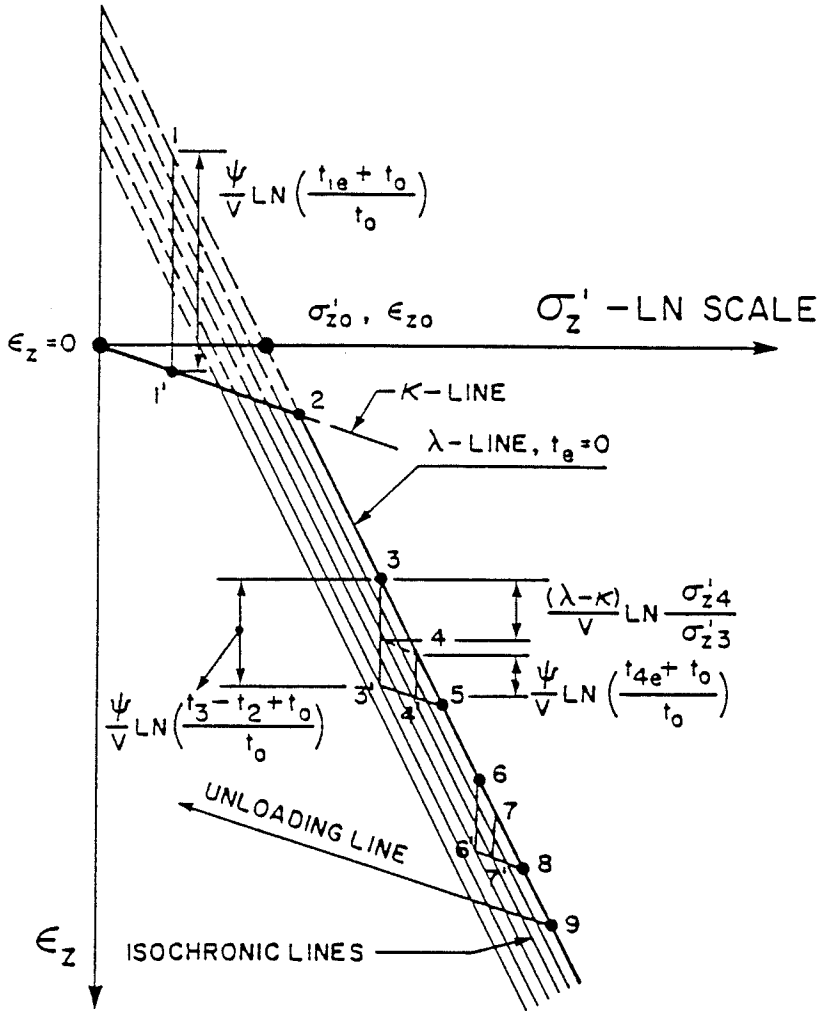

Fig.6.1 Schematic representation of 1-D EVP model for incremental loading

the $\varepsilon_z, \ln\sigma'_z$ relationship at stresses higher than σ'_{zc} (λ - linein Fig.6.1). Note that this is also the reference time line:

$$[6.2] \quad \varepsilon_z^{ep} = f^{ep}(\sigma'_z) = \varepsilon_{zo}^{ep} + \frac{\lambda}{V} \ln(\sigma'_z/\sigma'_{zo})$$

(3). Creep compression at constant σ'_z is assumed to be given by:

$$[6.3] \quad \varepsilon_z^{tp} = f^{tp}(t_e, \sigma'_z) = \frac{\psi}{V} \ln(\frac{t_o + t_e}{t_o})$$

This equation is a modification of the usual "secondary consolidation" relationship in which strains vary linearly with ln(time) but are not defined when time is zero. Note however that in [6.3] the creep strains are assumed to depend on only "equivalent times" and are defined when $t_e = 0$.

In these definitions of λ, κ and ψ (Eqns.[6.1], [6.2], [6.3]), V is the specific volume of the clay (1+e). The ε_{zo}^{e}, κ/V; ε_{zo}^{ep}, σ'_{zo}, λ/V; and t_o, ψ/V in Eqns.[6.1],[6.2],6.3] are all material parameters determined by fitting test data.

In Fig.6.1, the total strains at any point can be written from [5.5], using [6.2] and [6.3] as:

$$[6.4] \quad \varepsilon_z = \varepsilon_{zo}^{ep} + \frac{\lambda}{V} \ln(\sigma'_z/\sigma'_{zo}) + \frac{\psi}{V} \ln[(t_e + t_o)/t_o].$$

This is a specified general equation for stepped loading using logarithmic functions. The relation between the equivalent time t_e in [6.4] and real creep time t will be given in Sections 6.2,6.3.

6.2 Methodology for Determining Model Parameters

In order to apply [6.4] to calculate strains under stepwise loading, we have to know the parameters in this equation, and relate the equivalent time t_e to the real loading time t.

(1). Parameters in [6.1]:

The parameters in [6.1] can be estimated by fitting first loading or unloading/reloading data. Here we assume that the slope of first loading data and the slopes of unloading/reloading are the same, Fig.6.1,6.2. We know this is only an approximation.

(2). Parameters in [6.3]:

To determine parameters ψ/V and t_o and relate equivalent time t_e to real time t, we must first chose a reference state point. This point is on the reference time line, and t_e at this point is zero.

For example, assume we apply a single stage stress σ'_{z1} to the specimen, point 1 in Fig.6.2 and assume also that we know the strain vs. time curve like that in Fig.6.3 under the stress σ'_{z1}. Then, we can use point 1 as the reference point. The instant elastic strain in Fig.6.3 can be calculated from [6.1], the parameters in which are already known. As pointed out in Chapter 5, the real time dependent behavior of the soil skeleton can not be measured during the period of primary consolidation shown in Fig.6.3. Basically we use Eqn.[6.3] to fit

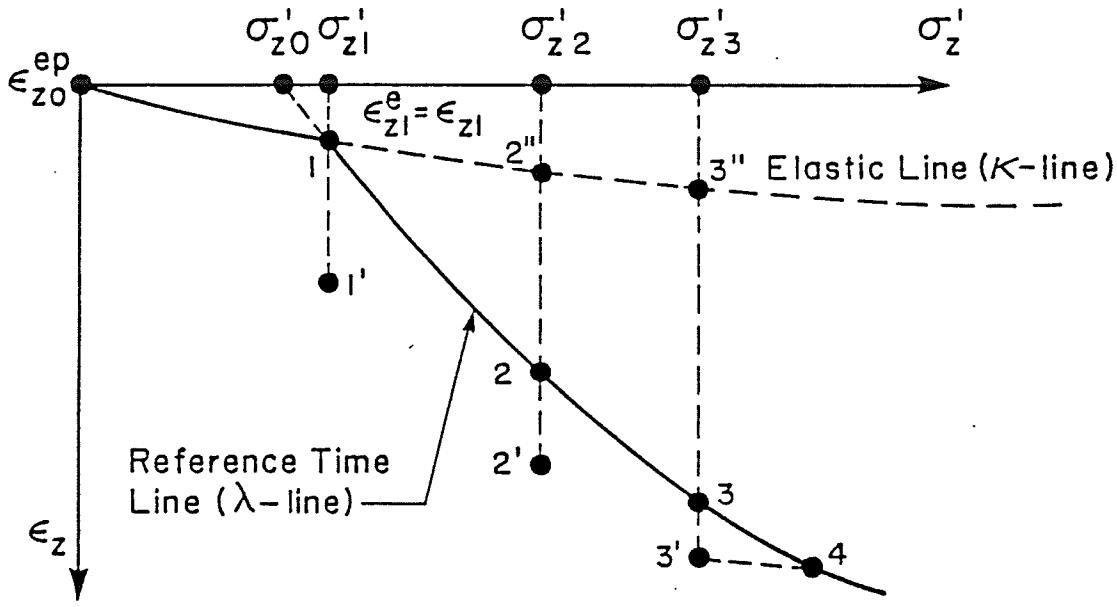

Fig.6.2 Schematic representation of creep tests for calculations of model parameters and apparent preconsolidation pressure

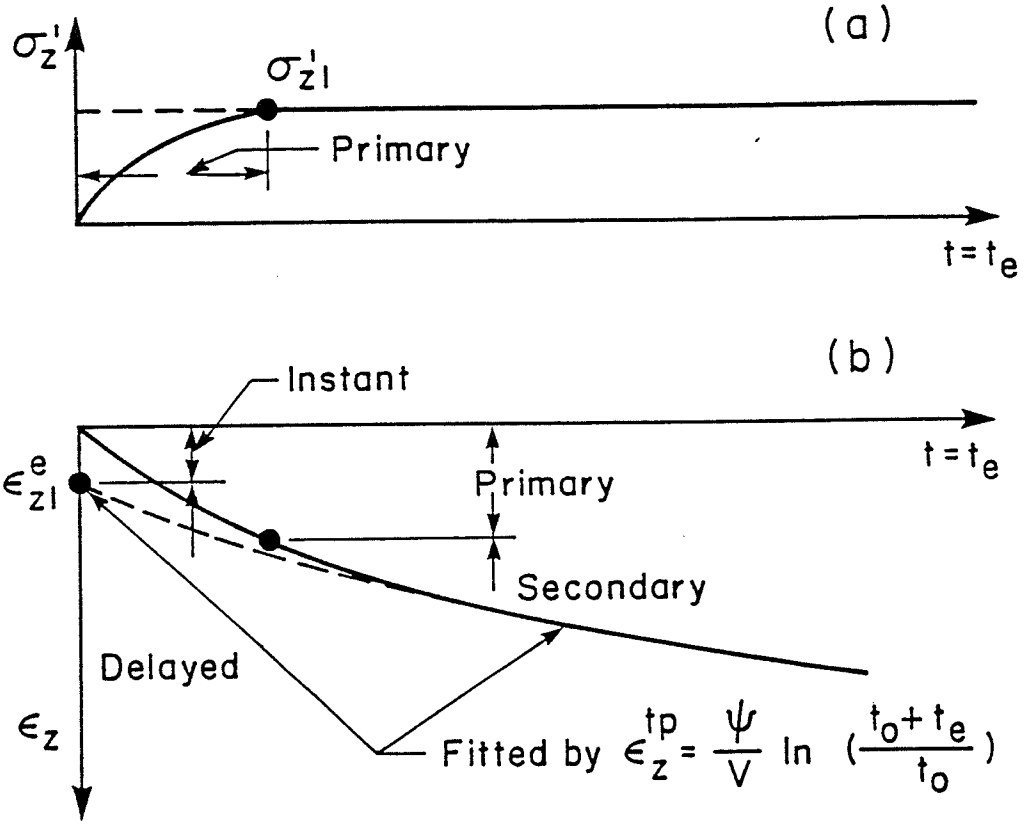

Fig.6.3 Schematic representation of creep test for determination of creep parameters t_o and ψ/V

between the data taken after the primary consolidation is complete and the point of the instant elastic strain determined from [6.1]. In this way, t_o and ψ/V are material parameters. In this particular case the equivalent t_e is equal in value to the real duration of loading time t. In other cases, specifically when the current state lies below the reference time line, for example in overconsolidated specimens, t_e and t are different. This is examined in a following section.

(3). Parameters in [6.2]:

Eqn.[6.2] is the reference time line that goes through reference point 1 in Fig.6.2. Supose we now have another single stage loading test, for example a creep test under stress σ'_{z2} in Fig.6.2. We can also obtain a strain vs. time curve similar to that in Fig.6.3 from this new test. This means that the final creep strain ε_{z2}, in Fig.6.2 is known under stress σ'_{z2} with duration t.

Relation between t_e and t:

The instant elastic strain at point 2" can be calculated from [6.1]:

$$[6.5] \quad \varepsilon_{z2"} = \varepsilon_z^e = \varepsilon_{zo}^e + \frac{\kappa}{V} \ln(\sigma'_{z2})$$

The equivalent time $t_{e2"}$ at point 2" can be found by the following procedure, using [6.4] and [6.5]:

$$[6.6] \quad \varepsilon_{zo}^{ep} + \frac{\lambda}{V} \ln(\sigma'_{z2}/\sigma'_{zo}) + \frac{\psi}{V} \ln \left(\frac{t_o + t_{e2"}}{t_o}\right) = \varepsilon_{zo}^e + \frac{\kappa}{V} \ln(\sigma'_{z2})$$

From which:

$$[6.7] \quad t_{e2"} = t_o \left[e^{(\varepsilon^e_{zo} - \varepsilon^{ep}_{zo})/(\psi/V)} \cdot (\sigma'_{z2})^{\kappa/\psi} \cdot (\sigma'_{z2}/\sigma'_{zo})^{-\lambda/\psi} - 1 \right]$$

As explained in Chapter 5, the equivalent time t_e above the reference time line is negative. The relation between $t_{e2'}$ and t is:

$$[6.8] \quad t_{e2'} = t + t_{e2"}$$

Equations for solving λ/V and σ'_{zo}:

From [6.4], the final creep strain $\varepsilon_{z2'}$, at point 2', using [6.4], [6.7] and [6.8] is:

$$[6.9] \quad \varepsilon_{z2'} = \varepsilon^{ep}_{zo} + \frac{\lambda}{V} \ln(\sigma'_{z2}/\sigma'_{zo}) + \frac{\psi}{V} \ln\left(\frac{t_o + t_{e2'}}{t_o}\right)$$

$$= \varepsilon^{ep}_{zo} + \frac{\lambda}{V} \ln(\sigma'_{z2}/\sigma'_{zo}) +$$

$$+ \frac{\psi}{V} \ln\left[\frac{t}{t_o} + e^{(\varepsilon^e_{zo} - \varepsilon^{ep}_{zo})/(\psi/V)} \cdot (\sigma'_{z2})^{\kappa/\psi} \cdot (\sigma'_{z2}/\sigma'_{zo})^{-\lambda/\psi}\right]$$

The reference state point 1 must be on the reference time line by definition. We know that t_{e1} at point 1 is zero and the strain ε_{z1} is equal to the instant elastic strain ε^e_{z1}. So using [6.4] and [6.1]:

$$[6.10] \quad \varepsilon^{ep}_{zo} + \frac{\lambda}{V} \ln(\sigma'_{z1}/\sigma'_{zo}) = \varepsilon^e_{zo} + \frac{\kappa}{V} \ln(\sigma'_{z1})$$

The parameters ε^e_{zo}, κ/V, t_o and ψ/V have been determined in the previous paragraphs. The constant ε^{ep}_{zo} is the initial strain before loading, so it is also known. Thus the meaning of parameter σ'_{zo} is that when $\sigma'_z = \sigma'_{zo}$, ε_z is equal to ε^{ep}_{zo}. The position of σ'_{zo} is shown in Fig.6.1 and 6.2. In Eqns.[6.9] and [6.10] there are only two

unknowns left, λ/V and σ'_{zo}. So they can be obtained by solving the two equations.

It is found that Eqns.[6.9] and [6.10] make up a non-linear equation system with unknowns λ/V and σ'_{zo} which can not be solved directly. We can use any approximate method to get the roots of this euqation system, for example using the simple bisection method or using more sophisticated Newton's second-order method.

Using the above procedure, only two single-stage creep tests are needed to find λ/V and σ'_{zo}. In practice, we may have more than two single-stage tests available. In this case, we may use another graphical approach to find λ/V and σ'_{zo}. In this approach, we try a number of assumed values of λ/V and σ'_{zo}, then see in graph whether the modelled values of σ'_z vs. ε_z are close to the measured values. This graphical approach is more flexible and should be used when only multi-stage test data are available or the fitting functions are more complicated than [6.1] - [6.3], we should use this graphic approach. This will be explained in the following Chapter.

6.3 Calculation of Apparent Preconsolidation Pressure

It is known that the preconsolidation pressure from first loading depends on creep times and strain rates (Graham et al. 1983, Crawford 1986, Leroueil et al. 1985). Apparent preconsolidation pressures resulted from creep strains due to aging has the same nature as

first-loading preconsolidation pressure. Eqn.[6.4] can be used to calculate the apparent preconsolidation pressure from single-stage loading creeping or multi-stage loading creeping.

Consider a single-stage loading creeping with stress σ'_{z3} and time t, see Fig.6.2. In terms of equivalent time, the final creep strain at point 3' is:

$$[6.11] \quad \varepsilon_{z3'} = \varepsilon^{ep}_{zo} + \frac{\lambda}{V} \ln(\sigma'_{z3}/\sigma'_{zo}) + \frac{\psi}{V} \ln(\frac{t_o + t_{e3'}}{t_o})$$

If the specimen is then loaded again, the "reloading" trace will move elastically to point 4 on the reference time line. The pressure σ'_{z4} at point 4 is the so-called preconsolidation pressure from aging. Thus the strain at 4 is:

$$[6.12] \quad \varepsilon_{z4} = \varepsilon_{z3'} + \frac{\kappa}{V} \ln(\sigma'_{z4}/\sigma'_{z3})$$

The state point $(\sigma'_{z4}, \varepsilon_{z4})$ is on the reference time line with $t_e = 0$:

$$[6.13] \quad \varepsilon_{z4} = \varepsilon^{ep}_{zo} + \frac{\lambda}{V} \ln(\sigma'_{z4}/\sigma'_{zo})$$

Combining [6.13] and [6.12] using [6.11], the apparent preconsolidation pressure resulting from aging under stress σ'_{z3} with creep time t is:

$$[6.14] \quad \sigma'_{z3,c} = \sigma'_{z4} = \sigma'_{z3} \, (\frac{t_o + t_{e3'}}{t_o})^{\psi/(\lambda-\kappa)}$$

where the equivalent time $t_{e3'}$ is found by using the same procedure as t_{e2}, from [6.7] and [6.8] in the single-stage loading case.

In the case of multi-stage loading, for example in Fig.5.5 loading from

point i-1 ($\varepsilon_{z,i-1}, \sigma'_{z,i-1}$) to point i ($\varepsilon_{zi}, \sigma'_{zi}$) with a real creep time t under stress σ'_{zi}, the apparent preconsolidation pressure referred to the reference time line is:

$$[6.15] \quad \sigma'_{zi,c} = \sigma'_{z,i+1} = \sigma'_{zi} \left(\frac{t_o + t_{ei'}}{t_o}\right)^{\psi/(\lambda-\kappa)}$$

The values of t_{ei}, in [6.15] is found from:

$$[6.16] \quad \varepsilon^{ep}_{zo} + \frac{\lambda}{V}\ln(\sigma'_{zi}/\sigma'_{zo}) + \frac{\psi}{V}\ln\left(\frac{t_o+t_{ei''}}{t_o}\right) = \varepsilon_{z,i-1} + \frac{\kappa}{V}\ln(\sigma'_{zi}/\sigma'_{z,i-1})$$

From which:

$$[6.17] \quad t_{ei''} = t_o\left[e^{(\varepsilon^{e}_{z,i-1}-\varepsilon^{ep}_{zo})/(\psi/V)} \left(\frac{\sigma'_{zi}}{\sigma'_{z,i-1}}\right)^{\kappa/\psi} (\sigma'_{zi}/\sigma'_{zo})^{-\lambda/\psi} - 1\right]$$

$$[6.18] \quad t_{ei'} = t + t_{ei''}$$

$$= t + t_o\left[e^{(\varepsilon^{e}_{z,i-1}-\varepsilon^{ep}_{zo})/(\psi/V)} \left(\frac{\sigma'_{zi}}{\sigma'_{z,i-1}}\right)^{\kappa/\psi} (\sigma'_{zi}/\sigma'_{zo})^{-\lambda/\psi} - 1\right]$$

Eqn.[6.18] gives a general relationship between equivalent t_e and real creep time t for single-stage loading or multi-stage loading. Eqn.[6.15] with [6.18] is therefore a general equation for calculating the apparent preconsolidation pressure from aging under any stepwise loading with respect to the reference time line, Fig.6.2.

As mentioned previously, the apparent preconsolidation pressure is defined with respect to the reference time line. The reference time line is not unique, but must be chosen by the analyst. Thus, the apparent preconsolidation pressure is itself also not unique.

Pressures determined from [6.14] or [6.15] should perhaps be called "reference" apparent preconsolidation pressures. According to the basic assumptions used in formulating the model, instant compression is exclusively elastic. However, the reference time line is not a line describing instant responses, so the true apparent preconsolidation pressure is the stress that can be applied after aging.

6.4 General $\sigma'_z - \dot{\sigma}'_z - \varepsilon_z - \dot{\varepsilon}_z$ Relationship for Continuous Loading

The preceding sections developed Eqns.[6.4],[6.18] using logarithmic functions for the case of stepped loading. In this section we will develop a more general constitutive equation for continous loading using the framework in Chapter 5.

According to Eqn.[5.7] in Chapter 5, using Eqn.[6.1] and [6.4], we have:

$$[6.19] \quad \dot{\varepsilon}_z = \frac{\kappa}{V} \frac{1}{\sigma'_z} \dot{\sigma}'_z + \frac{\psi/V}{t_o + t_e}$$

According to Eqn.[5.5], in the case specified by Eqn.[6.4], we find:

$$[6.20] \quad t_o + t_e = t_o \, e^{(\varepsilon_z - \varepsilon_{zo}^{ep})V/\psi} \, (\sigma'_z/\sigma'_{zo})^{-\lambda/\psi}$$

Substituting for (t_o+t_e) from [6.20] into [6.19]:

$$[6.21] \quad \dot{\varepsilon}_z = \frac{\kappa}{V}\frac{1}{\sigma'_z}\dot{\sigma}'_z + \frac{\psi}{Vt_o} e^{-(\varepsilon_z-\varepsilon_{zo}^{ep})V/\psi} (\sigma'_z/\sigma'_{zo})^{\lambda/\psi}$$

Eqn.[6.21] provides a general constitutive model specified by logarithmic functions for continuous reloading. The equation is valid for $\psi \neq 0$, and therefore includes the wide range of natural clays which show creep and strain-rate effects throughout their deformation process (Graham et al. 1983, Mesri and Choi 1984, Kabbaj et al. 1986). The unloading behavior is assumed to be completely elastic and time-independent. Eqns.[6.1] and [6.21] form a general σ'_z-$\dot{\sigma}'_z$-ε_z-$\dot{\varepsilon}_z$ constitutive model that describes the time dependent behaviour of clays under continuous one-dimensional loading, reloading or unloading.

6.5 Applications of the Model

This section develops the general equation [6.21] into applications for particular strain and stress conditions.

6.5.1 Creep

The condition for creep in [6.21] is when the effective vertical stress is constant ($\dot{\sigma}_z = 0$):

$$[6.22] \quad \dot{\varepsilon}_z = \frac{\psi}{Vt_o} \exp[-(\varepsilon_z-\varepsilon_{zo}^{ep})V/\psi](\sigma'_z/\sigma'_{zo})^{\lambda/\psi}$$

Integrating this equation with the initial conditions $\varepsilon_z = \varepsilon_{zi}$,

$\sigma'_z = \sigma'_{zi}$, $t = 0$ to produce the strains generated during creep, and using the equivalent time t_{ie} instead of ε_{zi} in [6.4] leads to:

$$[6.23] \quad \varepsilon_z = \varepsilon^{ep}_{zo} + \frac{\lambda}{V} \ln(\sigma'_{zi}/\sigma'_{zo}) + \frac{\psi}{V} \ln[(t + t_{ie} + t_o)/t_o]$$

This equation is the same as [6.4] for stepped loading but it has now been obtained from the model for continuous loading.

6.5.2 Relaxation

In geotechnical testing, relaxation tests are usually done by switching off the motor drive of the machine and allowing the energy stored in the test frame to drive the specimen with increasing strain at decreasing strain rates (Graham et al. 1983). However, using the classical condition $\dot{\varepsilon}_z = 0$ (ε_z = constant), assuming $\varepsilon^{ep}_{zo} = 0$, [6.21] becomes:

$$[6.24] \quad \frac{\kappa}{V} \dot{\sigma}'_z/\sigma'_z = -(\frac{\psi}{Vt_o}) \ (\sigma'_z/\sigma'_{zo})^{\lambda/\psi} \exp(-\varepsilon_z V/\psi)$$

As before, integrate the equation with initial conditions t_i, σ'_{zi} and ε_{zi}:

$$[6.25] \quad \sigma'_z = \sigma'_{zo} \ [\frac{\lambda}{\kappa} \frac{(t-t_i)}{t_o} + (\sigma'_{zi}/\sigma'_{zo})^{-\lambda/\psi} \exp(\varepsilon_{zi} V/\psi)]^{-\psi/\lambda} \exp(\varepsilon_{zi} V/\lambda)$$

The stress decreases with increasing time $(t-t_i)$ from the beginning of relaxation. Again using the equivalent time t_{ie} instead of ε_{zi}, [6.25] can also be written:

$$[6.26] \quad \sigma'_z = \sigma'_{zi} \left[\frac{t_{ie} + t_o}{(\lambda/\kappa)(t - t_i) + t_{ie} + t_o}\right]^{\psi/\lambda}$$

This equation contains the three modelling parameters λ, κ, and ψ combined in the interesting ratios (1) ψ/λ, the same as $C_{\alpha e}/C_c$ which Mesri and Godlewski (1977) suggest lies commonly in the range 0.04 - 0.08; and (2) κ/λ which commonly occurs in Critical State soil mechanics with values about 0.1 - 0.2.

Appendix 6.1 presents an alternative derivation of [6.26] based on the equivalence of $\varepsilon_z = \varepsilon_z^{sp} = 0$.

6.5.3 Constant rate of strain

The required condition is obtained by setting the strain rate term $\dot{\varepsilon}_z$ = constant and integrating the general equation [6.21], assuming $\varepsilon_{zo}^{ep} = 0$:

$$[6.27] \quad \sigma'_z = \sigma'_{zo}\left\{\left[\left(\frac{\sigma'_{zo}}{\sigma'_{zi}}\right)^{\lambda/\psi} - \frac{(\psi/V)/t_o}{\dot{\varepsilon}_z(1-\kappa/\lambda)} e^{\left(-\varepsilon_{zi}\frac{V}{\psi}\right)}\right] e^{\left[-\left(\frac{\lambda}{\kappa}\right)(\varepsilon_z-\varepsilon_{zi})\left(\frac{V}{\psi}\right)\right]} + \frac{(\psi/V)/t_o}{\dot{\varepsilon}_z(1-\kappa/\lambda)} e^{\left(-\varepsilon_z\frac{V}{\psi}\right)}\right\}^{-\psi/\lambda}$$

where σ'_{zi}, ε_{zi} are the initial conditions. Eqn.[6.27] can be used to express the effective stress vs. vertical strain relationship in the clay for different rates of straining, for example in CRSN tests. If a test is restarted after a period of unloading, then the initial values

should be reassigned. Eqn.[6.27] can also be written:

$$[6.28]\quad \varepsilon_z = \frac{\lambda}{V}\ln(\sigma'_z/\sigma'_{zo}) + \frac{\psi}{V}\ln\left\{\left[(\sigma'_{zo}/\sigma_{zi})^{\lambda/\psi} - \frac{(\psi/V)/t_o}{\dot{\varepsilon}_z(1-\kappa/\lambda)}\, e^{(-\varepsilon_{zi}V/\psi)}\right] x \right.$$

$$\left. x\, e^{[\varepsilon_z V/\psi - (\frac{\lambda}{\kappa})(\varepsilon_z-\varepsilon_{zi})(\frac{V}{\psi})]} + \frac{(\psi/V)/t_o}{\dot{\varepsilon}_z(1-\kappa/\lambda)}\right\}$$

Note that the slope of the log(stress)-strain curves for different constant strain rates is now slightly different from λ/V. This will be examined more closely in a later section.

An alternative formulation for CRSN tests is given in Appendix 6.2.

6.5.4 Constant rate of effective stress

The required condition in [6.21] is now $\dot{\sigma}'_z$= constant. By integration:

$$[6.29]\quad \varepsilon_z = \frac{\lambda}{V}\ln(\frac{\sigma'_z}{\sigma'_{zo}}) + \frac{\psi}{V}\ln\left\{e^{(\varepsilon_{zi}V/\psi)}(\sigma'_{zo}/\sigma'_{zi})^{\kappa/\psi}(\sigma'_{zo}/\sigma'_z)^{(\lambda-\kappa)/\psi} + \right.$$

$$\left. + \frac{\psi/t_o}{\dot{\sigma}'_z(\lambda-\kappa+\psi)}[\sigma'_z - \sigma'_{zi}(\sigma'_{zi}/\sigma'_z)^{(\lambda-\kappa)/\psi}]\right\}$$

It can be seen from [6.29] and Fig.6.4 that the slope of constant rate of stress tests in the VEP region is slightly steeper than λ/V. Note that because the behaviour is non-linear, the rate of straining $\dot{\varepsilon}_z$ and the rate of stressing $\dot{\sigma}'_z$ can not both be constant at the same time but

are related through [6.21].

6.6 Prediction and Comparison

The 1-D continuous EVP model will now be compared with published results from CRSN tests on two natural clays, and results from a stepped CRSN – relaxation test on reconstituted clay.

The model uses only three parameters λ, κ and ψ, all of which are relatively easily determined from stepped loading creep tests. The methodology for determining the parameters needed by the model was presented in Section 6.3. It is commonly found that the slope of the reference time line (λ-line) is close to the slope of stepped loading creep lines with constant duration (Bjerrum 1967a). Therefore, when using the method in this Section, we can first try the λ/V found from oedometer tests with constant duration loading.

In order to find ψ/V and t_o, at least two creep tests should last long enough to permit reliable determination of the two parameters. This is probably best done in the normally consolidated (EVP) range under the λ-line with $\sigma'_z > \sigma'_{zc}$. Although ψ/V is determined from straining only after primary consolidation has finished, it should be remembered that the same coefficient is used for the viscous component associated with slower straining under the κ-line, in non-equilibrated CRSN tests, and during primary consolidation. In this way, it differs fundamentally from the strain dependent C_α-parameter used by Mesri and his co-workers

(Mesri and Choi 1985a,b, Mesri and Castro 1987).

6.6.1 Modelling of Backebol clay

Sällfors (1975) presented MSL and CRSN tests on soft high-plastic clay from Bäckebol, Sweden. Basic classification information for the clay is given in Table 6.1. The rates used in the tests ranged from 5×10^{-7} to 1.67×10^{-5} s^{-1}. From comparable test results, it is estimated that $\varepsilon_{zo}^{ep} = 0$, $\lambda/V = 0.410$, $\kappa/V = 0.010$, and $\psi/V = 0.0205$. The resulting ratio $\kappa/\lambda = 0.0244$ is low but not totally unexpected for a highly sensitive clay. The value $\psi/\lambda = 0.050$ is in the range proposed by Mesri and Choi (1985a). A value of 600 s is found for t_o and this gives σ'_{zo} = 81 kPa. The initial values in the CRSN tests were σ'_{zi} = 10 kPa, ε_{zi}= 0.25 %. Fig.6.4 shows the λ-line and κ-line interpreted from MSL tests, and the curve obtained from [6.29] when the rate of effective stress applications is 1×10^{-3} kPa/sec. The values of κ,λ and ψ were then used in [6.27] to model CRSN tests run at strain rates of 7.5×10^{-6} s^{-1}, 2.0×10^{-6} s^{-1} and 5.0×10^{-7} s^{-1} respectively. The results are shown at logarithmic scale in Fig.6.5a and at arithmetic scale in Fig.6.5b. The calculated curves are in good agreement with the experimental data shown in the Figures.

The distance between the CRSN lines in Fig.6.5 is quite sensitive to the magnitude of the creep coefficient ψ — larger ψ-values produce wider separations between the various strain rate lines. Even though the value of $\psi/\lambda = 0.05$ is well within the range proposed by Mesri et

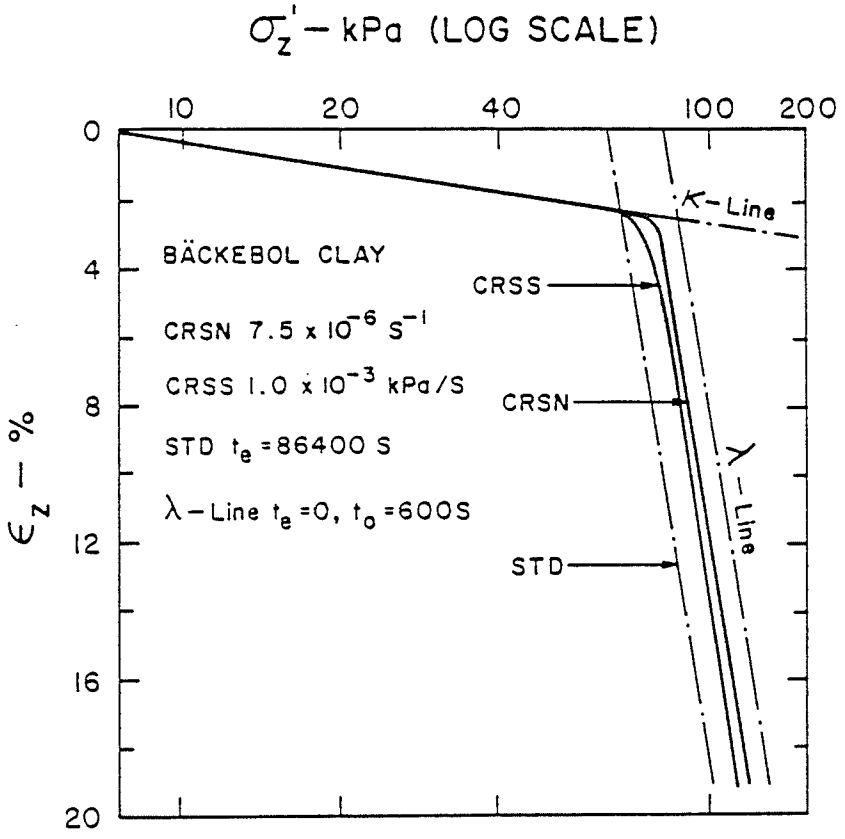

Fig.6.4 Modelling results for CRSS, CRSN and STD tests for Bäckebol clay (see also Sällfors 1975)

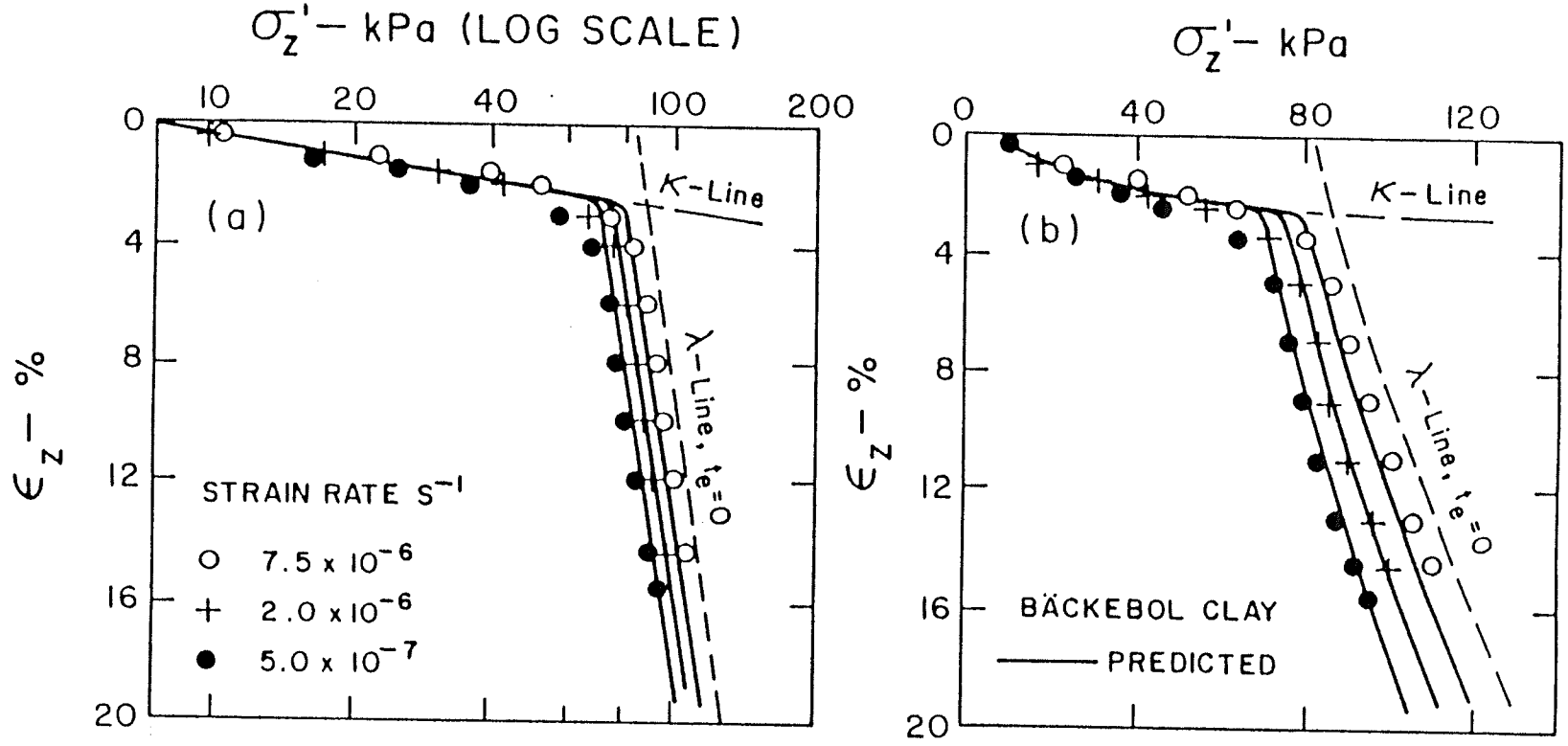

Fig.6.5 Comparison of predicted and measured σ'_z, ε_z results for Bäckebol clay (Sällfors 1975)

Choi (1985b), the separations predicted by the model are rather smaller than the measured ones. When $\psi/V = 0.0205 = 0.05\lambda/V$, a tenfold change in $\dot{\varepsilon}_z$ from 10^{-6} sec^{-1} to 10^{-5} sec^{-1} causes 12.2% change in σ'_z at ε_z = 5%. When ψ/V is increased to $0.0287 = 0.07\lambda/V$, the corresponding change in σ'_z is 17.5%. That is, increasing ψ increases the variability of σ'_z with $\dot{\varepsilon}_z$. Reasonable values of the parameter ψ therefore produce similar estimates of the dependency of σ'_{zc} on $\dot{\varepsilon}_v$ as the empirical parameter $\eta_{0.1}$ proposed by Graham et al. (1983).

Table 6.1 Properties of Clays

Clays	Depth (m)	W (%)	W_l (%)	W_p (%)	I_p (%)	S_t	σ_{zc} (kPa)	Clay Content (%)
Bäckebol Clay	7	102	99	34	65	25	72	70
Batiscan Clay	7.3	79.6	43	22	21	125	88	81
Reconstituted Illite		51	61	26	35		70	61

Fig.6.6 shows that [6.27] can also be used to find the relationship between effective stresses and strain rates at selected strain levels. The faster the strain rate, the higher will be the stress reached at a given strain. The predicted and measured results in Fig.6.6 are in fair agreement although once again the strain rate dependency was underpredicted by the ψ-value determined from STD tests.

The EVP model also permits calculation of the dependency of preconsolidation pressure on strain rate. In sensitive clays, it

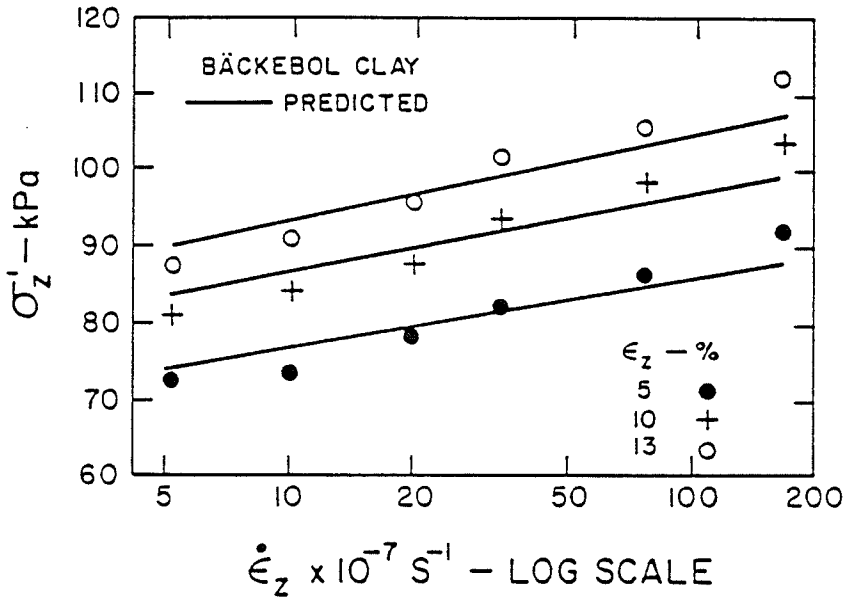

Fig.6.6 Stress-strain rate relationship at different strains (Bäckebol clay: Sällfors 1975)

appears reasonable (Graham et al. 1988) to assume that preconsolidation pressures are reached at about constant strain ε_z through the intersections between the κ-line and the λ-line for different strain rates. The finding by Leroueil et al. (1985) of a normalized effective stress (σ'_z/σ'_{zc})- strain (ε_z) relationship from CRSN tests supports this assumption. The value of ε_z^* at the κ-λ intersection can be found from [6.1],[6.2]:

$$[6.30] \quad \varepsilon_z^* = \frac{\lambda}{\lambda-\kappa} \left[\frac{\kappa}{V} \ln(\sigma'_{zo}/\sigma'_{zi}) - \varepsilon_{zi}\right]$$

For Bäckebol clay, $\varepsilon_z^* = 2.40$ % and this produces the prediction for the dependency of preconsolidation pressure on strain rate shown in Fig.6.7. Once again, the model tends to underpredict the dependency. Graham et al. (1983) also showed high strain rate dependencies in sensitive clays.

6.6.2 Modelling of Batiscan clay

Leroueil et al. (1985) presented creep and CRSN tests on Batiscan clay (Table 6.1). Published results have again been used to determine λ/V = 0.55, σ'_{zo}= 128 kPa; κ/V = 0.02; and t_o = 60s ψ/V = 0.022 for the EVP model, that is κ/λ = 0.0364, ψ/λ = 0.04. At strains larger than 16%, the σ'_z, ε_z-relationship becomes curved and the κ, λ and ψ parameters change. The published data show initial conditions σ'_{zi} = 68.4 kPa, ε_{zi} = 0. Using these values in [6.27] produces the stress-strain rate relations shown in Fig.6.8. The predicted curves agree well with the

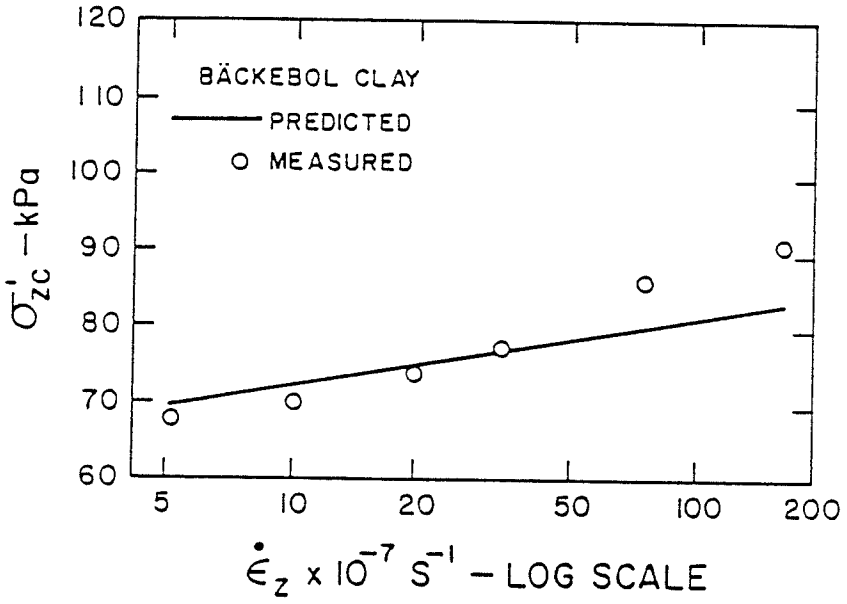

Fig.6.7 Preconsolidation pressure - strain rate relationship for Bäckebol clay (Sällfors 1975)

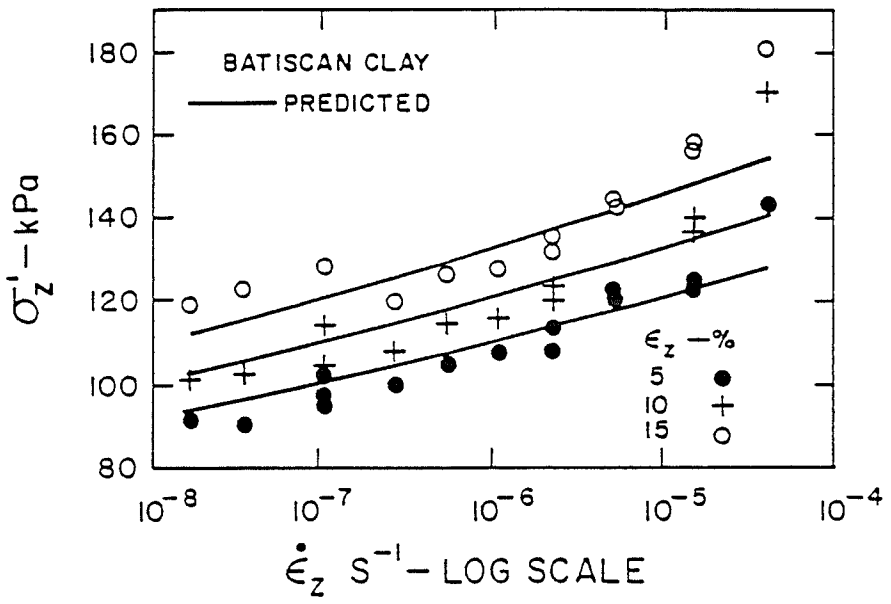

Fig.6.8 Stress-strain rate relationships at different strains (Batiscan clay: Leroueil et al. 1985)

test data but again underpredict the dependency on strain rate. Eqn.[6.27] has also been used to calculate the preconsolidation pressure - strain rate relationship shown in Fig.6.9.

6.6.3 Modelling of reconstituted illite

Specimens 256 mm diameter and 200 mm high were first prepared from slurry (Table 6.1) by one-dimensional consolidation to σ'_z = 70 kPa (Graham and Lau 1988). These were then cut into oedometer specimens 76 mm diameter 20 mm high and tested using 200 kPa back pressure to ensure saturation. The specimens were first consolidated to σ'_z = 200 kPa using a load increment ratio = 1.0 and increment durations of 24 hours. The 200 kPa stress was held for four days and then the specimens were unloaded to 2.4 kPa in four increments each lasting one day. This produced unloaded specimens with a known preconsolidation pressure.

Fig.6.10 shows results from one of these specimens run in a strain-controlled test in which the strain rate was changed at several stages during the test. At 24.6% strain, the machine drive was switched off to allow relaxation. As mentioned earlier, this does not produce the classic condition for relaxation because energy is fed into the specimen and some further straining occurs, in this case, an additional 0.3%.

The stepped loading portions of the test produced κ/V = 0.025; t_o = 600s, ψ/V = 0.004; λ/V= 0.10, σ'_{zo} = 47 kPa, from which κ/λ = 0.25, ψ/λ

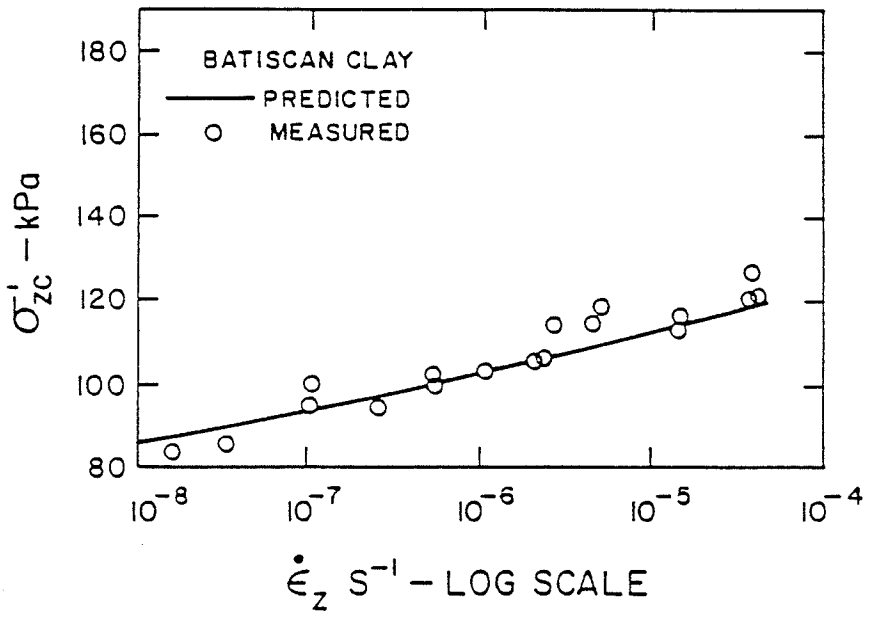

Fig.6.9 Preconsolidation pressure - strain rate relationship for Batiscan clay (Leroueil et al. 1985)

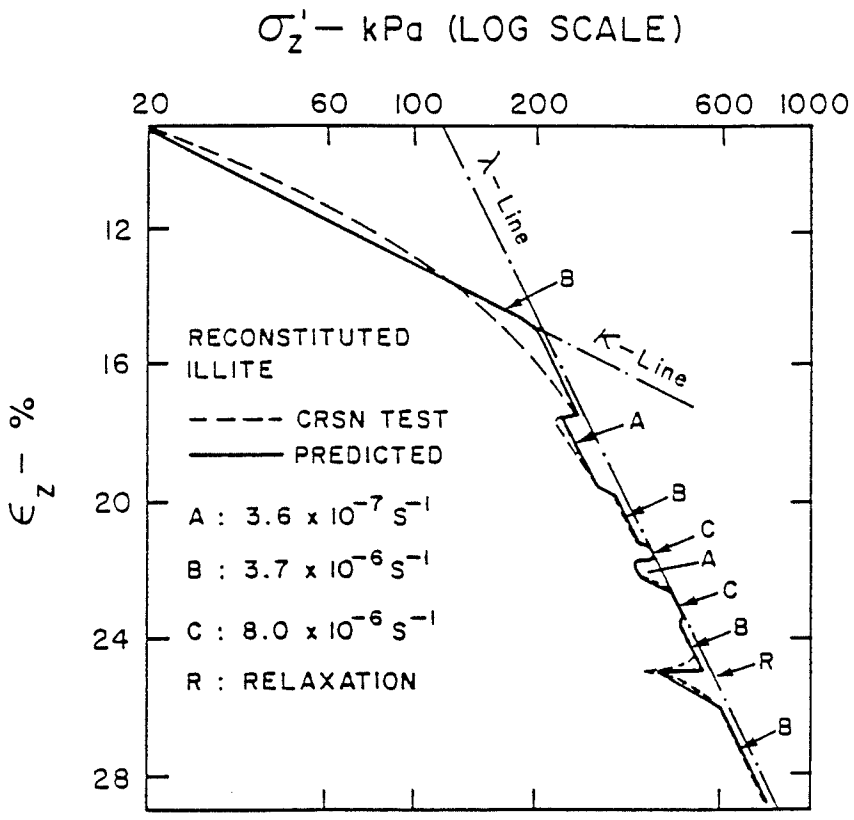

Fig.6.10 Measured and predicted step-change and relaxation results, reconstituted illite

= 0.04. These ratios indicate that the clay is a much more normal clay than either of the two highly sensitive clays described in preceding sections.

In the CRSN portion of the test, the initial values were ε_{zi} = 9.42% , σ'_{zi} = 22.8 kPa. Using these parameters in [6.27] produces the predicted stress-strain curves shown in Fig.6.10. When the strain rate is changed, the strain and stress at this point are used as initial values for the following section of the calculations. The calculated curve is in good agreement with the test data.

Fig.6.11 shows results calculated using [6.25] for the relaxation portion of the test. The measured stresses decreased more rapidly with time than the calculated values. However, since the specimens experienced some additional straining during this period, (as opposed to the constant strain assumption used in the analysis), the agreement is promising.

6.7 Discussion and Conclusions

Standard oedometer tests are easy to run and allow relatively easy determination of the parameters λ, κ and ψ. However natural strains (not engineering strains) may need to be used for plotting the data if large compressions are encountered and the normal consolidation line is slightly curved (Graham et al. 1982).

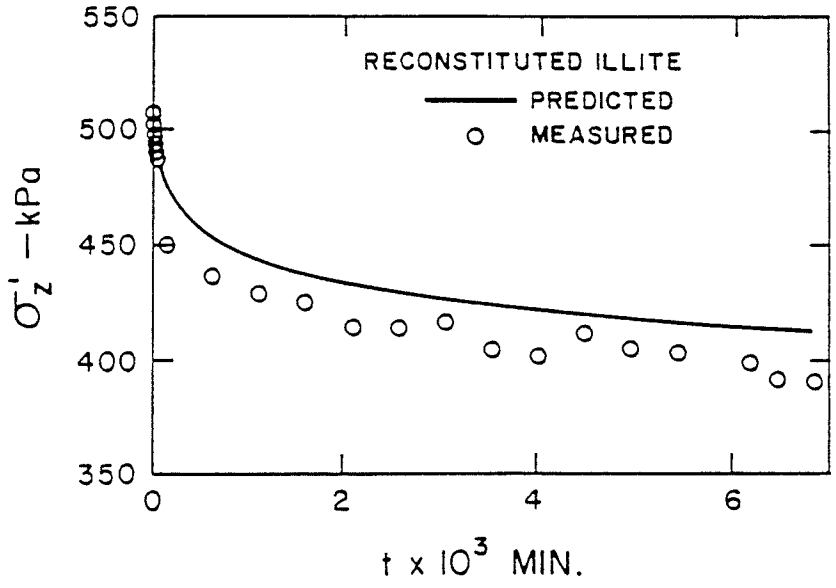

Fig.6.11 Stress-time relationships from relaxation test, reconstituted illite

Oedometer tests (and especially CRSN tests) are not ideal for finding effective stress relationships. The effective stresses are not measured directly, but must be evaluated on the basis of assumptions in each case. In MSL tests it is assumed that after EOP no excess porewater pressures exist in the specimen. In CRSN tests it is common to assume a parabolic porewater pressure distribution in the specimen provided the strain rate is not excessive. It is also common to ignore the effects of different stiffnesses as the preconsolidation front moves through the specimen with time (Walker and Raymond 1968).

In this Chapter three logarithmic functions have been used to fit test data. If the clay shows linearly elastic behaviour before yielding (Graham et al. 1988) then the κ parameter may be only an approximation of the true behaviour. Similarly, the ψ-parameter requires linearization of the creep data in log (time) and of course this only corresponds to attenuating primary creep. In some soils, λ-parameter is not a constant. However, once the three parameters have been determined, the model can then be used to predict the results that would be obtained from other types of tests.

The equations used in the model do not depend on the transient conditions of porewater pressure dissipation but instead deal with time-dependent hardening of the clay skeleton. The model can therefore be applied in principle to other materials such as ice, and frozen soils and provided the hardening laws [6.1], [6.2] and [6.3] can be defined for elastic hardening, for time-independent plastic hardening and for time-dependent plastic hardening. The model can also be

developed for isotropic consolidation and the prediction of times of consolidation.

The model agrees well with test results from reconstituted illite but tends to underestimate the influence of time-effects and strain rate effects in the two sensitive clays that have been examined. Graham et al. (1983) report large changes in undrained shear strength and preconsolidation pressure with changes in strain rate. This will require careful selection of model parameters or even selection of different functions to fit elastic, elastic-plastic (reference time line) and time-dependent behavior more accurately. Chapter 7 will present solutions developed using power functions for fitting experimental data.

Chapter 7

1-D EVP MODELLING USING POWER FUNCTIONS

7.1 Specified 1-D EVP Model

Chapter 6 developed a 1-D EVP model using logarithmic relationships with κ, λ, and ψ, Fig.7.1a. While these relationships are reasonable approximations for the behavior of many clays, there are other clays, particularly postglacial clays with high sensitivity, for which they are unsuitable, Fig.7.1b. Overconsolidated compression is often linear in σ'_z, ε_z-space, not $\ln(\sigma'_z), \varepsilon_z$-space. Normally consolidated behavior of natural clays is frequently curved, not straight in $\ln(\sigma'_z), \varepsilon_z$-space. Secondary consolidation (creep) is often curved in $\ln(\text{time}), \varepsilon_z$-space and the parameter ψ depends on time and vertical effective stress.

In this Chapter three power functions are used to fit (a) the instant elastic line, (b) the reference time line, and (c) creep strains. Using the framework in Chapter 5, a 1-D EVP model is developed and used to predict the time dependent behavior of Batiscan clay and Winnipeg clay. An improved prediction for Batiscan clay is obtained from this model.

Fig.7.2 and 7.3 show data obtained by Leroueil et al. (1985) from long duration constant stress tests on sensitive Champlain Sea clay from Batiscan, 100 km west of Québec City. The procedure involves finding

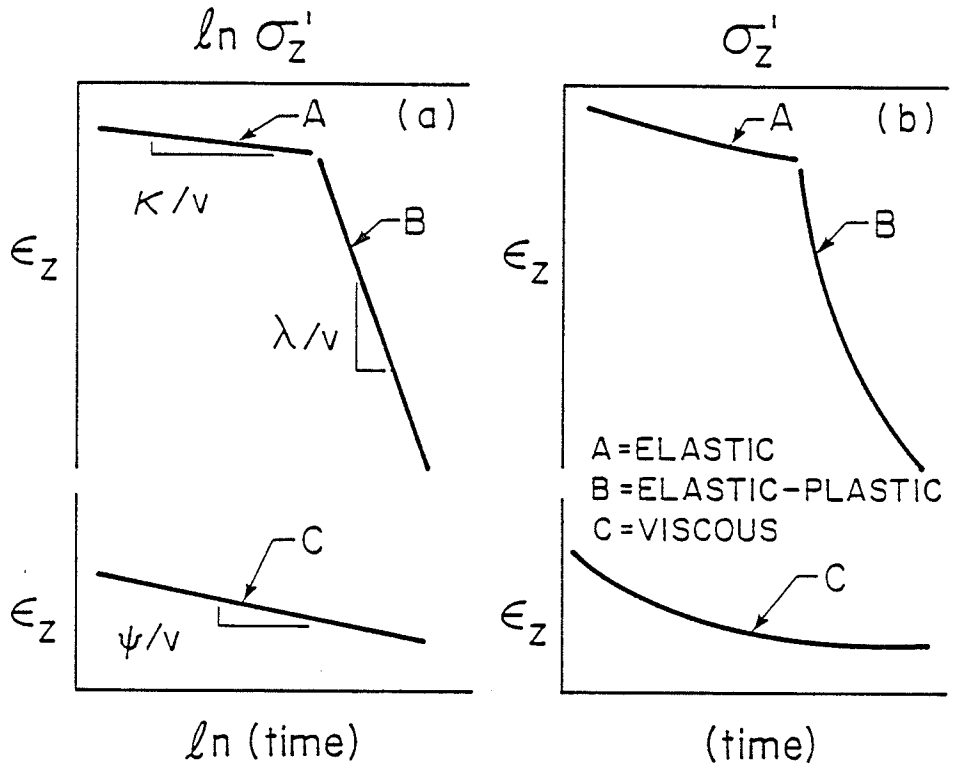

Fig.7.1 Schematic of elastic, elastic-plastic and creep modelling functions

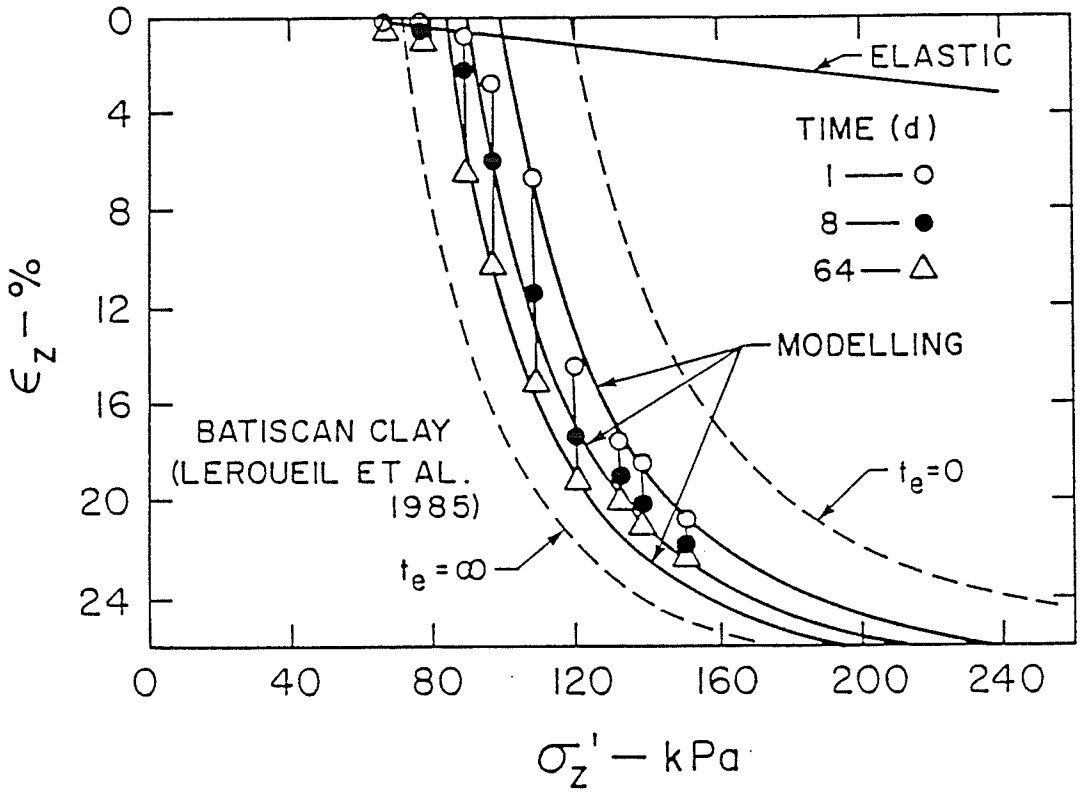

Fig.7.2 Curve fitting of σ_z', ε_z - t data - single-stage creep tests (Batiscan clay: Leroueil et al. 1985)

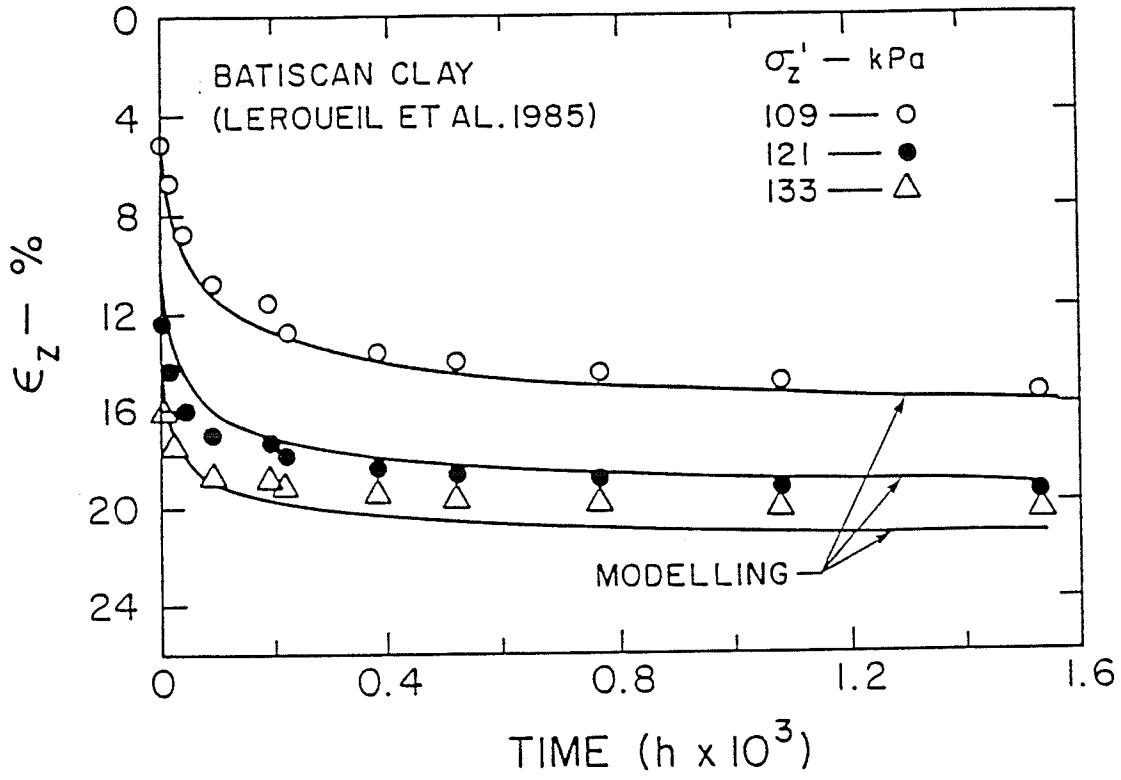

Fig.7.3 Curve fitting of ε_z, t - σ'_z data - single-stage creep tests (Batiscan clay: Leroueil et al. 1985)

the three functions f^e, f^{ep} and f^{tp} in Eqns.[5.2], [5.3], and [5.4] that best fit the experimental data in Figs.7.2 and 7.3 in the required range of stresses and time. The following functions have been used. Remember however that the model framework in Chapter 5 is general and any suitable functions can be used.

(1). For the elastic line:

$$[7.1] \quad \varepsilon_z^e = f^e = a_1 + a_2(\sigma'_z/\sigma'_u + \sigma'_{zoe}/\sigma'_u)^{n_1}$$

where σ'_u is unit stress which makes the equation dimensionless.

(2). For the elastic plastic line, the reference time line with $t_e = 0$ is:

$$[7.2] \quad \varepsilon_z^{ep} = f_o^{ep} = b_{1o}[1 - (\sigma'_{zo}/\sigma'_z)^{n_{2o}}]$$

and when with $t_e = \infty$ in the limiting case:

$$[7.3] \quad \varepsilon_z^{ep} = f_\infty^{ep} = b_{1\infty}[1 - (\sigma'_{z\infty}/\sigma'_z)^{n_{2\infty}}]$$

(3). For the viscous plastic strain vs. time:

$$[7.4] \quad \varepsilon_z^{tp} = f^{tp} = (f_\infty^{ep} - f_o^{ep})[1 - (\frac{t_o}{t_e+t_o})^{n_3}]$$

When the equivalent t_e in [7.4] is infinite, the limit of creep strains is $(f_\infty^{ep} - f_o^{ep})$.

Using Eqns.[7.2],[7.4] in Eqn.[5.5], the general equation for stepped

loading is:

$$[7.5] \quad \varepsilon_z = b_{1o}[1 - (\sigma'_{zo}/\sigma'_z)^{n_{2o}}] + (f_\infty^{ep} - f_o^{ep})[1 - (\frac{t_o}{t_e+t_o})^{n_3}]$$

Using Eqns.[7.1],[7.4] in Eqn.[5.7], we have:

$$[7.6] \quad \dot{\varepsilon}_z = a_2 n_1 (\sigma'_z/\sigma'_u - \sigma'_{zoe}/\sigma'_u)^{n_1-1} \dot{\sigma}'_z/\sigma'_u + (f_\infty^{ep} - f_o^{ep}) \frac{n_3}{t_o} (\frac{t_o}{t_e+t_o})^{n_3+1}$$

From [7.5]:

$$[7.7] \quad \frac{t_o}{t_e+t_o} = (1 - \frac{\varepsilon_z - f_o^{ep}}{f_\infty^{ep} - f_o^{ep}})^{1/n_3}$$

Using [7.7] in [7.6], the 1-D EVP model for Batiscan clay is:

$$[7.8] \quad \dot{\varepsilon}_z = a_2 n_1 (\frac{\sigma'_z}{\sigma'_u} - \frac{\sigma'_{zoe}}{\sigma'_u})^{n_1-1} \frac{\dot{\sigma}'_z}{\sigma'_u} + (f_\infty^{ep} - f_o^{ep}) \frac{n_3}{t_o} (1 - \frac{\varepsilon_z - f_o^{ep}}{f_\infty^{ep} - f_o^{ep}})^{(n_3+1)/n_3}$$

7.2 Determination of Model Parameters

As mentioned in Section 6.3 of Chapter 6, when the fitting functions are complicated or there are more test data than strictly required for solving model parameters, graphical approaches are more practical and simple.

The basic principle of the graphical approach for determining the model parameters is:

(a) Assume values of the paramters based on previous experience;

(b) Then use the model to fit all the available creep test data;

(c) If the calculated curves from the model are in a good visual agreement with these creep test data, then the parameter values that have been assumed are acceptable.

Using this graphical approach, we first can determine the instant elastic line in Fig.7.2. using the information from reloading data. The values of $a_1, a_2, \sigma'_{zoe}, n_1$ are given in Table 7.1.

Table 7.1 Parameters for Eqns.[7.1],[7.2],[7.3] and [7.4], Batiscan Clay (Leroueil et al. 1985) and Winnipeg Clay (Au 1982)

	Batiscan	Winnipeg		Batiscan	Winnipeg
a_1	-0.60	-0.10	n_{2o}	3.6	0.0240
a_2	0.42	0.0326	$b_{1\infty}$	0.284	5.54
σ'_u (kPa)	1.0	1.0	$\sigma'_{z\infty}$ (kPa)	72.3	190.0
σ'_{zoe} (kPa)	100.0	50.0	$n_{2\infty}$	2.9	0.0220
n_1	0.07	0.235	t_o (hours)	1.0	1.0
b_{1o}	0.262	5.50	n_3	0.27	0.28
σ'_{zo} (kPa)	119.3	289.0			

To determine the parameters in Eqns.[7.2],[7.3],[7.4], we have to first guess the parameters in [7.2] and [7.3], since Eqn.[7.4] contains all parameters. From experience, the shapes of [7.2] and [7.3] are similar to the shape of the time line with constant long durations from single-stage creep tests or multi-stage creep tests (Bjerrum 1967a).

Their shapes are different from the time line with short creep durations. In fact, the time line with infinite creep duration is the Eqn.[7.3] with $t_e = \infty$, independent of whether single-stage creep tests or multi-stage creep tests are used.

For Batiscan clay, $b_{1o} = 0.262$, $\sigma'_{zo} = 119.3$ kPa, $n_{2o} = 3.6$; $b_{1\infty} = 0.284$, $\sigma'_{z\infty} = 72.3$ kPa, $n_{2\infty} = 2.9$ have been chosen, so that the shapes of Eqns.[7.2] and [7.3] are similar to the shape of time line of 64 day duration in Fig.7.2. Then $t_o = 1.0$ hour, $n_3 = 0.27$ were selected in Eqn.[7.4] to fit the instant point from [7.1] and creep test data after primary comsolidation.

For example, to fit the creep data under a single-stage loading $\sigma'_z = 109$ kPa, using the parameter values in Table 7.1, the instant elastic strain is, from [7.1]:

$$[7.9] \quad \varepsilon_z^e = -0.6 + 0.42(109 + 100)^{0.07} = 0.01046$$

The strain at $t_e = 0$, from [7.2]:

$$[7.10] \quad \varepsilon_z^{ep} = f_o^{ep} = 0.262[1 - (119.3/109)^{3.6}] = -0.1006$$

The strain at $t = \infty$, from [7.3]:

$$[7.11] \quad \varepsilon_z^{ep} = f_\infty^{ep} = 0.284[1 - (72.3/109)^{2.9}] = 0.1976$$

So the limit of creep strain at $\sigma'_z = 121$ kPa is:

$$[7.12] \quad f_\infty^{ep} - f_o^{ep} = 0.1976 - (-0.1006) = 0.2982$$

The relation between equivalent t_e and real duration time t can be found as follows. The equivalent time t_{ei} at the instant point with $\varepsilon_{zi} = \varepsilon_z^e = 0.01046$ from [7.9] is, from Eqn.[7.6]

$$[7.13] \quad 0.01046 = -0.1006 + 0.2982[1 - (\frac{1}{t_{ei} + 1})^{0.27}]$$

from which:

$$[7.14] \quad t_{ei} = [1 - \frac{0.01046+0.1006}{0.2982}]^{-1/0.27} - 1 = 4.616 \text{ (hour)}$$

The equivalent time t_e is:

$$[7.15] \quad t_e = 4.616 + t$$

Therefore the equation for fiting the creep test data is, from [7.5]:

$$[7.16] \quad \varepsilon_z = -0.1006 + 0.2982 \ [1- (\frac{1}{4.616 + t + 1})^{0.27}]$$

For example when t = 1600 hours, the strain is 0.1570. The strains at 1 day, 8 days and 64 days are 0.07815, 0.1261, 0.1565 respectively. The curve fitting done on this basis is shown in Figs.7.2 and 7.3.

Using the same procedure, we can fit creep tests for effective vertical stresses 90 kPa, 98 kPa, 121 kPa, 133 kPa, 139 kPa and 151 kPa. Fig.7.2 shows the overall fittings for creep durations 1 day, 8 days and 64 days respectively. Fig.7.3 shows the typical curve fittings for stress 109 kPA, 121 kPa and 133 kPa. It is seen from the two figures that good agreement has been obtained, and so the curve fitting parametes shown in Table 7.1 can be used in the general model.

7.3 Validation of the 1-D EVP Model

As pointed out in previous Chapters, the validation of a constitutive model should be examined using the test data which was not used in calibrating the model. In this section, having calibrated the model from single-stage loading creep tests, we will use it to compare predicted and measured values from CRSN tests on Batiscan clay and from a step-changed Constant Rate of Strain (CRSN) test on Winnipeg clay.

7.3.1 Prediction of CRSN tests on Batiscan clay

Calibration parameters for the general EVP model in Eqn.[7.8] are shown in Table 7.1 for Batiscan clay. What now must be done is to examine whether the model based on creep loading data will predict results from other types of 1-D test and therefore by implication, field performance.

Figs.7.4 and 7.5 show results from CRSN tests on Batiscan clay (Leroueil et al. 1985). In Fig.7.4, predicted values of the ε_z, σ'_z-relationship are compared with experimental values for three different strain rates. The analyses used initial values $\varepsilon_{zi} = 0.001$, $\sigma'_{zi} = 67$ kPa. The agreement is good. Fig.7.5 shows the measured values of σ'_z which produced vertical strains of 5%, 10% and 15% for different straining rates. The Figure also shows values predicted by the earlier logarithmic modelling (Yin and Graham 1989a) in Chapter 6 and by the

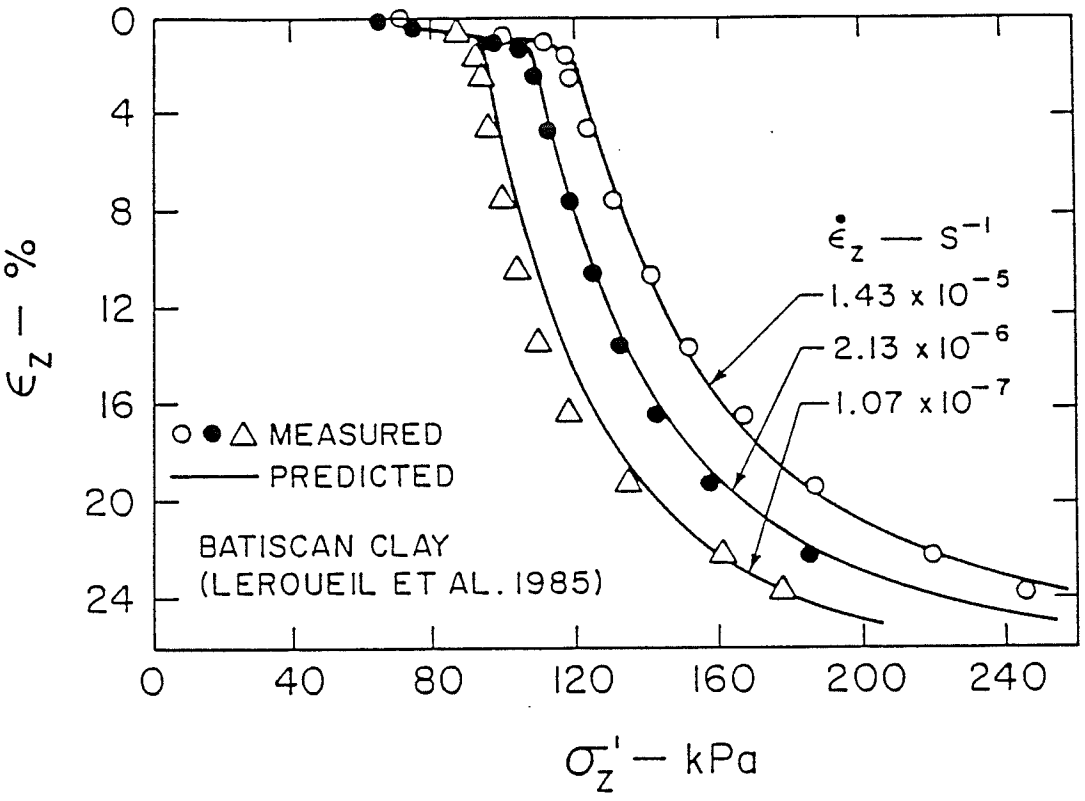

Fig.7.4 Prediction of σ'_z, ε_z-behavior for different strain rates - CRSN (Batiscan clay: Leroueil et al. 1985)

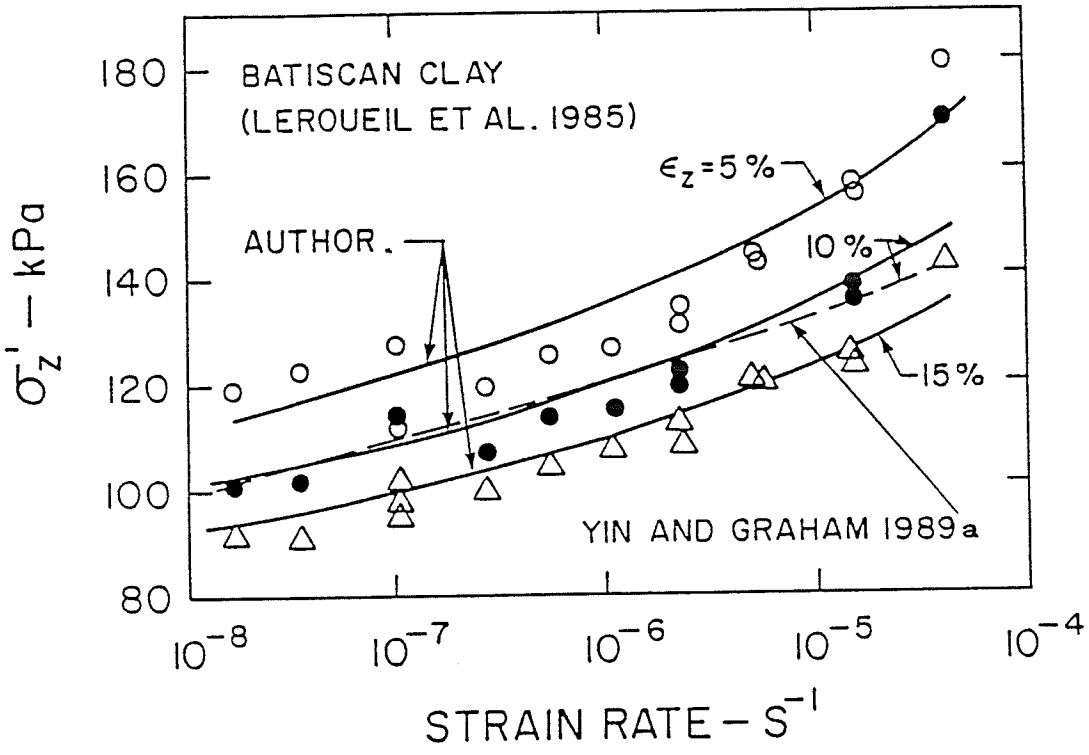

Fig.7.5 Prediction of σ_z', $\dot{\varepsilon}_z$-behavior for different strains - CRSN (Batiscan clay: Leroueil et al. 1985)

new modelling represented by Eqn.[7.8]. The $\varepsilon_z, \log(\sigma'_z)$-relationship for this clay is noticeably non-linear and thus the new power-law modelling in this Chapter produces improved agreement with the experimental results compared with the logarithmic modelling shown in Chapter 6.

7.3.2 Modelling of the coefficient of secondary consolidation $C_{\alpha\varepsilon}$

The conventional secondary consolidation coefficient $C_{\alpha\varepsilon}$ is defined in terms of real duration time (Graham et al. 1983):

[7.17] $C_{\alpha\varepsilon} = d\varepsilon_z^{tp}/d\log(t)$

It is found that $C_{\alpha\varepsilon}$ varys with vertical effective stresses and duration times (Graham et al. 1983, Clausen et al. 1984), see Figs.7.6 and 7.7. To calculate creep strains, we have to chose a proper value of $C_{\alpha\varepsilon}$, depending on the stress range and the time range (Mesri and Choi 1985a,b).

In the 1-D EVP model specified in Eqn.[7.4], the equivalent time t_e is used to calculate attenuating creep strains over the full range of stresses including overconsolidated range and normally consolidated range. The parameters used for specifying the creep behavior are constant, not like $C_{\alpha\varepsilon}$. According to Eqn.[7.4], the larger the equivalent times, the smaller will be the creep rates. The general euqation can be used to explain why $C_{\alpha\varepsilon}$ is smaller in the overconsolidated range even though the inherent creep behavior

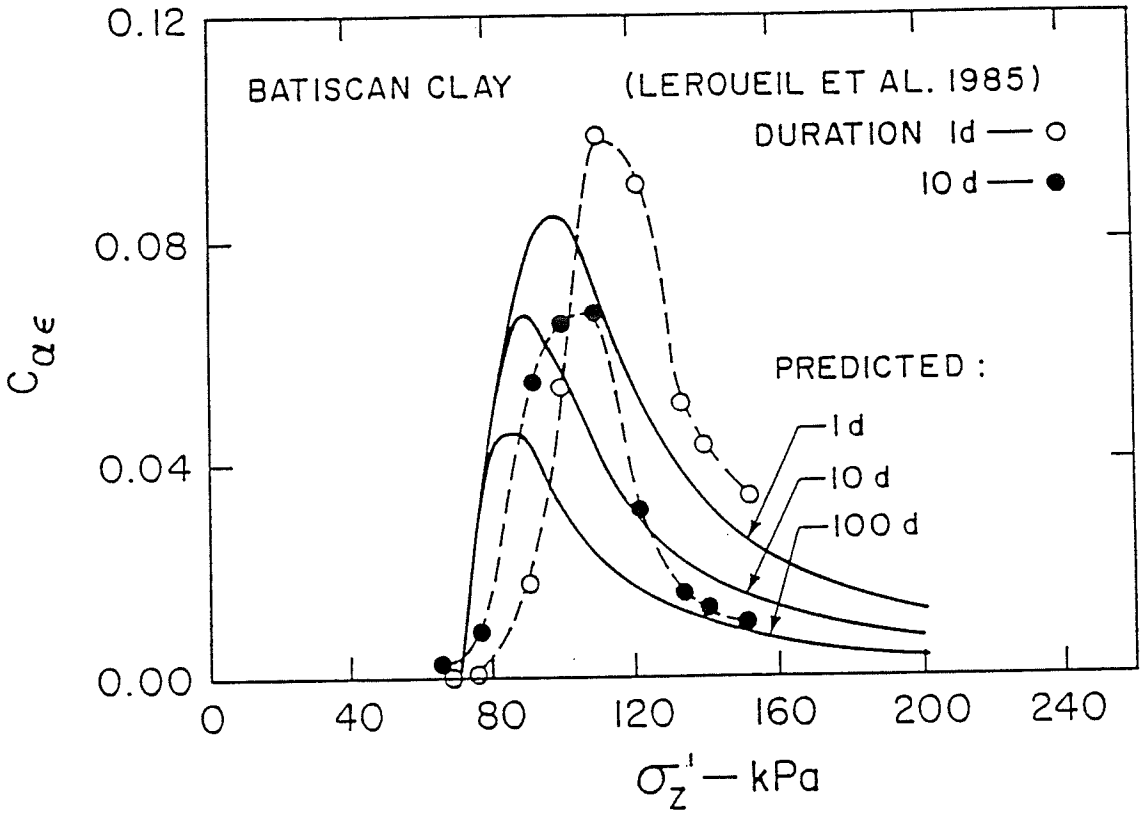

Fig.7.6 Predicted and measured $C_{\alpha\varepsilon}$ results - Single-stage creep tests (Batiscan clay: Leroueil et al. 1985)

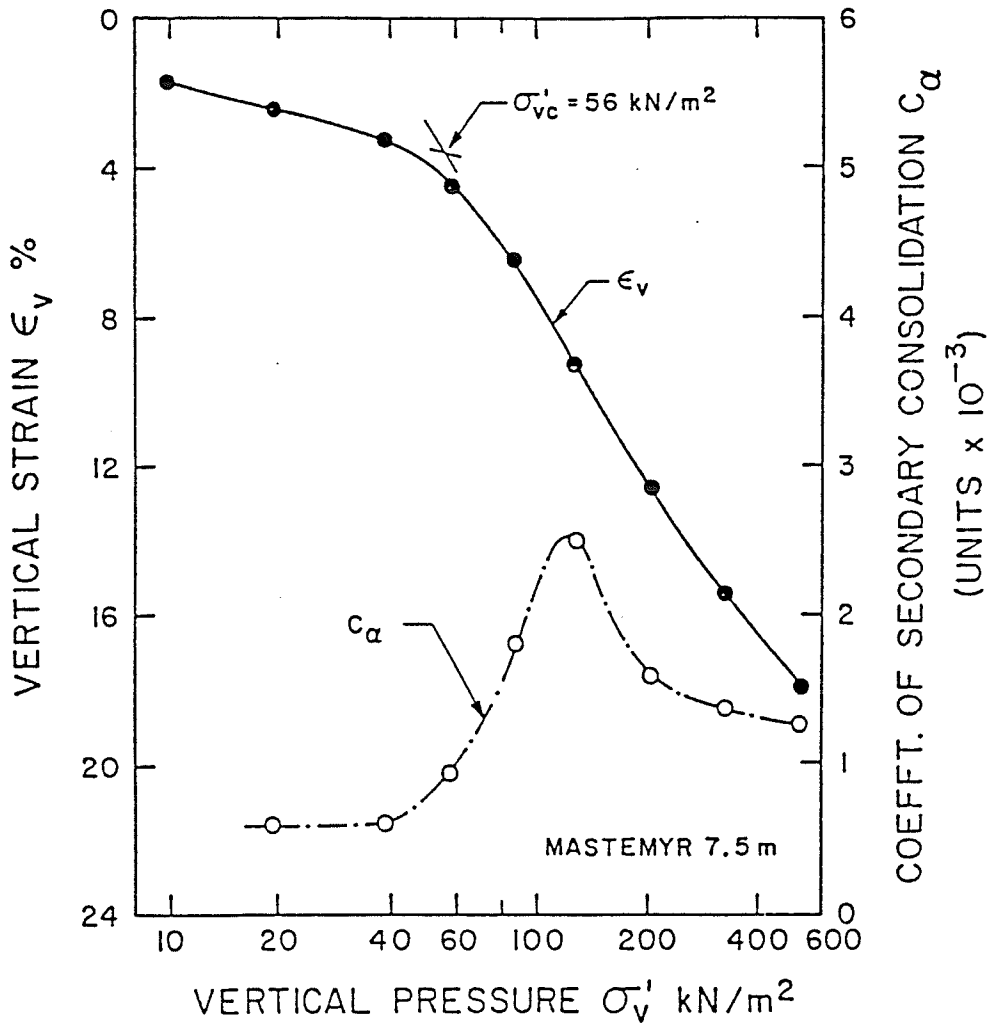

Fig.7.7 Measured $C_{\alpha e}$ results for Mastemyr clay (after Clausen et al. 1984)

parameters remain constant.

Using Eqns.[7.5] and [7.1], the equivalent time t_{ei} on the elastic line can be calculated from:

$$[7.18] \quad f_o^{ep} + (f_\infty^{ep} - f_o^{ep})[1 - (\frac{t_o}{t_{ei} + t_o})^{n_3}] = f^e$$

from which:

$$[7.19] \quad t_{ei} = t_o \left[1 - \frac{f^e - f_o^{ep}}{f_\infty^{ep} - f_o^{ep}}\right]^{-1/n_3} - t_o$$

We know that $t_e = t + t_{ei}$. So Eqn.[7.4] can be written:

$$[7.20] \quad \varepsilon_z^{tp} = f^{tp} = (f_\infty^{ep} - f_o^{ep})[1 - (\frac{t_o}{t + t_{ei} + t_o})^{n_3}]$$

According to the definition of $C_{\alpha\varepsilon}$ in [7.17]:

$$[7.21] \quad C_{\alpha\varepsilon} = \frac{d\varepsilon_z}{d\log(t)} = 2.303\ t \frac{d\varepsilon_z}{dt}$$

Then, differentiating Eqn.[7.20], from Eqn.[7.21]:

$$[7.22] \quad C_{\alpha\varepsilon} = 2.303\ n_3 \frac{t}{t_o} (f_\infty^{ep} - f_o^{ep}) (\frac{t_o}{t + t_{ei} + t_o})^{n_3+1}$$

It can be seen from [7.22] that $C_{\alpha\varepsilon}$ depends on stresses and times. Using the parameter values for Batiscan clay again in Table 7.1, Eqn.[7.22] can then be used to calculate the conventional secondary consolidation coefficient $C_{\alpha\varepsilon}$. Fig.7.6 shows the calculated curves for 1 day, 10 days and 100 days from [7.22] and the measured values for 1 day and 10 days. A written Discussion has been received from Mesri

(1990) on this topic. It will be interesting to see whether Mesri (Mesri and Choi 1985a,b), who has identified the stress-dependency of $C_{\alpha\varepsilon}$, has also identified time-dependency.

7.3.3 Prediction of a step-changed CRSN test on Winnipeg clay

The 1-D EVP model in Eqn.[7.8] is also calibrated using creep test data on Winnipeg clay. The values of model parameters are listed in Table 7.1. Fig.7.8 shows data measured from Winnipeg clay (Au 1982) using step-changed strain rates between 1.3×10^{-7} s^{-1} and 1.3×10^{-6} s^{-1}. Values predicted using initial values ε_{zi} = 0.0026 and σ'_{zi} = 63.7 kPa are in good agreement with the measured results.

7.4. Discussion and Conclusions

At first sight, 1-D oedometer testing is simple. In the common MSL tests, a load is applied, held constant until the induced porewater pressures dissipate, and then another load is added. This procedure clearly arose from the important early emphasis on hydrodynamic consolidation. More recently however it has become clear that clay behaviour depends quite strongly on strain rate. Thus, MSL tests in which strain rates vary continuously during a loading increment, give only an approximate, empirical indication of the behaviour of the clay unless careful attention is also given to secondary consolidation.

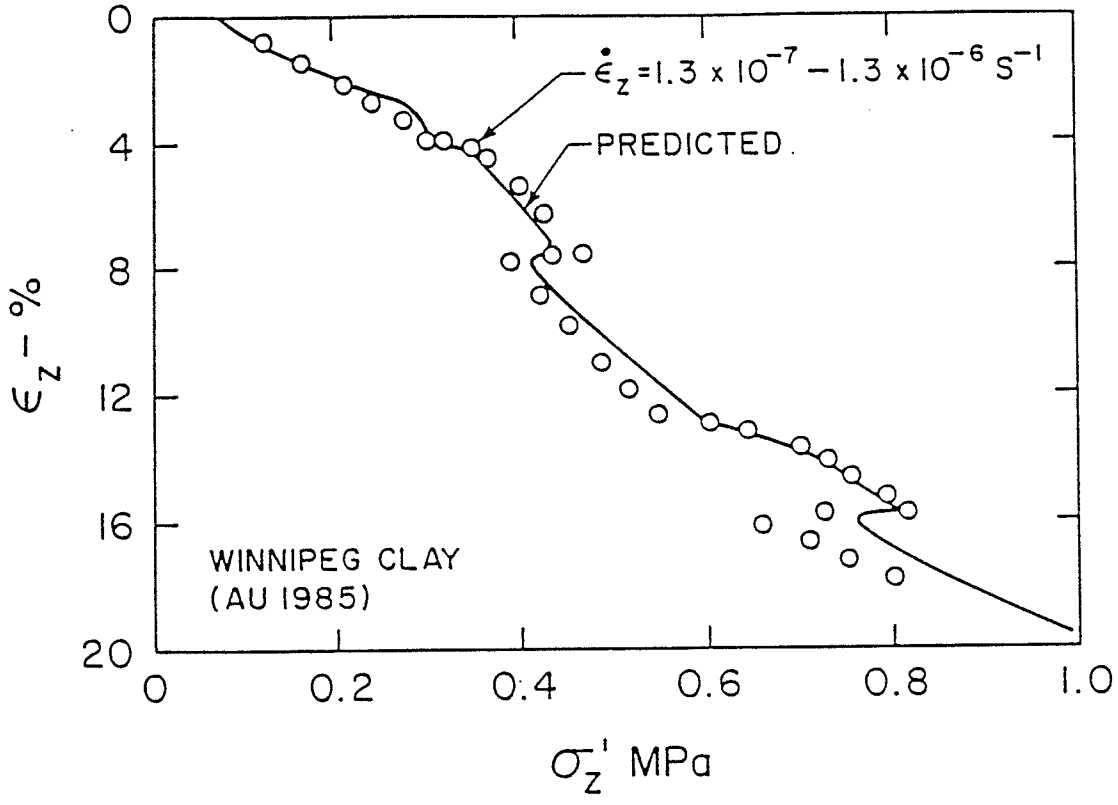

Fig.7.8 Predicted and measured σ'_z, ε_z results for step-changed CRSN test (Winnipeg clay: Au 1984)

That has been done in this Chapter, by writing functional expressions for elastic, elastic-plastic, and time-dependent compression, and by giving careful attention to defining the time-scale for time-dependent compression, it has been possible to write a general 1-D constitutive equation that can model a wide variety of test types. Figs.7.4,7.5,7.6,7.8 show that good agreement can be obtained between predicted and observed results for tests different from those used to form the model. The Figures show that successful agreement has been obtained for two very different types of clay, one a highly sensitive postplacial marine clay from Eastern Canada and the second a proglacial lacustrine plastic clay from Western Canada.

Perhaps the most important finding is the mathematical framework for understanding the secondary consolidation coefficient $C_{\alpha\varepsilon}$. Bjerrum (1967) showed that creep settlements of field structures depend strongly on the relationship between σ'_z and σ'_{zc}. Settlement rates were slow when $\sigma'_z < \sigma'_{zc}$, and higher when $\sigma'_z > \sigma'_{zc}$. Fig.7.6 shows that $C_{\alpha\varepsilon}$ is not constant but depends on stress level and stress duration.

Chapter 8

3-D ELASTIC VISCO-PLASTIC (EVP) MODELLING

8.1 Formulation of 3-D EVP Models

Chapters 3,4 developed hypoelasticity models for time independent stress-strain behavior of soils. Chapters 5,6,7 presented elastic visco-plastic models for time-dependent stress-strain behavior in 1-D straining (1-D EVP). All these models are applicable under certain restricted conditions. It is known that the stress-strain relationships of clays and frozen soils are time-dependent. In the field, the stress states are more complicated, usually in general three dimensional states where $\sigma'_1 \neq \sigma'_2 \neq \sigma'_3$. This Chapter will develop a constitutive model that can account for time and strain rate effects in general stress conditions.

As seen in Eqns.[5.7],[6.21] and [7.8], the vertical strain rate in 1-D straining was earlier divided into an elastic strain rate and a visco-plastic strain rate. It is reasonable to generalize this and to assume that in 3-D stress states, the strain rates ($\dot{\varepsilon}_{ij}$) consist of elastic strain rates ($\dot{\varepsilon}^{e}_{ij}$) and visco-plastic strain rates ($\dot{\varepsilon}^{vp}_{ij}$) (Perzyna 1963, 1966):

$$[8.1] \qquad \dot{\varepsilon}_{ij} = \dot{\varepsilon}^{e}_{ij} + \dot{\varepsilon}^{vp}_{ij}$$

An elastic constitutive law is needed to calculate the elastic strain rates. In general, the framework of hypoelastic models in Chapter 3 may be used. In simple cases, the time-independent behavior can be assumed to be isotropic elasticity. Thus, elastic strain rates are:

$$[8.2] \quad \dot{\varepsilon}^{e}_{ij} = [(\frac{1}{9K} - \frac{1}{6G})\delta_{ij}\delta_{kl} + \frac{1}{4G}(\delta_{ik}\delta_{jl}+\delta_{il}\delta_{jk})]\dot{\sigma}'_{kl}$$

The visco-plastic strain rates are considered to follow the flow rule:

$$[8.3] \quad \dot{\varepsilon}^{vp}_{ij} = S \frac{\partial F}{\partial \sigma'_{ij}}$$

where S is a scaling function which controls the magnitude of visco-plastic strain rates, and $S \geq 0$. The F in [8.3] is the visco-plastic potential function. The partial differentiation $\partial F/\partial \sigma'_{ij}$ controls the direction of visco-plastic strain rates, see Fig.8.1. It is found that the flow rule in [8.3] for calculating visco-plastic strain rates is similar to the flow rule for plastic strain increments in elastic plastic theory, see Appendix 8.2. The geometry represented by function F in stress space is called the flow surface which can go forwards and backwards, see Figs.8.1 and 8.2. It is seen that the flow surface is different from a yield surface which can go only forwards in strain hardening and may go backwards in strain softening. Perzyna (1963) proved that the flow surface must convex.

The flow surface F may be assumed to be elliptic, see Figs.8.1,8.2:

$$[8.4] \quad F = p'^{2} - p'_{m}p' + q^{2}/M^{2} = 0$$

As mentioned in Chapter 3, mean stress $p' = \sigma'_{kk}$, the general deviator

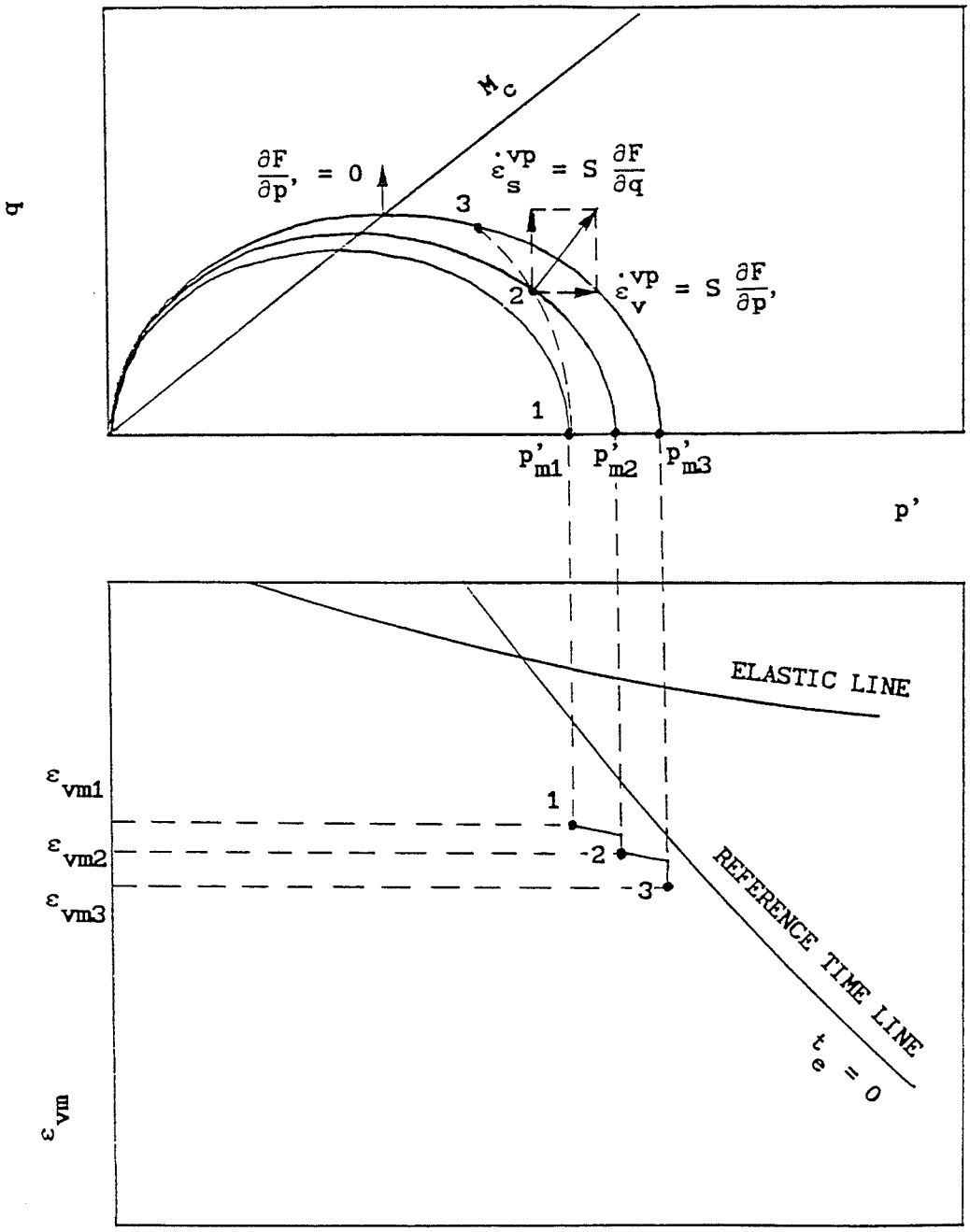

Fig.8.1 Illustration of flow rule and scaling methods

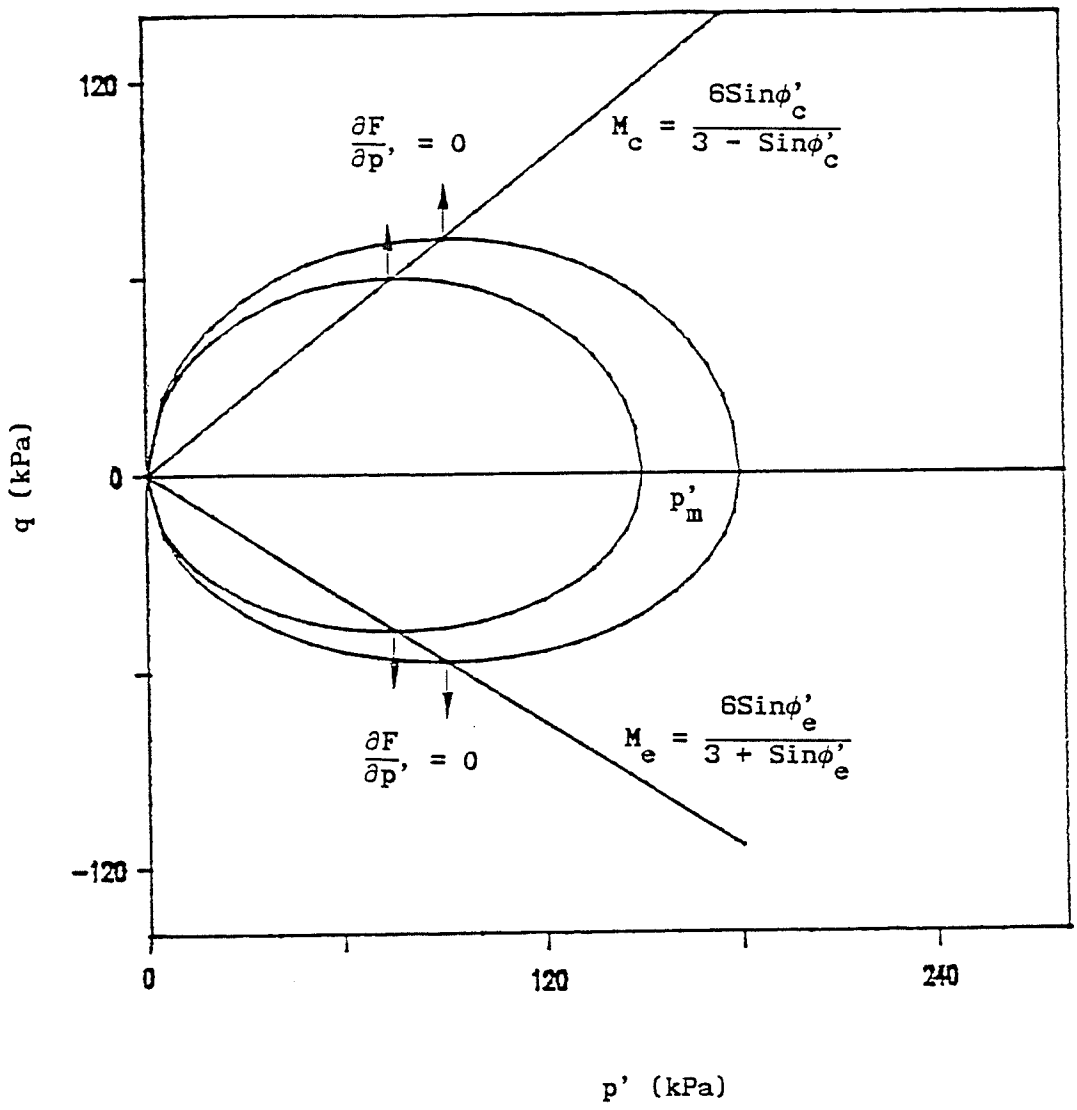

Fig.8.2 Flow surfaces and strength envelope in p-q space

stress q in [8.4] is $q = (3J_2)^{1/2} = (\frac{3}{2} S_{ij}S_{ij})^{1/2}$, where $S_{ij} = \sigma'_{ij} - \frac{1}{3}\sigma'_{kk}\delta_{ij}$. The p'_m in [8.4] is a stress parameter on the mean stress, p', coordinate axis, (Fig.8.1) that "scales" the various flow surfaces..

The strength envelope can then be defined as the line on which the strain rate vector directions are in the direction of deviator stress, q, coordinate axis. That is, where $\partial F/\partial p' = 0$, visco-plastic shear strain rate $\dot{\varepsilon}_s^{vp} \Rightarrow \infty$, see Figs.8.1,8.2. This definition is similar to the definition of the Critical State Line (Roscoe and Burland, 1968, Wroth and Houlsby 1985). From [8.4]:

$$[8.5] \quad \frac{\partial F}{\partial p'} = 2p' - p'_m$$

from which the mean stress at failure:

$$[8.6] \quad p'_f = p'_m/2$$

The equation of strength envelope in p',q-space is, from [8.4], using [8.6]:

$$[8.7] \quad F_f = q_f^2/p_f'^2 = \eta_f^2 = M^2$$

where M represents the strength envelope. A new technique is developed to generalize the flow surface Eqn.[8.4] and the strength envelope Eqn.[8.7] in p',q-space into expressions for general three dimensional stress states. It is assumed that the strength envelope in general stress states is expressed as:

$$[8.8a] \quad \eta_f^2 = \frac{M_c^2}{(1+\beta)^m}(1 + \beta\sin 3\theta)^m$$

where parameter θ is the Lode angle, defined as (Hill 1950):

[8.8b] $\sin 3\theta = \frac{3\sqrt{3}}{2} J_3/J_2^{3/2}$

where $J_2 = \frac{1}{2} S_{ij}S_{ij}$; $J_3 = \frac{1}{3} S_{ij}S_{jk}S_{ki}$ (Hill 1950). The m in [8.8a] is a parameter which controls the shape of the strength envelope on π planes (constant p'), see Fig.8.3. The parameter β in [8.8a] can be obtained as follows. When Lode angle $\theta = +30^{\circ}$, η_f must be equal to M_c denoting the triaxial compression (TC) strength of the soil, when $\theta = -30^{\circ}$, η_f must be equal to M_e denoting the triaxial extension (TE) strength, see Fig.8.3. Thus, from Eqn.[8.8a]:

[8.9a] $$\eta_f^2 = \frac{M_c^2}{(1+\beta)^m}(1+\beta)^m = M_c^2$$

[8.9b] $$\eta_f^2 = \frac{M^2}{(1+\beta)^m}(1-\beta)^m = M_e^2$$

The Eqn.[8.9b] is used to find β in [8.8]:

[8.10] $$\beta = \frac{(M_c/M_e)^{2/m} - 1}{1 + (M_c/M_e)^{2/m}}$$

We know:

[8.11a] $$M_c = \frac{6\mathrm{Sin}\phi'_c}{3 - \mathrm{Sin}\phi'_c}$$

[8.11b] $$M_e = \frac{6\mathrm{Sin}\phi'_e}{3 + \mathrm{Sin}\phi'_e}$$

where ϕ'_c and ϕ'_e are friction angles in compression and extension respectively. The strength envelope described by Eqns.[8.7]-[8.11] is a modification of the Mohr-Coulomb strength envelope, see Figs.8.2,8.3. The modified strength envelope has definition at corners of the

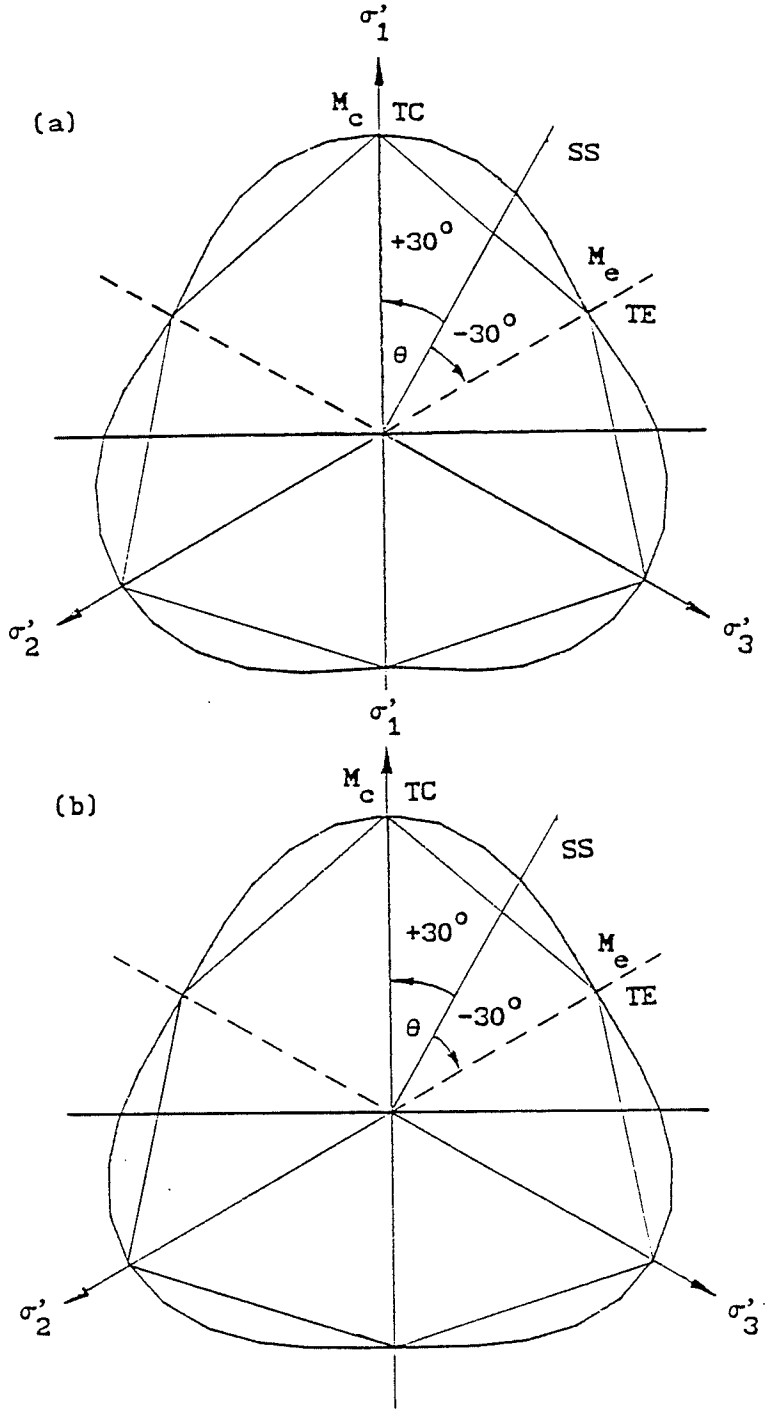

Fig.8.3 Strength envelopes on π-plane, $\phi'_c = \phi'_e = 20.67^\circ$, (a) m = 0.5, (b) m = 10

Mohr-Coulomb strength envelope in Fig.8.3. In Figs.8.2,8.3, $\phi'_c = \phi'_e = 20.67^o$, $M_c = 0.8$, $M_e = 0.6316$. It is seen in Fig.8.3a,b that when shape parameter m = 0.5, the strength envelope on π-plane is concave, when m = 10, the strength envelope is convex. The shape of the strength envelope therefore depends also on m as well as M_c and M_e. In elastic-plastic theory, the shape of the strength envelope and the yield surface should be convex on π-plane (Hill 1950). The parameter M in Eqn.[8.4] can be obtained from Eqns.[8.8a] and [8.7]. As shown in Fig.8.2, if $M_c \neq M_e$, the flow surface is not symmetric about the p'-axis in p',q-space.

Eqns.[8.1]-[8.4] form a general 3-D elastic visco-plastic model (EVP model) for any stress or strain conditions. Under trixial stress states, $q = \sigma_1 - \sigma_3$, $p' = (\sigma'_1 + 2\sigma'_3)/3$. Using [8.4], $\partial F/\partial p' = 2p' - p'_m$, $\partial F/\partial q = 2q/M^2$, the constitutive relationship for triaxial stress states is, from [8.1] and [8.3], see Fig.8.1:

$$[8.12] \quad \begin{cases} \dot{\varepsilon}_v = \dot{\varepsilon}^e_v + S\,(2p' - p'_m) \\ \dot{\varepsilon}_s = \dot{\varepsilon}^e_s + S\,2q/M^2 \end{cases}$$

From [8.4]:

$$[8.13] \quad p'_m = p' + \frac{q^2}{p'M^2}$$

and so, if a state point (p',q) is known, p'_m can be calculated from [8.13].

8.2 Scaling Methods

The scaling functions in Eqns.[8.3] and [8.12] control the magnitude of visco-plastic strain rates. This scaling function is similar to the scale factor in elastic-plastic models, which controls the magnitude of incremental plastic strains, see Appendix 8.2. In this section, we will introduce three methods for determining the scaling functions in the elastic visco-plastic model.

8.2.1 General p'_m-$\dot{p}'_m$-ε_{vm}-$\dot{\varepsilon}_{vm}$ relationship in isotropic stressing

The scaling function is related to a general constitutive equation for isotropic stressing. We will extend the work of 1-D EVP models in Chapters 5,6,7 for 1-D straining to formulate a general p'_m-$\dot{p}'_m$-ε_{vm}-$\dot{\varepsilon}_{vm}$ relationship for isotropic stressing.

It is assumed that in isotropic stress states, the total volumetric strain is devided into three components:

$$[8.14] \quad \varepsilon_{vm} = \varepsilon^{e}_{vm} + \varepsilon^{sp}_{vm} + \varepsilon^{tp}_{vm}$$

where recoverable instaneous elastic strains can be found from reloading or unloading tests, see Fig.8.1:

$$[8.15] \quad \varepsilon^{e}_{vm} = f^{e}(p'_m)$$

The elastic-plastic strain is (on the reference time line in Fig.8.1) is given by:

[8.16] $\varepsilon_{vm}^{ep} = \varepsilon_{vm}^{e} + \varepsilon_{vm}^{sp} = f^{ep}(p'_m)$

The time-dependent plastic strain is:

[8.17] $\varepsilon_{vm}^{tp} = f^{tp}(t_e, p'_m)$

where t_e is equivalent time as defined in Chapter 5. From [8.14] to [8.17], the equation for isotropic stepped loading is:

[8.18] $\varepsilon_{vm} = f^{ep}(p'_m) + f^{tp}(t_e, p'_m)$

In the same way as in 1-D EVP models, the equation for continuous loading is:

[8.19] $\dot{\varepsilon}_{vm} = (\frac{df^{e}}{dp'_m})\dot{p}'_m + \frac{\partial f^{tp}}{\partial t_e}$

Substituting t_e from [8.18] into [8.19], we can obtain a general p'_o-$\dot{p}'_o$-ε_v-$\dot{\varepsilon}_v$ relationship for isotropic stressing.

For example, if we use logarithmic functions:

[8.20] $f^{e} = \varepsilon_{vmo}^{e} + \frac{\kappa}{V} \ln(p'_m)$

[8.21] $f^{ep} = \varepsilon_{vmo}^{ep} + \frac{\lambda}{V} \ln(\frac{p'_m}{p'_{mo}})$

[8.22] $\varepsilon_{vm}^{tp} = \frac{\psi}{V} \ln(\frac{t_e + t_o}{t_o})$

where the parameters ε_{vmo}^{e}, κ/V; ε_{vmo}^{ep}, p'_{mo}, λ/V; and t_o, ψ/V can be determined using isotropic creep tests with the same methods as for 1-D EVP models in Chapters 5,6,7. Using Eqns.[8.18],[8.19] with

[8.20]-[8.22], we have:

$$[8.23] \quad \dot{\varepsilon}_{vm} = \frac{\kappa}{V}\dot{p}'_m/p'_m + \frac{\psi}{Vt_o} e^{-(\varepsilon_{vm}-\varepsilon^{e}_{vm}-\varepsilon^{sp}_{vm})V/\psi}$$

where ε^{e}_{vm} is from [8.20], and according to [8.16], $\varepsilon^{sp}_{vm} = f^{ep} - f^{e}$. Eqn.[8.23] is a p_m-$\dot{p}_m$-ε_{vm}-$\dot{\varepsilon}_{vm}$ relationship for any isotropic stressing, multi-stage, single-stage or continous loading specified by using logarithmic functions.

8.2.2 Method 1

Determining the scaling functions needs the use of an evolution law and a consistency condition in the same way as determining the scale factor in elastic-plastic models, see Appendix 8.2. The evolution law and consistency condition have to relate in some way the visco-plastic strain rates at any state point to the rates in isotropic stressing, see Fig.8.1.

The evolution law in Method 1 is that the rates of visco-plastic volumetric strain on the flow surface is kept constant. This means that the rates $\dot{\varepsilon}^{vp}_{v}$ at any state points are equal to $\dot{\varepsilon}^{vp}_{vm}$ on the mean stress p', axis. This law is similar to the strain hardening law in the modified Cam-Clay model in which the plastic volumetric strain is kept constant, see Appendix 8.2. From Eqn.[8.23], using [8.21]:

$$[8.24] \quad \dot{\varepsilon}^{vp}_{vm} = \frac{\psi}{Vt_o} e^{-(\varepsilon_{vm}-\varepsilon^{e}_{vm}-\varepsilon^{sp}_{vm})V/\psi}$$

$$= \frac{\psi}{Vt_o} e^{-(\varepsilon_{vm}-\varepsilon^{ep}_{vmo})V/\psi} \left(\frac{p'_m}{p'_{mo}}\right)^{\lambda/\psi}$$

The visco-plastic volumetric strain rate at any point is, from [8.12]

$$[8.25] \quad \dot{\varepsilon}^{vp}_{v} = S\,(2p' - p'_m)$$

Using the evolution law and $S \geq 0$, the scaling function is:

$$[8.26] \quad S = \frac{\psi}{Vt_o} e^{-(\varepsilon_{vm}-\varepsilon^{ep}_{vmo})V/\psi} \left(\frac{p'_m}{p'_{mo}}\right)^{\lambda/\psi} / |2p' - p'_m| \geq 0$$

where p'_m is found from Eqn.[8.13] for any state point using the consistency condition that the current point must be kept on the flow surface. The ε_{vm} in [8.26] can be obtained by solving Eqn.[8.27]:

$$[8.27] \quad \dot{\varepsilon}_{vm} = \frac{\kappa}{V} \dot{p}'_m/p'_m + \frac{\psi}{Vt_o} e^{-(\varepsilon_{vm}-\varepsilon^{ep}_{vmo})V/\psi} \left(\frac{p'_m}{p'_{mo}}\right)^{\lambda/\psi}$$

This procedure for determining the scaling function is quite complicated, and, to simplify this procedure, ε_v can be used instead of ε_{vm} in [8.26] to avoid solving the diferential equation [8.27]. The scaling function S is then:

$$[8.28] \quad S = \frac{\psi}{Vt_o} e^{-(\varepsilon_{v}-\varepsilon^{ep}_{vmo})V/\psi} \left(\frac{p'_m}{p'_{mo}}\right)^{\lambda/\psi} / |2p' - p'_m|$$

By comparing [8.23] with [8.12], we have:

$$[8.29] \quad \dot{\varepsilon}^{e}_{v} = \frac{\kappa}{V} \dot{p}'_m/p'_m = \frac{\kappa}{V} \dot{p}'/p'$$

where we can use p' instead of p'_m. This involves assuming that the

time-independent behavior is isotropic elasticity. Using this assumption, Eqn.[8.20] can be writen as:

$$[8.30] \quad \varepsilon_{vm}^{e} = \varepsilon_{v}^{e} = \varepsilon_{vmo}^{e} + \frac{\kappa}{V} \ln(p')$$

The 3-D EVP model for triaxial stress states is then:

$$[8.31] \quad \begin{cases} \dot{\varepsilon}_v = \frac{\kappa}{V} \dot{p}'/p' + \frac{\psi}{Vt_o} e^{-(\varepsilon_v - \varepsilon_{vmo}^{ep})V/\psi} \left(\frac{p'_m}{p'_{mo}}\right)^{\lambda/\psi} \\ \dot{\varepsilon}_s = \frac{1}{3G} \dot{q} + \frac{\psi}{Vt_o} e^{-(\varepsilon_v - \varepsilon_{vmo}^{ep})V/\psi} \left(\frac{p'_m}{p'_{mo}}\right)^{\lambda/\psi} \frac{2q/M^2}{|2p' - p'_m|} \end{cases}$$

where the elastic shear modulus G is estimated from unloading/reloading shear tests.

8.2.3 Method 2

This method considers the difference in the elastic strain and the time-independent plastic strain in Eqn.[8.23]. The ε_{vm}^{e} is from [8.30], ε_{vm}^{sp} is from:

$$[8.32] \quad \varepsilon_{vm}^{sp} = [\varepsilon_{vmo}^{ep} + \frac{\lambda}{V} \ln(\frac{p'_m}{p'_{mo}})] - [\varepsilon_{vmo}^{e} + \frac{\kappa}{V} \ln(p'_m)]$$

Thus the scaling function is:

$$[8.33] \quad S = \frac{\psi}{Vt_o} e^{-(\varepsilon_v - \varepsilon_{vmo}^{ep})V/\psi} \left(\frac{p'}{p'_m}\right)^{\kappa/\psi} \left(\frac{p'_m}{p'_{mo}}\right)^{\lambda/\psi} / |2p' - p'_m|$$

where we still use ε_v instead of ε_{vm} to simplify the scaling function.

Eqn.[8.33] can be used to write a similar equation system to [8.31] for triaxial stress states.

8.2.4 Method 3

The strength of overconsolidated clays and frozen soils depends on both time and strain rate, and it is not easy to determine a unique strength envelope. Sometimes however, it is possible to find the line on which the visco-plastic volumetric strain rates in shear tests are zero and this will be called the "neutral line". Consider for the moment that this line is known. Method 3 assumes that visco-plastic volumetric strain rates, $\dot{\varepsilon}_v^{vp}$ are zero on the "neutral line", are equal to $\dot{\varepsilon}_{vm}^{vp}$ on the mean stress, p', axis. Thus, we have:

$$[8.32] \quad S = \frac{\psi}{Vt_o} e^{-(\varepsilon_{vm}-\varepsilon_{vmo}^{ep})V/\psi} \left(\frac{p'_m}{p'_{mo}}\right)^{\lambda/\psi} /p'_m$$

to meet the required condition, that is, on the "neutral line":

$$[8.33] \quad \dot{\varepsilon}_v^{vp} = \frac{\psi}{Vt_o} e^{-(\varepsilon_{vm}-\varepsilon_{vmo}^{ep})V/\psi} \left(\frac{p'_m}{p'_{mo}}\right)^{\lambda/\psi} (2p'_n - p'_m)/p'_m = 0$$

wher p'_n is the stress on the "neutral line", and on the p' axis:

$$[8.34] \quad \dot{\varepsilon}_v^{vp} = \frac{\psi}{Vt_o} e^{-(\varepsilon_{vm}-\varepsilon_{vmo}^{ep})V/\psi} \left(\frac{p'_m}{p'_{mo}}\right)^{\lambda/\psi} (2p'_m - p'_m)/p'_m = \dot{\varepsilon}_{vm}^{vp}$$

As derived earlier for Eqn.[8.6] because of the assumption of an ellipse for the flow surface, $p'_n = p'_m/2$ in [8.35].

If ε_v is used instead of ε_{vm} in Eqn.[8.34], we have:

$$[8.37] \quad S = \frac{\psi}{Vt_o} e^{-(\varepsilon_v - \varepsilon_{vmo}^{ep})V/\psi} \left(\frac{p'_m}{p'_{mo}}\right)^{\lambda/\psi} / p'_m$$

The constitutive equations for triaxial stress states are, from [8.12] using [8.37]:

$$[8.38] \quad \begin{cases} \dot{\varepsilon}_v = \frac{\kappa}{V} \dot{p}'/p' + \frac{\psi}{Vt_o} e^{-(\varepsilon_v - \varepsilon_{vmo}^{ep})V/\psi} \left(\frac{p'_m}{p'_{mo}}\right)^{\lambda/\psi} \frac{2p' - p'_m}{p'_m} \\ \dot{\varepsilon}_s = \frac{1}{3G} \dot{q} + \frac{\psi}{Vt_o} e^{-(\varepsilon_v - \varepsilon_{vmo}^{ep})V/\psi} \left(\frac{p'_m}{p'_{mo}}\right)^{\lambda/\psi} \frac{2q/M^2}{p'_m} \end{cases}$$

Chapter 10 will show an application of this scaling method to a frozen sand.

In Eqns.[8.31],[8.38], the visco-plastic strain rates $\dot{\varepsilon}_v^{vp} \geq 0$ and $\dot{\varepsilon}_s^{vp} \geq 0$ in loading and unloading/reloading when $(2p' - p'_m) \geq 0$ and $2q/M^2 \geq 0$ respectively. In the case of unloading where $\Delta p' < 0$ and $\Delta q < 0$, it is found that the change in visco-plastic strain energy is $\Delta W^{vp} = \Delta p' \dot{\varepsilon}_v^{vp} \Delta t + \Delta q \dot{\varepsilon}_s^{vp} \Delta t \leq 0$. It is known in elastic material that the change in elastic strain energy $\Delta W^e \geq 0$ for unloading. That $\Delta W^e \geq 0$ implies that the elastic material possesses the potential of elastic strain energy in unloading, and can do work on objectives outside. While that $\Delta W^{vp} \leq 0$ in unloading implies that the visco-plastic material can not do work on objectives outside, but exhausts energy from outside even in the unloading process. Therefore

the Eqns.[8.31],[8.36] satisfy the second thermodynamic law and can be applied to calculate the time-dependent behavior in loading and unloading/reloading in the visco-plastic region.

8.3 Simulation of a CIŪ Test Using the Modified Cam-Clay Model and EVP Models

It was found in 1-D EVP modelling (Yin and Graham 1989a,b) that when the creep parameter ψ/V approached zero, the results from the model approached the elastic line and the elastic-plastic line (reference time line). This section will examine results from EVP modelling, and also the similarities and differences between EVP models and the modified Cam-Clay elastic plastic model. It will be remembered that the modefied Cam-Clay model takes no account of strain rate effects.

Formulation of the modified Cam-Clay model (Roscoe and Blurland 1968) is presented in Appendix 8.2. Using this model, the undrained effective stress path in p',q-space, started at a point $(0,p'_i)$ after isotropic consolidation, is:

$$[8.39] \quad q = Mp'[(p'_i/p')^{\lambda/(\lambda-\kappa)}{}_{-1}]^{1/2}$$

The $q-\varepsilon_s$ curve can be obtained by solving the following differentiation equation in conjunction with [8.39], see Appendix 8.2:

$$[8.40] \quad d\varepsilon_s = \frac{1}{3G}\,dq + \frac{\lambda-\kappa}{Vp'_m p'(2p'-p'_m)}\,[(2p'-p'_m)\,\frac{2q}{M^2}\,dp' + (\frac{2q}{M^2})^2 dq]$$

Eqns.[8.39],[8.40] are used to model the stress-strain behavior of a

undrained CI$\bar{U}$ test, see Figs.[8.4]-[8.9].

Effective stress paths and q-ε_s curves for the CI$\bar{U}$ test are obtained from EVP models by solving the following differentiation equation system. From Eqn.[8.12], using the undrained condition $\dot{\varepsilon}_v = 0$:

$$[8.39] \quad \begin{cases} \dot{p}' = (Vp'/\kappa)\, S\, (2p' - p'_m) \\ \dot{\varepsilon}_s = \frac{1}{3G}\,\dot{q} + S\, 2q/M^2 \end{cases}$$

Three different scaling functions can be obtained using the three methods given in the previous sections.

The parameters used in the modelling were: $\kappa/V = 0.025$ ($\kappa/\lambda = 0.25$), $\varepsilon^e_{mvo} = -0.0963$; $\lambda/V = 0.1$, $p'_{mo} = 47$ KPa, $\varepsilon^{ep}_{mvo} = 0$; $\psi/V = 0.004,\ 0.0004$ ($\psi/\lambda = 0.04,\ 0.004$), $t_o = 1$ hour; $M_c = 0.8$, $G = 1000$ KPa. The initial point used in all calculations was chosen on the referemce time line: $p'_i = 100$ KPa, $q_i = 0$, $\varepsilon_{vi} = \lambda/V \ln(p'_i/p'_{oo}) = 0.0755$, $t_i = 0$ hour.

Fig.8.4 shows the simulated q-ε_s and effective stress path of the CI$\bar{U}$ test using the modified Cam-Clay model and a EVP model with scaling function in Eqn.[8.26] in Method 1. The creep parameter ψ/V used was 0.004. Fig.8.5 shows the simulation of the same test, where the creep parameter ψ/V was reduced to 0.0004.

In Figs.8.6 and 8.7, the scaling function [8.31] in Scaling Method 2 was used in EVP modelling of the same CI$\bar{U}$ test. The creep parameter ψ/V was 0.004 in Fig.8.6, and 0.0004 in Fig.8.7. Figs.8.8 and 8.9 used

the scaling function [8.35] in Method 3 with ψ/V = 0.004 and 0.0004 respectively.

It is seen in Figs.8.4-8.9 that the stress-strain curves and effective stress paths were strain rate dependent and sensitive to the parameter ψ/V in EVP modelling. When the creep parameter ψ/V approached zero, the simulated curves from EVP models using Scaling Method 2 and Method 3 approached the curves from the modified Cam-Clay model. However, curves from the EVP model using Scaling Method 1 were not. The general shapes of the curves are similar to those found in CI$\bar{U}$ tests at different straining rates. The modified Cam-Clay model is a particular example, when viscosity is zero, of the more general EVP model with rigorous scaling of the function [8.26]

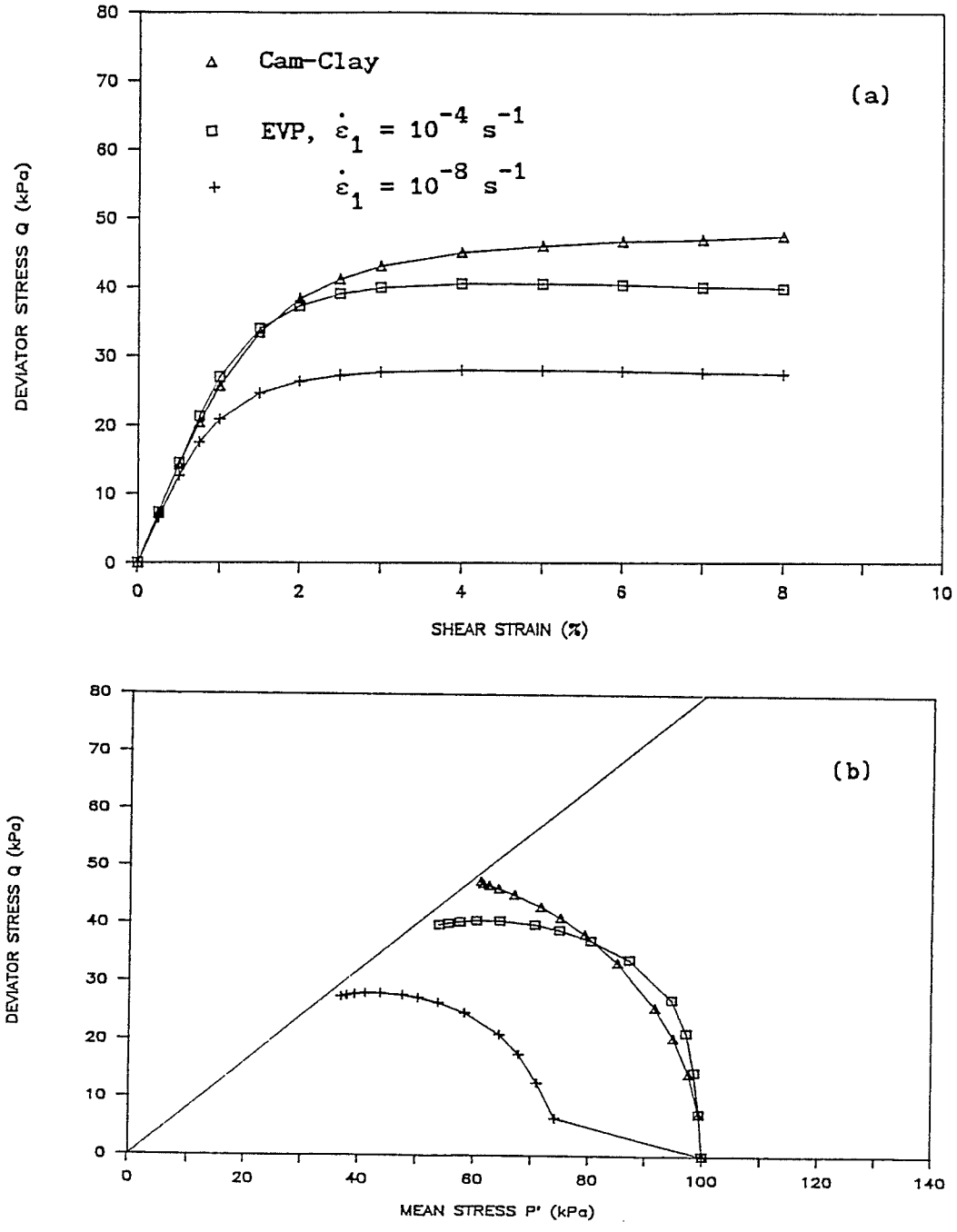

Fig.8.4 Simulation of a CI$\bar{U}$ test using modified Cam-Clay model and 3-D EVP model - Scaling Method 1, $\psi/V = 0.004$
(a) q vs. ε_s, (b) q vs. p'

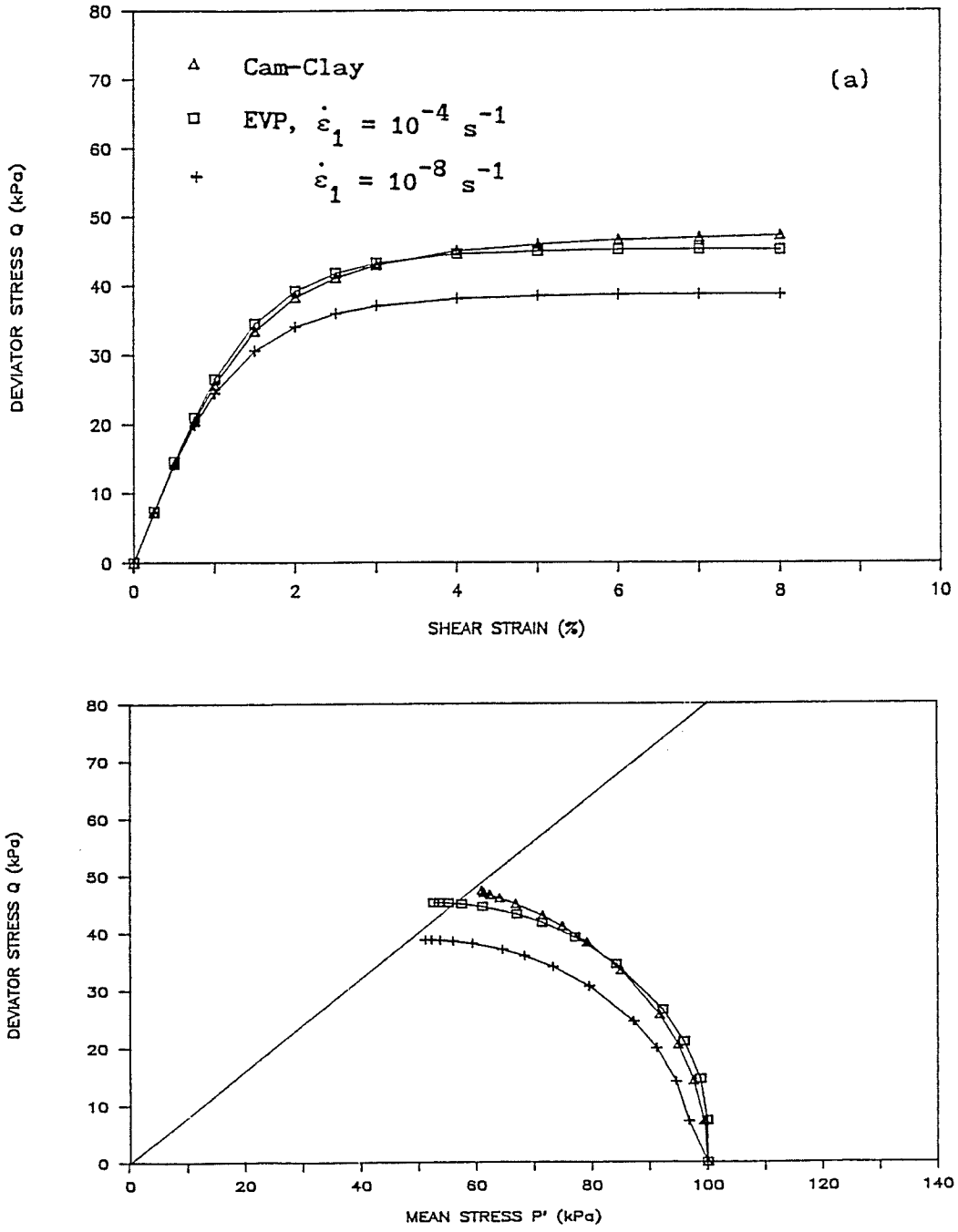

Fig.8.5 Simulation of a CIŪ test using modified Cam-Clay model and 3-D EVP model - Scaling Method 1, $\psi/V = 0.0004$ (a) q vs. ε_s, (b) q vs. p'

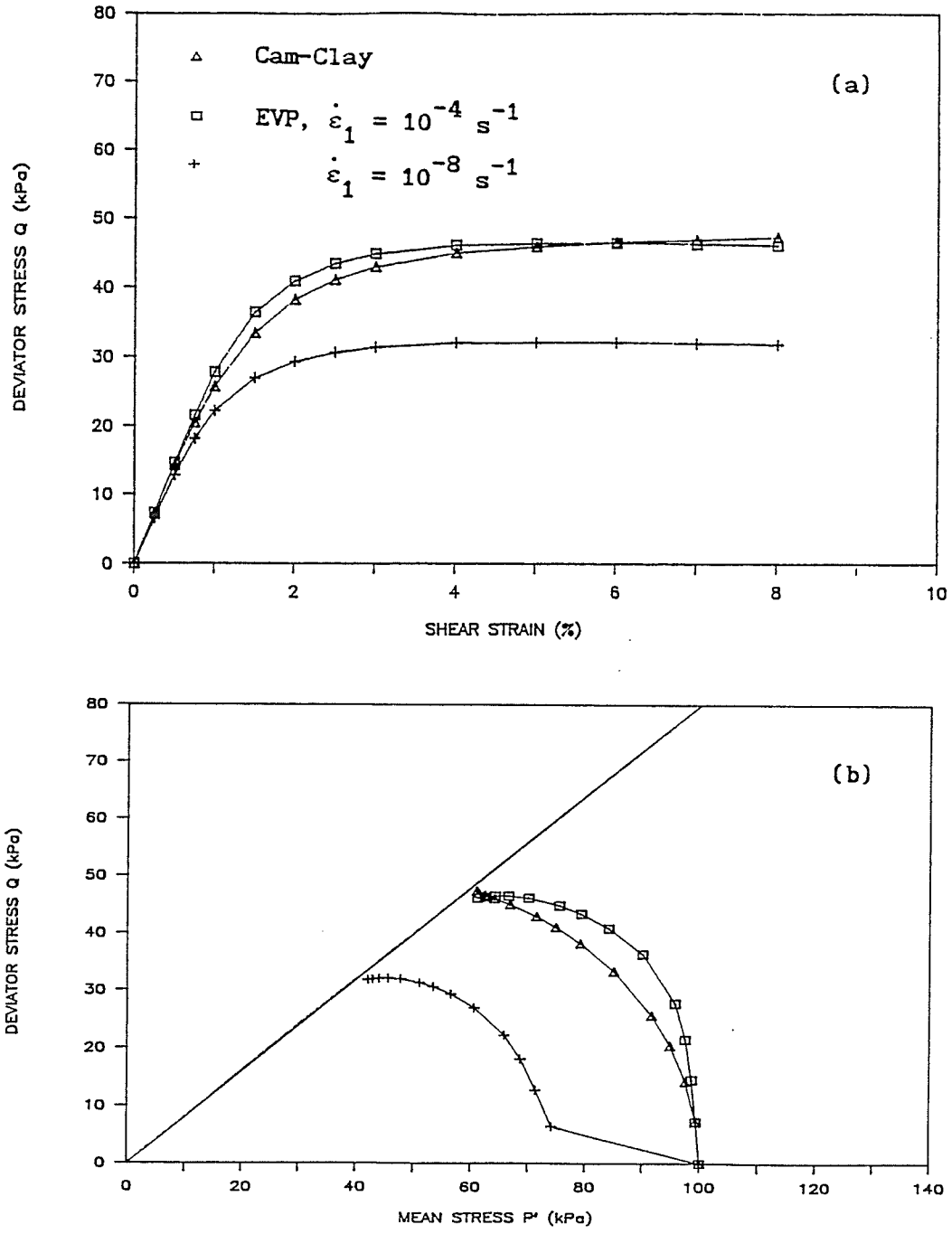

Fig.8.6 Simulation of a CI$\bar{U}$ test using modified Cam-Clay model and 3-D EVP model - Scaling Method 2, $\psi/V = 0.004$
(a) q vs. ε_s, (b) q vs. p'

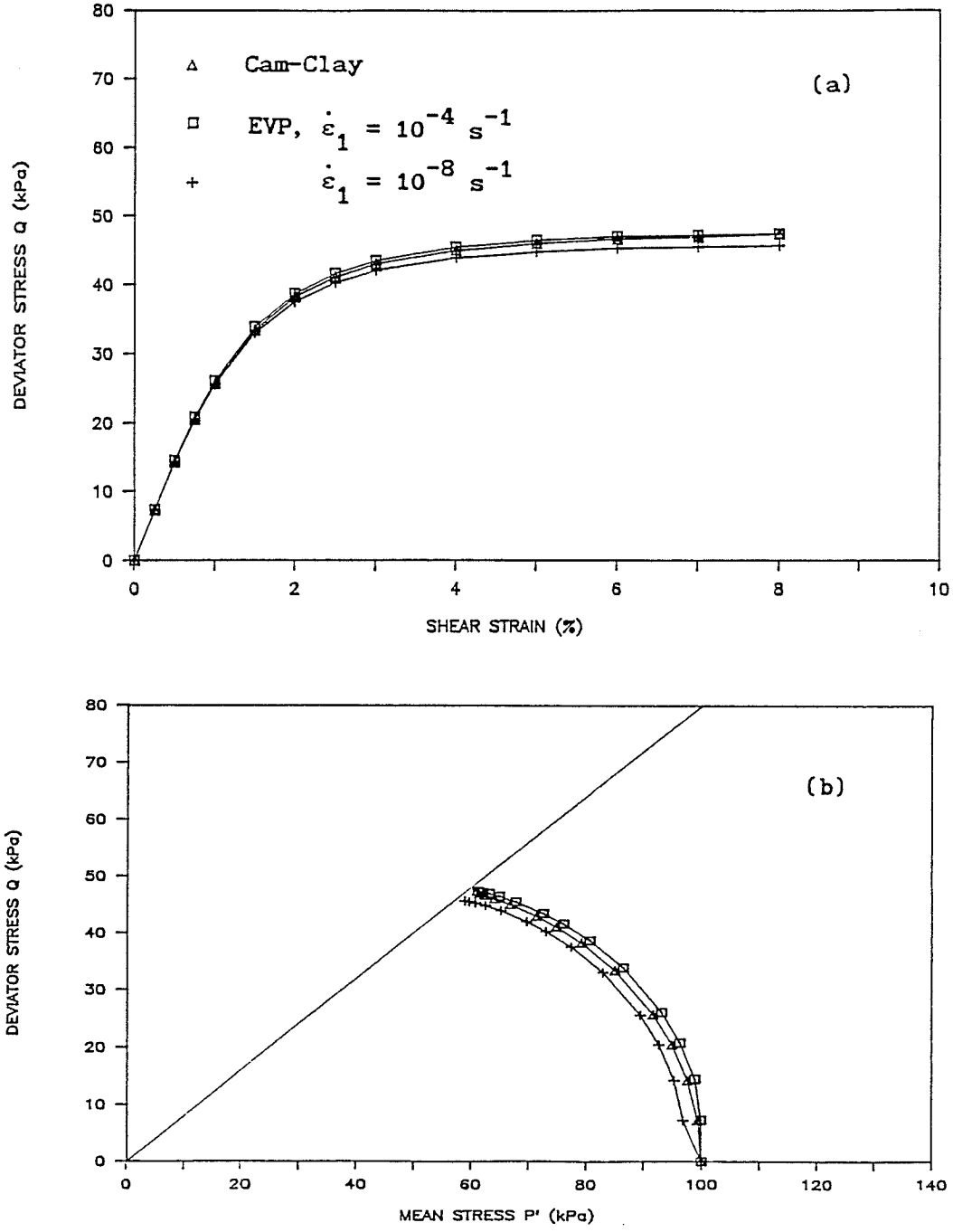

Fig.8.7 Simulation of a CI$\bar{U}$ test using modified Cam-Clay model and 3-D EVP model - Scaling Method 2, $\psi/V = 0.0004$ (a) q vs. ε_s, (b) q vs. p'

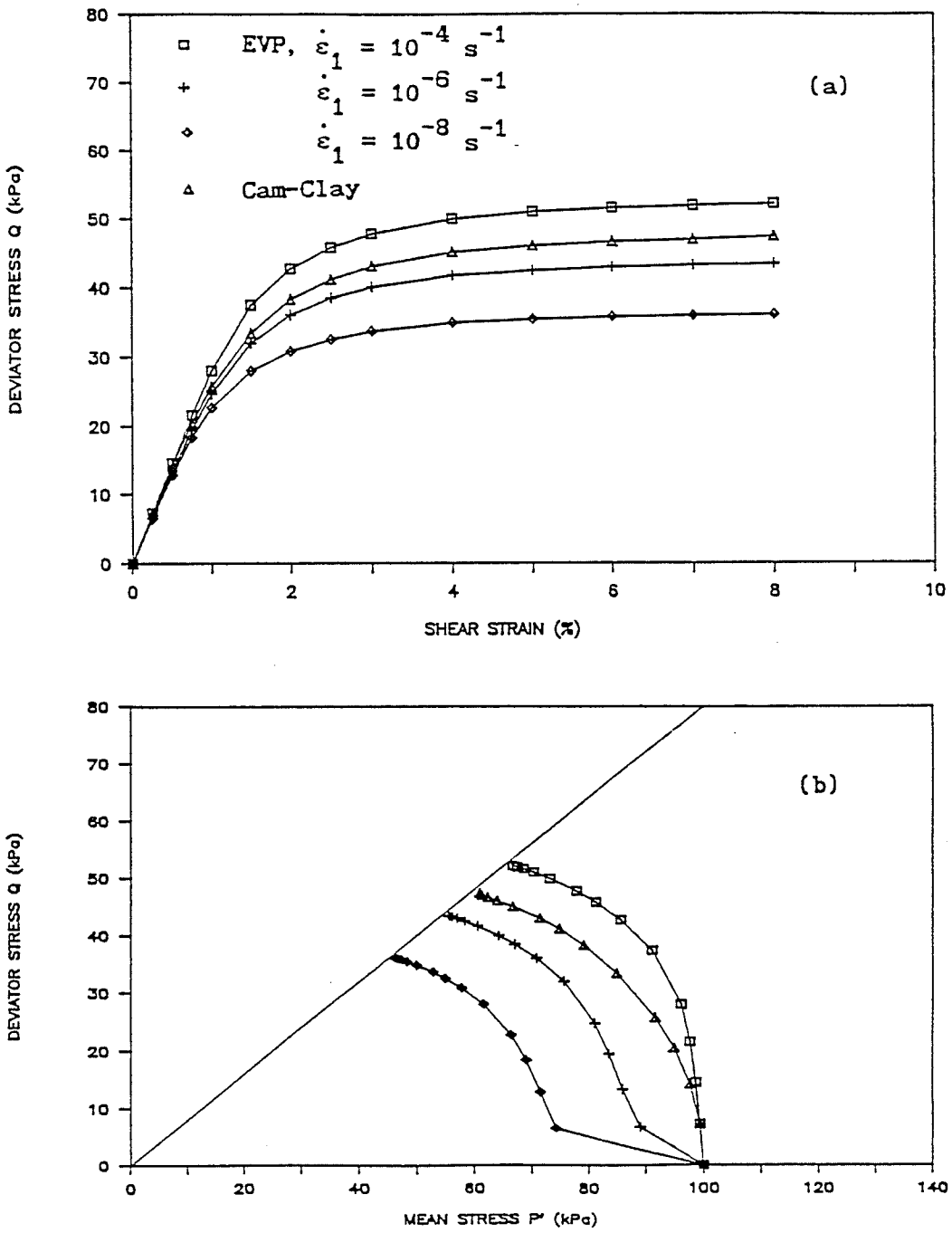

Fig.8.8 Simulation of a CIŪ test using modified Cam-Clay model and 3-D EVP model - Scaling Method 3, $\psi/V = 0.004$
(a) q vs. ε_s, (b) q vs. p'

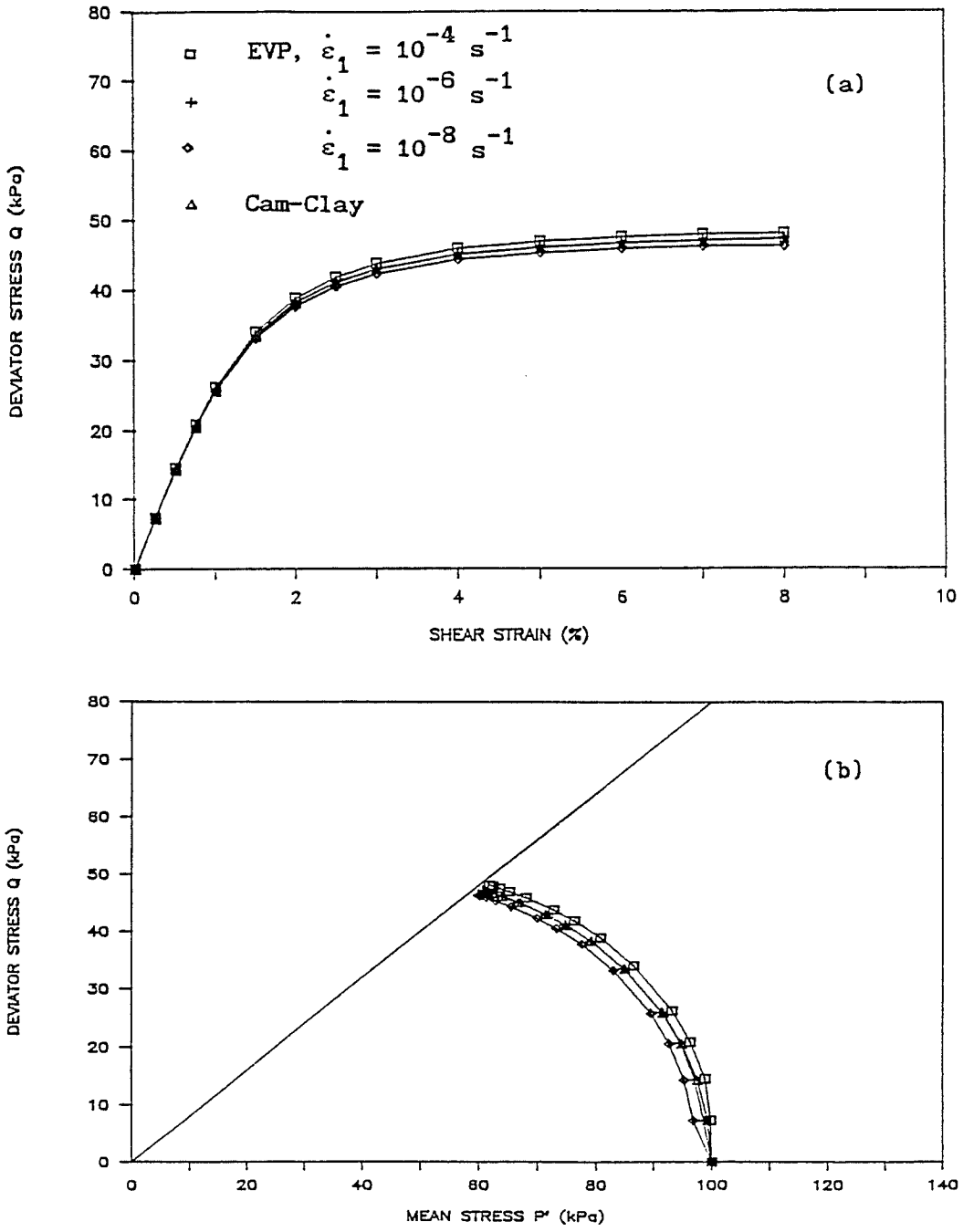

Fig.8.9 Simulation of a CIŪ test using modified Cam-Clay model and 3-D EVP model - Scaling Method 3, $\psi/V = 0.0004$
(a) q vs. ε_s, (b) q vs. p'

Chapter 9

ELASTIC VISCO-PLASTIC (EVP) MODELLING OF SAND-BENTONITE BUFFER MATERIAL

Chapter 8 developed the framework of 3-D elastic visco-plastic (EVP) models to simulate the time dependent stress-strain behavior of soils. In this Chapter, we apply this framework to the sand-bentonite buffer material that has been proposed for use in the Canadian Fuel Waste Management Program (see also Graham et al. 1989). An EVP model is developed for this material and calibrated using available test data. It is then verified using test data that has not previously been used in building the model.

9.1 Test Program and Results

A test program was performed by the author to collect additional test data from triaxial tests on the buffer material. These data have been combined with previous test results presented, for example, by Graham and Saadat (1987), Graham et al. (1989), and will be used for the calibration and verification of the proposed EVP model.

9.1.1 Preparation and properties of specimens

In specimen preparation, an improved compaction frame (Yarechewski 1988) was used to produce high density specimens at 95% ASTM Modified Standard Density, γ_d = 1.67 Mg/m^3 (Graham et al. 1988). The properties of specimens T1001, T1002 after compaction, are in Table 9.1. The targeted dry density was 1.67 Mg/m^3. As usual in experimental work, the measured values deviated from the targeted ones. In Table 9.1, the subscript "o" denotes the measured properties right after compaction of those specimens. The γ_{di} in Table 9.1 is the corrected dry density after installation of the specimen in triaxial cell, see Appendix 9.1.

Table 9.1 Properties of Specimens T1001 and T1002

Specimen	γ_{do} Mg/m^3	w_o %	S_{ro} %	e_o	V_o	γ_o Mg/m^3	G_s	γ_{di} Mg/m^3
T1001	1.678	22.33	99.04	0.6089	1.6089	2.053	2.7	1.517
T1002	1.696	20.63	94.10	0.592	1.592	2.046	2.7	1.685

9.1.2 Triaxial tests and results

The triaxial cells used in the program were Brainerd-Killman (B.K.) cells with capacity 3500 kPa. These were installed in an ELE loading frame with loading capacity 10,000 kg and a wide speed range, 0.00005

mm/min to 0.125 mm/min. An improvement in this test program in comparison with the previous test programs described by Sun (1986), Wan (1987) and Saadat (1989) was that a double drainage system was used in the B.K. cells. The advantages of such a drainage system are:

(1). In consolidation or drained tests, if both top and bottom ends are allowed to drain, the process of consolidation or porewater pressure dissipation can be accelerated. If only the top end is drained, then the bottom end can be closed and used to measure porewater pressure at the bottom of the specimen. In this way, the process of porewater pressure dissipation can be monitored.

(2). In undrained shear tests, the two drains are closed and used to measure the porewater pressure.

In the test program, two types of shear tests were designed, one was a multi-stage q creep shear test under undrained condition (on specimen T1001). The second was a step-changed constant strain rate shear test under undrained condition (on specimen T1002). The two specimens were first isotropically consolidated for a long time under multi-stage isotropic pressures (184.5 days for T1001 and 217.5 days for T1002). The resulting consolidation data will be used to determine the scaling function in the EVP model. The undrained shear test data will be used mostly to examine the validation of the EVP model.

9.1.2.1 Isotropic consolidation tests

As mentioned in the preceding paragraph, specimens T1001 and T1002 were isotropically consolidated using multi-stage loading. The back pressure used was 500 kPa. The principal results of the consolidation tests are in Table 9.2 and complete details are given in Appendix 9.2. In Table 9.2, the consolidation pressure $p_{con} = \sigma_3 - u_b$, the excess porewater pressure $\Delta u = u - u_b$, where σ_3 is the cell pressure, u_b is the back pressure, u is the porewater pressure. In the test program, the same filter paper strips (Whatman #1) as used in previous tests (Sun 1986, Wan 1987, Saadat 1989) were put on the lateral surface of the specimen for radial drainage. However, It has been found by James M. Oswell (personal communication) that the permeability of the filter paper strips is very low and impermeable at pressures higher than 800 kPa. It was assumed that the relationship between the back pressure applied at the top of the specimen and the porewater pressure measured at the bottom is parabolic, and the effective mean stress p' values in Table 9.2 were estimated from the relationship $(p_{con} - \frac{2}{3}\Delta u)$.

Table 9.2 Results of Isotropic Consolidation Tests

Specimen	p_{con} kPa	t hour	ε_v %	Δu kPa	p' kPa
T1001	200	227.6	-13.85		200
	800	1558.4	-7.15	-285	990
	3000	2642.9	1.88	468	2688
T1002	200	231.4	-10.13	4	197.3
	1000	2955.3	-1.82	30	980
	3000	2034.1	2.62	89	2940.7

During specimen preparation, there are usually some deviations from the targeted dry density and the saturation is not 100 %. Furthermore when installing specimen in the test cells, the dry density of specimens might be changed. Appendix 9.1 presents a technique for the calculation of volumetric strains considering these variations in dry density and unsaturation. The ε_v values in Table 9.2 are the corrected values.

Figs.9.1-9.3 show the curves of volumetric strain vs. time (ε_v vs. t) and excess porewater pressure vs. time (Δu vs. t) for specimen T1001. Figs.9.4-9.6 show the same curves for specimen T1002. The data of volumetric strain vs. effective mean stress (ε_v vs. p') at the final stage of each multi-stage loading are shown in Figs.9.9 and 9.8. In Fig.9.2, the porewater pressure was negative but the volumetric strain was increasing. It was subsequently found that the hole accessing the porewater pressure transducer was blocked and the negative porewater

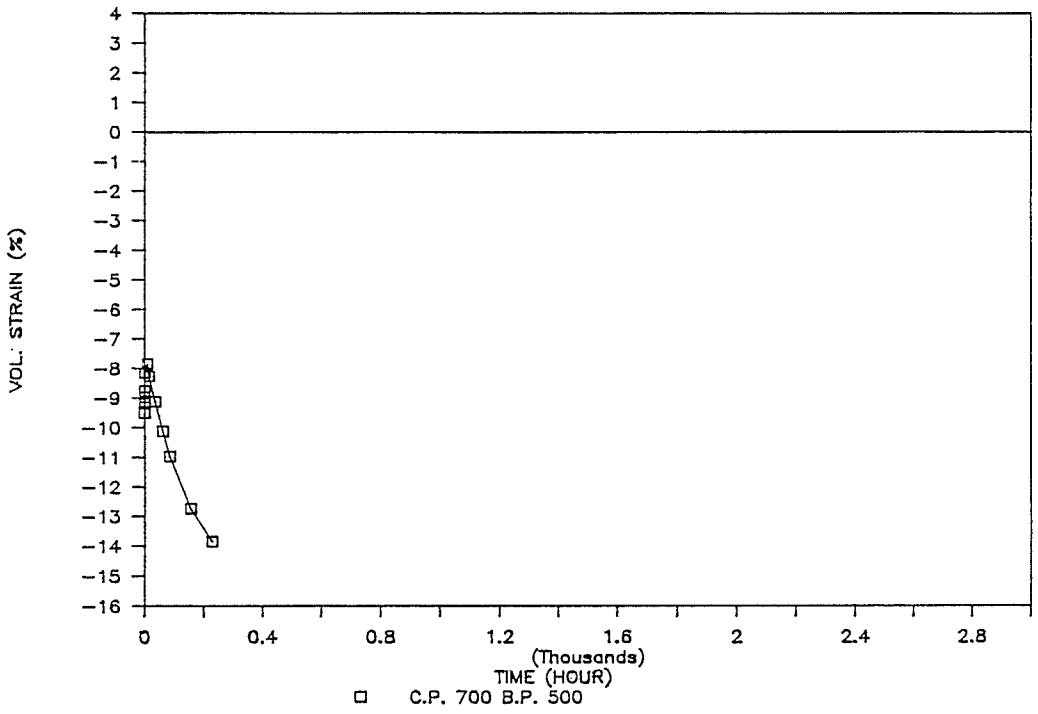

Fig.9.1 Isotropic consolidation test - T1001, p_{con} = 200 kPa, ε_v, t-relationship

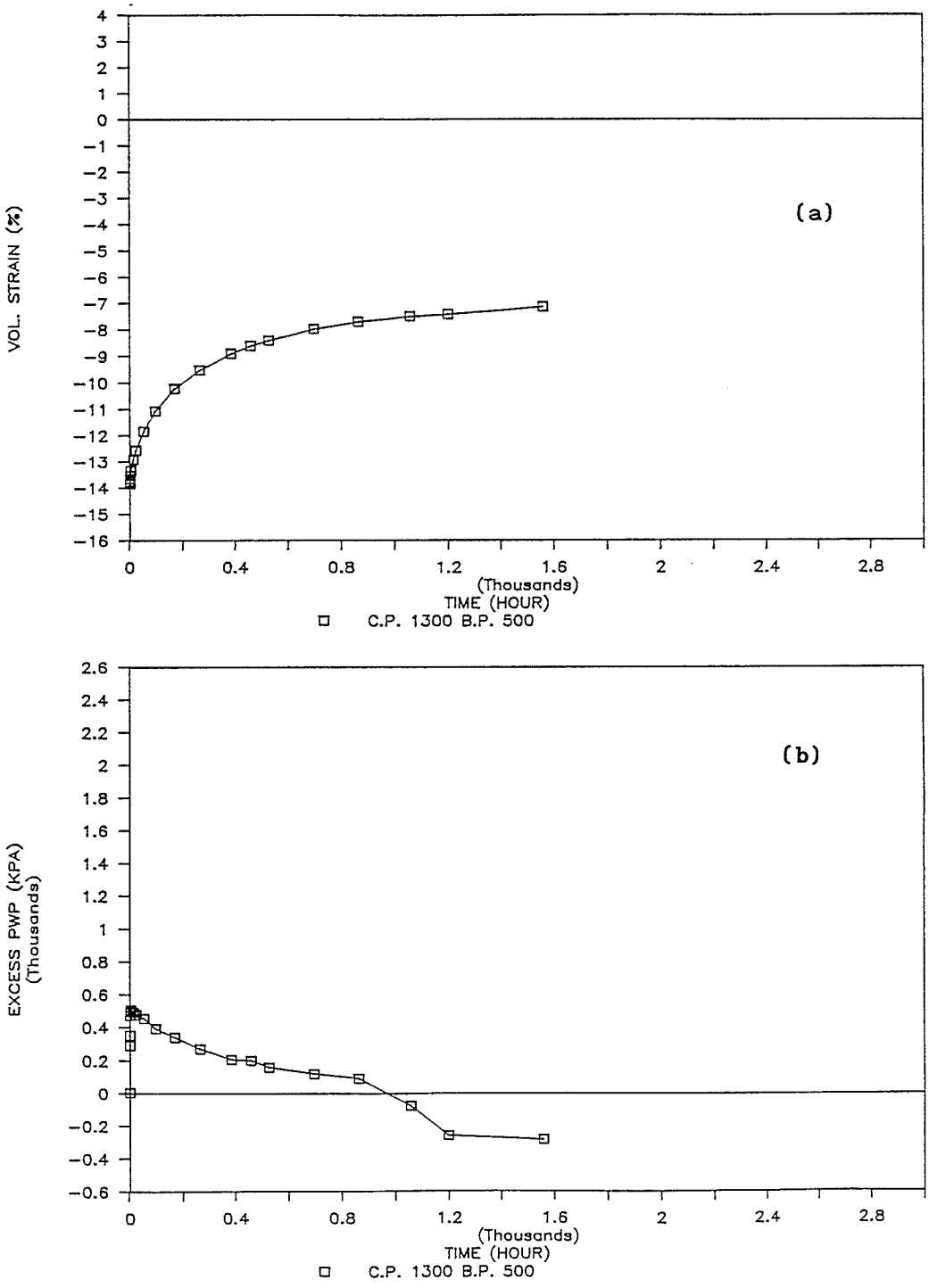

Fig.9.2 Isotropic consolidation test - T1001, p_{con} = 800 kPa, (a) ε_v, t-relationship, (b) Δu, t-relationship

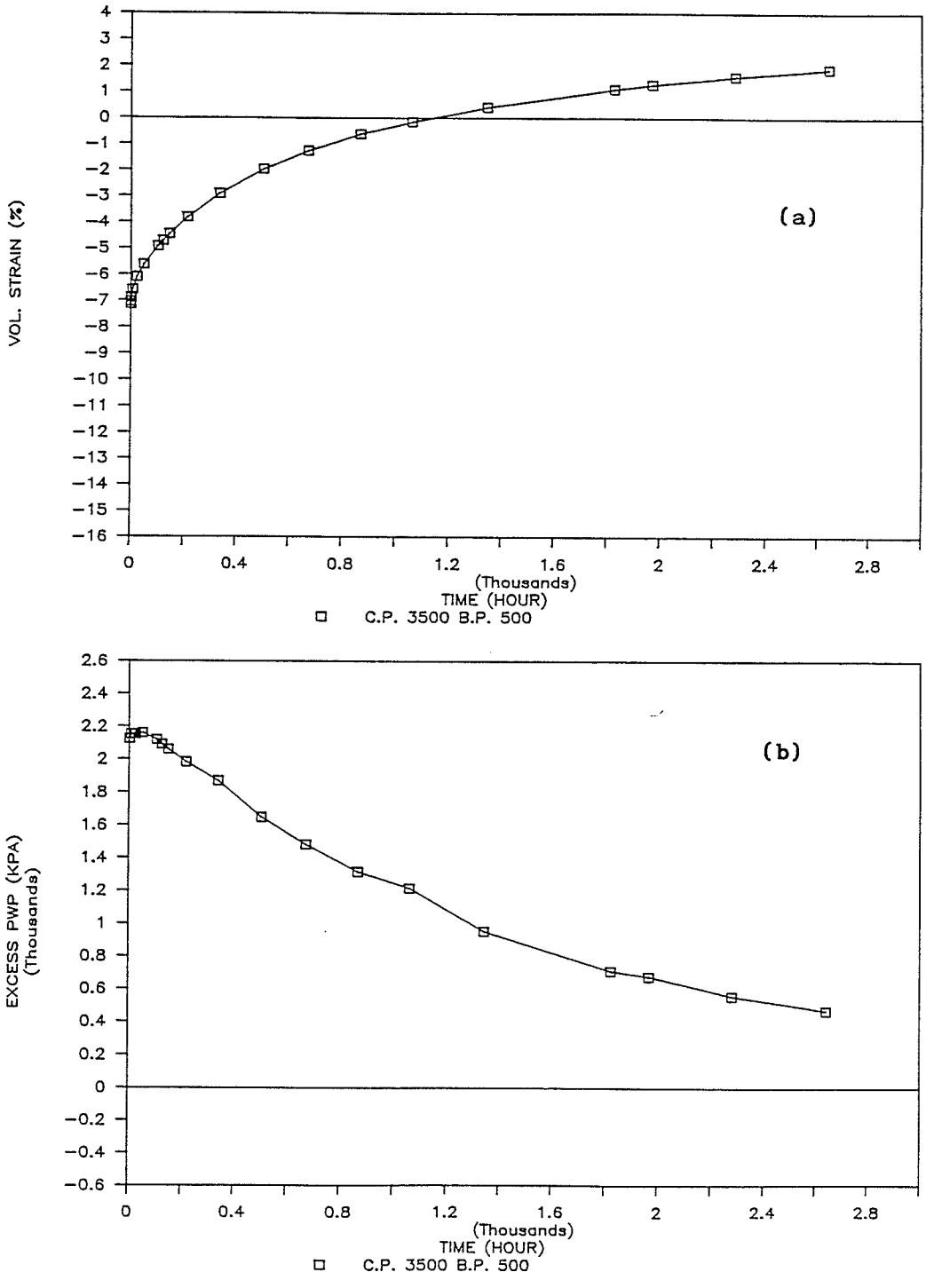

Fig.9.3 Isotropic consolidation test - T1001, p_{con} = 3000 kPa, (a) ε_v, t-relationship, (b) Δu, t-relationship

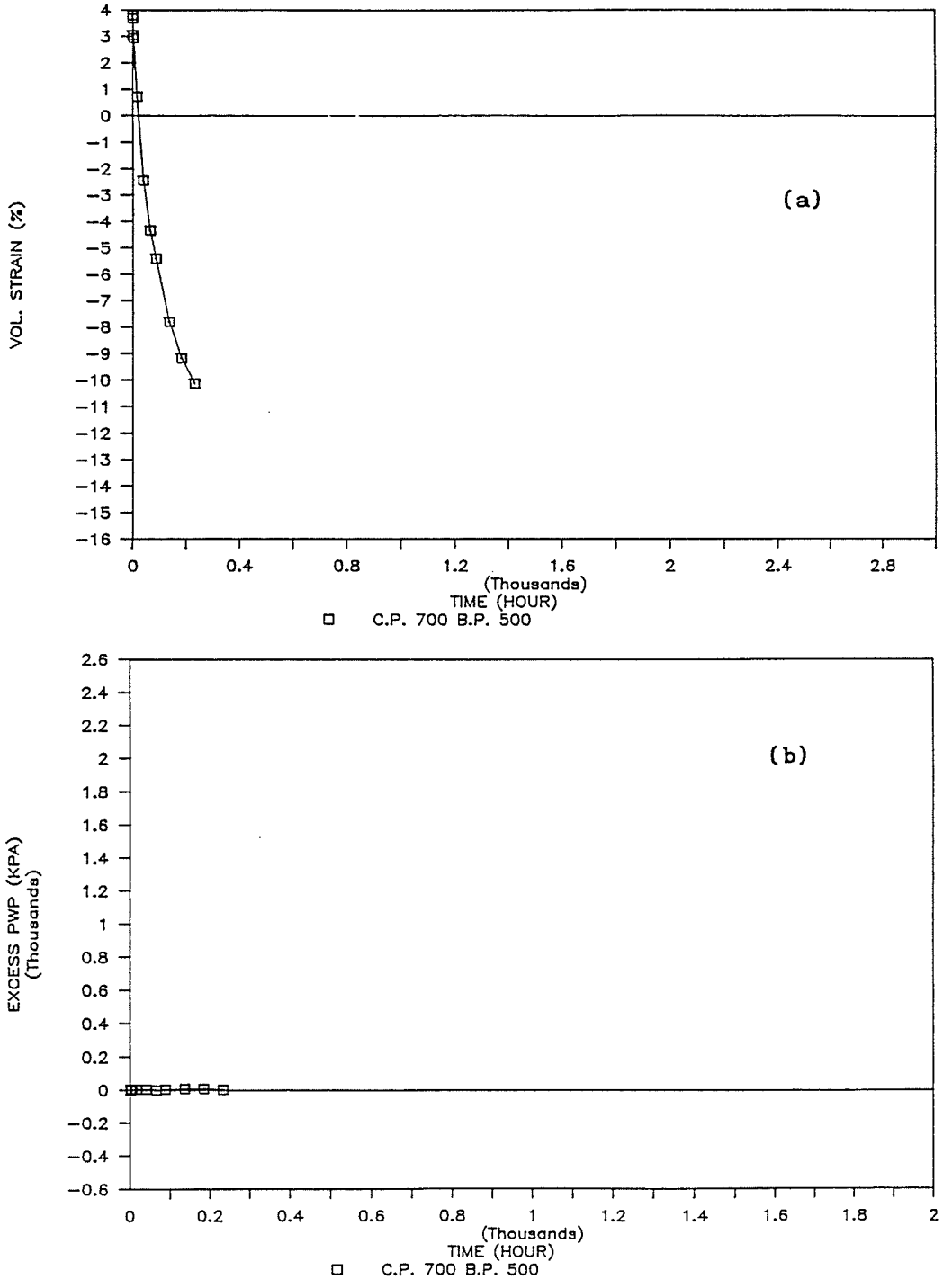

Fig.9.4 Isotropic consolidation test - T1002, p_{con} = 200 kPa, (a) ε_v, t-relationship, (b) Δu, t-relationship

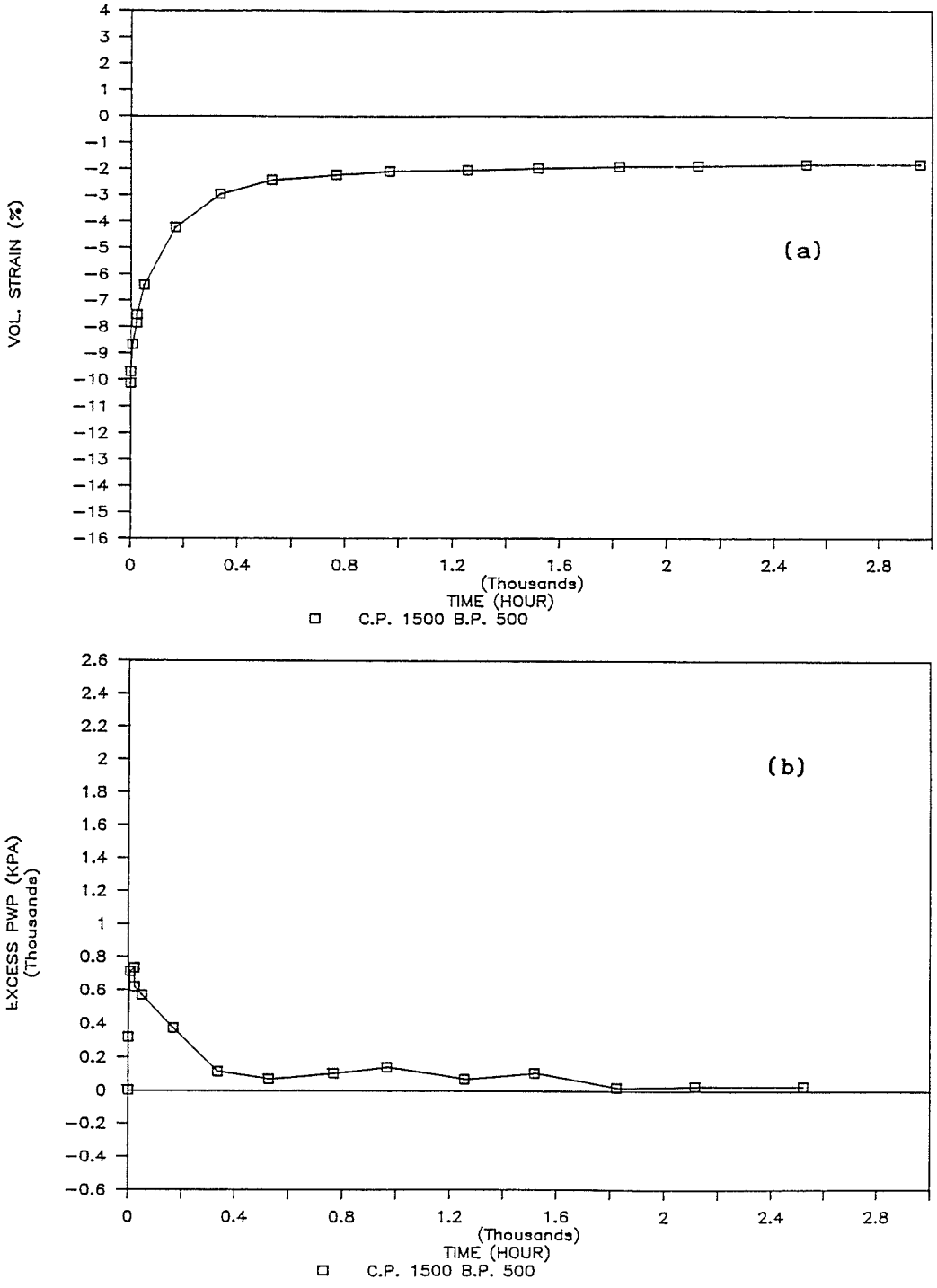

Fig.9.5 Isotropic consolidation test - T1002, p_{con} = 1000 kPa, (a) ε_v, t-relationship, (b) Δu, t-relationship

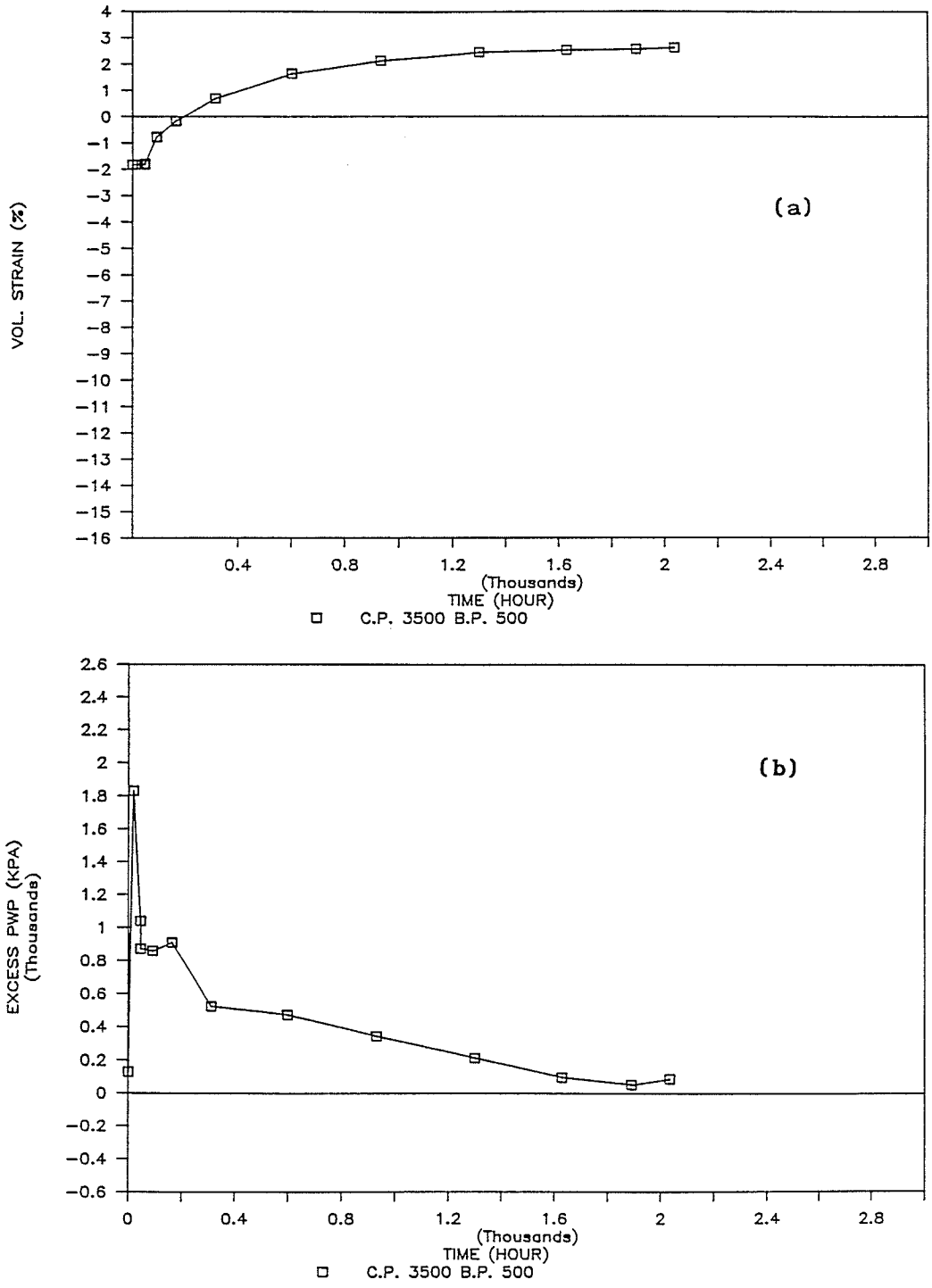

Fig.9.6 Isotropic consolidation test - T1002, p_{con} = 3000 kPa, (a) ε_v, t-relationship, (b) Δu, t-relationship

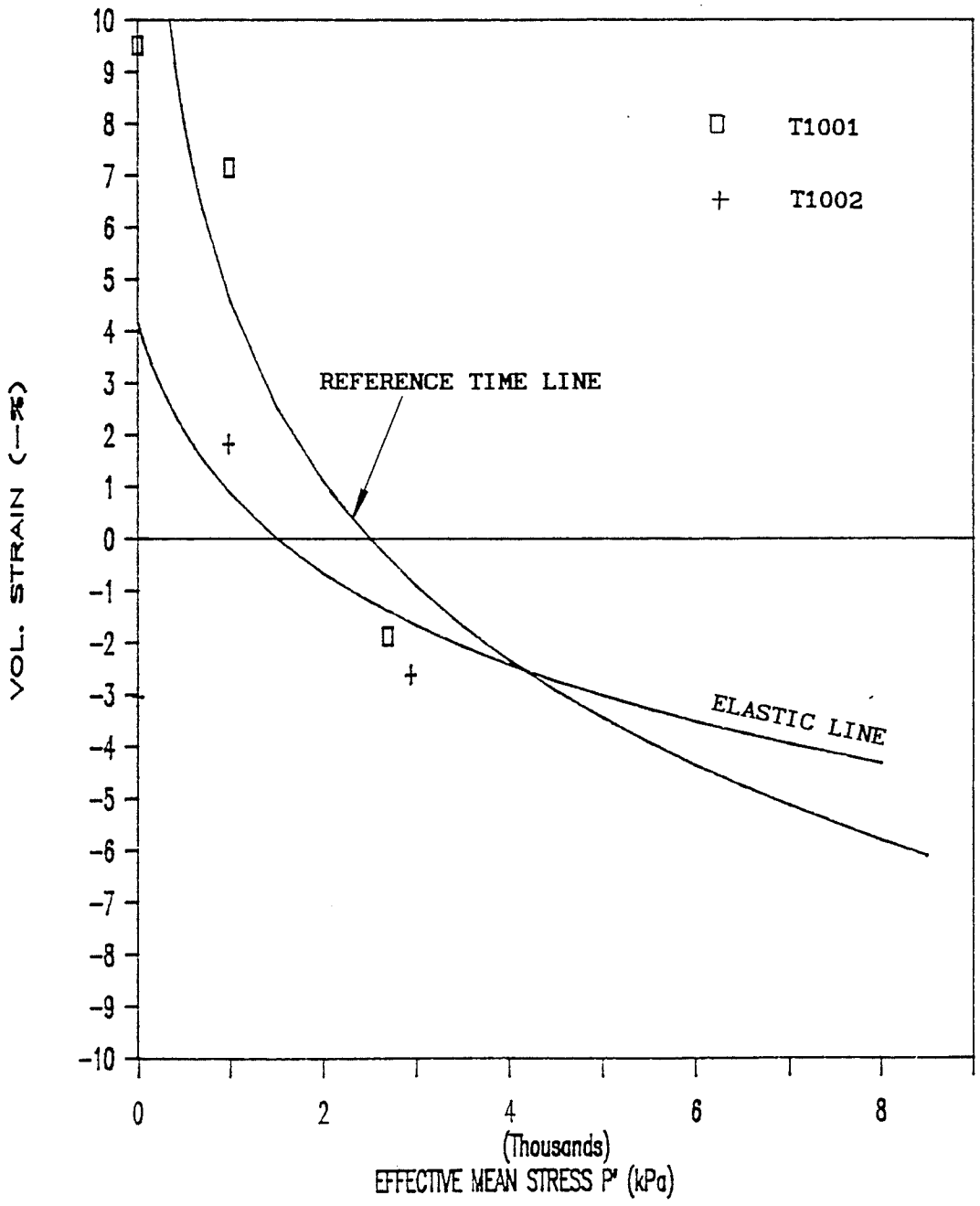

Fig.9.7 p',ε_v-relationship, elastic line and reference time line

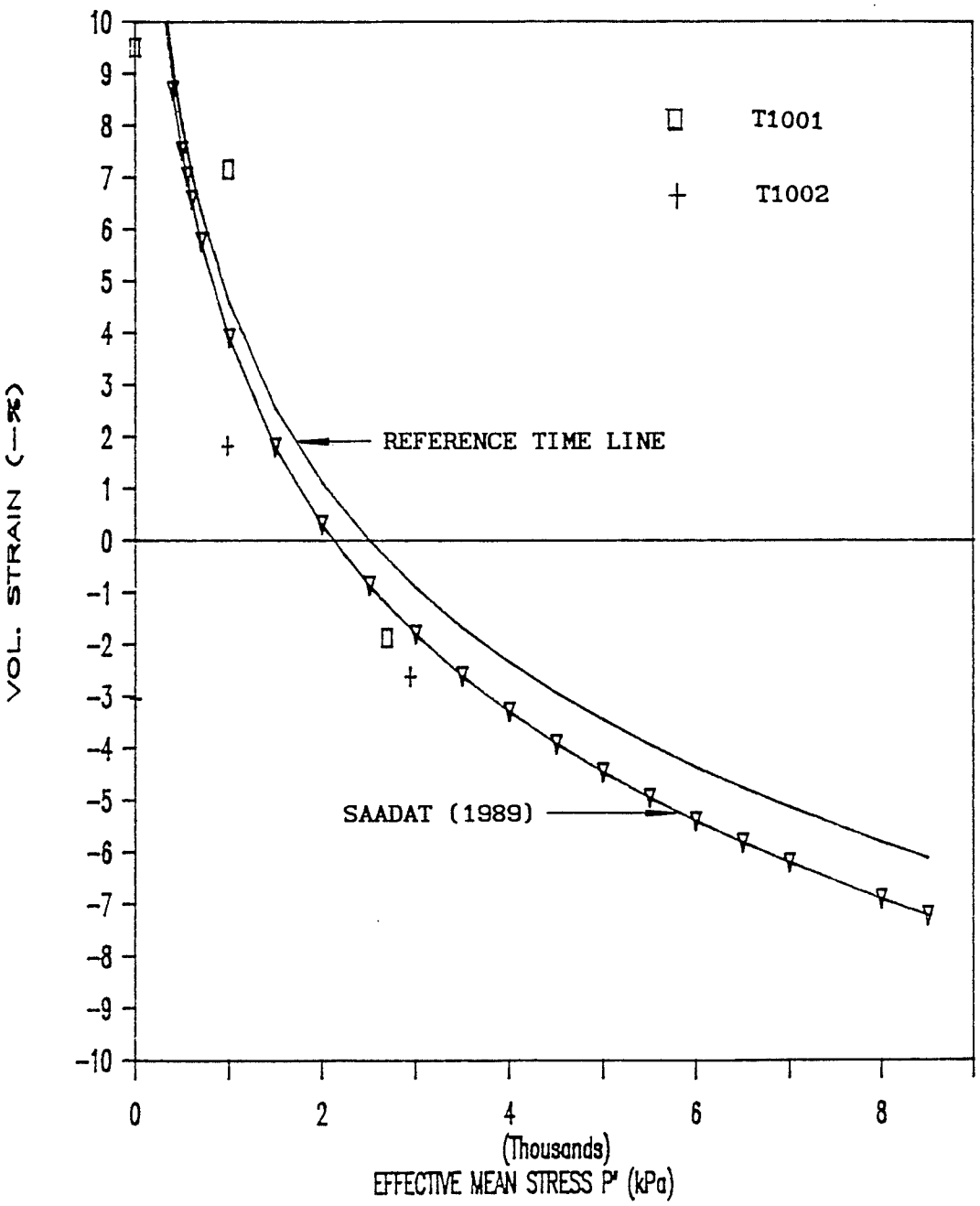

Fig.9.8 Comparison of reference time line and equation by Saadat (1989)

pressures seem to be related to temperature changes rather than to swelling potential. In Fig.9.5, the excess porewater was close to zero and the volumetric strain approaches a constant. However, in both specimens, there were some residual excess porewater pressures left at the final stage of consolidation. In T1001, there was 468 kPa left after 2642.9 hours of consolidation, while in T1002 there was 89 kPa left after 2034.1 hours of consolidation.

9.1.2.2 Triaxial shear tests

In specimen T1001, after multi-stage isotropic consolidation, there was 468 kPa excess porewater pressure at the bottom end of the specimen but of course zero at the top end where the back pressure was applied. The porewater pressure distribution was not uniform. If shearing then commenced immediately, we could not measure the true response of porewater pressure, since the distribution of porewater pressure would be changing as a result of the initial porewater gradients and shear-induced porewater pressures. In order to equalize the initial porewater pressures, the drainage valve at the top was closed, and the specimen was relaxed for 213.3 hours under undrained conditions. At the end of this relaxation, the porewater pressure at the top was the same as the pressure at the bottom, with an excess porewater pressure magnitude of 1045 kPa. The specimen was then sheared by applying multi-stage constant deviator stresses under undrained conditions. At each stage, the deviator stress increment was

applied suddenly, then was kept constant, and delayed compression movements were allowed to occur. Due to the increase in section area of the specimen, the deviator stress decreased by small amounts. The complete test data of this test are presented in Appendix 9.2.

Fig.9.9 shows the curves of shear strain vs. time (ε_s vs. t) and excess porewater pressure vs. time (Δu vs. t) for deviator stresses 315.7, 686.8, 866.0, 1041.9, 1077.0 kPa respectively. The following characteristics are found:

(1). For each suddenly applied deviator stress, there were "instant" responses of shear strain and porewater pressure. These may be treated as time-independent behavior.

(2). The rates of shear strain $\dot{\varepsilon}_s$ changes decreased with time for q = 315.7, 686.8 and 866.0 kPa. So did the excess porewater pressure changes Δu, except for some scatter of $\Delta u, t$ data for q = 686.8 kPa. This means the specimen will not fail due to delayed straining when the deviator stress is below 866.0 kPa.

(3). When q = 1041.9 kPa, the rate $\dot{\varepsilon}_s$ increased with time in the final stage of loading. The specimen exhibited accelerating creep and this is a definition of failure (Vaid and Campanella 1977). The corresponding rate $\Delta\dot{u}$ decreased with time, indicating the specimen was tending to expand during shear.

(4). When q was increased to 1077.0 kPa, the rate $\dot{\varepsilon}_s$ was increased further and failure followed after about 30 minutes.

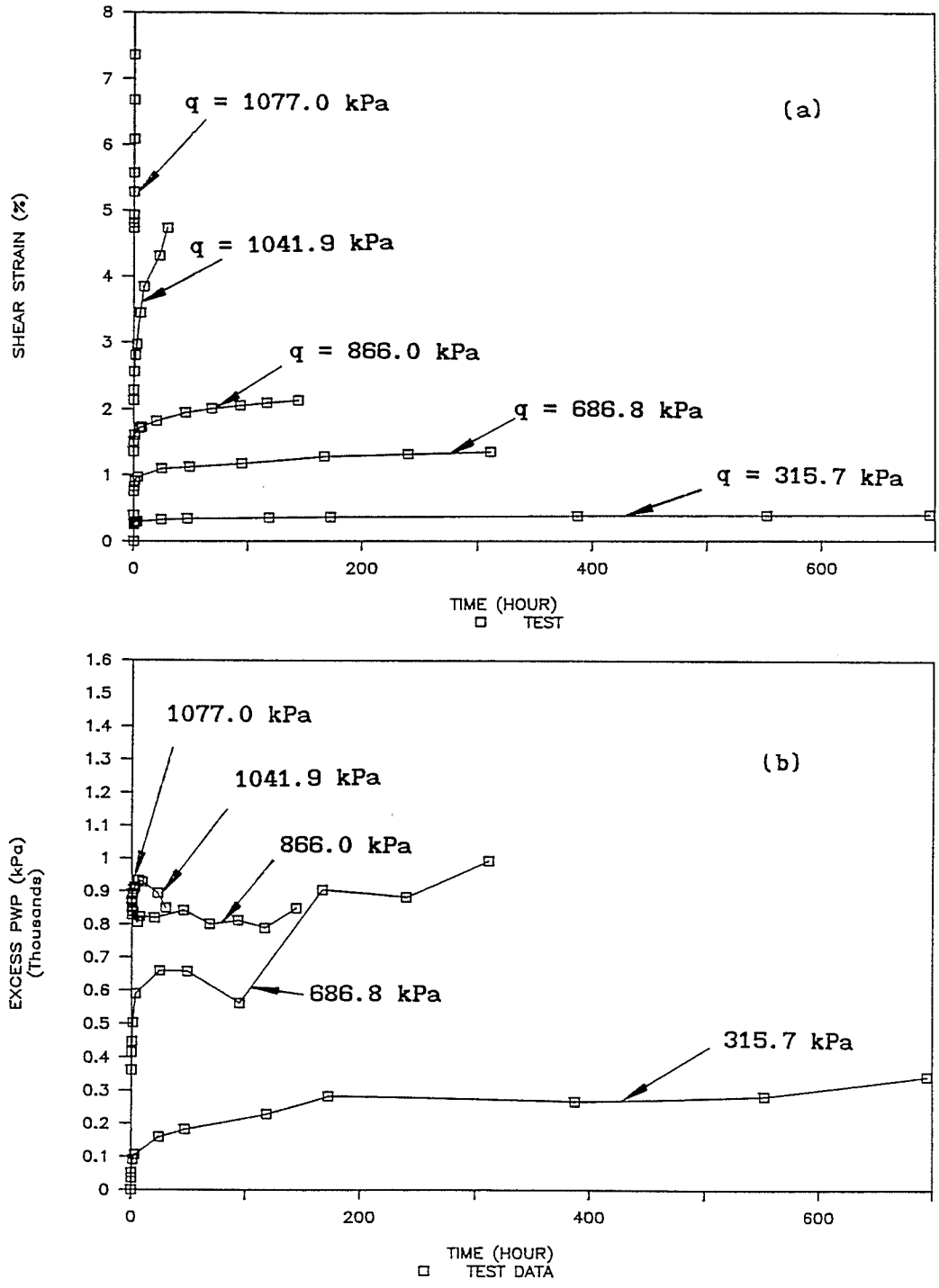

Fig.9.9 Undrained multi-stage q creep shear test - T1001, (a) ε_s,t-relationship, (b) Δu,t-relationship

Fig.9.10 shows the effective stress path in the test. It is noted that the instantaneous effective stress paths responding to the suddenly applied deviator stresses, were not vertical, but inclined to right side ($\Delta q/\Delta p' > 0$) in q,p'-space. The ratios of $\Delta q/\Delta p'$ for q = 315.7 and 686.8 kPa were 3.636 and 2.667 respectively. We know that if the elastic behavior of a soil is isotropic, the instant effective stress paths would be vertical, namely $\Delta q/\Delta p' = \infty$. The instantaneous effective stress paths measured in the test indicated that the time-independent behavior is anisotropic. This result is consistent with some findings reported by Graham and Saadat (1987) and Graham et al (1989).

In specimen T1002, at the end of consolidation, there was only 89 kPa excess porewater pressure left. In order to make the distribution of porewater pressure in the specimen uniform, the specimen was isotropically relaxed for 32.5 hours after consolidation under undrained conditions. After relaxation, the excess porewater pressure increased to 306.6 kPa. The effective mean stress p' at this stage was 2693.4 kPa. The specimen was then sheared using step-changed constant strain rates under undrained condition. The strain rates used were 0.00036 h^{-1}, 0.0058 h^{-1} and 0.094 h^{-1}. The complete test data for this specimen are in Appendix 9.2

Fig.9.11 shows the curves of deviator stress vs. shear strain (q vs. ε_s) and excess porewater pressure vs. shear strain (Δu vs. ε_s) for the

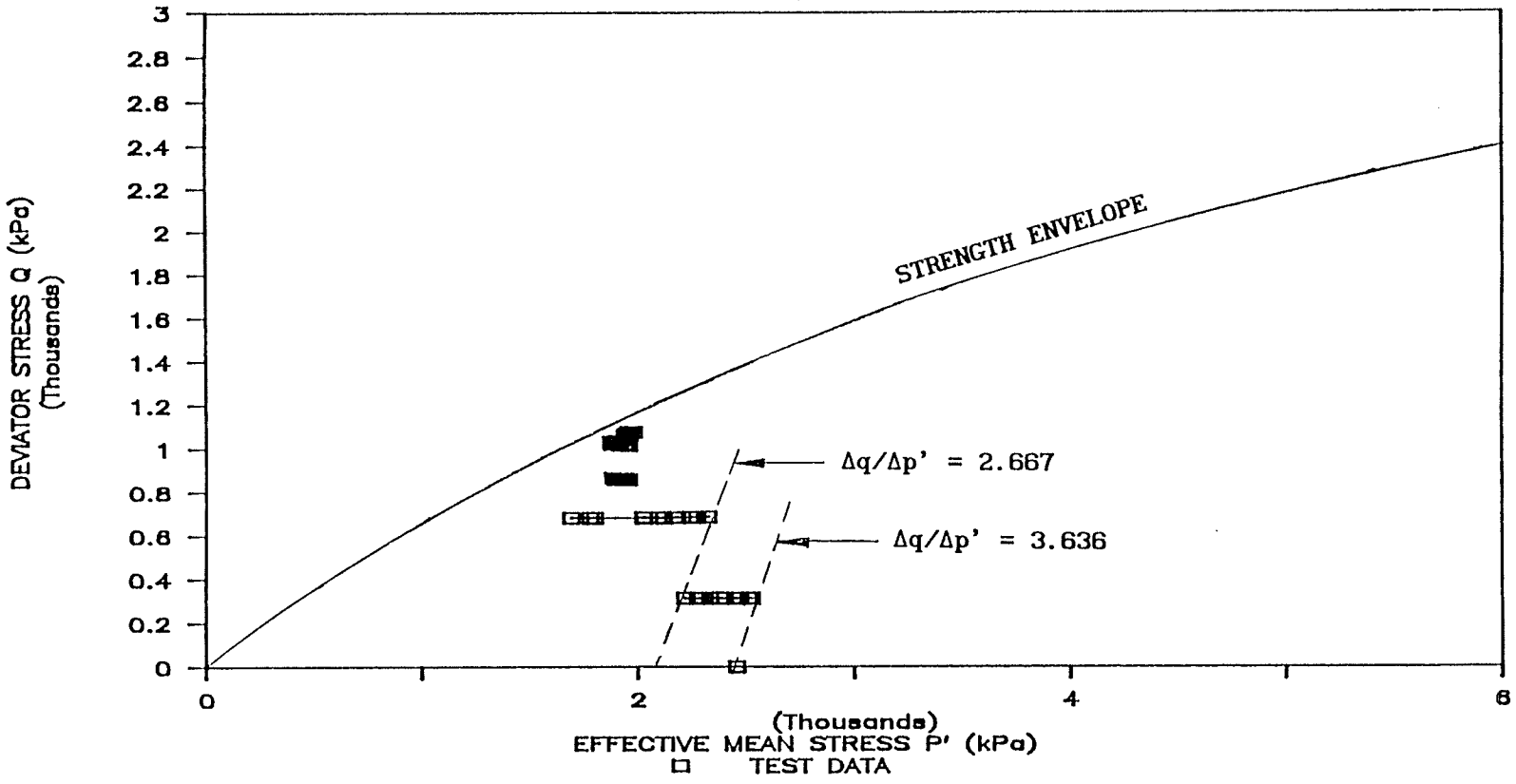

Fig.9.10 Effective stress path - T1001

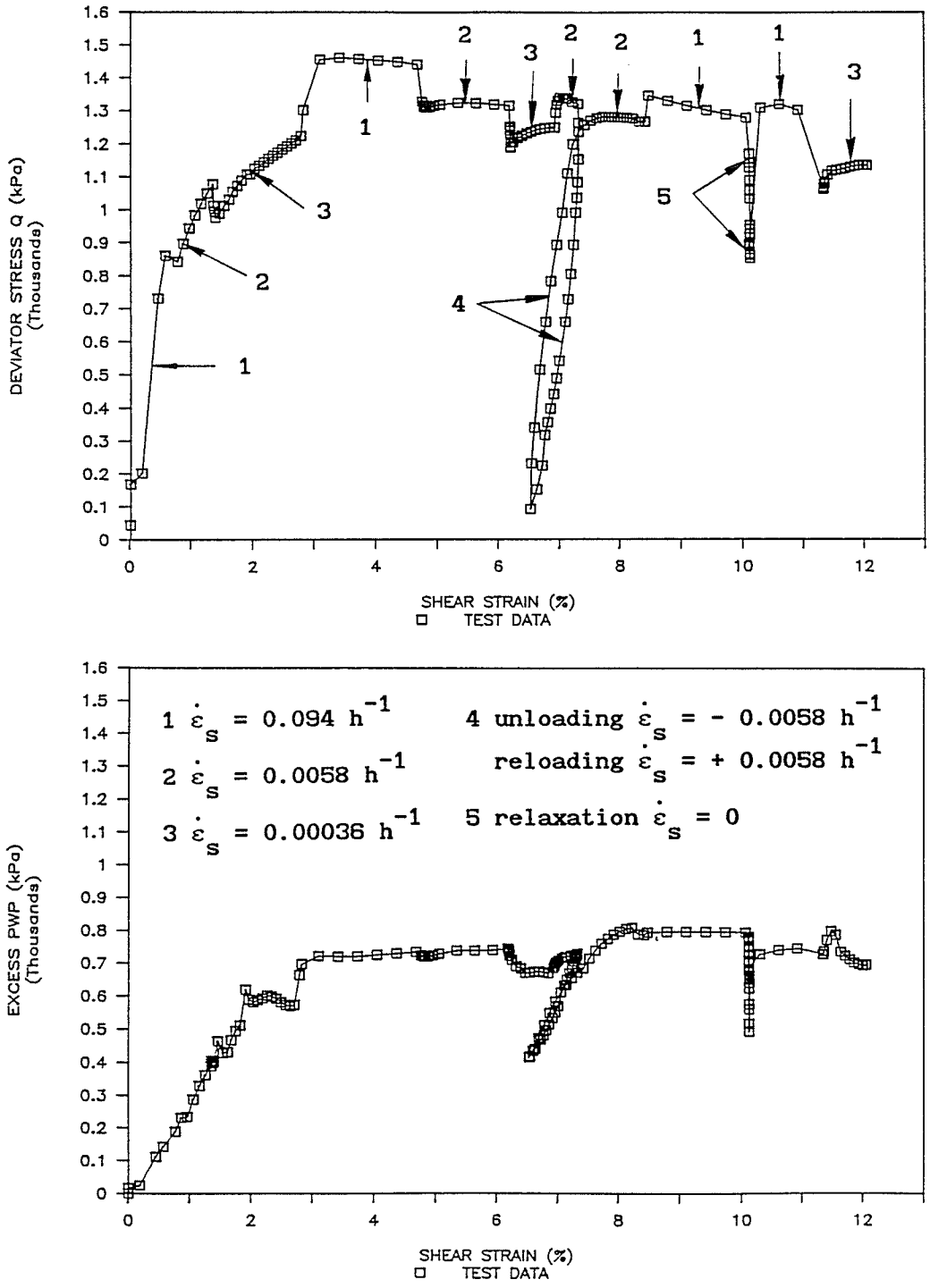

Fig.9.11 Undrained step-changed constant strain rate test - T1002, (a) q, ε_s-relationship, (b) $\Delta u, \varepsilon_s$-relationship

test. In the test, the specimen was unloaded and reloaded at ε_s = 7.31 % with strain rate $\dot{\varepsilon}_s$ = -0.0058 1/h for unloading and 0.0058 1/h for reloading, see Fig.9.11. At ε_s = 10.06 %, the driving machine was shut off and the specimen was relaxed for 46.6 hours. During shear relaxation, the deviator stress decreased with time and approached a constant, see Figs.9.11 and 9.12.

The effective stress path of the test is shown in Fig.9.13. It is found that the first part of effective stress path in the undrained shear was straight and inclined to the right side. The ratio of $\Delta q/\Delta p'$ for this part was 5.455. The effective stress path in unloading and reloading was also inclined towards the right side on average. The ratio of $\Delta q/\Delta p'$ in the unloading/reloading was 12.903. All of this indicated again that the time-independent behavior of the high density specimens is anisotropic.

9.2 EVP Model and Its Calibration

This section develops an EVP model for the sand-bentonite buffer material using the framework given in Chapter 8 and considering the characteristics of the material measured in T1001 and T1002. The scaling function will be determined using the data from isotropic consolidation. The strength envelope for the model is taken from previous test results given by Graham and Saadat (1987) and Graham et al. (1989).

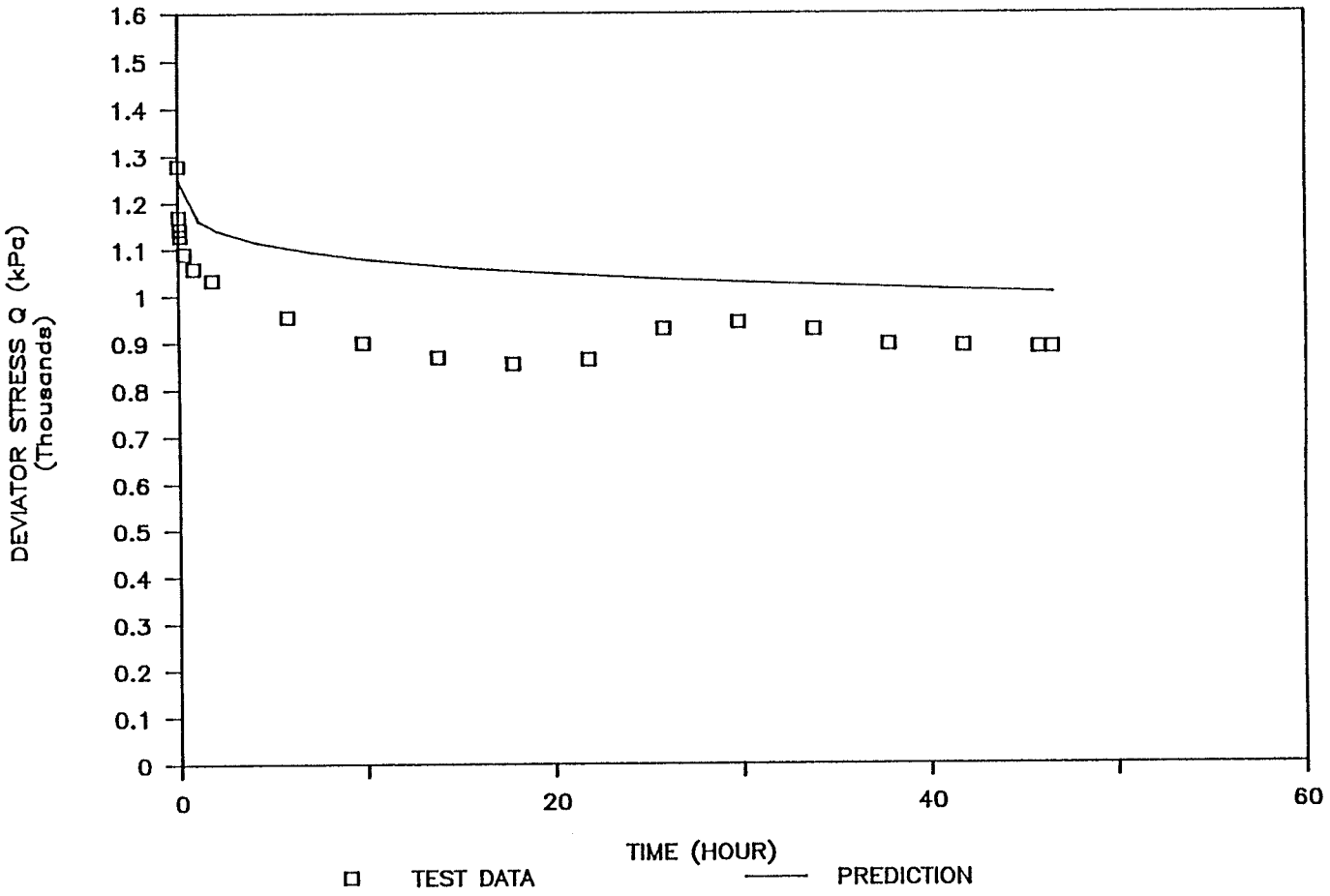

Fig.9.12 Measured and predicted q,t-relationships in relaxation - T1002

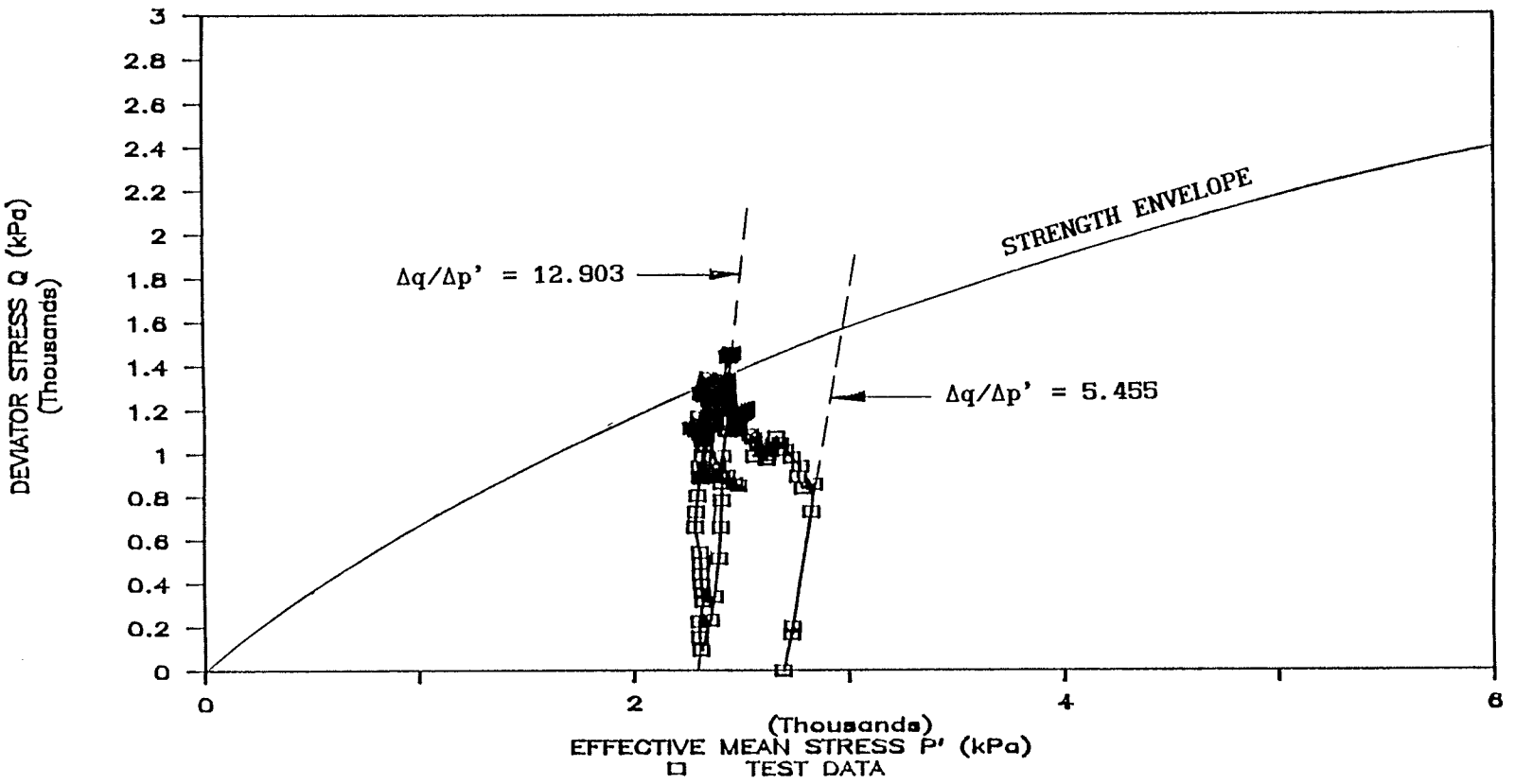

Fig.9.13 Effective stress path - T1002

9.2.1 Equations of EVP model

As discussed in the previous section, the effective stress paths of time-independent behavior of the high density specimens (T1001 and (T1002) were straight and inclined to right side ($\Delta q/\Delta p' > 0$) in undrained shear conditions, (see Figs.9.10, 9.13). This type of effective stress path can also be found in Fig.9.14 (Graham and Saadat, 1987) and Fig.9.15 (Graham et al, 1989). However in these Figures, more effective stress paths turn to left side ($\Delta q/\Delta p' < 0$). This may be explained by (1) excess porewater pressures remaining after consolidation that were not measured and corrected in the plots; (2) the dry density was low so that the initial state was close to normally consolidated states and visco-plastic behavior dominated the effective stress paths. Graham et al. (1989) say that these specimens are at "Swelling Equilibrium". That the ratio of $\Delta q/\Delta p'$ is larger than zero implies that deviator stresses produce negative volumetric strains i.e. a tendency to shear- expansion in constant-volume tests.

The KGJ model developed in Chapter 4 can be employed to describe the anisotropic time-independent behavior. Here, we make the same assumption used earlier, that total strain rates are the sum of time-independent strain rates and visco-plastic strain rates. Referring to Eqns.[8.1], [8.3] and [8.12], the constitutive equation for triaxial stress states can then be expressed as:

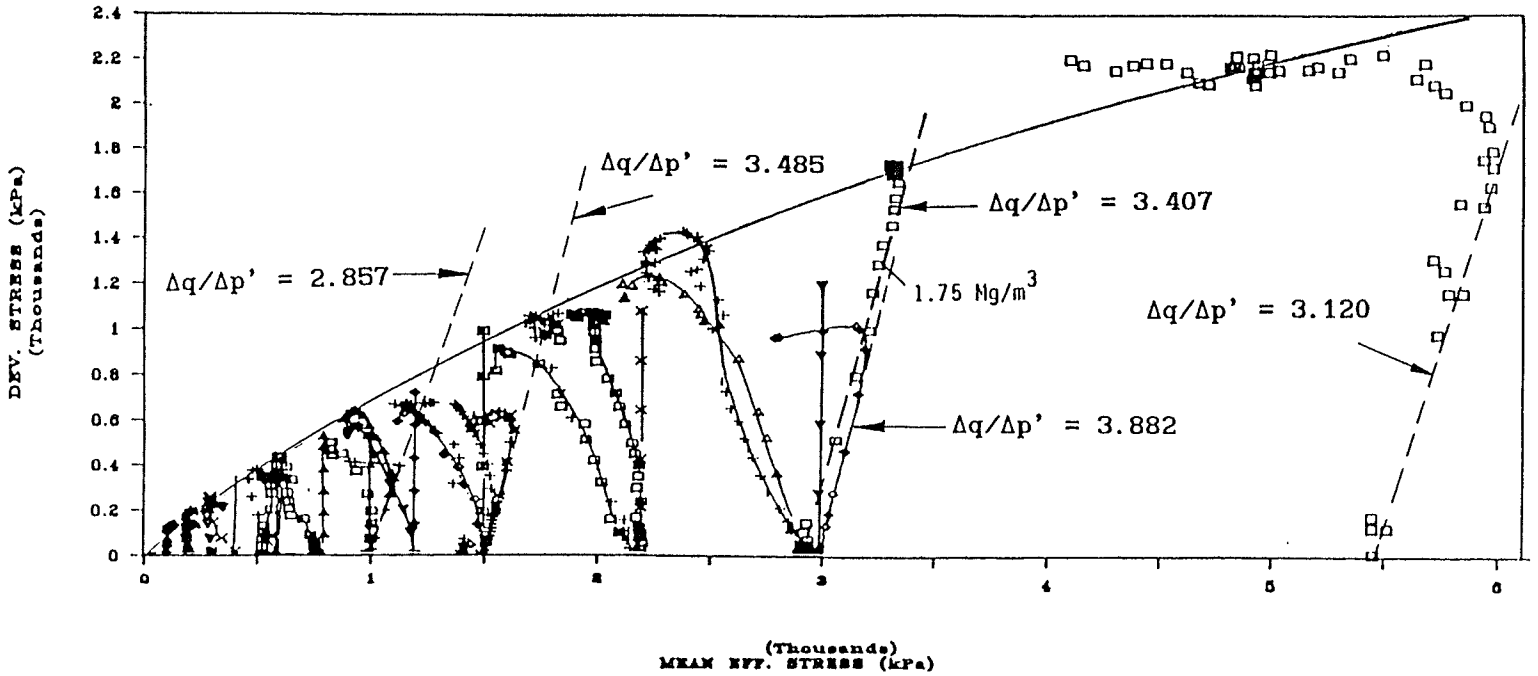

Fig.9.14 Effective stress paths and strength envelope
(after Graham and Saadat 1987)

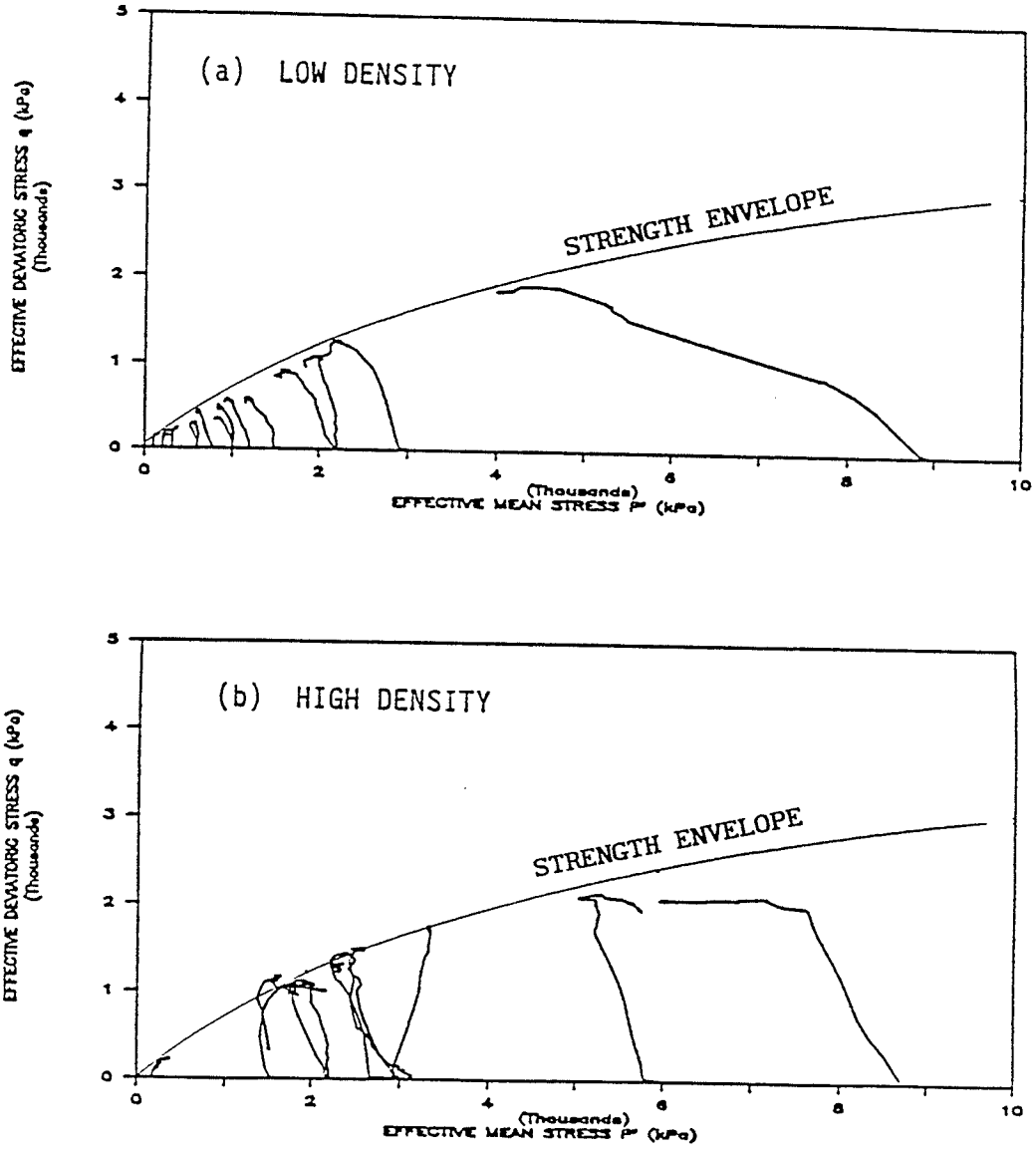

Fig.9.15 Effective stress paths and strength envelope (after Graham et al 1989)

$$[9.1] \quad \begin{cases} \dot{\varepsilon}_v = (\frac{1}{K}\dot{p}' + \frac{1}{J}\dot{q}) + S\,(2p' - p_m) \\ \dot{\varepsilon}_s = (\frac{1}{J}\dot{p}' + \frac{1}{3G}\dot{q}) + S\,(2q/M^2) \end{cases}$$

where in the absence of detailed test data it is assumed that the flow surface is an ellipse (Fig.10.16), expressed by Eqn.[8.4]. It is found from Figs.9.14,9.15 (Graham et al. 1989) that the strength envelope is curved. A hyperbolic function can be used to fit these data in Figs.9.14,9.15:

$$[9.2] \quad q_f = \frac{p'_f}{a + b\,p'_f}$$

where the parameters a and b were 1.3 and 0.0002 kPa^{-1} respectively, see Figs.9.14,9.15,9.16. From Eqns.[8.6],[8.7] it is known from Fig.9.16 that $p'_f = p'_m/2$ and $q_f/p'_f = M$. Thus from [9.2] the parameter M is:

$$[9.3] \quad M = M_c = \frac{1}{a + bp'_f} = \frac{1}{a + 0.5bp'_m}$$

Introducing this expression for M into [8.4] and solving for the stress parameter p'_m gives:

$$[9.4] \quad p'_m = \frac{(p'-abq^2) - \sqrt{(p'-abq^2)^2 - 4(0.5bq)^2(a^2q^2+p'^2)}}{2(0.5bq)^2}$$

It should be pointed out that in Eqn.[9.1], the KGJ model is used to

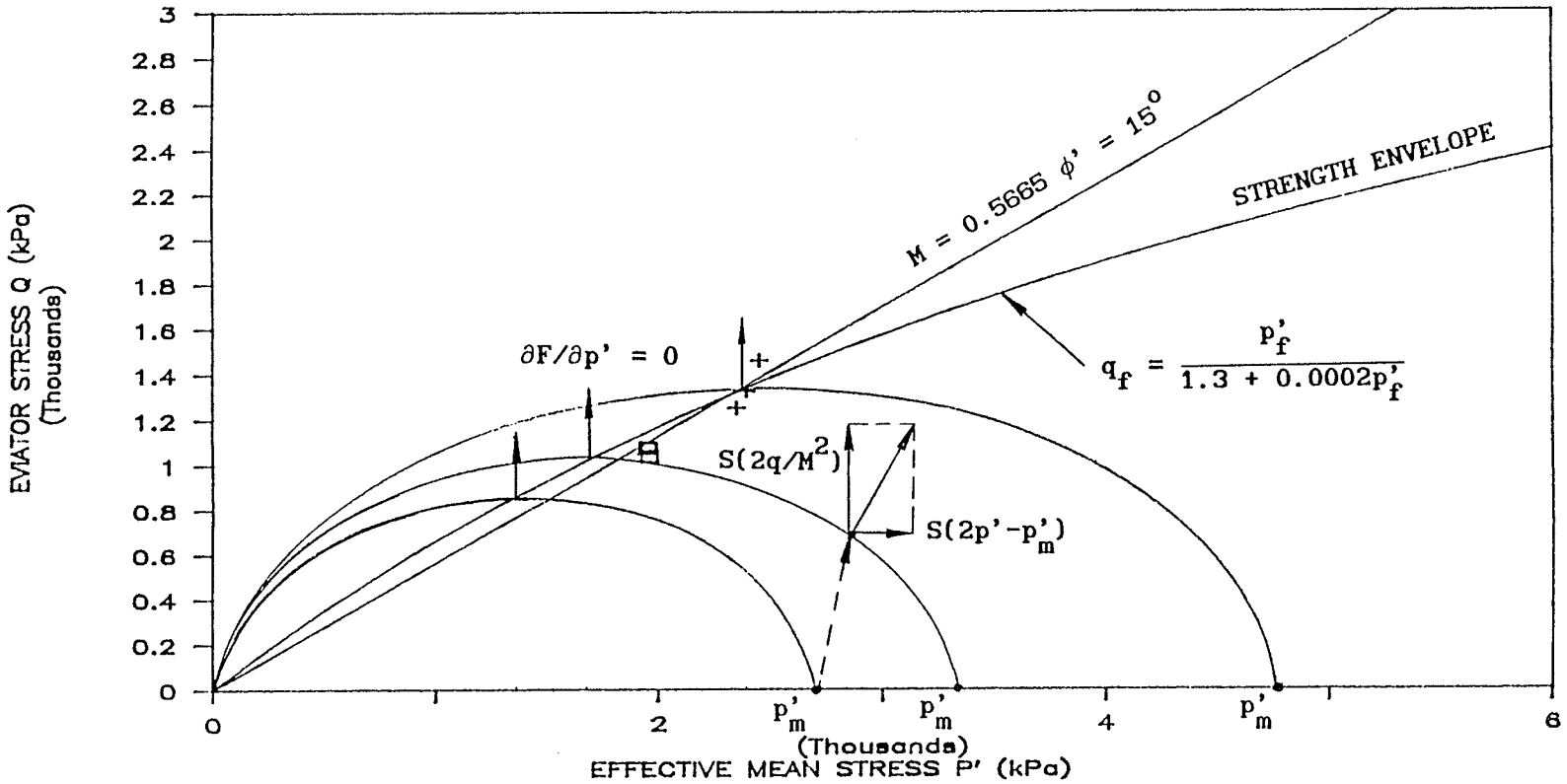

Fig.9.16 Flow surfaces, flow rule and strength envelopes

describe the time-independent behavior which may or may not be elastic. The strain responses defined by the KGJ model may depend on the stress paths and may not be fully reversible. Usable test data are not yet available.

9.2.2 Conceptual model for isotropic swelling and creep

To determine the scaling function S in Eqn.[9.1], we have to use the isotropic creep test data shown earlier in Figs.[9.1]-[9.8]. However, the behavior of the sand-bentonite buffer material is very complicated. This material exhibits both swelling and creep characteristics (Graham et al. 1986, Graham et al. 1989). In order to describe these phenomena, an extended conceptual model is developed from the model suggested by Graham et al. (1986).

As shown in Fig.9.17, the swelling equilibrium line (SEL) is reached by swelling (expansion) of an infinite time. The new model introduces a "creep equilibrium line" (CEL) which is reached by creep compression of an infinite time. In general, one would expect the SEL to be below the CEL as shown in Fig.9.17. According to this definition of SEL and CEL, the specimen at the state points below the SEL will swell to approach to SEL. The specimen at the state points above the CEL will compress to approach to the CEL. At the state points between the CEL and SEL, the behavior will be neutral, with neither creep nor swell being observed, and the behavior is completely time-independent. According

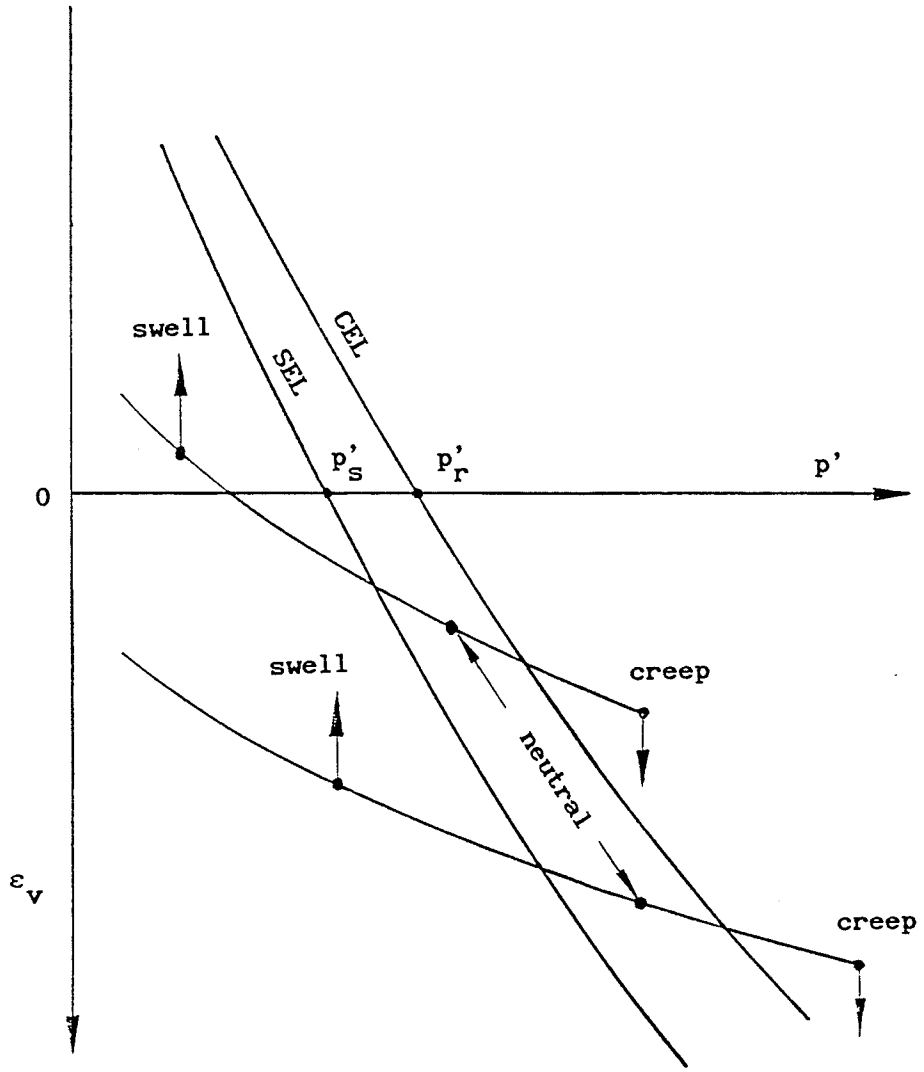

Fig.9.17 Conceptual model for swelling and creep behavior in isotropic stressing

to this model, the swelling pressure, p'_s at a given specific volume is the pressure on the SEL at which the volumetric strain, ε_v, is constant, (Fig.9.17). Similarly, the relaxation pressure, p'_r at a given specific volume is the pressure on the CEL and which the volumetric strain, ε_v is constant.

This conceptual model explains why in some soils there are large creep movements, whereas in other soils like sand, the behavior is almost completely time-independent. According the model in Fig.9.17, when the SEL is far on the left side of the CEL, then there is only creep behavior above the CEL and time-independent behavior below the CEL. If both the SEL and CEL are further separated, then the behavior is completely time-independent. The sand-bentonite mixture in the program has both swelling and creep. So there must exist both a SEL and a CEL in the ε_v,p'-space. The determination of the SEL and CEL by testing is difficult due to the coupling of hydrodynamic consolidation. No detailed examination of existing data or new testing specifically aimed at distinguishing the SEL and CEL have yet been undertaken, (see for example Graham et al. 1989b).

9.2.3 Determination of scaling function S

The difficulty in determining the scaling function S in Eqn.[9.1] is that there are at this stage no completely reliable creep ε_v,p' data available from isotropic consolidation tests. These would normally be

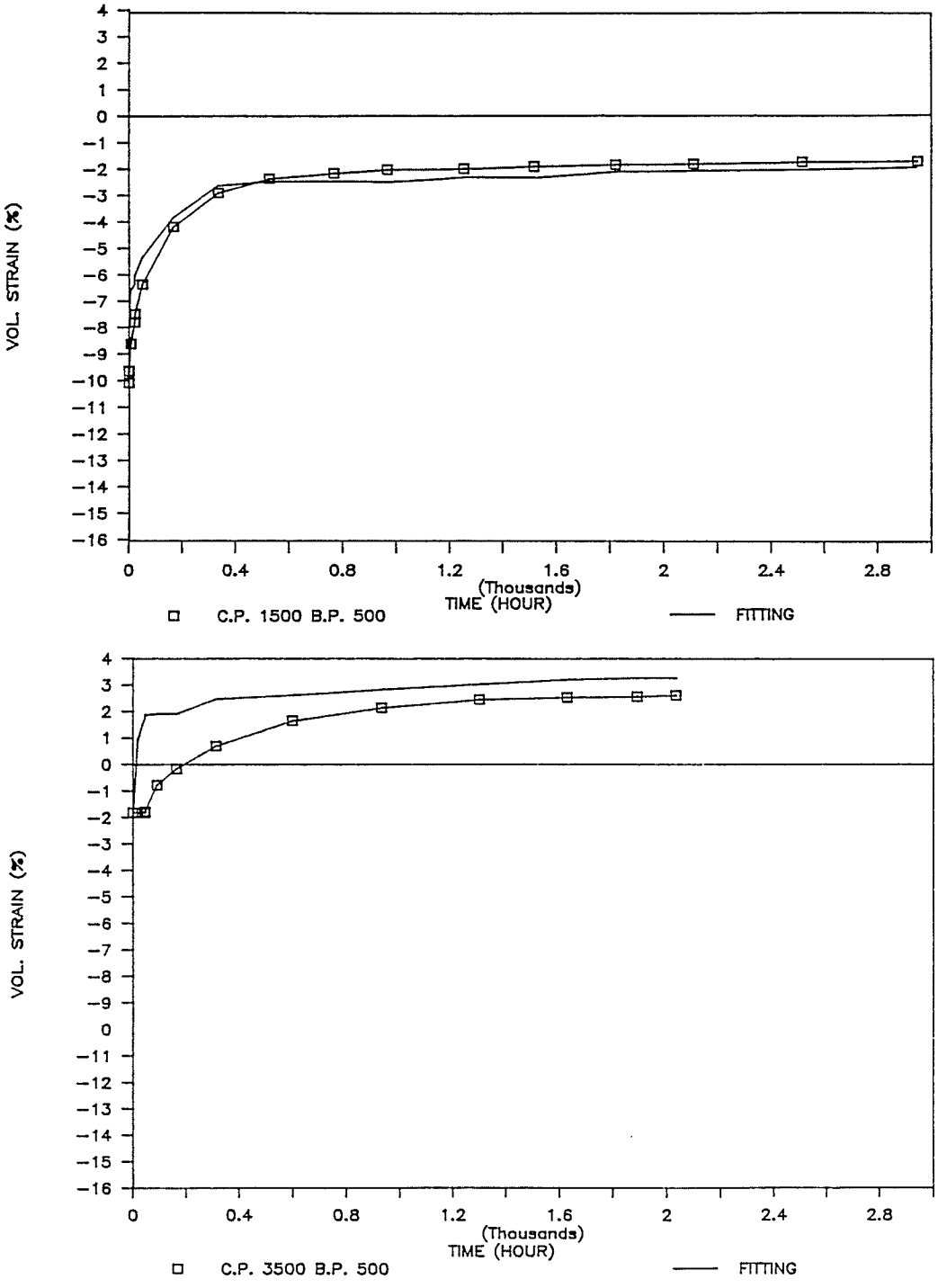

Fig.9.18 Measured and fitted ε_v,t-relationships - T1002
(a) p_{con} = 1000 kPa (b) p_{con} = 3000 kPa

needed to find the reference time line, the elastic time line and the creep parameters required in the scaling function. The permeability of the sand-bentonite mixture is very low, of the order 10^{-12} - 10^{-13} m/s. The dissipation of excess porewater pressures will not finish in a long time for consolidation pressures higher than p_{con} = 3000 kPa, see Figs.9.3,9.6, (see also Saadat 1989). In this case, the effective mean stress p' is increasing all the time and is not constant, so the data are not technically creep data at all. At lower pressures, for example p_{con} = 200 kPa, the soil swells and the swelling will not finish in a long time, see Figs.9.1,9.4 and the same comment holds. Even the relationship of ε_v,p' for unloading and reloading is also time-dependent, and cannot be measured accurately due to excess porewater pressures in the specimen. In the following section, the elastic line, reference time line and creep parameters will be estimated using the available information combined with present understanding of the behavior of the material.

The elastic line:

$$[9.5] \quad \varepsilon^{e}_{vm} = \frac{\kappa}{V} \ln(p'_{o1} + p'_{m}) - \varepsilon^{e}_{vmo}$$

has been assigned the values $\kappa/V = 0.03$, p'_{o1} = 500 kPa, see Fig.9.7. The parameter ε^{e}_{vmo} will not be used in the modelling.

The reference time line:

$$[9.6] \quad \varepsilon^{ep}_{vm} = \frac{\lambda}{V} \ln\left(\frac{p'_{o2} + p'_{m}}{p'_{o3}}\right)$$

has values $\lambda/V = 0.05$, $p'_{o2} = 0.5$ kPa, $p'_{o3} = 2500$ kPa, see Fig.9.8. This estimated reference time line is close to the equation of "end-of-consolidation" used by Saadat (1989), see Fig.9.8.

The creep equation:

$$[9.7] \quad \varepsilon_{vm}^{tp} = \frac{\psi}{V} \ln\left(\frac{t_o}{t_o + t_e}\right)$$

has been assigned $\psi/V = 0.0025$, $t_o = 0.1$ hour.

The equation for calculating creep strains under any stepwise isotropic loading is, using [9.6] and [9.7]:

$$[9.8] \quad \varepsilon_{vm}^{ep} = \frac{\lambda}{V} \ln\left(\frac{p'_{o2} + p'_m}{p'_{o3}}\right) + \frac{\psi}{V} \ln\left(\frac{t_o}{t_o + t_e}\right)$$

Using the method in Chapter 8, the general constitutive equation for continuous isotropic stressing is:

$$[9.9] \quad \dot{\varepsilon}_{vm} = \frac{\kappa/V}{p'_{o1} + p'_m} \dot{p}'_m + \frac{\psi}{t_o V} e^{-(V/\psi)\varepsilon_{vm}} \left(\frac{p'_{o2} + p'_m}{p'_{o3}}\right)$$

Using the scaling Method 2 in Chapter 8, the scaling function in Eqn.[9.1] is:

$$[9.10] \quad S = \frac{\psi}{V t_o} e^{-(V/\psi)\varepsilon_v} \left(\frac{p'_{o1} + p'}{p'_{o1} + p'_m}\right)^{\kappa/\psi} \left(\frac{p'_{o2} + p'_m}{p'_{o3}}\right)^{\lambda/\psi} / \left|2p' - p'_m\right|$$

The parameters in Eqns.[9.5]-[9.7] have been best-estimated by the graphical method explained in Chapter 8. The curves fitted by using

[9.8] are shown in Fig.9.18a,b. The details of the graphical method will be presented in Chapter 10.

9.2.4 Determination of moduli K,G,J

Using Method 1 in Chapter 3, the data from isotropic unloading and reloading consolidation tests are used to find the bulk modulus K. Data from undrained unloading and reloading shear tests are used to find the coupling modulus J and the shear modulus G. The modulus K is obtained by differentiating [9.5] or taken from [9.9]:

$$[9.11] \quad K = \frac{\kappa/V}{p'_{o1} + p'_m} = \frac{\kappa/V}{p'_{o1} + p'} = \frac{0.03}{500 + p'}$$

Here again, the use of p' instead of p'_m assumes that K is independent of deviator stresses.

The J modulus is found to be:

$$[9.12] \quad J = -K \frac{dq}{dp'} = -4.601\ K$$

The effective stress paths of the time-independent responses were linear, see Figs.9.10, 9.13, 9.14 and 9.15. The average value of dq/dp' for 6 specimens tested by Saadat (1989) and for T1001 and T1002 in this test program is 4.601.

The apparent modulus D (Eqn.[3.11]) is found to be 45000 kPa, using the data from the unloading and reloading tests given in Fig.9.11. The

shear modulus G is found from Eqn.[3.12], using [9.12] and D:

$$[9.13] \quad G = \frac{DJ^2}{J^2 + 3DK} = D \frac{1}{1 + 3DK/J^2} = 45000 \frac{1}{1 + 6377.2/K}$$

where K is given by [9.11].

9.3 Verification of the EVP Model

In the preceding section, the EVP model was formulated and calibrated for the sand-bentonite buffer material. Now the model will be used to predict two different type of tests. One is an undrained multi-stage q creep shear test, and the other is an undrained step-changed constant strain rate shear test.

9.3.1 Modelling of an undrained multi-stage q creep shear test

After isotropic consolidation and relaxation, specimen T1001 was sheared using multi-stage deviator stresses under undrained conditions. The loading history for this undrained shear test is in Table 9.3. The detailed data are given in Appendix 9.2.

Table 9.3 Loading History, Initial Conditions and Measured and Calculated ε_s, p' Data at the End of Each Loading

q (kPa)	315.7	686.8	866.0	1041.9	1077.0
Duration (hour)	695.2	311.2	144.3	29.7	0.53
p'_i (kPa) (initial)	2455	2200.9	2080.3	1986.4	1941.2
ε_{si} (initial)	0	.0053	.0132	.0211	.0341
ε_{vi} (initial)	0.0188	0.0188	0.0188	0.0188	0.018
p' (kPa) (calcu.)	2200.9	2080.3	1986.4	1941.2	1945.5
p' (kPa) (test)	2215.5	1690.8	1897.6	1959.9	1941.8
ε_s (calcu.)	.0053	.0132	.0211	.0341	.0350
ε_s (test)	.0039	.0136	.0214	.0473	.0976

In the test, each deviator stress increment was applied to the specimen suddenly (over a period of a few seconds), and then held constant. From Eqn.[9.1] the instantaneous responses due to the sudden loading are given by:

$$[9.14] \quad \begin{cases} \Delta\varepsilon_v = \frac{1}{K}\Delta p' + \frac{1}{J}\Delta q \\ \Delta\varepsilon_s = \frac{1}{J}\Delta p' + \frac{1}{3G}\Delta q \end{cases}$$

Using the undrained condition $\Delta\varepsilon_v = 0$ into the first equation in [9.14], the ratio $\Delta q/\Delta p' = -J/K$, and this has been measured to be 4.601. Using this ratio in the second equation in [9.14], the shear strain is:

[9.15] $\Delta\varepsilon_s = (\frac{1}{4.601\ J} + \frac{1}{3G})\ \Delta q$

So if the deviator stress increment, Δq, is known, Eqn.[9.15] can be used to calculate the instant shear strain increment, $\Delta\varepsilon_s$.

Using conditions $\dot{\varepsilon}_v = 0$ and $\dot{q} = 0$ from Eqn.[9.1], the effective mean stress p', and shear strain ε_s, during undrained creep under the deviator stresses are:

[9.16] $$\begin{cases} \dot{p}' = -K\ S\ (2p' - p'_m) \\ \dot{\varepsilon}_s = \frac{1}{J}\ \dot{p}' + S\ 2q/M^2 = [\frac{K}{J}\ (2p' - p'_m) + 2q/M^2]\ S \end{cases}$$

Note here that the creep shear strain rate $\dot{\varepsilon}_s$ depends on the current stress state p',q. The excess porewater pressure, Δu, is:

[9.17] $\Delta u = p'_i + q/3 - p'$

where p'_i is the initial effective mean stress on p'-axis.

The initial conditions used in calculating the p',t- and ε_s,t-relationships for different deviator stresses are shown in Table 9.3. Note that when the deviator stress is newly increased, new initial conditions should be used. These new initial conditions are the final values at the end of the last deviator stress, see Table 9.3. Eqns.[9.15],[9.16] are used to calculate the relationships of p' vs. t and ε_s vs. t. Eqn.[9.16] is a non-linear differential equation system for which no analytical solution can be obtained. The fourth-order

Runge-Kutta method was used to solve [9.16] numerically. The computer program for using this method is given in Appendix 9.3. Eqn.[9.17] is used to calculate the relationship of Δu vs. t. Table 9.3 shows the initial values, final predicted p', ε_s values, and their equivalent measured test values for each deviator stress q.

Fig.9.19 shows the comparison of the measured and predicted shear strain vs. time (ε_s vs. t) relationships for five different deviator stresses. It is seen in the Figure that the calculated curves agrees well with the test data. The calculated Δu vs. t in Fig.9.20 and q vs. p' in Fig.9.21 for q = 315.7 kPa agree with the measured data. However, the model tends to underpredict the porewater pressures (and hence the p',q,t-relationships) for higher deviator stresses.

9.3.2 Modelling of an undrained step-changed constant strain rate shear test

Specimen T1002 was sheared using step-changed constant strain rates under undrained conditions after isotropic consolidation and relaxation were completed. The detailed data are given in Appendix 9.2. The schedule for changing the strain rates is shown in Table 9.4 as a function of the shear level during the test.

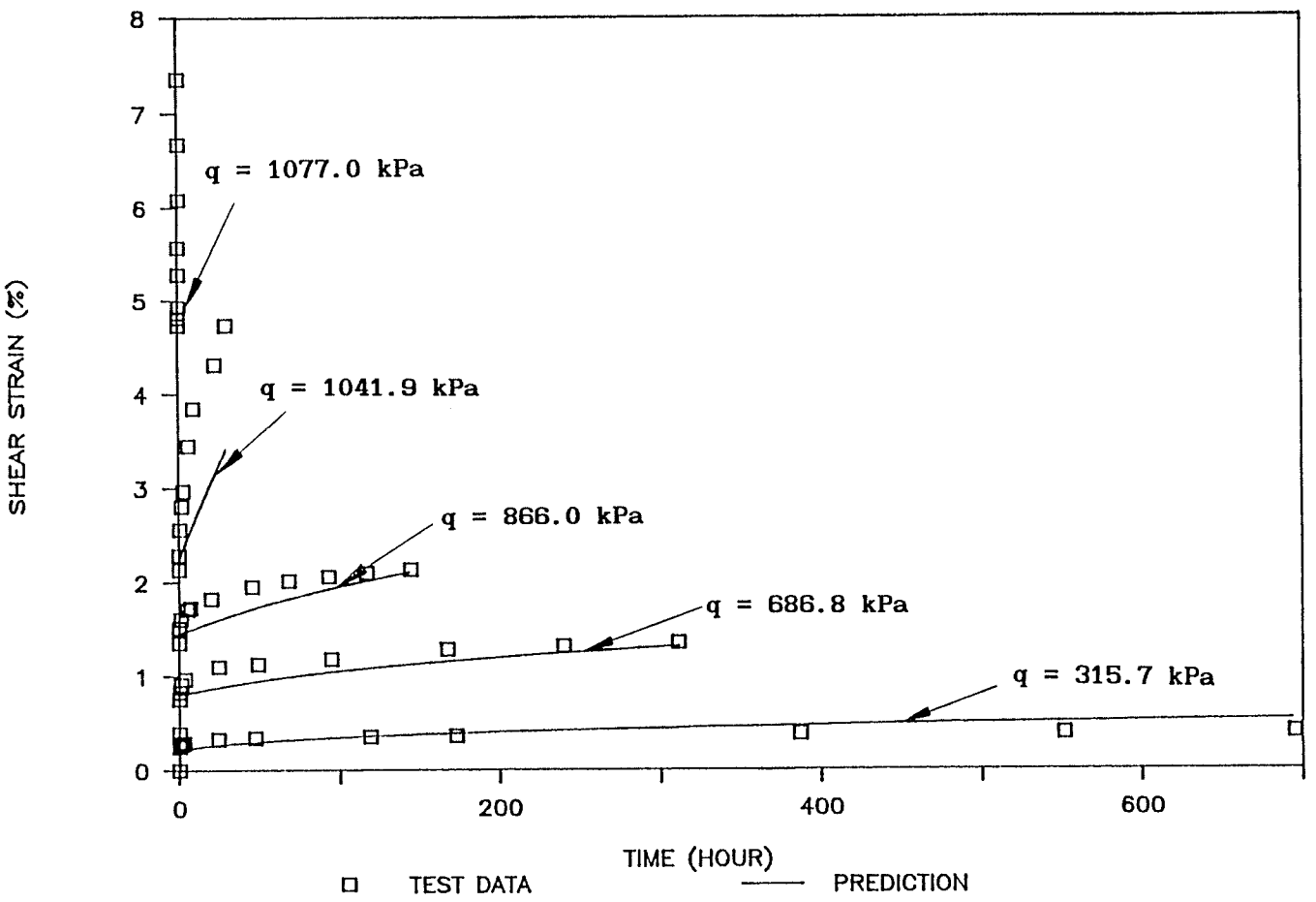

Fig.9.19 Measured and predicted ε_s,t-relationships - T1001

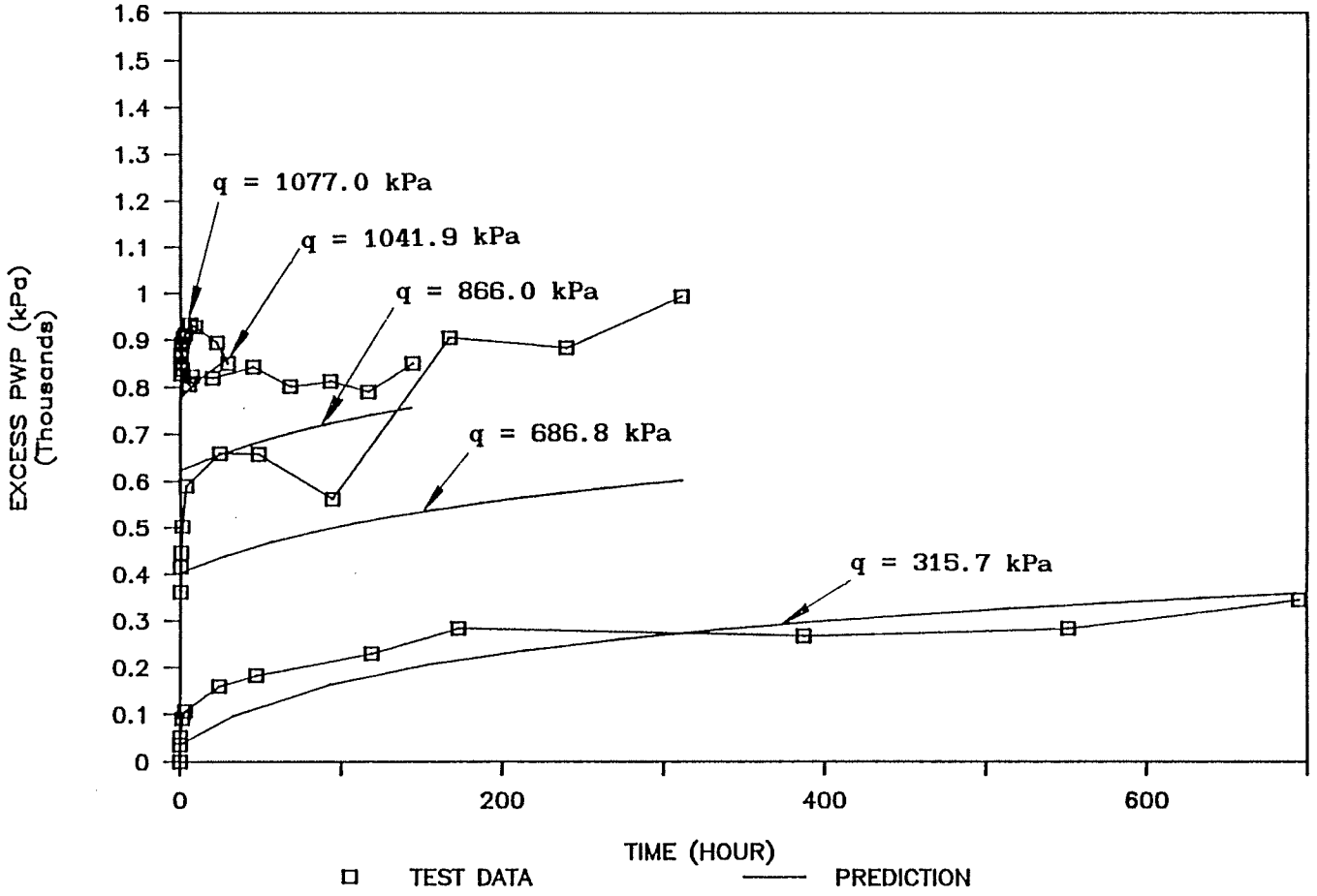

Fig.9.20 Measured and predicted Δu,t-relationships - T1001

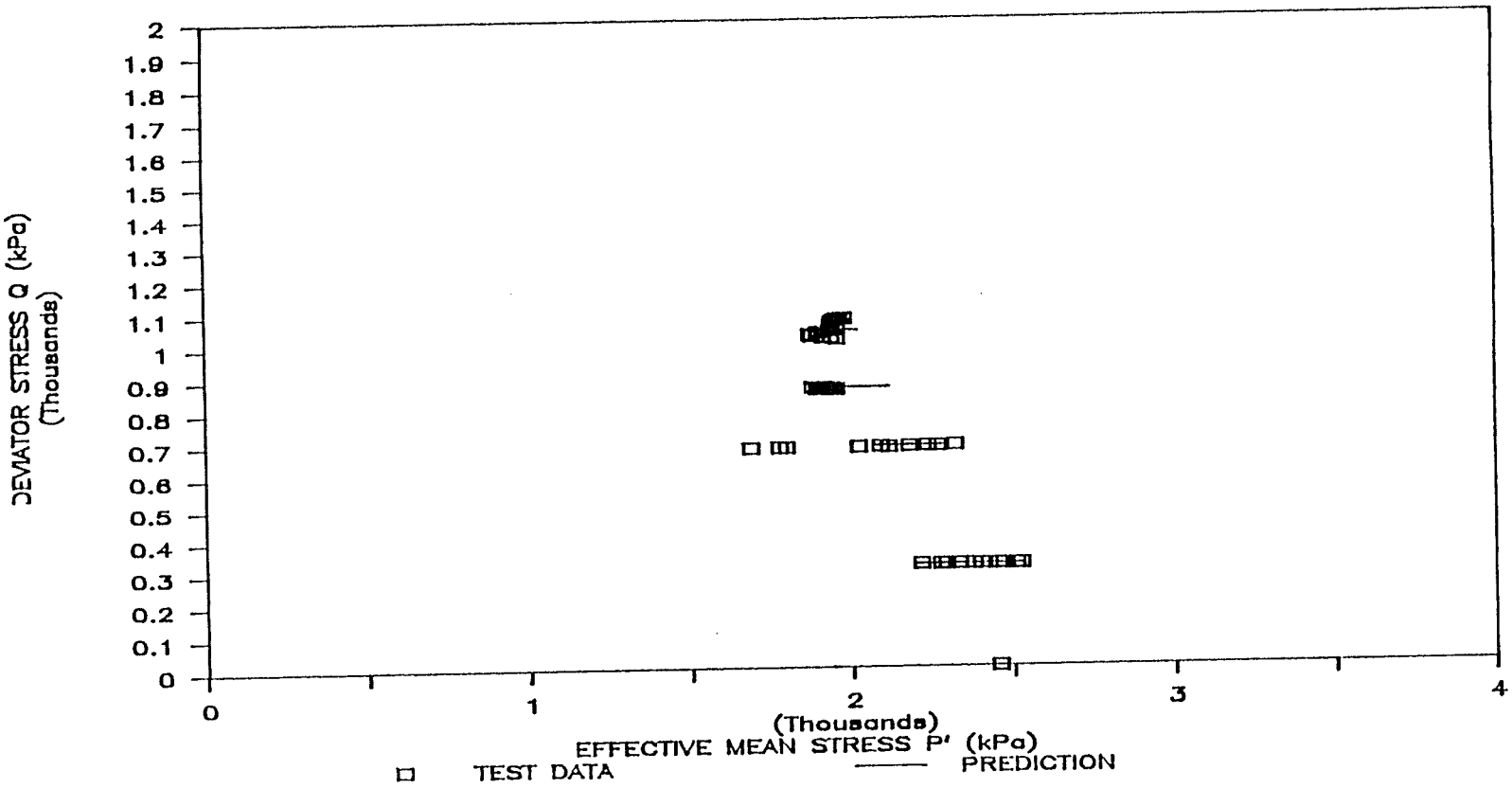

Fig.9.21 Measured and predicted effective stress paths - T1001

Table 9.4 Schedule of Strain Rate Changes

ε_s	0	.0057	.0135	.0280	.0468	.0619	.0692
$\dot{\varepsilon}_s$	.094	.0058	.00036	.094	.0058	.00036	.0058

ε_s	.0731	.0653	.0841	.1006	.1012	.1092	.1134
$\dot{\varepsilon}_s$	-.0058	+.0058	.094	0	.094	.00036	end

The equations for calculating p' vs. ε_s and q vs. ε_s are obtained from [9.1], using the condition $\dot{\varepsilon}_v = 0$:

$$[9.18] \quad \begin{cases} \dot{p}' = -K\,[\frac{1}{J}\,\dot{q} + S(2p' - p'_m)] \\ \dot{q} = 3G\,[\dot{\varepsilon}_s - \frac{1}{J}\,\dot{p}' - S(2q/M^2)] \end{cases}$$

The initial condition at the beginning was $q_i = 0$, $p'_i = 2693$ kPa and $\varepsilon_{si} = 0$, $\varepsilon_{vi} = 0.0262$. The strain rate was 0.094 h^{-1}. If the strain rate was changed, then the new strain rate and new initial values should be used in the calculation of [9.18]. The new initial values are the final values at the end of shearing with the previous strain rate. The computer program for solving [9.18] numerically is in Appendix 9.4.

For comparison purposes, Figs.9.22,9.23,9.24 present the measured and predicted q,ε_s-relationships, $\Delta u,\varepsilon_s$-relationships and effective stress paths respectively. The modelling is generally good. It is seen in Fig.9.22 that the model overestimates q values in the shear strain

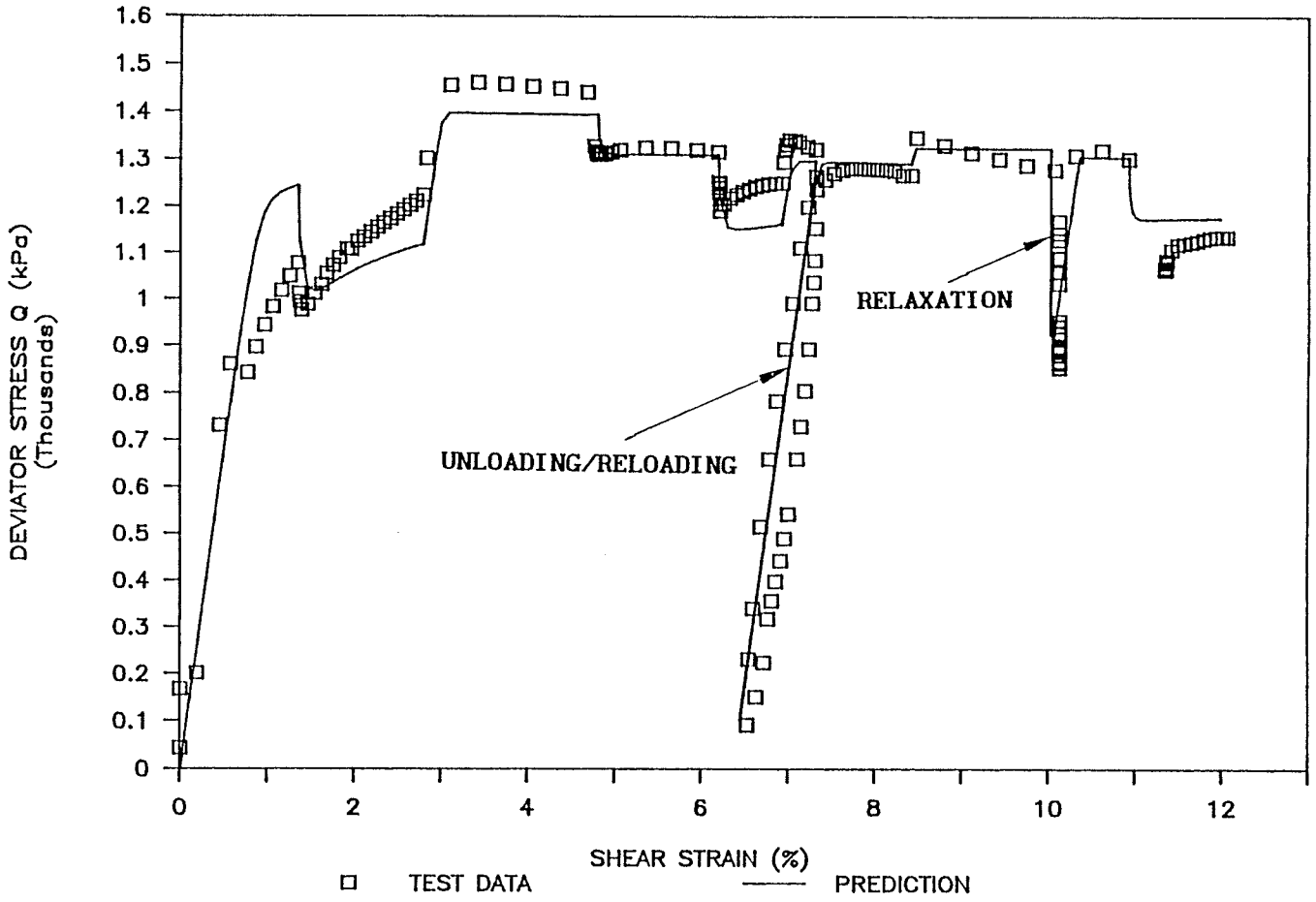

Fig.9.22 Measured and predicted q,ε_s-relationships - T1002

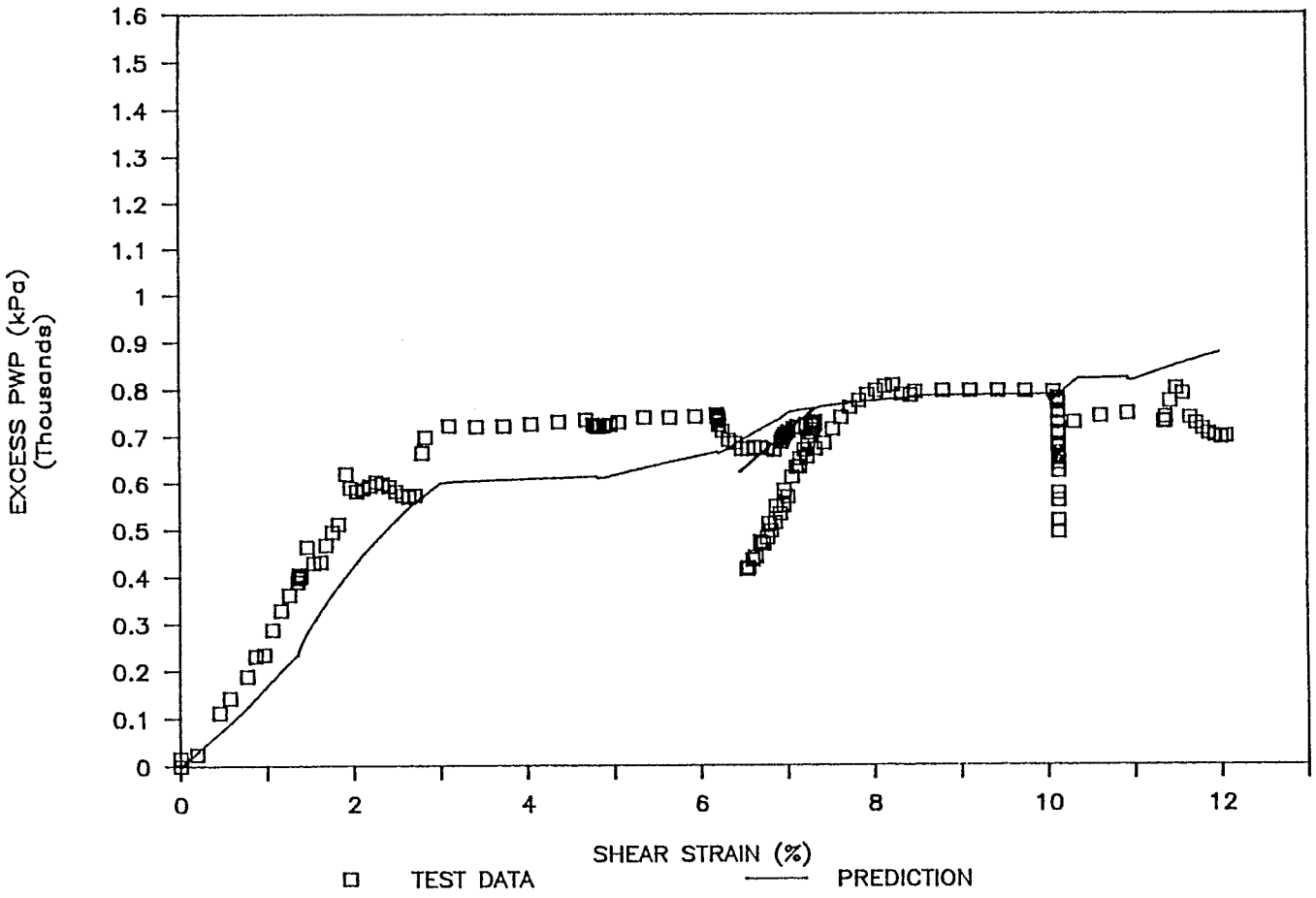

Fig.9.23 Measured and predicted $\Delta u, \varepsilon_s$-relationships - T1002

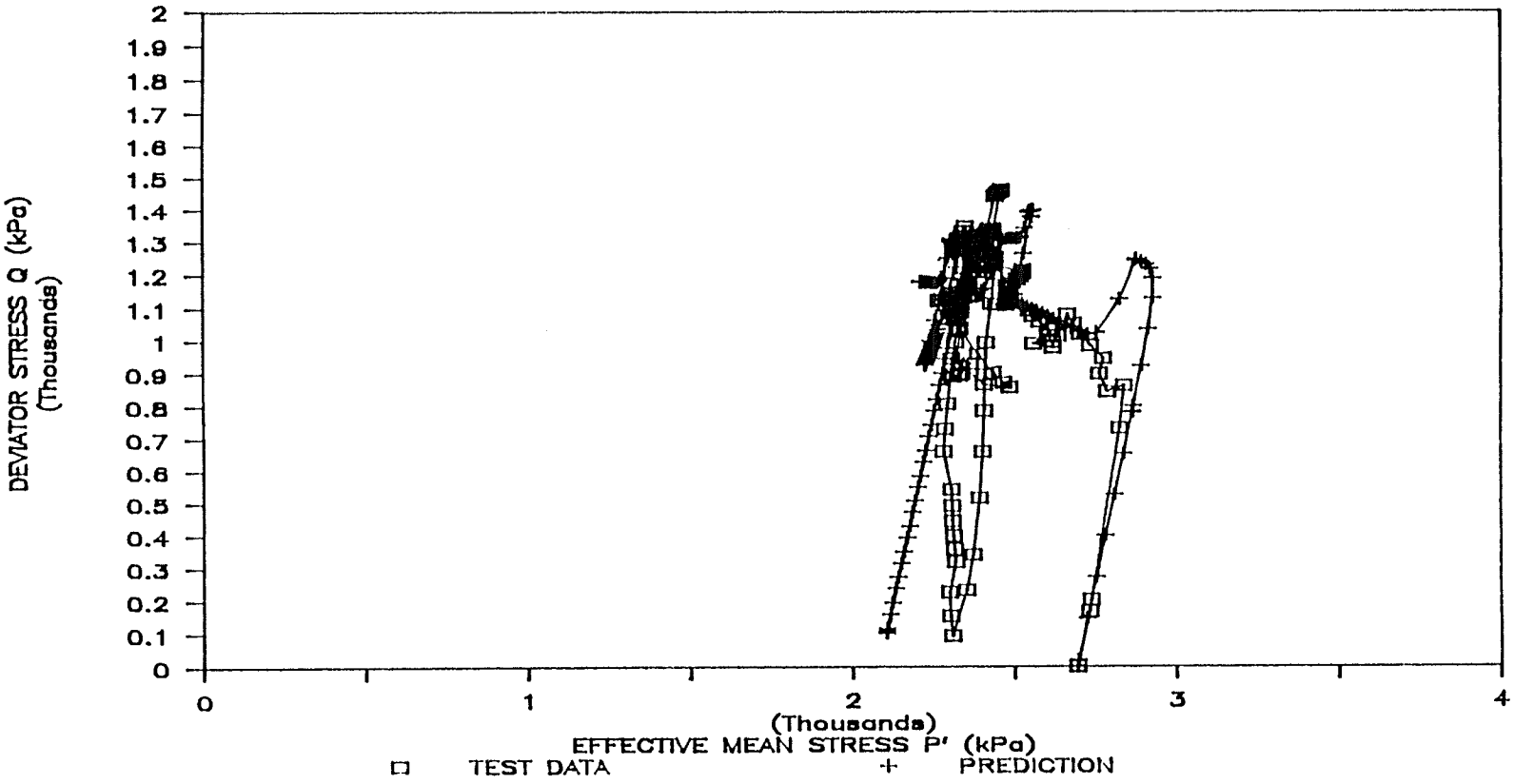

Fig.9.24 Measured and predicted effective stress paths - T1002

range 0.5 % - 1.35 %. Because of the way the model was formulated, it did not reproduce the loop in the unloading and reloading measured in the test, see Figs.9.22,9.24. In Fig.9.12 the predicted q,t data are compared with the test data. The model overestimates the q-values.

Fig.9.25 shows a simulation of constant strain rate shear tests (CRSN) which have not yet been produced in the laboratory. Fig.9.26 shows the comparison of the $q, \dot{\varepsilon}_s$-values measured from the step-changed constant strain rate shear test (T1002) and calculated in the simulated CRSN tests. We can see the strain effects produced by the EVP model.

It is seen from these comparisons that some of modelled values are not especially close to the corresponding test data. However, bearing in mind the restricted data base that was used to calibrate the model for "buffer", some encouraging features of the EVP model can be seen from these Figures. The model can simulate the effects of varying strain rate, relaxation and creep. It is also interesting to note that Eqn.[9.18] can model unloading and reloading cycles simply by using negative and positive strain rates respectively without any additional condition.

9.4 Discussion

The sand-bentonite buffer material has both swelling and creep

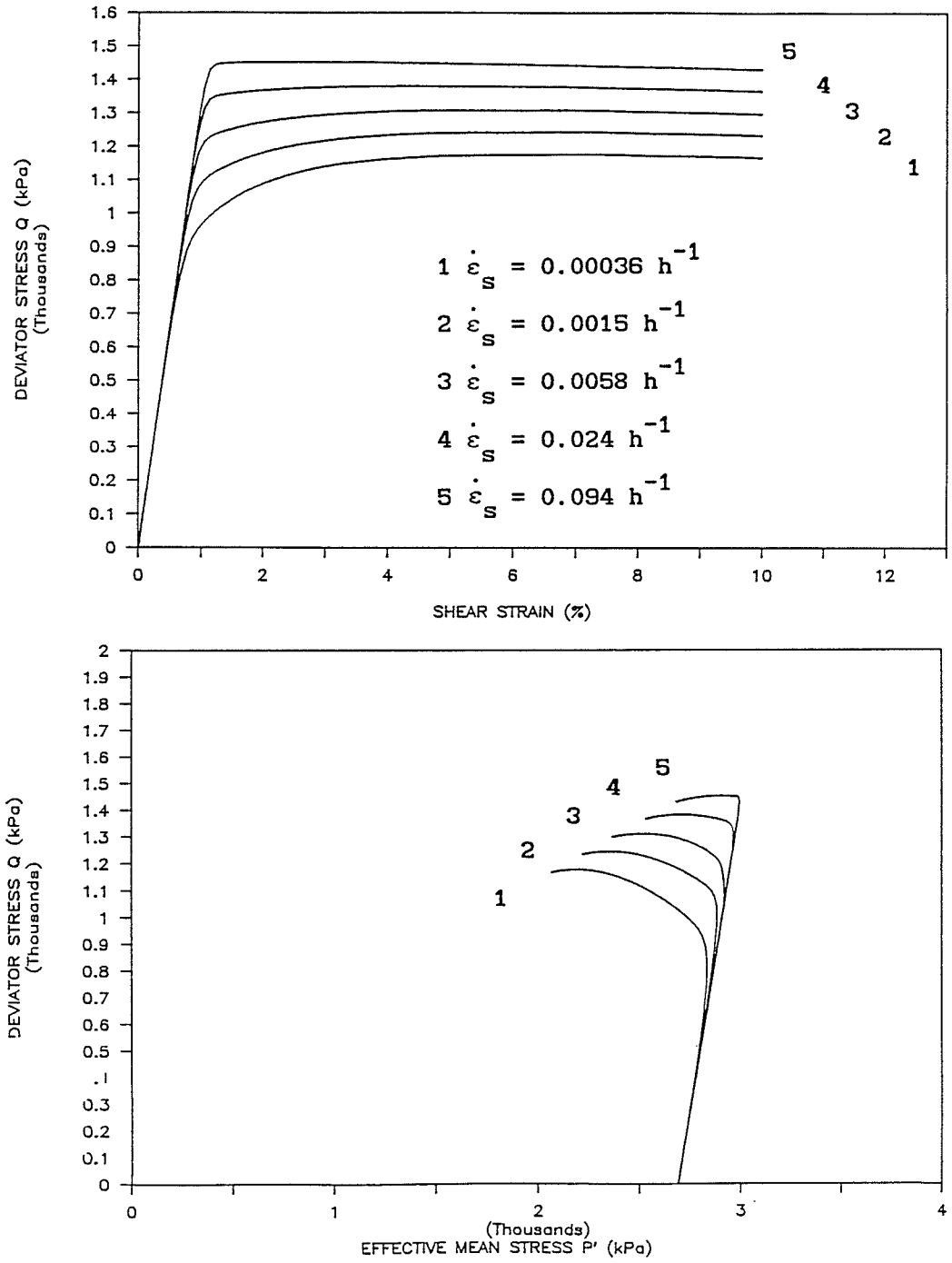

Fig.9.25 Simulation of constant strain rate shear tests - CRSN

(a) q,ε_s-relationships (b) effective stress paths

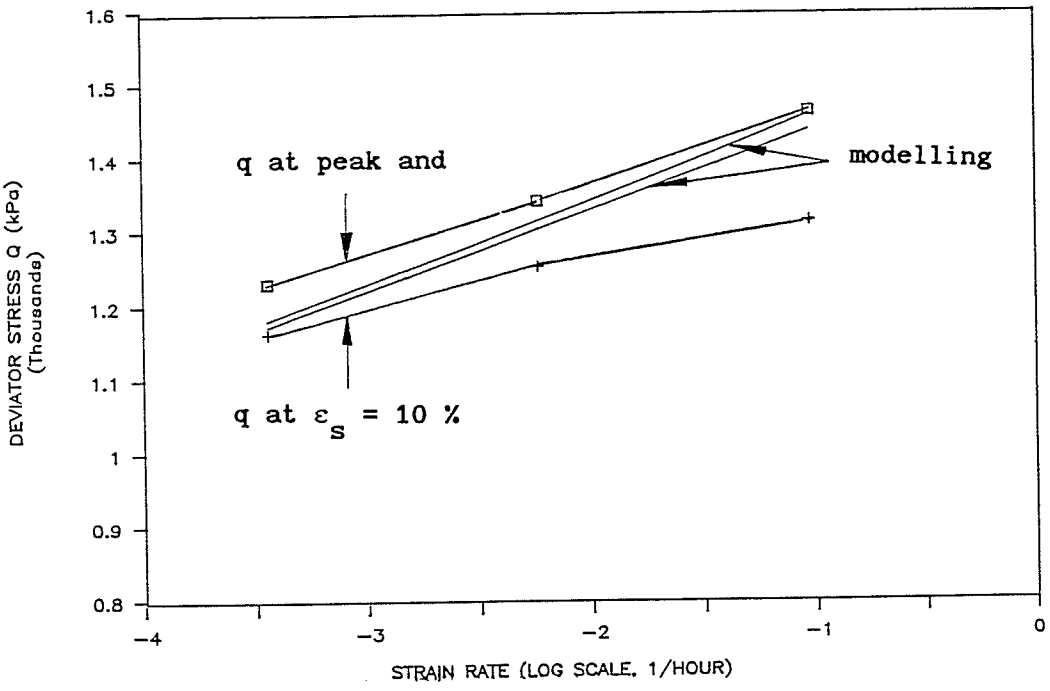

Fig.9.26 Comparison of the $q,\dot{\varepsilon}_s$-relationships measured in T1002 and calculated in CRSN

characteristics. Time-dependent behavior of this material is therefore complicated and difficult to measure. Due to the coupling of hydrodynamic consolidation and low permeability (10^{-12} to 10^{-13} m/s, Dixon and Gray 1985), it is in principle difficult to separate effects of time dependency such as creep or swelling from time dependent behavior related to dissipation of porewater pressure. The result is that it is difficult to get reliable creep p', ε_v-data required in the determination of the scaling function. All the parameters in the scaling function have been estimated using engineering judgement. There are therefore experimental uncertainties in some of the parameters, and this of course directly affects the quality of the model predictions. No systematic study of the influence of these errors has been undertaken in the thesis.

In determining the K,G,J moduli, it was assumed that the apparent modulus D and the ratio J/K were constant. It is considered possible that they might depend on stress levels. The time-independent behavior of the buffer needs further examination in an extended laboratory program. In the formulation of the EVP model, an elliptic flow surface was assumed, and an associated flow rule was used. The true shape of this surface and the flow rule require to be examined by stress-probe tests. Such work is currently being undertaken in the University of Manitoba by doctoral candidate J.M. Oswell.

The EVP model developed in this chapter is used to model time-dependent stress-strain behavior which is related to volumetric creep

in p', ε_v-space. In other words, this model applies only to state points above the swelling equilibrium line (SEL) in Fig.9.17. This model can not at this stage deal with any time effects resulting from swelling. It does include the normal time-independent behavior associated with the Cam-Clay modelling in the overconsolidated range. The work in this chapter is very preliminary. More work needs to be done.

Chapter 10

ELASTIC VISCO-PLASTIC (EVP) MODELLING OF A FROZEN SAND

10.1 Introduction

Considerable laboratory testing of frozen soils and modelling of the stress-strain-time relationship, have been carried out. To date, no one single model has gained universal acceptance because of the complexity and variability of the behaviour of the soils. Essentially, the behaviour includes components of elasticity, plasticity, and viscosity. Some models combine two of these components, for example, Budkowska and Fu, 1989, and Sun et al., 1989. Other models are not based on the behaviour of ideal materials, but simply analyze the behaviour in terms of strain rates which are related to such factors as stress level, time, and temperature for a given material. Most models are based on uniaxial deformation. In this Chapter, a 3-D EVP model is developed from on the framework presented in Chapter 8. This model incorporates all the aforementioned components. It is applied to the results of triaxial compression creep tests carried out on a frozen sand by Rahman 1988.

Many creep theories assume that frozen soils are incompressible and their creep behaviour is not influenced by mean (hydrostatic) stress level. However, experimental results show that volumetric creep rates

are significant and depend on both time and mean stress (Domaschuk et al. 1985). The 3-D EVP model in this Chapter can account for volumetric and shear creep under general stress conditions.

10.2 Equations of the EVP Model for a Frozen Sand

Here, the frozen sand is treated as one phase material, and thus no distinction is made between total stresses and effective stresses.

In the proposed model, elastic responses are assumed to be isotropic, using Eqn.[8.2]. The flow surface is assumed to be an ellipse, using Eqn.[8.4]. Under triaxial stress states, the constitutive relationship for the frozen sand is:

$$[10.1] \quad \begin{cases} \dot{\varepsilon}_v = \frac{1}{K}\dot{p} + S\,(2p - p_m) \\ \dot{\varepsilon}_s = \frac{1}{3G}\dot{q} + S\,(2q/M^2) \end{cases}$$

A strength envelope is also required for the model. It was found from creep shear test data that the strength envelope, defined as $\partial\varepsilon_s/\partial\varepsilon_v = \infty$, was not unique, but time-dependent (Rahman 1988). These data therefore could not be used to determine the strength envelope. However, Fig.10.1 shows the "zero volumetric strain rate line" found from those creep tests. The behaviour below the line was compressive, the behaviour above the line was expansive, and the behaviour on the line was zero, namely $\dot{\varepsilon}_v = \dot{\varepsilon}_v^e + \dot{\varepsilon}_v^{vp} = 0$. Since both deviator stress and mean stress at any point on the line are constant, the elastic

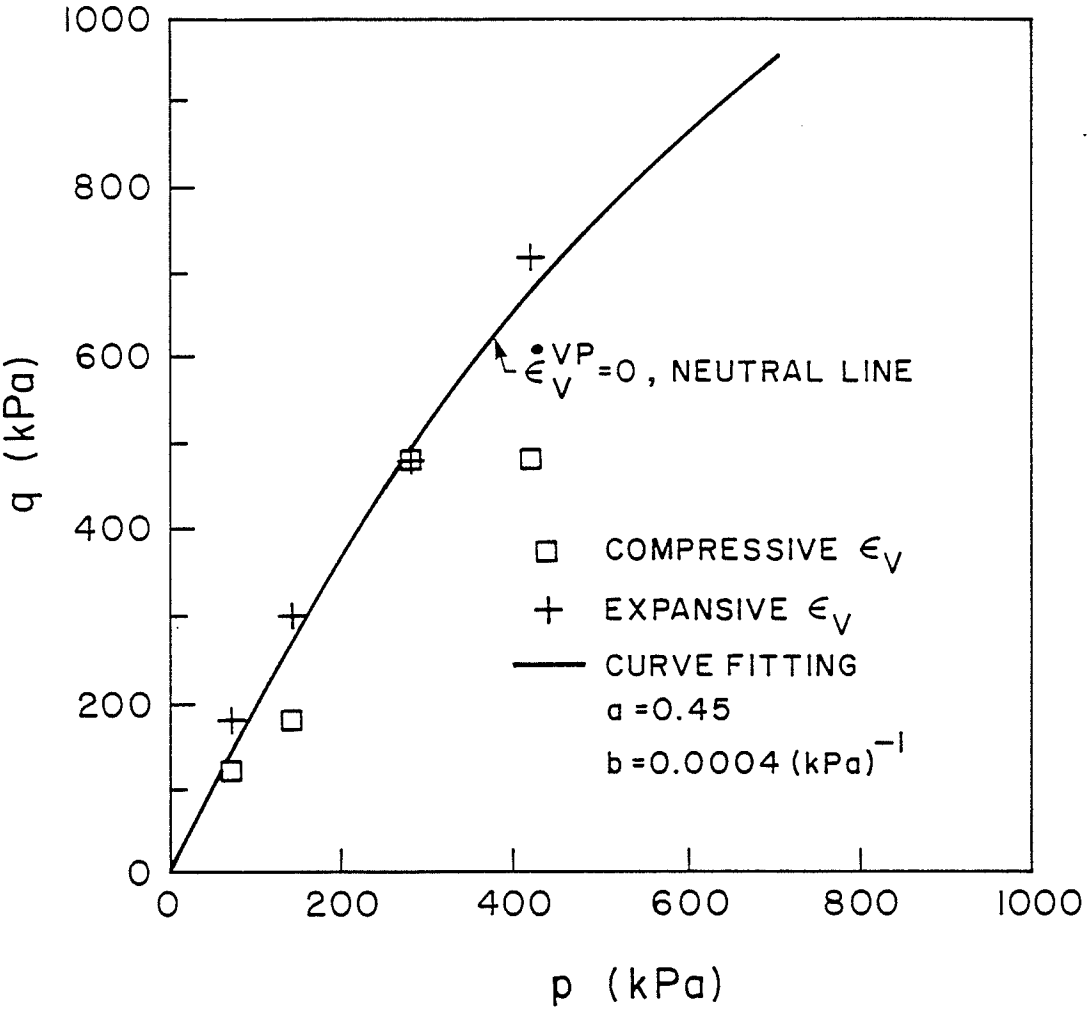

Fig.10.1 Neutral line, $\dot{\varepsilon}_v^{vp} = 0$ - multi-stage, constant p, triaxial compression creep tests

strain rate should be zero $\dot{\varepsilon}_v^e = 0$. Therefore the visco-plastic volumetric strain rates on the line were also zero, that is $\dot{\varepsilon}_v^{vp} = 0$. In Chapter 8, the envelope on which visco-plastic volumetric strain rates are zero was defined as a "neutral lines", see Fig.10.1.

For the frozen sand in this test series, the zero $\dot{\varepsilon}_v^{vp}$ envelope (that is the neutral line in q,p-space in triaxial compression tests) was curved. It has been fitted by a hyperbolic function:

$$[10.2] \quad q_{nc} = \frac{p_{nc}}{a + bp_{nc}}$$

where q_{nc} and p_{nc} are stresses on the neutral line in compression. Using graphical technique, the constants in [10.2] a = 0.45, and b = 0.0004 $(kPa)^{-1}$. This line is shown in Fig.10.1.

Because $\dot{\varepsilon}_v^{vp} = 0$ on this line, Eqn.[10.1] requires that $\partial F/\partial p$ is also zero = 0 on the neutral line, since $S \neq 0$. This implies that the visco-plastic volumetric strain rate vectors of the visco-plastic potential F on the neutral line are vertical in q-p space. Using the condition that $\partial F/\partial p = 0$ in combination with Eqn.[8.4]:

$$[10.3] \quad p_{nc} = p_m/2$$

and

$$[10.4] \quad F_n = q_{nc}^2/p_{nc}^2 = M^2$$

Using Eqn.[10.2], the parameter, M, in [8.4] or [10.4] is written:

$$[10.5] \quad M = M_c = \frac{1}{a + bp_{nc}} = \frac{1}{a + 0.5bp_m}$$

Introducing this expression for M into [8.4] and solving for the stress parameter p_m gives:

$$[10.6] \quad p_m = \frac{(p-abq^2) - \sqrt{(p-abq^2)^2 - 4(0.5bq)^2(a^2q^2+p^2)}}{2(0.5bq)^2}$$

Given any stress point (p,q), the point $(p_m,0)$ intercepted by the elliptical flow surface with the p coordinate, can be calculated from [10.6].

Creep shear tests in triaxial extension may be used to find the neutral line in extension, namely M_e. Then applying Eqns.[8.7],[8.8], the flow surface and the zero $\dot{\varepsilon}_v^{vp}$ envelope in q,p-space can be generalized for general 3-D stress states (Fig.8.3).

10.3 Determination of Scaling Function

Eqn.[10.1] provides a general framework for the time-dependent stress-strain behaviour of the frozen sand. For applications, the scaling function S in [10.1] must be determined from test data.

Scaling Method 3 (using a neutral line) in Chapter 8 is used here to determine S. This method can meet the condition that the visco-plastic volumetric strain rates, $\dot{\varepsilon}_{vnc}^{vp}$, must always be zero for the stress

points (p_{nc}, q_{nc}) on the neutral line, namely:

[10.7] $$\dot{\varepsilon}^{vp}_{vnc} = S\,(2p_{nc} - p_m) = S\,[2(p_m/2) - p_m] = 0$$

Under isotropic stress conditions, from [10.1]:

[10.8] $$S = \dot{\varepsilon}^{vp}_{vm}/p_m$$

where $\dot{\varepsilon}^{vp}_{vm}$ is the visco-plastic strain volumetric rate when q = 0. This strain rate can be found by using the procedure in Chapter 8.

Only one isotropic multi-stage loading creep test was available from the earlier tests on the frozen sand (Figs. 10.2, 10.3). The data from this test were used to determine all the parameters necessary for calculating the visco-plastic strain rate $\dot{\varepsilon}^{vp}_{vm}$. It should be pointed out that the numerical procedures are simpler, if a number of single stage loading creep tests are performed.

The following fitting functions illustrated in Fig. 10.2 were used to model the isotropic test data.

Elastic line (elastic strain):

[10.9] $$\varepsilon^{e}_{vm} = \frac{\kappa}{V} \ln\left(\frac{p_{o1} + p_m}{p_{o1}}\right)$$

in which: $\kappa/V = 0.0013$, $p_{o1} = 10$ kPa. It was assumed that this equation was valid for all stress states.

Reference time line (elastic plastic strain, $t_e = 0$):

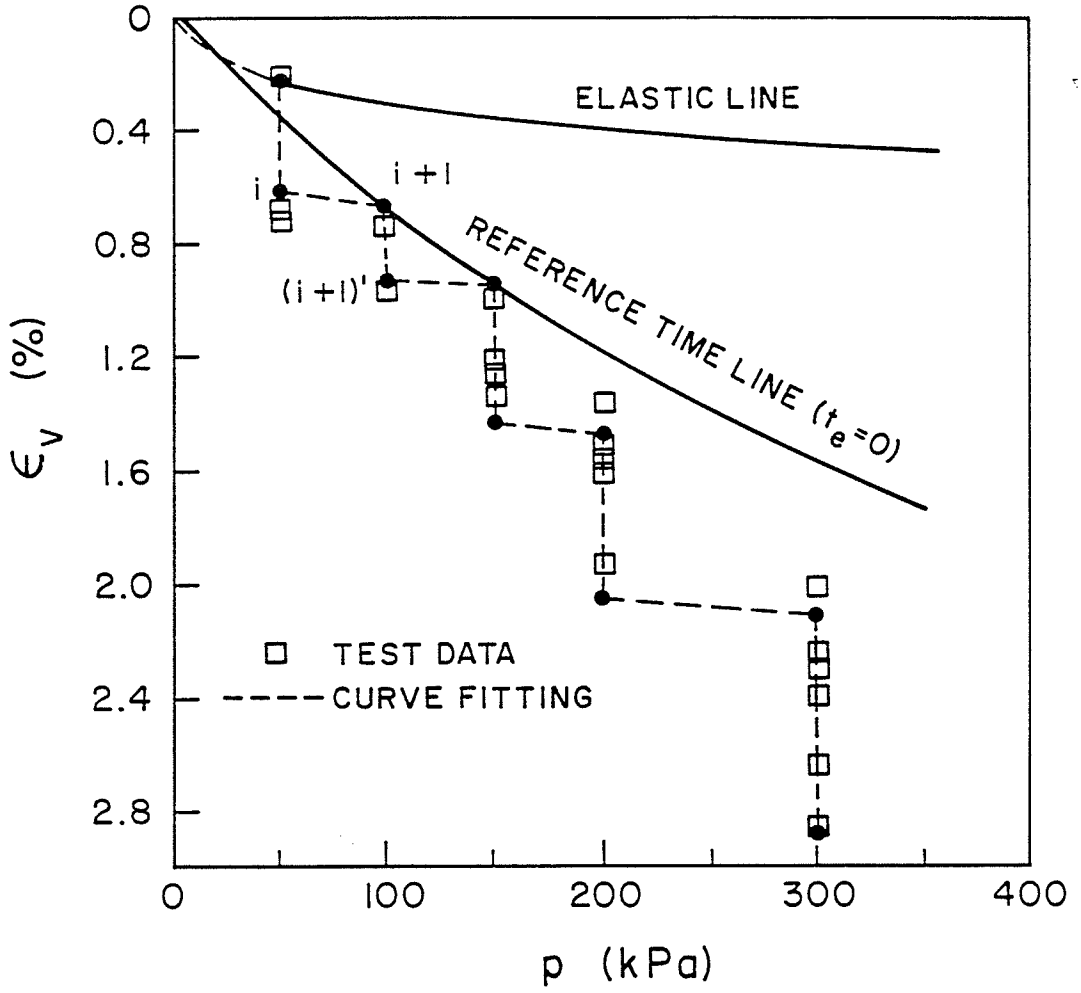

Fig.10.2 Elastic line, reference time line and curve fitting of creep test data - an isotropic multi-stage loading creep test

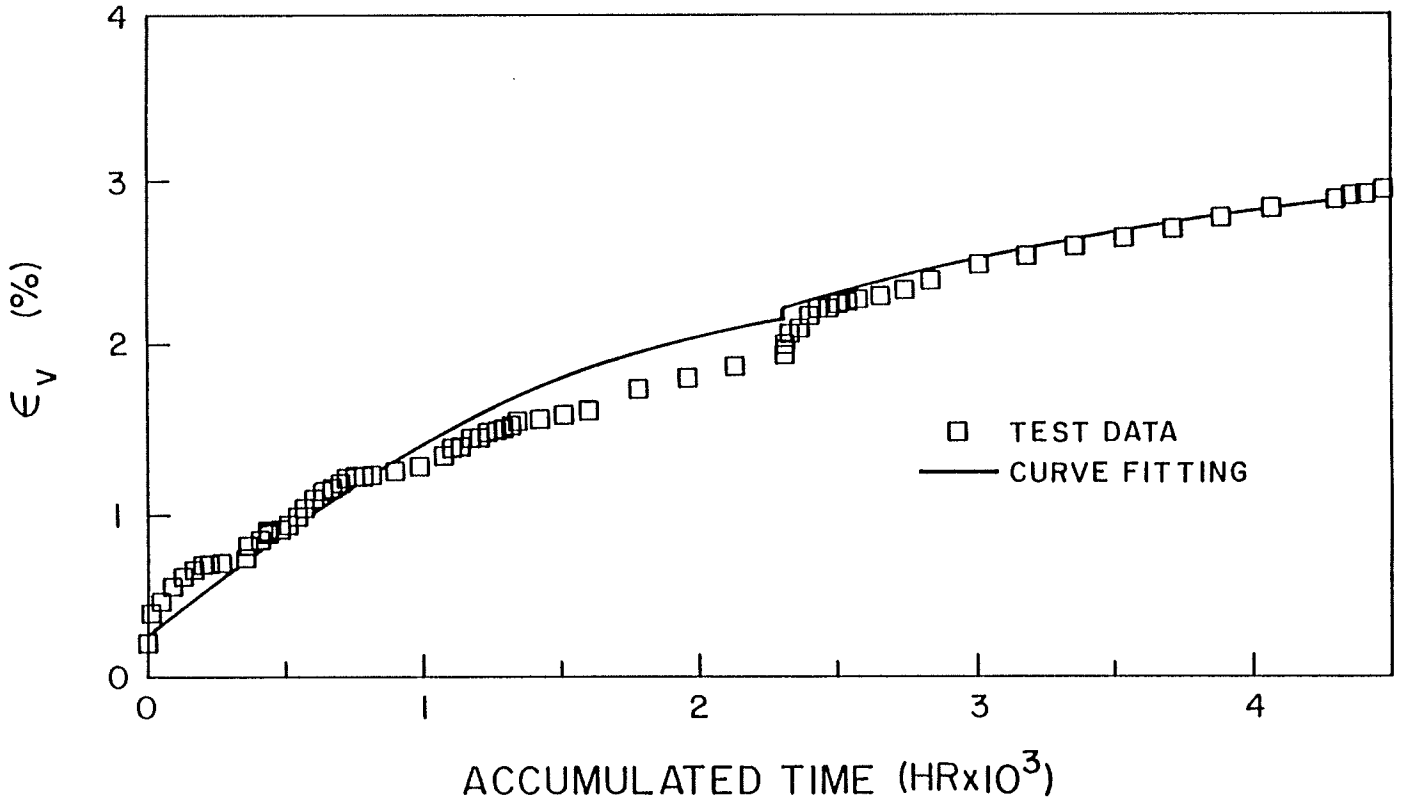

Fig.10.3 Curve fitting of creep test data - an isotropic multi-stage loading creep test

$$[10.10] \quad \varepsilon_{vm}^{ep} = \frac{\lambda}{V} \ln\left(\frac{p_{o2} + p_m}{p_{o3}}\right)$$

where $\lambda/V = 0.017$, $p_{o2} = 190$ kPa, and $p_{o3} = 195$ kPa.

Creep equation (time dependent plastic strain):

$$[10.11] \quad \varepsilon_{vm}^{tp} = \frac{\psi}{V} \ln\left(\frac{t_o + t_e}{t_o}\right)$$

where $\psi/V = 0.007$, $t_o = 600$ hr, t_e is equivalent time.

Using [10.10] and [10.11], the equation for calculating creep strains under any stepwise isotropic loading is:

$$[10.12] \quad \varepsilon_v = \frac{\lambda}{V} \ln\left(\frac{p_{o2} + p_m}{p_{o3}}\right) + \frac{\psi}{V} \ln\left(\frac{t_o + t_e}{t_o}\right)$$

Then using the method in Chapter 8, the general constitutive equation for continuous isotropic stressing can be written:

$$[10.13] \quad \dot{\varepsilon}_{vm} = \frac{\kappa/V}{p_{o1} + p_m} \dot{p}_m + \frac{\psi}{t_o V} e^{-(V/\psi)\varepsilon_{vm}} \left(\frac{p_{o2} + p_m}{p_{o3}}\right)^{\lambda/\psi}$$

In this way, the mathematical functions [10.9], [10.10] and [10.11] are used to describe the characteristics of the soil behaviour. The basic principle for determining the parameters in [10.9], [10.10], and [10.11] is that the parameters are chosen so that the calculated curve from [10.12] or [10.13] best matches the test data from isotopic loading shown in Figs. 10.2, 10.3. Details of the curve fitting calculations are in Table 10.4 of Appendix 10.1.

Introducing [10.13] into [10.1], and replacing the bulk modulus with the expression $(p_{o1} + p)/(\kappa/V) = K$, the expression for the elastic strain rate can be written:

$$[10.14] \quad \dot{\varepsilon}^{e}_{vm} = \frac{\kappa/V}{p_{o1} + p_m} \dot{p}_m = \frac{\kappa/V}{p_{o1} + p} \dot{p}$$

The use of p instead of p_m in this relationship again means assuming that the elastic volumetric strain is independent of deviator stresses, that is, isotropic elasticity. According to Rahman (1988), the average elastic shear modulus for the frozen sand was G = 112,500 kPa.

The visco-plastic strain rate is, from [10.13]:

$$[10.15] \quad \dot{\varepsilon}^{vp}_{vm} = \frac{\psi}{t_o V} e^{-(V/\psi)\varepsilon_{vm}} \left(\frac{p_{o2} + p_m}{p_{o3}}\right)^{\lambda/\psi}$$

So from [10.8] and [10.15] the scaling function is:

$$[10.16] \quad S = \frac{\psi}{t_o V} e^{-(V/\psi)\varepsilon_v} \left(\frac{p_{o2} + p_m}{p_{o3}}\right)^{\lambda/\psi} / p_m$$

where again ε_{vm} is replaced by ε_v.

10.4 Modelling Multi-stage Creep Tests

In the previous section (10.2), the EVP model was scaled and calibrated for frozen sand. In the section, the model is used to predict the results of two triaxial compression tests performed on specimens of the same sand. The stress paths in these tests were different from those used to calibrate the model. One test was a multi-stage, constant mean

normal stress, test, while the other was a multi-stage, constant cell pressure test. A comparison is then made between the observed creep strains and those predicted by the model.

10.4.1 Equations for multi-stage creep tests

In multi-stage creep tests in which q and p were kept constant at each stage, the initial elastic responses after applying mean stress p and deviator stress q are:

$$[10.17] \quad \begin{cases} \Delta\varepsilon_v^e = \frac{1}{K}\,\Delta p, \\ \Delta\varepsilon_s^e = \frac{1}{3G}\,\Delta q \end{cases}$$

The incremental visco-plastic strain responses from [10.1] and [10.16] are:

$$[10.18] \quad \begin{cases} d\varepsilon_v^{vp} = \frac{\psi}{t_o V}\, e^{-(V/\psi)\varepsilon_v} \left(\frac{p_{o2}+ p_m}{p_{o3}}\right)^{\lambda/\psi} \frac{(2p - p_m)}{p_m}\, dt \\ d\varepsilon_s^{vp} = \frac{\psi}{t_o V}\, e^{-(V/\psi)\varepsilon_v} \left(\frac{p_{o2}+ p_m}{p_{o3}}\right)^{\lambda/\psi} \frac{(2q/M^2)}{p_m}\, dt \end{cases}$$

Integrating [10.18] with initial conditions: $t = 0$, $\varepsilon_v^{vp} = \varepsilon_{vi}^{vp}$ and $\varepsilon_s^{vp} = \varepsilon_{si}^{vp}$, the total visco-plastic strains are:

$$[10.19]\quad \begin{cases} \varepsilon_v^{ep} = \dfrac{\psi}{V}\ln\left[\dfrac{t}{t_o}\left(\dfrac{p_{o1}+p}{p_{o1}}\right)^{(-\kappa/\psi)}\left(\dfrac{p_{o2}+p_m}{p_m}\right)^{\lambda/\psi}\left(\dfrac{2p-p_m}{p_m}\right) + e^{(V/\psi)\varepsilon_{vi}^{vp}}\right] \\ \varepsilon_s^{vp} = \dfrac{2q/M^2}{2p-p_m}\left(\varepsilon_v^{vp} - \varepsilon_{vi}^{vp}\right) + \varepsilon_{si}^{vp} \end{cases}$$

where the initial strains are: $\varepsilon_{vi}^{vp} = \varepsilon_{vi} - \varepsilon_{vi}^{e}$; and $\varepsilon_{si}^{vp} = \varepsilon_{si} - \varepsilon_{si}^{e}$.

The total strains are:

$$[10.20]\quad \begin{cases} \varepsilon_v = \dfrac{\kappa}{V}\ln\left(\dfrac{p_{o1}+p}{p_{o1}}\right) + \varepsilon_v^{vp} \\ \varepsilon_s = \dfrac{q}{3G} + \varepsilon_s^{vp} \end{cases}$$

Loading from point (p_i, q_i) to (p_{i+1}, q_{i+1}) with creep time t at (p_{i+1}, q_{i+1}) the total strains after shearing, using [10.19] and [10.20], are:

$$[10.21]\quad \begin{cases} \varepsilon_v - \varepsilon_{v,iso} = \left\{\dfrac{\psi}{V}\ln\left[\dfrac{t}{t_o}\left(\dfrac{p_{o1}+p_{i+1}}{p_{o1}}\right)^{(-\frac{\kappa}{\psi})}\left(\dfrac{p_{o2}+p_m}{p_3}\right)^{\lambda/\psi}\left(\dfrac{2p_{i+1}-p_m}{p_m}\right) + \right.\right. \\ \qquad \left.\left. + e^{\varepsilon_{vi}^{vp}\, V/\psi}\right] + \dfrac{\kappa}{V}\ln\left(\dfrac{p_{o1}+p_{i+1}}{p_{o1}}\right)\right\} - \varepsilon_{v,iso} \\ \varepsilon_s - \varepsilon_{s,iso} = \left\{\dfrac{2q(a+.5bp_m)^2}{2p_{i+1}-p_m}\left[\left(\left(\varepsilon_v - \varepsilon_{v,iso}\right) + \varepsilon_{v,iso} - \right.\right.\right. \\ \qquad \left.\left.\left. - \dfrac{\kappa}{V}\ln\left(\dfrac{p_{o1}+p_{i+1}}{p_{o1}}\right)\right) - \varepsilon_{vi}^{vp}\right] + \right. \\ \qquad \left. + \left(\varepsilon_{si} - \dfrac{q_i}{3G}\right) + \dfrac{q_{i+1}}{3G}\right\} - \varepsilon_{s,iso} \end{cases}$$

where $\varepsilon_{v,iso}$ is the strain after isotropic stressing, and is given by:

$$[10.22] \quad \varepsilon_{v,iso} = \frac{\lambda}{V} \ln\left(\frac{p_{o2} + p_{iso}}{p_{o3}}\right) + \frac{\psi}{V} \ln\left(\frac{t_o + t_e}{t_o}\right)$$

$$= \frac{\lambda}{V} \ln\left(\frac{p_{o2}+p_{iso}}{p_{o3}}\right) + \frac{\psi}{V} \ln\left[\frac{t}{t_o} + \left(\frac{p_{o1}+p_{iso}}{p_{o1}}\right)^{\frac{\kappa}{\psi}} \left(\frac{p_{o2}+p_{iso}}{p_{o3}}\right)^{-\frac{\lambda}{\psi}}\right]$$

The shear strain, $\varepsilon_{s,iso}$ in [10.21] is the strain after isotropic stressing and is equal to zero from [10.1]. The stress p_m in [10.21] is found from [10.5] when we know the current stress state (p,q).

10.4.2 Prediction of test MST2

The mean stress p = 280 kPa was kept constant throughout the test. The deviator stress increment, Δq, was 120 kPa. Temperature was -3 C^o. The loading history is given in Table 10.1.

Table 10.1 Loading History of MST2, p = 280 kPa

q (kPa)	0	120	240	360	480	600
Duration (hrs)	596	475	504	1006	1393	984

Eqn.[10.21] was used to predict the $(\varepsilon_v - \varepsilon_{v,iso})$ vs. t and $(\varepsilon_s - \varepsilon_{s,iso})$ vs. t relations. Fig.10.4 shows the comparison between the predicted and the observed volumetric and shear creep strains. Generally, the model overpredicted the shear strains and underpredicted

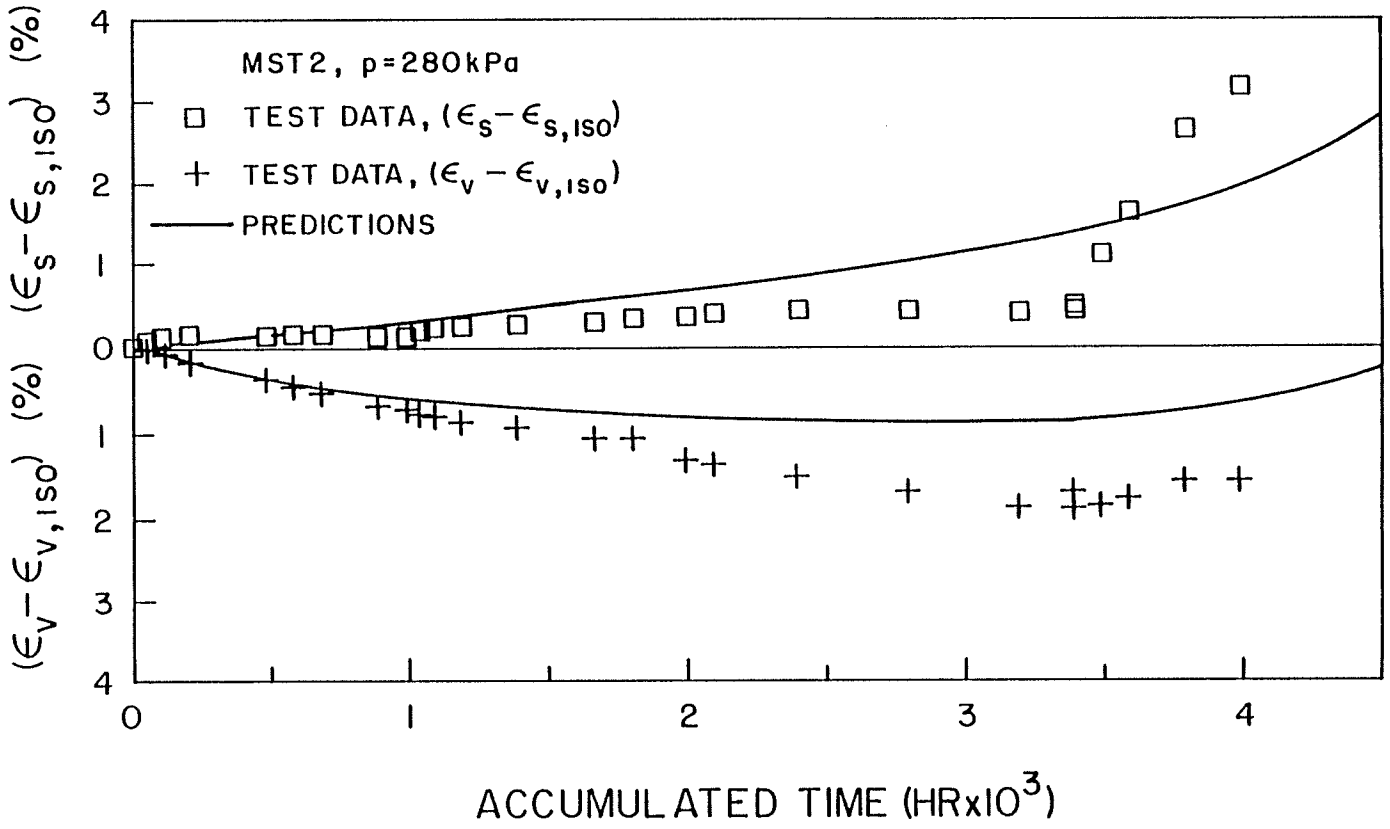

Fig.10.4 Predicted and measured (ε_s-$\varepsilon_{s,iso}$) vs. t and (ε_v-$\varepsilon_{v,iso}$) vs. t for a multi-stage, constant p, triaxial compression creep test - MST2

the volumetric strains. The difference between predicted and observed tended to increase with elapsed time. However the model showed some interesting features. Its prediction of the start of dilation and the onset of tertiary creep corresponded with the observed time, which was approximately 3300 hours. This is very significant in view of the fact that the model was calibrated by means of an isotropic compression test which did not involve shear strains. Details of this prediction are in Table 10.5. of Appendix 10.2.

10.4.3 Prediction of test MST10

This was a constant cell pressure triaxial compression test. Temperature was -3 C^{o}. The loading history is given in Table 10.2.:

Table 10.2 Loading History of MST10, σ_3 = 70 kPa

q (kPa)	0	20	40	60	80	100
p (kPa)	70	76.7	83.3	90	96.7	103.3
Duration (hrs)	407	226	503	117	144	144

120	140	160	180	200	240	280	320	360
110	116.7	123.3	130	136.7	150	163.3	176.7	190
312	503	1549	720	1223	719	807	1319	959

Eqn.[10.21] in conjunction with [10.22] is used to make the prediction.

Details are in Table 10.6 of Appendix 10.2. A comparison of the observed shear and volumetric strains with those predicted by the model, is shown in Fig. 10.5. It is seen that the agreement between the observed and predicted shear strains is quite good. On the other hand there is poor agreement between predicted and observed volumetric strains.

10.5 Discussion and Conclusions

In calibrating the EVP model, determining the scaling function is very important because it controls the magnitude of all the visco-plastic strain rates. Thus, any error in this function, significantly affects the predictive accuracy of the model. In this particular study, only one multi-stage isotropic test was available for determining the scaling function. The fact that it was a multi-stage test rather than a series of single-stage tests, made the procedure for finding the scaling function more complicated than necessary and subject to inaccuracies. This may be the source of the obtained discrepancies between measured and predicted creep strains, particularly volumetric creep strains.

Accurate establishment of the neutral line in Fig. 10.1 is essential to the model predictive capability. In this study, the neutral line was based on results from constant mean normal stress triaxial tests. The increments of stress used in the tests were relatively large and this made it impossible to define the neutral line accurately. Further

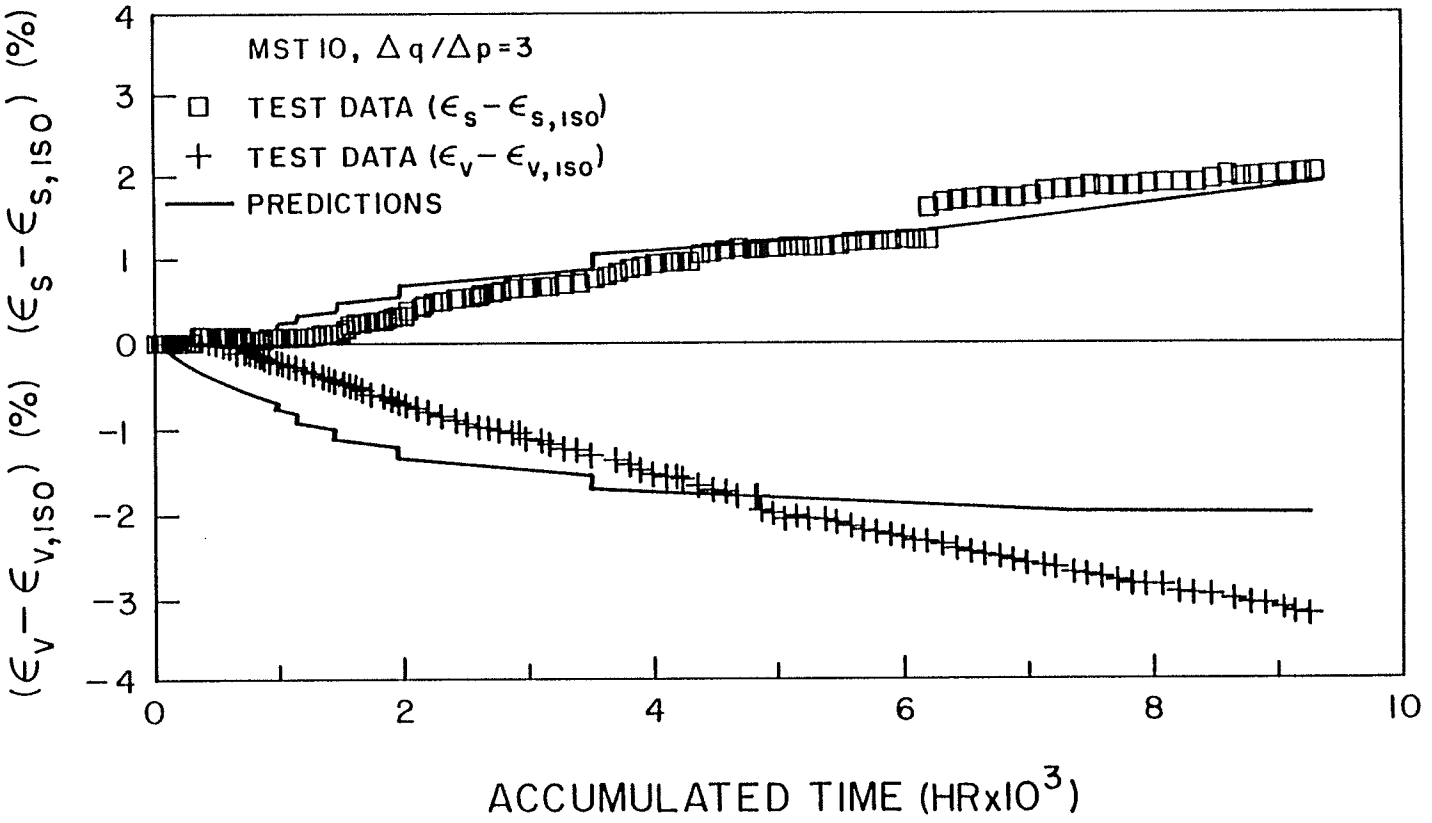

Fig.10.5 Predicted and measured (ε_s-$\varepsilon_{s,iso}$) vs. t and (ε_v-$\varepsilon_{v,iso}$) vs. t for a multi-stage, constant σ_3, triaxial compression creep test - MST10

tests with smaller stress increments would improve the accuracy of the model.

It should be noted that there are a number of assumptions in the model. The flow rule in Eqn.[10.1] assumes that the visco-plastic strain rates are normal to a flow surface which is identical to a visco-plastic potential function. This flow rule is similar to the associated flow rule used in elasto-plastic theory. It is assumed that the flow surface is an ellipse in q-p space. The real surface should be determined from a series of tests. The time-independent part of strains is assumed to be isotropically elastic. The scaling function S is simplified by using ε_v instead of ε_{vm}. As pointed out for 1-D EVP models in Chapter 5, some assumptions are made to find $\dot{\varepsilon}^{vp}_{vm}$ in the scaling function S.

Despite the differences between observed creep strains and those predicted by the model, the model presents a rational framework representing the complex behaviour of frozen soil. Further testing is now needed to examine and refine the assumptions used in the model, and to provide additional data for its validation.

Chapter 11

CONCLUSIONS AND SUGGESTIONS FOR FURTHER WORK

Chapters 3 and 4 discussed the framework of three-modulus hypoelasticity models and their applications to three different soils. Chapters 5, 6, and 7 presented the general theoretical work of 1-D Elastic Visco-Plastic (EVP) models and the detailed construction, calibration and verification of the models. Chapters 8, 9 and 10, contained the framework of 3-D EVP models and their applications to sand-bentonite buffer materials and a frozen sand. The features and limitations of these models have been discussed following the presentation of each model. This chapter will summarize those discussions starting with 3-D models, draw some conclusions from the models, and make some suggestions for further research in this field.

11.1 3-D Elastic Visco-Plastic (EVP) Models

The features of 3-D EVP models may be summarized according to the structure, calibration methods and functions of the models.

1. Structure of 3-D EVP models:

(1). Total strains are the sum of time-independent strains (not

necessary elastic) and time-dependent strains.

(2). The time-independent part of total strains may be modeled by a isotropic model as for the frozen sand, or by an anisotropic KGJ model as for the sand-bentonite material.

(3). The time-dependent part of the total strains is calculated using a flow rule.

(4). The flow surface defined in Chapter 8 may be elliptical as used here in the models for the sand-bentonite material and the frozen sand, or some other shapes.

(5). The strength envelope (or zero $\dot{\varepsilon}_v^{vp}$ line) may be curved in q,p-space and smooth on the π-plane as used in the model for sand-bentonite (or in the model for the frozen sand).

2. Methods for determining model parameters:

(1). A number of single-stage isotropic consolidation tests at different confining pressures are preferred to find the parameters for scaling functions. The procedure using this type of tests is simple. A multi-stage isotropic consolidation test may also be used to find all parameters in the scaling function as shown in the modelling of the frozen sand. However, in this case the procedure for finding those parameters is more complicated than that using single-stage tests.

(2). The ultimate strength envelope used in the model for the sand-

bentonite material may be found from a number of undrained or drained shear tests. The zero $\dot{\varepsilon}_v^{vp}$ line in the model for the frozen sand can be found from a number of multi-stage q creep tests at constant mean stresses.

(3). The moduli K,G,J (or K,G) can be determined using the same procedure as that in hypoelasticity models using unloading/reloading data in isotropic consolidation tests and undrained shear tests.

(4). The flow surface here was basically assumed and further work is required on its experimental determination.

3. The models can consider the following characteristics of soil behavior:

(1). **Non-linearity:** models are sets of nonlinear differential equations.

(2). **Irreversibility:** no unloading/reloading criteria are needed if using a logarithmic function for creep, i.e. Eqn,[8.22], [9.7] or [10.11]. For loading, positive strain rates (or positive stress rates) are used. Negative strain rates (or negative stress rates) are used to model unloading.

(3). **Inherent anisotropy** is described by the KGJ model; **induced anisotropy** is described through the flow rule equations.

(4). **Time and strain effects:** like creep, relaxation and strain rate

dependency.

(5). **Loading history:** if only final states are the same, but the loading histories to the states are different, then the final stresses or strains will be different.

The work of 3-D EVP modelling is still at preliminary stage. There are a number of uncertainties and limitations in the models at this stage.

1. Uncertainties:

(1). The flow function was assumed. The real shape of this flow function in q,p-space and on π-planes may be identified by using appropriate tests.

(2). It is unclear what is the suitable evolution law for different soils, that is experimental studies are required to examine what evolution law are most suitable to desribe the behaviour of soils.

(3). The suitable scaling function is also not known with certainty.

(4). The stress path dependency of time-independent behavior is largely unknown. Adequate testing program have not yet been undertaken.

2. Limitations:

(1). The models can not consider any time or strain rate effects related to the swelling potential of soils such as the

sand-bentonite material described in the Chapters 8,9. The work on sand-bentonite therefore relates only to its compression (not expansive) behavior.

(2). The models can not produce the hysteritic loops in unloading-reloading as found in all soils.

Based on the research done so far on 3-D EVP modelling, the following suggestions are made for its further development.

1. Better understanding is required for the physical basis of the flow rule, flow surface and visco-plastic potential function.

2. The evolution law in Scaling Methods 1,2,3 of Chapter 8 should be given further study.

3. Other scaling methods should be developed. For example, use oedometer tests to find the scaling function.

4. Develop test techniques to measure the shape of flow surface.

5. The constructed models need more verification for different soils and more general stress states.

6. At a later stage the models should be incorporated into numerical analyses, such as finite element analysis.

11.2 1-D Elastic Visco-Plastic (EVP) Models

Compared with 3-D EVP models, the study of 1-D EVP models is more complete. The features of this type of models are:

1. Structure of 1-D EVP models:

(1). Total strains are the sum of time-independent elastic strains (i.e. instant) and time-dependent visco-plastic strains.

(2). Some important concepts are defined and used in constructing the EVP models. These include the "instant time line", "equivalent time", and "reference time line".

(3). The general framework that has been developed provides wide applicability of 1-D EVP models to different soils. For example, logarithmic functions or power functions may be used to particularize the general formulation depending on the nature of the soil.

2. Methods for determining the model parameters:

(1). The number of parameters depends on the fitting functions.

(2). Two methods have been developed, an analytical method and a graphic method.

(3). It is preferable that a number of single-stage creep tests at different pressures are used to find the parameters. In this

case, we may use the analytical method or the graphic method depending on the complex of the fitting functions.

(4). multi-stage creep tests can also be used to find the modelling parameters. However in this case, only the graphic method may be used. In general, the procedure in finding the parameters is quite complex.

3. The model has the following capabilities:

(1). **Non-linearity.**

(2). **Time effects:** such as creep, relaxation.

(3). **Strain rate effects.**

(4). **First loading and unloading/reloading:** no unloading/reloading criteria are needed if a logarithmic function is used for creep i.e. Eqn.[6.3]. If a power function is used with limits to the region of creep behavior (for example Eqn.[7.4]), then the left side of the infinite time line (see Fig.7.2) is pure elastic, the right side is elastic visco-plastic behavior.

The uncertainties in the models are:

1. The slope of the elastic line in the models may depend on loading history.

2. The infinite time line is extrapolated.

The limitations of the models are:

1. They can not consider any time and strain rate effects resulting from the swelling potentials in the soil.

2. The capabilities of models need further validation.

Suggestions for further research:

1. Apply the models to solve consolidation problems, compare calculated values with measured values. Thus validation of the model can be examined.

2. Apply the model to different soils, and compare the predicted results with test data measured in the laboratory.

11.3 Three-Modulus Hypoelasticity Models

The proposed three modulus hypoelasticity models are used for describing time-independent stress-strain behavior. The features of the model are:

1. The structure of the models is simple. There are three moduli in the model.

2. New methods have been suggested to determine these moduli functions using isotropic consolidation tests and undrained shear tests or drained shear tests.

3. The model can account for non-linearity, anisotropy, and the coupling of q, ε_v and p', ε_s.

The limitations of the model are:

1. The model can not consider time effects, or cyclic effects.

2. The applicability of the models to general stress states and more complicated loading conditions, like unloading/reloading, needs further examination.

3. In general, the model should be applied only to monotonic or propotional loading conditions.

The suggestion for the development of hypoelasticity models is to apply the models to solve boundary value problems, and to examine the validation of the models under general loading conditions.

APPENDIX 6.1 Alternative Derivation of [6.26] for Relaxation Tests

During relaxation the total strain ε_z is kept constant and it appears reasonable to assume that the total time-independent plastic strain ε_z^{sp} is also constant. That is, the viscous creep strain ε_z^{tp} increases, while the elastic strain ε_z^e decreases at the same rate (Fig.6.12). This is similar in principle to the condition $\varepsilon_v^e = -\varepsilon_v^p$ in undrained triaxial tests in Critical State modelling. Using this assumption at a point such as (i+n) for example in Fig.6.12, the increase of viscous creep strain from [6.4] must equal the decrease of elastic strain from [6.1]:

$$[6.31] \quad -\frac{\kappa}{V} \ln \frac{\sigma'_{z,i+n}+d\sigma'_{z,i+n}}{\sigma'_{z,i+n}} = \frac{\psi}{V} \ln \frac{t_{i+n,e}+dt_{i+n}+t_o}{t_{i+n,e}+t_o}$$

Since $d\sigma'_{z,i+n}$, dt_{i+n} are small, [6.31] reduces to:

$$[6.32] \quad -\frac{\kappa}{V} \frac{d\sigma'_{z,i+n}}{\sigma'_{z,i+n}} = \frac{\psi}{V} \frac{dt_{i+n}}{t_{i+n,e}+t_o}$$

Eqn.[6.32] can not be integrated directly because the equivalent time t_e in the denominator is different from real time t. However a relationship between t and t_e can be found as follows. Relaxation from point i to point i+1 in Fig.6.12 produces the relationship:

$$[6.33] \quad \frac{\psi}{V} \ln \frac{t_{i+1,e}+t_o}{t_o} = \frac{\psi}{V} \ln \frac{t_{ie}+dt_i+t_o}{t_o} + \frac{\lambda-\kappa}{V} \ln \frac{\sigma'_{zi}}{\sigma'_{zi}+d\sigma'_{zi}}$$

When dt_i and $d\sigma'_{zi}$ are small, [6.32] and [6.33] can be combined to give:

$$[6.34] \quad t_{i+1,e} = t_{ie} + \frac{\lambda}{\kappa} dt_i$$

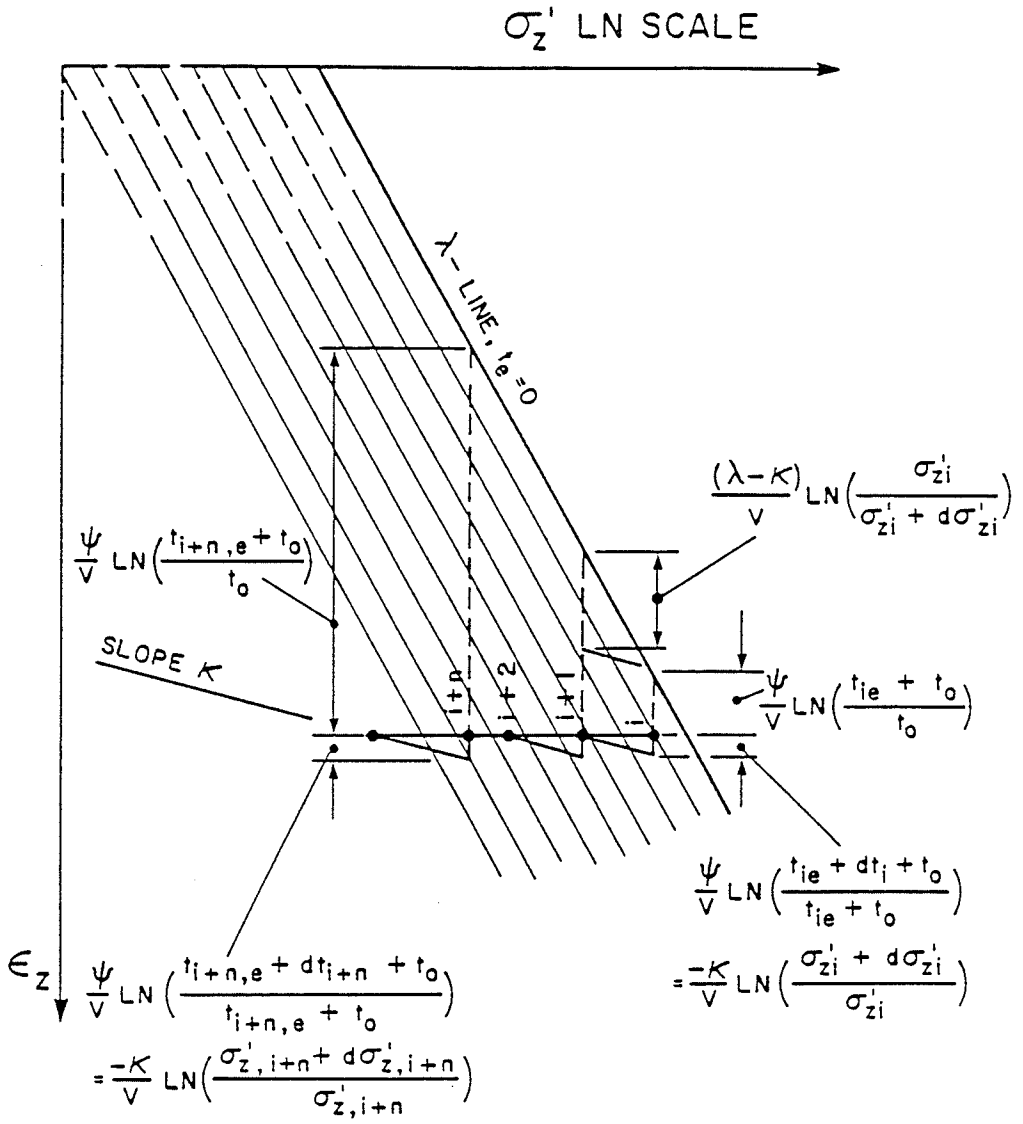

Fig.6.12 Schematic representation of $\varepsilon^{tp}, \varepsilon^{e}$-relationships for generalization of relaxation test

Using the same procedure from point (i+1) to (i+2) in Fig.6.12:

$$[6.35] \quad t_{i+2,e} = t_{i+1,e} + \frac{\lambda}{\kappa} dt_{i+1}$$

Now replace $t_{i+1,e}$ with [6.34]:

$$[6.36] \quad t_{i+2,e} = t_{ie} + \frac{\lambda}{\kappa} (dt_i + dt_{i+1})$$

Similarly for any general point (i+n):

$$[6.37] \quad t_{i+n,e} = t_{ie} + \frac{\lambda}{\kappa} (dt_i + dt_{i+1} + dt_{i+2} + \cdots + dt_{i+n-1})$$

When $n \Rightarrow \infty$, [6.37] becomes:

$$[6.38] \quad t_e = t_{ie} + \frac{\lambda}{\kappa} t$$

Substituting [6.38] into the relaxation equation [6.32] for any general point produces:

$$[6.39] \quad -\frac{\kappa}{V} \frac{d\sigma'_z}{\sigma'_z} = \frac{\psi}{V} \frac{dt}{t_{ie} + \frac{\lambda}{\kappa} t + t_o}$$

Integrating [6.39] with initial values $t = t_i$, $\sigma'_z = \sigma'_{zi}$ produces the same equation as [6.26].

APPENDIX 6.2 An Empirical Modelling Equation for the CRSN Test

Under CRSN conditions, the theoretical solution [6.28] shows that stress-strain lines for different strain rates are parallel, with approximately equal separations for each tenfold change in strain rate Figs.5a,b. The slope of these CRSN lines is almost (but not completely) equal to the slope of corresponding lines in STD tests, see Eqn.[6.28], Figs.4,5a,5b. From this, the following empirical equation is suggested to fit experimental data:

$$[6.40] \quad \varepsilon_z = \bar{\lambda} \ln(\sigma'_z/\sigma'_{zo}) + \bar{\psi} \ln(\frac{\bar{\psi}/t_o}{\dot{\varepsilon}_z})$$

where $\bar{\lambda}$ is now evaluated from the slope of CRSN tests in ln(stress)-vertical strain space. The value of the viscous plastic parameter $\bar{\psi}$ can be found from CRSN data as follows. In Fig.5a, when points A and B have the same strain $\varepsilon_{zA} = \varepsilon_{zB}$, then:

$$[6.41] \quad \varepsilon_{zA} = \bar{\lambda} \ln(\sigma'_{zA}/\sigma'_{zo}) + \bar{\psi} \ln(\frac{\bar{\psi}/t_o}{\dot{\varepsilon}_{zA}})$$

$$[6.42] \quad \varepsilon_{zB} = \bar{\lambda} \ln(\sigma'_{zB}/\sigma'_{zo}) + \bar{\psi} \ln(\frac{\bar{\psi}/t_o}{\dot{\varepsilon}_{zB}})$$

and these two equations can be solved for $\bar{\psi}$:

$$[6.43] \quad \bar{\psi} = \bar{\lambda} \ln(\sigma'_{zA}/\sigma'_{zB})/\ln(\dot{\varepsilon}_{zA}/\dot{\varepsilon}_{zB})$$

In Bäckebol clay (Sällfors 1975) $\bar{\lambda}$ is 0.41, at this accuracy, the same as the value of λ/V given earlier. Eqn.[6.43] then predicts $\bar{\psi} = 0.030$ and allows σ'_{zo} and t_o to be found from [6.41] and [6.42]. From these

it is easy to calculate the relationship between stress and strain rate for different strains in [6.40]. Fig.6.13 shows that results computed from [6.40] agree well with the measured test data.

If it is again assumed that the preconsolidation pressures σ'_{zc} corresponding to different strain rates all occur at the same vertical strain ε_z = constant, then [6.40] can also be used to evaluate the relationship between σ'_{zc} and $\dot{\varepsilon}_z$. Fig.6.14 shows that the modelling matches the test data closely. Equation [6.40] has the same mathematical form as that suggested by Kabbaj et al. (1986) but the new formulation gives clearer insight into the mechanisms of strain rate dependency in CRSN testing.

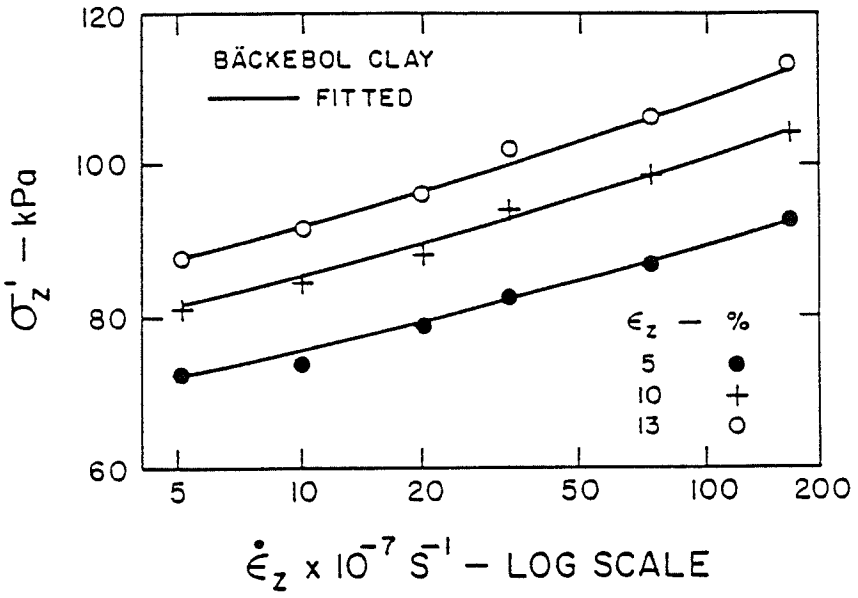

Fig.6.13 Alternative fitted modelling of stress - strain rate relationships (Bäckebol clay: Sällfors 1975)

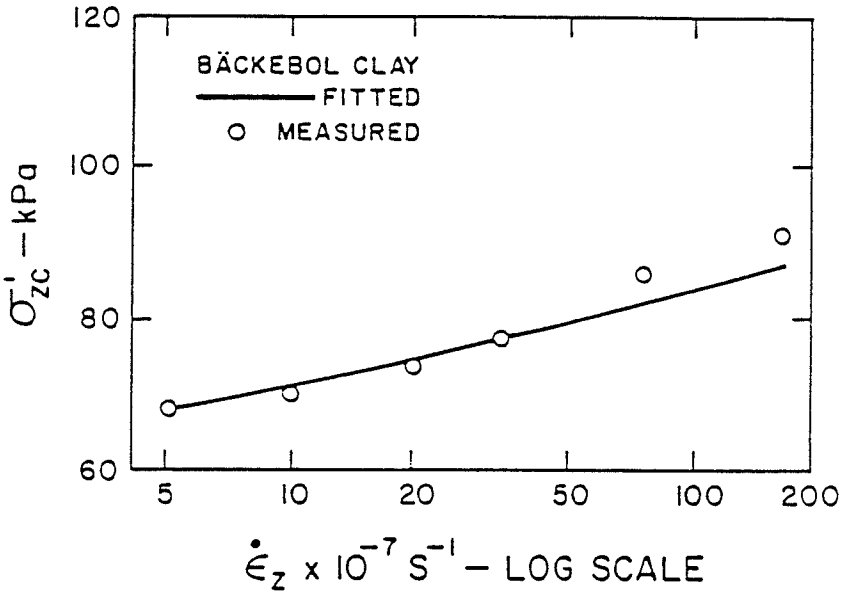

Fig.6.14 Alternative fitted modelling of preconsolidation pressure - strain rate relationships (Bäckebol clay: Sällfors 1975)

APPENDIX 8.1 Flow Surface and Strength Envelope for Anisotropic Soils

It was shown by earlier researches that the yield loci of natural clays are not symmetric to the p' axis in q,p' space, and are time dependent (Crooks and Graham 1976, Tavenas et al. 1978, Graham et al. 1983, Graham et al. 1988). The "yield loci" or " yield surfaces" used by these authors are called "flow surfaces" in the elastic visco-plastic modelling that has been developed here.

This Appendix will develop an appropriate mathematical function to model both asymmetric flow surfaces and strength envelope. This function may be used in EVP models to describe the time dependent stress-strain behavior of anisotropic soils.

Asymmetric flow surfaces in p',q-space may be described by the following mathematical equation:

$$[8.42] \quad F = q^2 + Ap'^2 - Bp'q - Ap'^{(2-n)}_m \, p'^n = 0$$

where parameters A may depend on Lode angle as defined in [8.9], B is a constant controlling the degree of asymmetry of the flow surface, n is a constant which controlls the shape of the flow surface in p',q-space (Figs.8.10, 8.11). In Eqn.[8.42] p'_m is a parameter on mean stress, p', axis. From [8.42]:

$$[8.43] \quad p'_m = [(q^2 + Ap'^2 - Bp'q) / A\, p'^n]^{1/(2-n)}$$

If a state point (p',q) is known, using [8.41] we can find p'_m. The flow surface in Eqn.[8.42] is a modification of the yield function

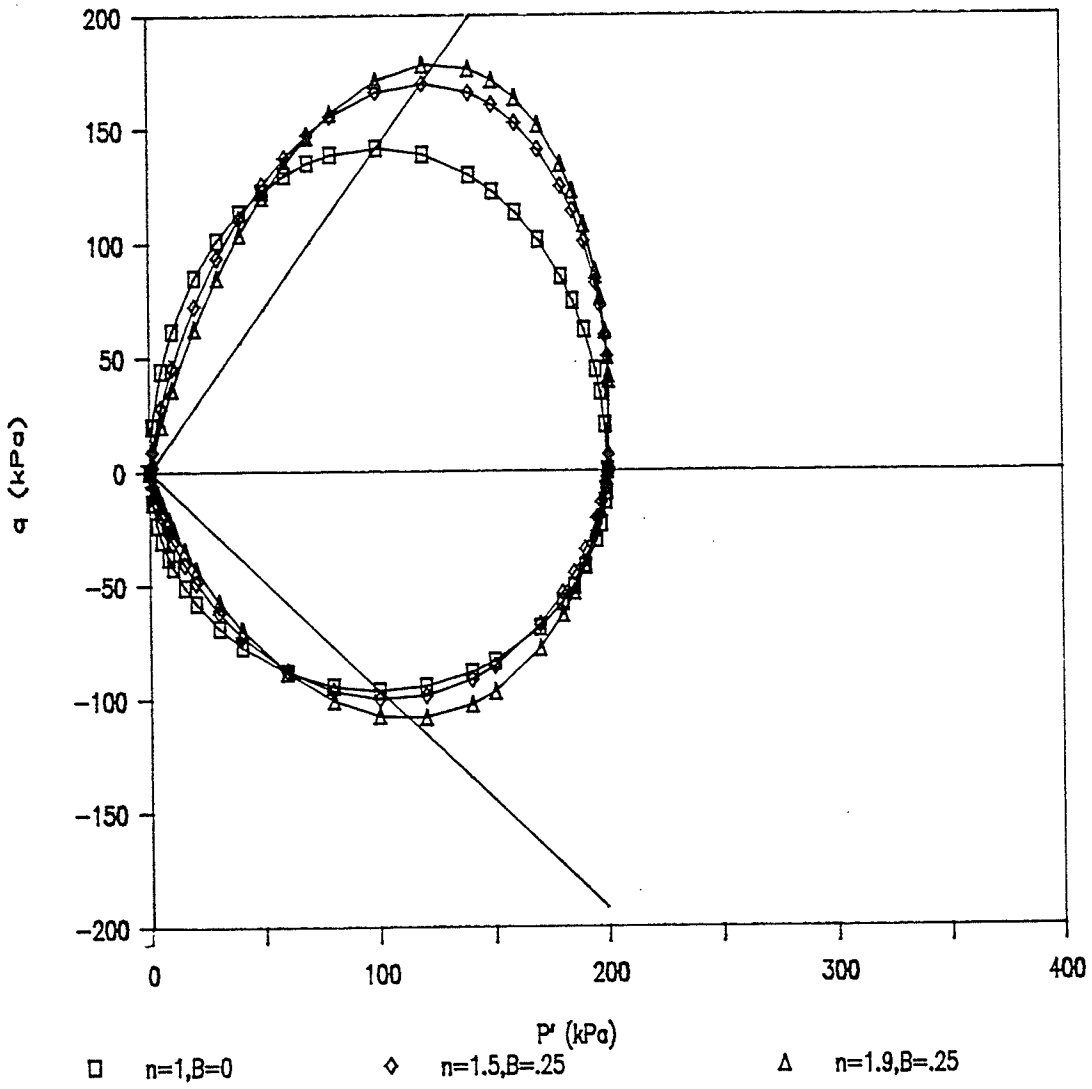

Fig.8.10 Asymmetric flow surfaces and strength envelope in p-q space - n = 1, B = 0; n = 1.5, B = 0.25; n = 1.9, B = 0.25

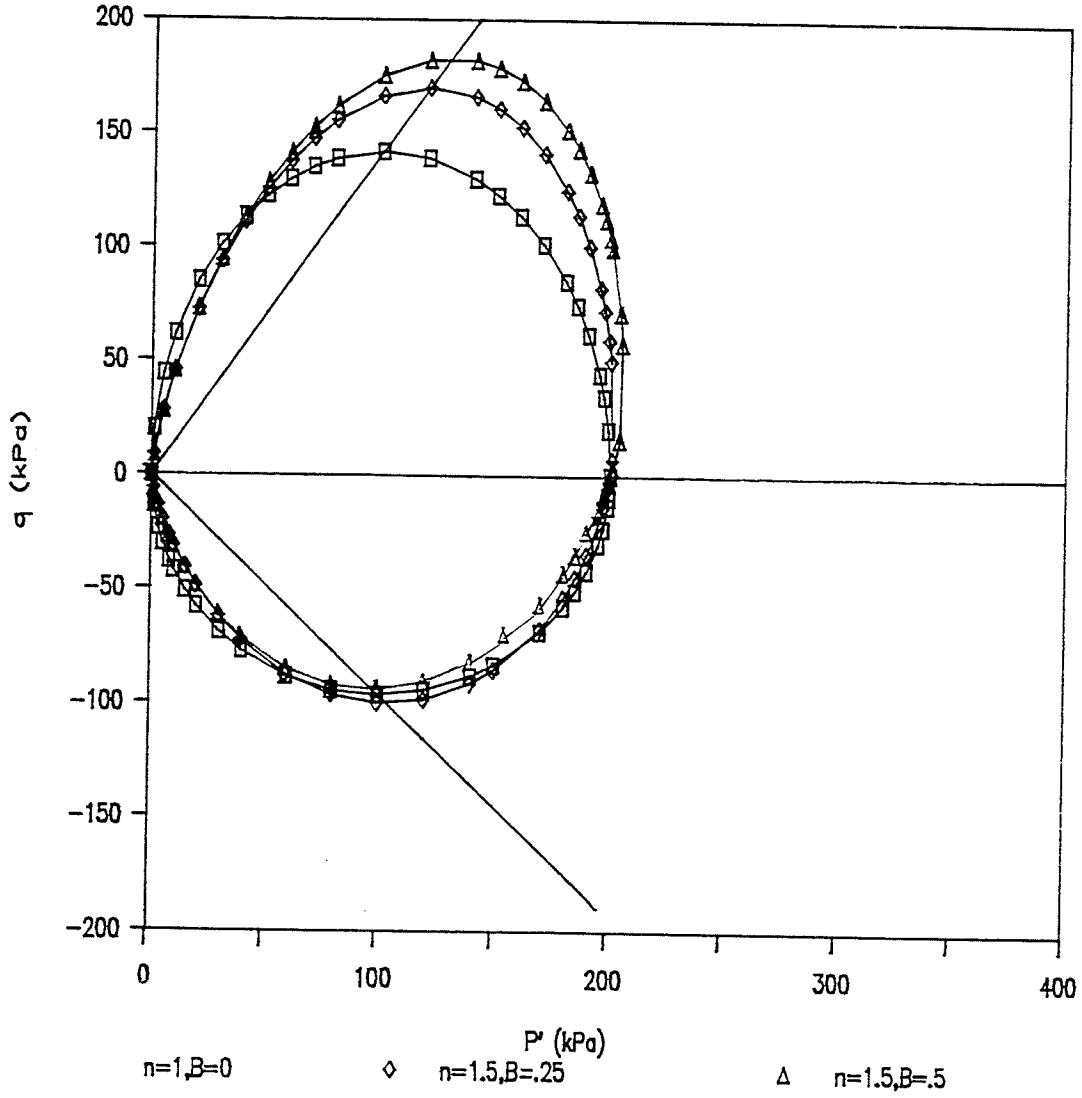

Fig.8.11 Asymmetric flow surfaces and strength envelope in p-q space - n = 1, B = 0; n = 1.5, B = 0.25; n = 1.5, B = 0.5

proposed by Desai et al. (1986, 1987) for initically isotropic soils.

The strength envelope is again defined by points on successive flow surfaces where normal vectors are perpendicular to p' axis, namely $\partial F/\partial p' = 0$, see Fig.8.10. From [8.42]:

$$[8.44] \quad \frac{\partial f}{\partial p'} = 2Ap' - Bq - Anp'^{(2-n)}_m p'^{n-1} = 0$$

from which:

$$[8.45] \quad 2A - B\eta_f - Anp'^{(2-n)}_m p'^{n-2}_f = 0$$

where $\eta_f = q_f/p'_f$. On the strength envelope, Eqn.[8.42] can be written:

$$[8.46] \quad \eta_f^2 + A - B\eta_f - Ap'^{(2-n)}_m p'^{n-2}_f = 0$$

Using [8.45] into [8.46]:

$$[8.47] \quad \eta_f^2 - (1 - \frac{1}{n})B\eta_f + (1 - \frac{2}{n})A = 0$$

Eqn.[8.47] is the strength envelope in p',q-space. A new technique is developed to generalize the flow function F in Eqn.[8.42] and the strength envelope in Eqn.[8.47] in p',q-space into expressions for general three-dimensional stress states.

The three dimensional strength envelope is assumed to be:

$$[8.48] \quad \eta_f = \frac{M_c}{(1 + \beta)^m} (1 + \beta \sin 3\theta)^m$$

where M_c is the slope of the strength envelope in compression in p',q-space, θ is the Lode angle as defined in Eqn.[8.9], m is a

constant controlling the shape of the strength envelope on π-plane (Fig.8.12). The parameter β in [8.48] can be found as follows. When $\theta = -30^{\circ}$ $\eta_f = M_e$ in triaxial extension, from [8.48]:

$$[8.49] \quad \eta_f = \frac{M_c}{(1 + \beta)^m} (1 - \beta)^m = M_e$$

from which:

$$[8.50] \quad \beta = \frac{1 - (M_e/M_c)^{1/m}}{1 + (M_e/M_c)^{1/m}}$$

The parameter A in [8.42] is then found from [8.46] using [8.47]:

$$[8.51] \quad A = - \frac{\eta_f^2 - (1 - 1/n)B\eta_f}{1 - 2/n} = \left\{ [\frac{M_c}{(1 + \beta)^m} (1 + \beta\sin3\theta)^m]^2 + \right.$$

$$\left. - B(1 - 1/n) \frac{M_c}{(1 + \beta)^m} (1 + \beta\sin3\theta)^m \right\} / (1 - 2/n)$$

When $\eta_f = M_c$ in the case of triaxial compression tests in p',q-space:

$$[8.52] \quad A = - \frac{M_c^2 - (1 - 1/n)BM_c}{1 - 2/n}$$

When $\eta_f = M_e$ in the case of triaxial extension tests in p',q-space:

$$[8.52] \quad A = - \frac{M_e^2 + (1 - 1/n)BM_e}{1 - 2/n}$$

Using Eqn.[8.42]:

$$[8.53] \quad q = 0.5\{ Bp' \pm \sqrt{(-Bp')^2 - 4A[p'^2 - p_m'^{(2-n)}p'^n)]} \}$$

Eqn.[8.53] can be used to calculate the flow surfaces in p',q-space. For example, the stress parameter p_m' = 200 kPa, the friction angle ϕ_c' =

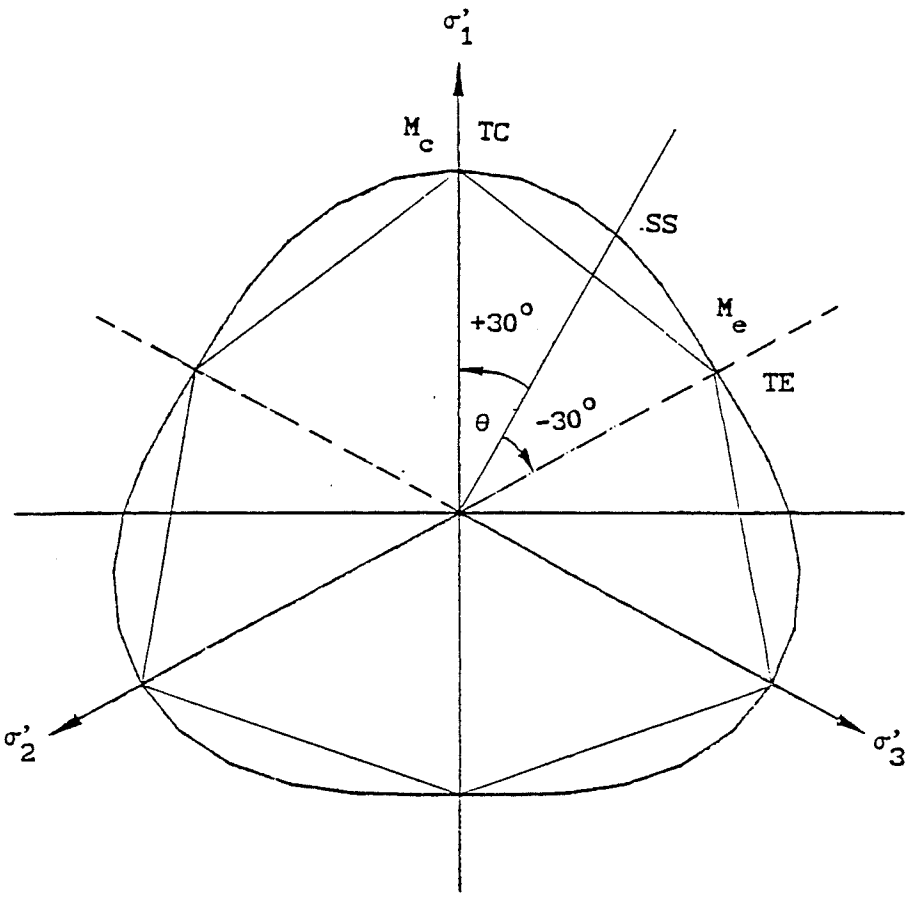

Fig.8.12 Strength envelopes on π-plane, $\phi'_c = \phi'_e = 35^\circ$, m = 0.5

$\phi'_e = 35^o$ which leads to $M_c = 1.418$ and $M_e = 0.963$. Fig.8.10 shows the comparison of the flow surfaces in which the parameters n = 1, B = 0; n = 1.5, B = 0.25; n = 1.9, B = 0.25 respectively. It is seen from this figure that when n = 1, B = 0, the above flow surface is half an ellipse with axis length $M_c p'_m$ in q direction; the below flow surface is half an ellipse with axis length $M_e p'_m$ in q direction. The influence of the parameter n on the flow surfaces can be seen from Fig.8.10 when n = 1.5, B = 0.25; n = 1.9, B = 0.25 respectively. Fig.8.11 shows the influence of the parameter B on the flow surfaces when n = 1.5, B = 0.25; n = 1.5, B = 0.5 respectively. The larger the value of the parameter B is, the more stronger the anisotropy of the flow surface will be.

Eqn.[8.48] is the equation of the strength envelope for general stress states. The strength envelope in p',q-space is represented in this model by two straight lines with a slope M_c in compression and M_e in extension, see Figs.8.10, 8.11. The strength envelope on π-plane is shown in Fig.8.12. It is seen in Fig.8.12 that the strength envelope, Eqn.[8.48], is smooth at the corners of the Mohr-Coulomb strength envelope.

APPENDIX 8.2 Modified Cam-Clay Model

The Modified Cam-Clay Model has been suggested for time independent stress- strain behavior (Burland 1969, Roscoe and Burland 1969). This model uses:

(1). Total incremental strains are divided into elastic incremental strains and plastic incremental strains:

$$[8.54] \quad d\varepsilon_{ij} = d\varepsilon^{e}_{ij} + d\varepsilon^{p}_{ij}$$

where the elasticity is isotropic. Graham and Houlsby (1983) suggested a simplified transverse anistropic elasticity to calculate the elastic strains.

(2). Associated flow rule:

$$[8.55] \quad d\varepsilon^{p}_{ij} = dS \frac{\partial F}{\partial \sigma'_{ij}}$$

where F is a yield function which is identical to the plastic potential function for the soil. The geometry of the yield function is a yield surface which is assumed a ellipse:

$$[8.56] \quad F = p'^{2} - p'_{m}p' + q^{2}/M^{2} = 0$$

where the parameter p'_{m} is:

$$[8.57] \quad p'_{m} = p' + \frac{q^{2}}{p'M^{2}}$$

(3) Logarithmic strain hardening law from isotropic stressing:

$$[8.58] \quad d\varepsilon_{vm}^{p} = \frac{\lambda-\kappa}{V} dp'_m/p'_m$$

Under triaxial stress states, the constitutive relationship is:

$$[8.59] \quad \begin{cases} d\varepsilon_v = \frac{\kappa}{Vp'} dp' + dS \frac{\partial F}{\partial p'} \\ d\varepsilon_s = \frac{1}{3G} dq + dS \frac{\partial F}{\partial q} \end{cases}$$

where the isotropic elasticity is characterized by two moduli, bulk modulus $p'V/\kappa$ and shear modulus G. The plastic volumetric strain at any point is:

$$[8.60] \quad d\varepsilon_v^p = dS \frac{\partial F}{\partial p'} = dS \ (2p' - p'_m)$$

The strain hardening law states that the plastic volumetric strain on the yield surface is kept the same. Using this condition, that is $d\varepsilon_v^p = d\varepsilon_{vm}^p$, from Eqns.[8.58] and [8.60], the scale factor dS is:

$$[8.61] \quad dS = \frac{\lambda-\kappa}{V} \frac{dp'_m}{p'_m(2p' - p'_m)}$$

Using the consistency condition, that is the current stress point must be kept on the yield surface, from Eqn.[8.56] or [8.57]:

$$[8.62] \quad dp'_m = [(2p' - p'_m) \ dp' + \frac{2q}{M^2} dq] \ / \ p'$$

Thus Eqn.[8.61] becomes:

$$[8.63] \quad dS = \frac{\lambda-\kappa}{V} \frac{dp'_m}{p'_m p'(2p' - p'_m)} [(2p' - p'_m) \ dp' + \frac{2q}{M^2} dq]$$

Using [8.63] into [8.59]:

$$[8.64]\quad \begin{cases} d\varepsilon_v = \dfrac{\kappa}{Vp'}\,dp' + \dfrac{\lambda-\kappa}{Vp'_m p'(2p'-p'_m)}\,[(2p'-p'_m)\,dp' + \dfrac{2q}{M^2}\,dq]\,(2p'-p'_m) \\ d\varepsilon_s = \dfrac{1}{3G}\,dq + \dfrac{\lambda-\kappa}{Vp'_m p'(2p'-p'_m)}\,[(2p'-p'_m)\,dp' + \dfrac{2q}{M^2}\,dq]\,\dfrac{2q}{M^2} \end{cases}$$

which can be written:

$$[8.65]\quad \begin{Bmatrix} d\varepsilon_v \\ d\varepsilon_s \end{Bmatrix} = \begin{bmatrix} \dfrac{\kappa}{Vp'} & 0 \\ 0 & \dfrac{1}{3G} \end{bmatrix} \begin{Bmatrix} dp' \\ dq \end{Bmatrix} + \dfrac{\lambda-\kappa}{Vp'_m p'(2p'-p'_m)} \begin{bmatrix} (p'-p'_m)^2 & \dfrac{2q}{M^2}(2p'-p'_m) \\ \dfrac{2q}{M^2}(2p'-p'_m) & (\dfrac{2q}{M^2})^2 \end{bmatrix} \begin{Bmatrix} dp' \\ dq \end{Bmatrix}$$

This is a matrix form of the modified Cam-Clay model under triaxial stress conditions.

APPENDIX 9.1 Corrections in the Calculation of Volumetric Strains in Isotropic Consolidation Tests

The calculation of volumetric strains in isotropic consolidation tests on sand-bentonite buffer materials is not as simple as is commonly assumed. Specimens of sand-bentonite compacted in the usual way with a hydraulic jack in a compaction mould are not fully saturated. The dry density obtained after compaction is not equal to the designed dry density which is γ_d = 1.67 Mg/m^3. In installing the specimen into a triaxial cell, the specimen may get access to water and swell. This happens, for example, when the top valve (and/or bottom valve) is open or when there is excess water on pedestal. Then the specimen absords water and swells before taking the initial burette readings used for establishing volume changes. The dry density of the specimen is changed by this process. Subsequent volume change readings do not reflect the real volume changes taking place in the specimen when expressed in terms of water content or specific volume. Sucking some water before taking burette readings is usually identified by measuring the final water content at the end of the test. In the testing of sand-bentonite buffer materials at the University of Manitoba, many tests have been done on low density buffer, γ_d = 1.50 Mg/m^3. We may want to use them together with the test data on high density buffer to study the behavior of the sand-bentonite mixtures. In this Appendix, we present some techniques to correct these variations and to calculate the real volumetric strains, using the data of T1001 and T1002 as an example.

Correction on dry density:

The targeted dry density was $\gamma_d = 1.67$ Mg/m^3. The dry density after compaction and before putting in a triaxial cell is γ_{do} which may not equal γ_d. The engineering strains are defined referring to the targeted dry density. This means that the configuration represented by the targeted dry density is used to be a reference at which the volumetric strains are zero. This reference can be chosen arbitrarily, but as long as it is determined, it should be used in all calculations of volumetric strains, specifically when relating them to specific volumes in the specimens.

Volumetric strain is:

$$[9.19] \quad \varepsilon_v = \frac{V_t - V}{V_t}$$

where V_t is targeted specific volume referring to $\gamma_d = 1.67$ Mg/m^3, V is current specific volume. Using V_o to denote the specific volume corresponding to the dry density γ_{do} after compaction, [9.19] can be written:

$$[9.20] \quad \varepsilon_v = \frac{V_t - V_o + V_o - V}{V_t V_o} V_o = \frac{V_t - V_o}{V_t} + \frac{V_o - V}{V_o} \frac{V_o}{V_t}$$

We know that $V_o = G_s\gamma_w/\gamma_{do}$, $V_t = G_s\gamma_w/\gamma_d$. Using ε_{vo} to denote the volumetric strain referring to V_o, the configuration after compaction, [9.20] becomes:

[9.21] $\varepsilon_v = (1 - \gamma_d/\gamma_{do}) + \varepsilon_{vo}\, \gamma_d/\gamma_{do}$

This equation allows for differences of targeted dry density and measured dry density. The difference in the dry densities has a relatively large correction on volumetric strains. For example when γ_{do} = 1.57 and 1.77, with respect to γ_d = 1.67, the starting values of $(1 - \gamma_d/\gamma_{do})$ = -6.369 % and 5.114 % respectively.

Correction on volume changes in installation

When being installed, a specimen may get access to water such as any excess water on the filter stone, or water in a burette where valve is not closed. As a result, the water content and voids ratio of the specimen increase, and the dry density decreases. The increase in water content can be found by comparing the measured water content at the end of the test and the water measured in the burette with the initial water content after compaction. The change in initial water content should considered in the calculation of volumetric strains.

Let w_i denote the increased water content after installation, and w_e denote the water content at the end of test, for example in a CI$\bar{U}$ test, at the end of undrained shearing. Also let ΔV_w denote the water volume measured in the burette. We have the following equation of water conservation, assuming there is no leakage:

$$[9.22] \quad w_i = w_e + \frac{\Delta V_w \gamma_w}{W_s}$$

where W_s is the total weight of soil in the specimen and is unchanged throughout the test.

$$[9.23] \quad W_s = G_s \gamma_w V_s = G_s \gamma_w \frac{V_o}{1 + e_o}$$

where e_o is initial void ratio after compaction, V_o is the total volume of the specimen after compaction. The void ratio increase in the installation is, using [9.22],[9.23]:

$$[9.24] \quad e_i = \frac{G_s w_i}{S_{ri}} = G_s [w_e + \frac{\Delta V_w (1+e_o)}{G_s V_o}] / S_{ri}$$

The dry density decrease in the installation is:

$$[9.25] \quad \gamma_{di} = \frac{G_s}{1 + e_i} \gamma_w$$

The corresponding volume of the specimen increase in the installation is:

$$[9.26] \quad V_i = (1 + e_i) \, W_s / (G_s \gamma_w)$$

Example 1, T1001:

$$[9.26] \quad W_s = 2.7 \frac{202.11}{1 + 0.6089} = 337.47 \text{ (g)}$$

$$[9.27] \quad w_i = 0.2179 + \frac{23.06}{337.47} = 0.2862$$

$$[9.28] \quad e_i = \frac{2.7 \times 0.2862}{0.9904} = 0.7803$$

where S_{ri} is assumed to be S_{ro} = 0.9904 which is the initial degree of saturation after compaction.

[9.29] $\gamma_{di} = \frac{2.7}{1 + 0.7803} = 1.5166\ (Mg/m^3)$

[9.30] $V_i = 337.47\ (1 + 0.7803)\ /2.7 = 222.52\ (cm^3)$

Example 2, T1002:

[9.31] $W_s = 2.7\ \frac{201.49}{1 + 0.5920} = 341.72\ (g)$

[9.32] $w_i = 0.2075 + \frac{0.88}{341.72} = 0.2100$

[9.33] $e_i = \frac{2.7 \times 0.2100}{0.9410} = 0.6028$

where S_{ri} is assumed to be S_{ro} = 0.9410.

[9.34] $\gamma_{di} = \frac{2.7}{1 + 0.6028} = 1.6846\ (Mg/m^3)$

[9.35] $V_i = 341.72\ (1 + 0.6028)\ /2.7 = 202.85\ (cm^3)$

Correction for unsaturation

The compacted specimens are not fully saturated. However they become saturated after using back pressure and long consolidation time. During the process of saturation, the specimens need to take in some water and this is recorded with the burette readings. The changes of burette readings partially compensate the saturation and do not reflect directly the real volume changes. We know that when the specimen is not saturated, the water content $w = S_r e/G_s$; when saturated $w = e/G_s$.

The difference on water contents is:

$$[9.36] \quad \Delta w = (1-S_r)\frac{e_o}{G_s} = (1 - S_r)(\frac{G_s}{\gamma_{do}}\gamma_w - 1)/G_s$$

The amount of water taken in to make the specimen saturated can be calculated as follows:

$$[9.37] \quad \Delta W = \Delta w\, W_s = \Delta w\, G_s V_s \gamma_w = \Delta w\, G_s \gamma_w \frac{V}{1 + e_o}$$

where V is total volume of the specimen. The volume of ΔW, using [9.36],[9.37], is:

$$[9.38] \quad \Delta V = \Delta W/\gamma_w = (1-S_r)\frac{e_o}{1 + e_o} V$$

For example in T1001:

$$[9.39] \quad \Delta V = (1 - 0.9904)\frac{0.6089}{1 + 0.6089} 201.11\ (cm^3) = 0.7307\ (cm^3)$$

For example in T1002:

$$[9.40] \quad \Delta V = (1 - 0.9410)\frac{0.5920}{1 + 0.5920} 201.49\ (cm^3) = 4.4206\ (cm^3)$$

The final corrections in the calculation of volumetric strains are, using [9.21] and previous data:

for T1001:

$$[9.41] \quad \varepsilon_v = (1 - \frac{1.67}{1.517}) + \frac{(\Delta V + 0.7307)}{222.5} \times \frac{1.67}{1.517}$$

for T1002:

$$[9.42] \quad \varepsilon_v = \left(1 - \frac{1.67}{1.685}\right) + \frac{(\Delta V + 4.4206)}{202.85} \times \frac{1.67}{1.685}$$

where $(\Delta V + 0.7307)$ is the volume change modified on unsaturation for T1001. The equivalent expression for T1002 is $(\Delta V + 4.4206)$. The corrected volumetric strains are in Appendix 9.2

APPENDIX 9.2 Test Data in Isotropic Consolidation Tests and Undrained Shear Tests

1. Isotropic Consolidation Tests

(1). T1001

Dry density = 1.517 Mg/m^3, designed dry density = 1.67 Mg/m^3

ELAPSED TIME (HOUR)	CELL PRESSURE kPa	PWP AT BOTTOM kPa	GIAL GUAGE mm	VOL. CHANGE ml	VOL. STRAIN %	EXCESS PWP kPa	P' ESTIMATED kPa
Back pressure = 500 kPa							
Drained at both top and bottom ends							
0	696	501	2.52	10.2	-9.50760		
0.016666			2.645	9.55	-9.18664		
0.033333			2.66	9.45	-9.13726		
0.116666			2.7	9.1	-8.96443		
0.283333			2.735	8.67	-8.75210		
1.5			2.749	7.45	-8.14968		
8.67			2.69	6.83	-7.84353		
15.57			2.52	7.7	-8.27313		
35.35			2.341	9.42	-9.12245		
61.03			2.225	11.45	-10.1248		
84.65			1.4	13.16	-10.9692		
154.15			0.71	16.74	-12.7369		
227.62			0.38	19	-13.8529		
Drained at top end							
0	1309	506	0.375	19	-13.8529	6	796
0.033333		791	0.18	18.9	-13.8035	291	606
0.083333		852	0.246	18.8	-13.7542	352	565.3333
0.55		971	0.246	18.6	-13.6554	471	486
1.466666		999	0.259	18.36	-13.5369	499	467.3333
4.033333		1008	0.259	17.96	-13.3394	508	461.3333
12.15		992	0.259	17.11	-12.9197	492	472
22.56666		977	0.259	16.38	-12.5592	477	482
51.38333		953	0.26	14.94	-11.8481	453	498
96.11666		893	0.261	13.36	-11.0679	393	538
168.35		840	0.261	11.65	-10.2236	340	573.3333
264.45		771	0.309	10.25	-9.53229	271	619.3333
382.9		705	0.309	9	-8.91505	205	663.3333
458.28		700	0.309	8.4	-8.61878	200	666.6666
525.93		658	0.308	8	-8.42126	158	694.6666
695.75		619	0.305	7.11	-7.98179	119	720.6666
862.45		590	0.306	6.55	-7.70527	90	740
1055.4		424	0.36	6.14	-7.50281	-76	850.6666
1199.1		240	0.359	5.98	-7.42381	-260	973.3333
1558.43		215	0.205	5.42	-7.14728	-285	990
1 day pwp equilibrium with both top and bottom ends closed							
Drained at top end							
0	3490	2625	2.372	5.42	-7.14728	2125	1583.333

0.03		2625	2.372	5.21	-7.04359	2125	1583.333
0.95		2626	2.372	4.9	-6.89051	2126	1582.666
6.37		2654	2.372	4.28	-6.58436	2154	1564
23.33		2654	2.372	3.3	-6.10045	2154	1564
49.08		2661	2.372	2.34	-5.62641	2161	1559.333
102.17		2620	2.372	0.94	-4.93510	2120	1586.666
121.81	burette	2592	2.372	0.5	-4.71783	2092	1605.333
121.82	adjusted	2592	2.372	9.02	-4.71783	2092	1605.333
146.2		2561	2.37	8.5	-4.46106	2061	1626
214.85		2483	2.37	7.2	-3.81913	1983	1678
338.38		2368	2.369	5.37	-2.91550	1868	1754.666
504.2		2147	2.371	3.45	-1.96742	1647	1902
672.77		1980	2.373	2.02	-1.26130	1480	2013.333
867.77	burette	1815	2.432	0.71	-0.61443	1315	2123.333
867.77	adjusted	1815	2.432	17.05	-0.61443	1315	2123.333
1060.33		1716	2.425	16.12	-0.15521	1216	2189.333
1343.09		1454	2.458	14.98	0.407708	954	2364
1824.12		1209	2.456	13.57	1.103952	709	2527.333
1967.35		1174	2.456	13.21	1.281717	674	2550.666
2280.75		1056	2.484	12.6	1.582929	556	2629.333
2642.85		968	2.512	12	1.879204	468	2688

(2). T1002

Dry density = 1.685 Mg/m^3, designed dry density = 1.67 Mg/m^3

ELAPSED TIME (HOUR)	CELL PRESSURE kPa	PWP kPa	GIAL GUAGE mm	VOL. CHANGE ml	VOL. STRAIN %	EXCESS PWP kPa	P' ESTIMATED kPa
Back pressure = 500 kPa							
Drained at top end							
0	700	500		24.86	3.050053	0	200
0.05		501		23.55	3.690102	1	199.3333
0.417		507.9		23.32	3.802477	7.9	194.7333
3.73		504.4		25.1	2.932792	4.4	197.0666
16.2		505.8		29.64	0.714609	5.8	196.1333
39.4		506		36.11	-2.44654	6	196
64.3		500		40	-4.34714	0	200
87.1	burette	505		42.18	-5.41226	5	196.6666
87.1	adjusted	505		26.5	-5.41226	5	196.6666
135.7		509		31.4	-7.80634	9	194
182.8		509		34.2	-9.17438	9	194
231.4		504		36.16	-10.1320	4	197.3333
Drained at top end							
0	1500	504		36.17	-10.1368	4	197.3
0.45		820.5		35.27	-9.69717	320.5	400
6.68		1212		33.18	-8.67602	712	500
21.36		1233.5		31.5	-7.85519	733.5	511
22.9		1121		30.88	-7.55227	621	586
50.7		1070.6		28.55	-6.41386	570.6	619.6
167.1		875		24.1	-4.23965	375	750
335.1		616		21.5	-2.96933	116	922.6666

527		571	20.4	-2.43188	71	952.6666
767.3		604	19.97	-2.22179	104	930.6666
965.8		643	19.71	-2.09476	143	904.6666
1254		571	19.62	-2.05079	71	952.6666
1517.4		609	19.46	-1.97261	109	927.3333
1823.5		520	19.36	-1.92375	20	986.6666
2114.3		530	19.3	-1.89444	30	980
2521.2		530	19.15	-1.82115	30	980
2955.3		530	19.15	-1.82115	30	980
Drained at top end						
0	3500	629	19.15	-1.82115	129	980
18.9		2330	19.15	-1.82115	1830	1780
44.5		1540	19.15	-1.82115	1040	2306.666
44.6		1371	19.07	-1.78206	871	2419.333
90.5		1358	17	-0.77069	858	2428
162.5		1409	15.76	-0.16484	909	2394
311.3		1021	14	0.695066	521	2652.666
598.3		972	12.07	1.638038	472	2685.333
931.4		844	11.05	2.136396	344	2770.666
1299.6		713	10.41	2.449092	213	2858
1627.2		595	10.25	2.527265	95	2936.666
1890.2		553	10.18	2.561467	53	2964.666
2034.1		589	10.06	2.620097	89	2940.666

2. Undrained Shear Tests

(1). T1001

Dry density = 1.517 Mg/m^3, designed dry density = 1.67 Mg/m^3

ELAPSED TIME Hour	CELL PRESSURE kPa	PWP kPa	GIAL GUAGE mm	AXIAL STRAIN %	EXCESS PWP kPa	P' ESTIMATED kPa	q kPa
Back pressure = 500 kPa							
Isotropic consolidation							
4428.9	3500	968	2.512		468	2688	0
Step 1: q = 315.7 kPa. After 213.3 hour isotropic undrained relaxation							
0	3500	1045	4.9	0	0	2455	0
0.016666		1081	5.15	0.251458	36	2524.5	315.7041
0.117		1097	5.166	0.267551	52	2508.5	315.6531
1.23		1137	5.186	0.287668	92	2468.5	315.5895
2.92		1152	5.195	0.296720	107	2453.5	315.5608
23.85		1205	5.226	0.327901	160	2400.5	315.4621
46.9		1228	5.241	0.342989	183	2377.5	315.4144

118.6		1275	5.255	0.357071	230	2330.5	315.3698
172.5		1329	5.261	0.363106	284	2276.5	315.3507
386.9		1313	5.278	0.380205	268	2292.5	315.2966
551.3		1329	5.285	0.387246	284	2276.5	315.2743
695.2		1390	5.292	0.394286	345	2215.5	315.2520
Step 2: q = 686.8 kPa							
0	3500	1407	5.29	0.392275	362	2322.833	686.7952
0.0167		1460	5.652	0.756387	415	2269.833	684.2847
0.18		1492	5.725	0.829812	447	2237.833	683.7784
1.2		1548	5.805	0.910279	503	2181.833	683.2236
3.57		1636	5.866	0.971635	591	2093.833	682.8005
24.51		1705	5.995	1.101388	660	2024.833	681.9059
48.7		1703	6.021	1.127539	658	2026.833	681.7256
94.7		1608	6.075	1.181854	563	2119.117	681.3511
167.1		1950	6.178	1.285455	905	1779.833	680.6367
239.7		1929	6.215	1.322671	884	1800.833	680.3801
311.2		2039	6.249	1.356869	994	1690.833	680.1443
Step 3: q = 866.0 kPa							
0		1908	6.249	1.356869	863	1884.633	865.9880
0.03		1873	6.405	1.513779	828	1919.633	864.6105
1.1		1883	6.5	1.609334	838	1909.633	863.7716
5.22		1850	6.602	1.711929	805	1942.633	862.8709
7.08		1868	6.621	1.731040	823	1924.633	862.7031
20		1865	6.715	1.825588	820	1927.633	861.8731
45.3		1888	6.841	1.952323	843	1904.633	860.7605
68.5		1847	6.902	2.013679	802	1945.633	860.2219
93.5		1858	6.945	2.056930	813	1934.633	859.8422
116.8		1835	6.985	2.097163	790	1957.633	859.4890
144.3		1895	7.023	2.135385	850	1897.633	859.1534
Step 4: q = 1041.9 kPa							
0		1895	7.023	2.135385	850	1959.866	1041.866
0.0167		1916	7.175	2.288271	871	1938.866	1040.239
0.67		1938	7.445	2.559847	893	1916.866	1037.347
1.67		1950	7.691	2.807282	905	1904.866	1034.713
2.58		1957	7.855	2.972238	912	1897.866	1032.957
5.85		1979	8.325	3.444980	934	1875.866	1027.924
9.08		1973	8.725	3.847314	928	1881.866	1023.641
22.5		1939	9.185	4.309997	894	1915.866	1018.715
29.72		1895	9.605	4.732448	850	1959.866	1014.218
Step 5: q = 1077.0 kPa							
0		1895	9.605	4.732448	850	1981.833	1076.999
0.0167		1907	9.685	4.812914	862	1969.833	1076.089
0.17		1919	9.803	4.931603	874	1957.833	1074.748
0.32		1927	10.15	5.280627	882	1949.833	1070.802
0.4		1933	10.44	5.572319	888	1943.833	1067.504
0.467		1936	10.95	6.085294	891	1940.833	1061.705
0.5		1938	11.54	6.678736	893	1938.833	1054.996
0.52		1935	12.22	7.362703	890	1941.833	1047.264
0.533		1935	14.6	9.756588	890	1941.833	1020.201

(2). T1002

Dry density = 1.685 Mg/m^3, designed dry density = 1.67 Mg/m^3

NOTES AND SPEED	EPLASED TIME Hour	AXIAL DISPL. mm	VERTICAL FOCRE N	PWP kPa	CELL PRESSURE kPa	AXIAL STRAIN %	q kPa	PWP AFTER SHEAR kPa	p' kPa	STRAIN RATE 1/hour
Back pressure = 500 kPa										
Isotropic consolidation										
	5220.8			589	3500		0		2940.7	
After 32.48 hour isotropic undrained relaxation, start undrained shear										
	0.183333	1.700603	589.2747	806.554	3564.05	0	0	0	2693.446	
0.15	0.25	2.322544	839.5026	837.9288	3563.35	0	167.7052	16.6752	2732.672	
mm/min		2.51	911	846	3567	0.188341	202.6407	24.7464	2736.246	
		2.77	1988	934	3567	0.449568	731.7281	112.7464	2824.608	
		2.89	2253	964	3567	0.570135	860.9985	142.7464	2837.699	
0.01	0.416666	3.086778	2220.181	1009.891	3561.95	0.767842	843.1997	188.6382	2785.874	
mm/min	0.583333	3.181224	2331.427	1052.274	3560.55	0.862735	896.8715	231.021	2761.382	0.005693
	0.75	3.285079	2429.983	1056.096	3556.35	0.967080	944.1411	234.8424	2773.317	0.006260
	0.916666	3.378529	2512.311	1108.900	3554.6	1.060971	983.4820	287.6472	2733.626	0.005633
	1.083333	3.476153	2585.195	1150.588	3553.2	1.159056	1018.092	329.3352	2703.475	0.005885
	1.25	3.571659	2652.769	1183.244	3551.8	1.255013	1050.065	361.9908	2681.476	0.005757
	1.416666	3.665109	2712.080	1210.689	3550.05	1.348904	1077.969	389.4354	2663.333	0.005633
0.0006	1.583333	3.677569	2577.523	1218.331	3548.65	1.361423	1012.270	397.0782	2633.791	0.000751
mm/min	1.75	3.684858	2539.753	1227.016	3547.25	1.368747	993.7929	405.7632	2618.947	0.000439
	2.25	3.703548	2504.343	1222.153	3541.3	1.387525	976.3550	400.8996	2617.998	0.000375
	4.25	3.777249	2530.901	1285.38	3523.8	1.461574	988.5487	464.1264	2558.835	0.000370
	6.25	3.853068	2581.359	1249.597	3499.65	1.537751	1012.326	428.3442	2602.543	0.000380
	8.25	3.932999	2622.080	1253.071	3493.35	1.618059	1031.290	431.8182	2605.391	0.000401
	10.25	3.996358	2672.539	1288.506	3497.9	1.681718	1055.129	467.253	2577.902	0.000318
	12.25	4.071118	2712.080	1316.298	3497.2	1.756831	1073.512	495.045	2556.238	0.000375
	14.25	4.140644	2746.604	1334.016	3493	1.826686	1089.491	512.7624	2543.847	0.000349
	16.25	4.226868	2786.735	1441.362	3616.2	1.913316	1107.974	620.109	2442.661	0.000433
	18.25	4.279823	2789.391	1410.791	3487.05	1.966521	1108.659	589.5378	2473.461	0.000266
	20.25	4.349349	2825.391	1402.453	3472.35	2.036376	1125.290	581.2002	2487.342	0.000349
	22.25	4.420994	2846.636	1408.707	3467.1	2.108360	1134.736	587.4534	2484.238	0.000359
	24.25	4.500988	2869.653	1415.307	3480.05	2.188731	1144.925	594.054	2481.033	0.000401
	26.25	4.575748	2894.144	1423.297	3480.75	2.263844	1155.870	602.0442	2476.692	0.000375
	28.25	4.647393	2915.390	1419.476	3475.85	2.335827	1165.269	598.2228	2483.646	0.000359
	30.25	4.721094	2935.455	1413.918	3468.85	2.409876	1174.058	592.6644	2492.134	0.000370
	32.25	4.800028	2957.881	1402.453	3463.6	2.489183	1183.906	581.2002	2506.881	0.000396
	34.25	4.873729	2977.357	1394.811	3459.75	2.563232	1192.381	573.5574	2517.349	0.000370
	36.25	4.950544	3000.078	1390.989	3458.35	2.640410	1202.364	569.736	2524.498	0.000385
	38.25	5.019074	3020.733	1394.463	3459.75	2.709264	1211.440	573.21	2524.049	0.000344
	40.25	5.106294	3050.241	1485.829	3586.45	2.796896	1224.518	664.5762	2437.042	0.000438
0.15	41.02	5.138504	3213.126	1518.832	3606.75	2.829257	1302.294	697.5792	2429.964	0.000420
mm/min	41.05	5.414679	3542.435	1542.803	3606.4	3.106737	1456.191	721.5498	2457.293	0.092493
	41.08333	5.725183	3563.976	1541.413	3576.65	3.418707	1461.780	720.1602	2460.545	0.093590
	41.11666	6.038739	3565.746	1542.456	3565.8	3.733743	1457.853	721.2024	2458.194	0.094510
	41.15	6.355409	3567.222	1546.624	3564.75	4.051909	1453.734	725.3712	2452.653	0.095449
	41.18333	6.665913	3567.222	1551.141	3564.4	4.363879	1449.008	729.8874	2446.561	0.093590

-------	41.21666	6.979469	3560.730	1555.657	3564.05	4.678915	1441.178	734.4036	2439.435	0.094510
0.01	41.25	7.060459	3322.895	1544.540	3563.7	4.760288	1328.056	723.2868	2412.844	0.024411
mm/min	41.28333	7.079149	3299.879	1542.803	3563.7	4.779066	1316.968	721.5498	2410.885	0.005633
	41.31	7.091609	3291.027	1542.456	3563.35	4.791585	1312.632	721.2024	2409.787	0.004694
	41.32388	7.100954	3288.666	1541.761	3563	4.800974	1311.392	720.5076	2410.069	0.006760
	41.35527	7.120703	3286.601	1541.413	3562.65	4.820816	1310.148	720.1602	2410.001	0.006321
	41.38861	7.137274	3287.191	1541.413	3561.95	4.837466	1310.196	720.1602	2410.017	0.004995
	41.45	7.178829	3291.027	1542.108	3561.25	4.879217	1311.424	720.855	2409.732	0.006800
	41.58333	7.253589	3301.945	1544.540	3559.85	4.954330	1315.514	723.2868	2408.664	0.005633
	41.75	7.353269	3313.158	1550.098	3557.75	5.054481	1319.387	728.8452	2404.396	0.006009
	42.25	7.646079	3333.223	1559.826	3551.45	5.348673	1324.680	738.5724	2396.433	0.005883
	42.75	7.939948	3340.305	1559.826	3545.85	5.643930	1323.849	738.5724	2396.156	0.005905
	43.25	8.234814	3340.895	1561.910	3539.55	5.940188	1319.966	740.6568	2392.778	0.005925
-------	43.67444	8.480899	3339.420	1566.774	3534.65	6.187435	1315.813	745.5204	2386.530	0.005825
0.0006	43.75055	8.487129	3202.503	1561.215	3533.95	6.193695	1252.281	739.962	2370.911	0.000822
mm/min	43.76416	8.491303	3193.650	1560.520	3533.6	6.197889	1248.123	739.2672	2370.219	0.003081
	43.79583	8.489184	3176.241	1558.783	3533.25	6.195760	1240.084	737.5302	2369.277	-0.00067
	43.82916	8.491303	3151.454	1557.046	3532.9	6.197889	1228.571	735.7932	2367.176	0.000638
	43.95	8.498529	3069.127	1551.835	3531.5	6.205150	1190.332	730.5822	2359.641	0.000600
	44.25	8.505819	3101.290	1543.845	3528.35	6.212473	1205.140	722.592	2372.567	0.000244
	45.25	8.545254	3103.651	1530.991	3517.15	6.252095	1205.724	709.7382	2385.615	0.000396
	47.25	8.612788	3131.388	1511.537	3494.05	6.319947	1217.687	690.2838	2409.058	0.000339
	49.25	8.687548	3150.274	1505.631	3471.65	6.395060	1225.443	684.378	2417.549	0.000375
	51.25	8.760189	3167.093	1491.735	3455.55	6.468045	1232.258	670.482	2433.716	0.000364
	53.25	8.837068	3181.552	1491.735	3459.05	6.545286	1237.916	670.482	2435.602	0.000386
	55.25	8.906594	3195.421	1495.209	3461.85	6.615142	1243.388	673.956	2433.952	0.000349
	57.25	8.984469	3203.978	1495.557	3462.55	6.693384	1246.290	674.3034	2434.572	0.000391
	59.25	9.055118	3211.355	1492.777	3461.15	6.764366	1248.740	671.5242	2438.168	0.000354
	61.25	9.135049	3217.257	1489.651	3459.05	6.844674	1250.380	668.3976	2441.841	0.000401
-------	63.25	9.214979	3219.912	1505.979	3483.55	6.924983	1250.523	684.7254	2425.561	0.000401
0.01	63.28333	9.228499	3316.699	1512.579	3485.65	6.938566	1294.833	691.326	2433.731	0.004074
mm/min	63.31666	9.246129	3370.993	1518.485	3487.75	6.956280	1319.541	697.2318	2436.061	0.005314
	63.35	9.263760	3397.256	1523.001	3489.85	6.973994	1331.358	701.748	2435.484	0.005314
	63.41666	9.301140	3419.387	1528.907	3493.35	7.011551	1340.986	707.6538	2432.787	0.005633
	63.5	9.353099	3419.682	1535.508	3498.25	7.063754	1340.368	714.2544	2425.981	0.006264
	63.58333	9.401879	3413.485	1540.371	3502.1	7.112765	1336.818	719.118	2419.934	0.005881
	63.75	9.501559	3397.256	1545.235	3510.5	7.212916	1327.938	723.9816	2412.110	0.006009
-------	63.91666	9.596069	3385.452	1550.446	3517.85	7.307871	1321.175	729.1926	2404.645	0.005697
Unload	63.95	9.602299	3262.109	1550.098	3519.25	7.314131	1264.614	728.8452	2386.138	0.001877
-0.01	63.98333	9.602299	3019.848	1545.235	3521	7.314131	1153.696	723.9816	2354.029	0
mm/min	64.01666	9.589839	2867.587	1540.024	3522.4	7.301612	1084.131	718.7706	2336.052	-0.00375
	64.05	9.577379	2762.243	1533.423	3523.45	7.289093	1036.033	712.17	2326.620	-0.00375
	64.08333	9.559685	2665.162	1526.128	3524.85	7.271316	991.7638	704.8746	2319.159	-0.00533
	64.16666	9.521309	2449.754	1507.716	3528	7.232758	893.4662	686.4624	2304.805	-0.00462
	64.25	9.476639	2256.181	1489.651	3531.5	7.187878	805.1518	668.3976	2293.432	-0.00538
	64.33333	9.434089	2088.576	1470.891	3534.3	7.145127	728.6457	649.638	2286.689	-0.00513
	64.41666	9.390479	1937.790	1453.174	3537.1	7.101311	659.7947	631.9206	2281.456	-0.00525
	64.58333	9.290799	1679.595	1389.252	3481.45	7.001160	541.8938	567.999	2306.078	-0.00600
	64.66666	9.243014	1565.989	1370.493	3480.75	6.953150	489.9573	549.2394	2307.525	-0.00576
	64.75	9.198345	1461.531	1353.470	3480.05	6.908270	442.1586	532.2168	2308.615	-0.00538
	64.83333	9.147509	1364.745	1334.363	3479.7	6.857193	397.8698	513.1098	2312.959	-0.00612
	64.91666	9.101780	1275.630	1317.688	3478.65	6.811249	357.0444	496.4346	2316.026	-0.00551
	65	9.056114	1190.352	1301.707	3478.3	6.765368	317.9449	480.4542	2318.973	-0.00550
	65.08333	9.010449	987.0426	1288.854	3477.25	6.719486	224.4199	467.6004	2300.652	-0.00550
	65.25	8.919054	830.0600	1261.756	3476.2	6.627660	152.2351	440.5032	2303.687	-0.00550
-------	65.41666	8.822489	699.6346	1235.701	3475.15	6.530639	92.17410	414.4482	2309.722	-0.00582

Reload	65.5	8.834949	1002.386	1239.175	3474.45	6.543158	231.9278	417.9222	2352.833	0.001502
0.01	65.58333	8.886845	1238.450	1255.851	3474.1	6.595299	340.7171	434.5974	2372.420	0.006256
mm/min	65.75	8.974065	1619.103	1294.412	3472.7	6.682931	515.3639	473.1588	2392.241	0.005257
	65.91666	9.070630	1932.774	1332.973	3471.3	6.779952	659.7671	511.7202	2401.648	0.005821
	66.08333	9.155794	2204.542	1369.450	3469.55	6.865518	784.1913	548.1972	2406.645	0.005133
	66.25	9.248185	2444.737	1403.843	3468.5	6.958346	893.8037	582.5898	2408.790	0.005569
	66.41666	9.341635	2660.146	1432.677	3467.1	7.052237	991.8037	611.424	2412.623	0.005633
	66.58333	9.422625	2922.177	1455.258	3466.05	7.133609	1111.138	634.005	2429.820	0.004882
	66.75	9.515079	3116.339	1475.755	3465	7.226499	1199.007	654.5016	2438.613	0.005573
	66.91666	9.607469	3201.618	1492.083	3463.95	7.319326	1236.849	670.8294	2434.899	0.005569
	67.08333	9.707149	3250.601	1504.589	3464.65	7.419477	1257.913	683.3358	2429.414	0.006009
	67.25	9.807889	3281.879	1534.813	3507.35	7.520692	1270.827	713.5596	2403.495	0.006072
	67.41666	9.905450	3300.469	1558.783	3538.5	7.618714	1277.963	737.5302	2381.903	0.005881
	67.58333	10.00724	3311.977	1580.67	3560.55	7.720993	1281.794	759.4164	2361.294	0.006136
	67.75	10.10898	3315.518	1595.608	3576.65	7.823209	1281.987	774.3546	2346.420	0.006132
	67.91666	10.20449	3316.699	1608.114	3589.25	7.919166	1281.189	786.861	2333.648	0.005757
	68.08333	10.30522	3317.879	1616.452	3597.65	8.020381	1280.317	795.1986	2325.019	0.006072
	68.25	10.40596	3317.584	1624.442	3602.55	8.121596	1278.774	803.1888	2316.515	0.006072
	68.41666	10.49941	3315.518	1628.611	3606.05	8.215487	1276.531	807.3576	2311.598	0.005633
	68.58333	10.59803	3298.699	1608.462	3565.1	8.314574	1267.535	787.2084	2328.749	0.005945
-------	68.75	10.69771	3302.240	1605.682	3557.75	8.414725	1267.753	784.4292	2331.601	0.006009
0.15	68.78333	10.75484	3477.517	1613.673	3557.4	8.472123	1346.205	792.4194	2349.761	0.017219
mm/min	68.81666	11.06946	3451.845	1616.104	3557.05	8.788224	1329.989	794.8512	2341.924	0.094830
	68.85	11.38613	3428.829	1616.104	3556.7	9.106390	1315.016	794.8512	2336.933	0.095449
	68.88333	11.70180	3408.469	1615.757	3556.35	9.423555	1301.317	794.5038	2332.714	0.095149
	68.91666	12.01536	3391.944	1615.41	3556	9.738592	1289.423	794.1564	2329.097	0.094510
-------	68.95	12.33826	3378.370	1614.367	3555.65	10.06301	1278.759	793.1142	2326.584	0.097327
Relaxa.	68.98333	12.38810	3133.159	1600.819	3555.3	10.11309	1169.168	779.5656	2303.603	0.015022
0	69.01666	12.39122	3075.618	1594.566	3554.95	10.11622	1143.580	773.3124	2301.326	0.000938
mm/min	69.05	12.39227	3041.979	1589.702	3554.25	10.11728	1128.630	768.4488	2301.207	0.000319
	69.25	12.39333	2955.226	1570.248	3551.45	10.11835	1090.099	748.9944	2307.818	0.000053
	69.75	12.39539	2885.882	1547.319	3544.8	10.12041	1059.287	726.066	2320.475	0.000041
	70.75	12.39645	2828.341	1527.517	3532.55	10.12148	1033.728	706.2642	2331.757	0.000010
	74.75	12.39956	2650.998	1443.794	3485.3	10.12461	954.9587	622.5408	2389.224	0.000007
	78.75	12.39956	2526.474	1381.262	3439.1	10.12461	899.6750	560.0088	2433.328	0
	82.75	12.40162	2455.950	1338.184	3406.55	10.12667	868.3452	516.9312	2465.963	0.000005
	86.75	12.40162	2425.852	1314.561	3399.9	10.12667	854.9831	493.308	2485.132	0
	90.75	12.40162	2445.327	1396.200	3463.25	10.12667	863.6291	574.947	2406.375	0
	94.75	12.39956	2592.867	1494.167	3561.25	10.12461	929.1509	672.9138	2330.249	-0.00000
	98.75	12.39433	2624.441	1523.696	3582.95	10.11935	943.2235	702.4428	2305.411	-0.00001
	102.75	12.40579	2588.736	1460.817	3565.45	10.13087	927.2523	639.5634	2362.966	0.000028
	106.75	12.39956	2519.097	1476.45	3556.7	10.12461	896.3999	655.1964	2337.049	-0.00001
	110.75	12.39956	2509.950	1483.050	3540.95	10.12461	892.3388	661.797	2329.095	0
	114.75	12.39539	2501.983	1499.378	3522.05	10.12041	888.8432	678.1248	2311.602	-0.00001
-------	115.4833	12.39645	2503.163	1502.852	3517.85	10.12148	889.3567	681.5988	2308.299	0.000014
0.15	115.5166	12.58023	3455.386	1548.709	3517.85	10.30613	1309.425	727.4556	2402.465	0.055395
mm/min	115.55	12.88133	3491.091	1561.910	3517.5	10.60865	1320.775	740.6568	2393.047	0.090755
-------	115.5833	13.19077	3458.927	1567.121	3517.5	10.91955	1302.028	745.8678	2381.587	0.093271
0.0006	115.895	13.60712	2935.750	1550.446	3516.1	11.33787	1066.779	729.1926	2319.846	0.013421
mm/min	115.9077	13.60918	2930.439	1550.446	3516.1	11.33993	1064.428	729.1926	2319.062	0.001616
	115.9833	13.60712	2939.291	1549.404	3516.1	11.33787	1068.330	728.1504	2321.405	-0.00027
	116.25	13.61753	2965.258	1550.098	3514.7	11.34832	1079.575	728.8452	2324.459	0.000391
	116.75	13.62999	2979.127	1558.783	3512.6	11.36084	1085.495	737.5302	2317.747	0.000250
	118.25	13.67771	3030.176	1593.176	3505.25	11.40879	1107.248	771.9228	2290.606	0.000319
	120.25	13.75041	3058.504	1619.926	3495.1	11.48184	1118.722	798.6726	2267.680	0.000365
	122.25	13.82412	3067.651	1609.851	3481.8	11.55588	1121.782	788.598	2278.775	0.000370

124.25	13.90722	3077.094	1557.394	3464.65	11.63939	1124.844	736.1406	2332.253	0.000417
126.25	13.97887	3085.356	1545.582	3452.75	11.71137	1127.531	724.329	2344.960	0.000359
128.25	14.05051	3097.749	1533.771	3448.55	11.78335	1132.013	712.5174	2358.266	0.000359
130.25	14.12004	3104.241	1524.043	3447.15	11.85321	1133.943	702.7902	2368.636	0.000349
132.25	14.19586	3110.733	1519.180	3447.15	11.92938	1135.787	697.9266	2374.115	0.000380
134.25	14.26856	3114.274	1515.358	3446.8	12.00243	1136.384	694.1052	2378.135	0.000365
135.6666	14.32046	3115.749	1518.138	3446.8	12.05457	1136.352	696.8844	2375.345	0.000368

APPENDIX 9.3 Computer Program for the Calculation of Undrained Multi-stage q Creep Shear Tests

```
10 CLS:
20 REM FILENAME BCQKGJ-2, SCALING METHOD 2
30 PRINT:PRINT:PRINT
40 PRINT"EVP KGJ Modelling of Undrained Multi-stage q Creep Shear Tests"
50 PRINT"Using Elliptical Flow Surface and Hyperbolic Strength Envelope"
60 PRINT:PRINT:PRINT
70 INPUT "LOTUS Data Filename";X$
80 OPEN X$+".PRN" FOR OUTPUT AS #1
90 INPUT"Mater. Parameters, T0,P0(sec, kPa)";T0,P0
100 INPUT"Mater. Param. Lambda,Kappa,Psi(1/V)";LAMBDA,KAPPA,PSI
110 INPUT"Mater. Param. A,B(kPa^-1),D(kPa)";A,B,D
120 INPUT"Initial Values,Ti(h),Ei,EVi,Pi(kPa),Qi(kPa)";TI,EI,EVI,PI,QI
130 INPUT"Time Incre. and q Incre., H(h),DQ(kPa)";H,DQ
140 INPUT"Time Range, TRNG(h)";TRNG
150 REM        TO SOLVE DIFFERENTIAL EQUATION
160 PRINT:PRINT:PRINT
170 PRINT"                          Calculation in Progress"
180 PRINT"                       Order 4 Runge & Kutta's Method"
190 PRINT:PRINT:PRINT
200 DIM T(2500),E(2500),P(2500)
210 B1=KAPPA/LAMBDA:B2=LAMBDA/PSI
220 GOSUB 570
230 T(0)=TI:E(0)=EI+DES:P(0)=PI:II=5
240 FOR I=1 TO 2500
250 IF I=5 THEN H=10*H
260 IF I=10 THEN H=10*H
270 IF I=15 THEN H=10*H
280 IF I=20 THEN H=10*H
290 T1=T(I-1)
300 Y1=P(I-1)
310 GOSUB 620
320 K1=Z1:L1=Z2
330 T1=T(I-1)+.5*H
340 Y1=P(I-1)+.5*H*K1
350 GOSUB 620
360 K2=Z1:L2=Z2
370 Y1=P(I-1)+.5*H*K2
380 GOSUB 620
390 K3=Z1:L3=Z2
400 T1=T(I-1)+H
410 Y1=P(I-1)+H*K3
420 GOSUB 620
430 K4=Z1:L4=Z2
440 T(I)=T(I-1)+H
450 P(I)=P(I-1)+H*(K1+2*K2+2*K3+K4)/6
460 E(I)=E(I-1)+H*(L1+2*L2+2*L3+L4)/6
470 IF T(I)>TRNG GOTO 500
480 IF (E(I)-E(0))>.1 GOTO 500
490 NEXT I
```

```
500 FOR J=0 TO I STEP II
510 WRITE #1,T(J),E(J)*100,P(J)
520 IF J>50 II=10
530 NEXT J
540 CLOSE #1
550 END
560 REM CALCULATION OF ELASTIC RESPONCES
570 DP=DQ/4.601:PI=PI+DP:QI=QI+DQ
580 K=(500+PI)/KAPPA:JM=-4.601*K:G=D*JM*JM/(JM*JM+3*D*K)
590 DES=DP/JM+DQ/3/G
600 RETURN
610 REM ELASTIC VISCOUS PLASTIC MODEL
620 BB=(Y1-A*B*QI*QI)/(.5*B*QI)^2:CC=(A*A*QI*QI+Y1*Y1)/(.5*B*QI)^2
630 PM=.5*4*CC/(BB+(BB*BB-4*CC)^.5)
640 M=1/(A+.5*B*PM)
650 A2=2*Y1-PM:A3=2*QI/M/M
660 K=(500+Y1)/KAPPA:JM=-4.601*K:G=D*JM*JM/(JM*JM+3*D*K)
670 C1=PSI/T0*(EXP(-EVI/LAMBDA)*((.5+PM)/P0)*((500+Y1)/(500+PM))^B1)^B2
680 Z1=-K*C1*A2/ABS(A2)
690 Z2=Z1/JM+C1*A3/ABS(A2)
700 RETURN
```

APPENDIX 9.4 Computer Program for the Calculation of Undrained Constant Strain Rate Shear Tests

```
10 CLS:
20 REM FILENAME BUDKGJ-2, SCALING METHOD 2
30 PRINT:PRINT:PRINT
40 PRINT"EVP KGJ Modelling of Undrained Constant Strain Rate Shear Tests"
50 PRINT"Using Elliptical Flow Surface and Hyperbolic Strength Envelope"
60 PRINT:PRINT:PRINT
70 INPUT "LOTUS Data Filename";X$
80 OPEN X$+".PRN" FOR OUTPUT AS #1
90 INPUT"Mater. Parameters, T0,P0 (sec,kPa)";T0,P0
100 INPUT"Mater. Param, Lambda,Kappa,Psi (1/V)";LAMBDA,KAPPA,PSI
110 INPUT"Mater. Param,A,B(kPa^-1),D(kPa)";A,B,D
120 INPUT"Initial Values, TI,EI,EVI,PI,QI";TI,EI,EVI,PI,QI
130 INPUT"Strain Rate & Time Incre., REPSI (1/h),H(h)";REPSI,H
140 REM        TO SOLVE DIFFERENTIAL EQUATION
150 PRINT:PRINT:PRINT
160 PRINT"                          Calculation in Progress"
170 PRINT"                        Order 4 Runge & Kutta's Method"
180 PRINT:PRINT:PRINT
190 DIM T(2500),E(2500),P(2500),Q(2500)
200 B1=KAPPA/LAMBDA:B2=LAMBDA/PSI
210 T(0)=TI:E(0)=EI*100:P(0)=PI:Q(0)=QI
220 FOR I=1 TO 2500
230 IF I=5 THEN H=10*H
240 IF I=10 THEN H=10*H
250 IF I=15 THEN H=10*H
260 IF I=20 THEN H=10*H
270 T1=T(I-1)
280 Y1=P(I-1):Y2=Q(I-1)
290 GOSUB 550
300 K1=Z1:L1=Z2
310 T1=T(I-1)+.5*H
320 Y1=P(I-1)+.5*H*K1:Y2=Q(I-1)+.5*H*L1
330 GOSUB 550
340 K2=Z1:L2=Z2
350 Y1=P(I-1)+.5*H*K2:Y2=Q(I-1)+.5*H*L2
360 GOSUB 550
370 K3=Z1:L3=Z2
380 T1=T(I-1)+H
390 Y1=P(I-1)+H*K3:Y2=Q(I-1)+H*L3
400 GOSUB 550
410 K4=Z1:L4=Z2
420 T(I)=T(I-1)+H:E(I)=E(I-1)+REPSI*H*100
430 P(I)=P(I-1)+H*(K1+2*K2+2*K3+K4)/6
440 Q(I)=Q(I-1)+H*(L1+2*L2+2*L3+L4)/6
450 IF E(I)>10 GOTO 480
460 NEXT I
470 II=10
480 FOR J=0 TO I STEP II
490 WRITE #1,T(J),E(J),P(J),Q(J)
```

```
500 IF E(J) >3 THEN II=20
510 NEXT J
520 CLOSE #1
530 END
540 REM ELASTIC VISCO-PLASTIC MODEL
550 IF Y2<.01 THEN GOTO 570
560 GOTO 590
570 PM=Y1
580 GOTO 610
590 BB=(Y1-A*B*Y2*Y2)/(.5*B*Y2)^2:CC=(A*A*Y2*Y2+Y1*Y1)/(.5*B*Y2)^2
600 PM=.5*4*CC/(BB+(BB*BB-4*CC)^.5)
610 M=1/(A+.5*B*PM)
620 A2=2*Y1-PM:A3=2*Y2/M/M
630 C1=PSI/T0*(EXP(-EVI/LAMBDA)*((.5+PM)/P0)*((500+Y1)/(500+PM))^B1)^B2
640 K=(500+Y1)/KAPPA:JM=-4.601*K:G=D*JM*JM/(JM*JM+3*D*K)
650 Z1=+Z2/4.601-K*C1*A2/ABS(A2)
660 Z2=3*G*(REPSI-Z1/JM-C1*A3/ABS(A2))
670 RETURN
```

APPENDIX 10.1. Curve Fitting of a Multi-Stage Isotropic Creep Test

In the test program (Rahman 1988), the soil used in the tests was uniform, quartz-carbonate medium-grain sand with uniformity (D_{60}/D_{10}) 2.0. The specific weight was 2.70. Specimen preparation involved three stages, namely, (1) sand deposition, (2) saturation, and (3) freezing. The specimen size was 76 mm diameter and 200 mm height. Stage 1 attempted to make the density of the specimen uniform and constant. However the maximum variation of was 7% in density. In stage 2, each specimen was saturated under a vacuum pressure of 55 kPa applied at the top. In stage 3, the specimen was placed in a chest freezer with temperature $-20^{o}C$ for 48 hours. The specimen was then prepared for triaxial testing in a cold room at temperature $-3^{o}C$ (Rahman 1988).

In the multi-stage isotropic stress creep test, the isotropic stress was applied to the specimen suddenly, and was then held a constant for a period of time until the next load was added. The loading history is shown in Table 10.3.

Table 10.3 Loading History for a Multi-Stage p Creep Test

P (kPa)	50	100	150	200	300
Duration (hrs)	313.5	216.5	527.5	1247.5	2159.5
Total Elap. (hrs)	313.5	530	1057.5	2305	4464.5

In the following calculations, all stress states are isotropic, and for simplicity, the subscript "m" has been deleted.

The general equation [10.12] for calculating creep strains in multi-stage isotropic creep tests is:

$$[10.23] \quad \varepsilon_v = \frac{\lambda}{V} \ln\left(\frac{p_{o2} + p}{p_{o3}}\right) + \frac{\psi}{V} \ln\left(\frac{t_o + t_e}{t_o}\right)$$

The equivalent time t_e is different from the duration time t of loading (see Chapter 8). The time t_e is negative for state points above the reference time line, positive below the line and zero on this line. The t_e for a state point (p, ε_v) is the time that would be required for the specimen to creep under the constant stress from the reference time line to this point no matter what the loading history was to reach this state point.

Considering a load increment from point i to (i+1) in Fig.10.2 and then creeping from point (i+1) to (i+1)' under the stress p_{i+1} with real duration time t, the equivalent time $t_{e,i+1}$ at point (i+1) is, from [10.23]:

$$[10.24] \quad t_{e,i+1} = t_o \left[e^{\varepsilon_{v,i+1}(V/\psi)} \left(\frac{p_{o2} + p_{i+1}}{p_{o3}}\right)^{-\lambda/\psi} - 1 \right]$$

The equivalent time t_e in [10.23] in terms of real duration time t is:

$$[10.25] \quad t_e = t + t_{e,A}$$

Using Eqns.[10.23]-[10.25], the final creep strain at point (i+1)' is:

$$[10.26] \quad \varepsilon_v = \frac{\lambda}{V} \ln\left(\frac{p_{o2}+p_{i+1}}{p_{o3}}\right) + \frac{\psi}{V} \ln\left[\frac{t}{t_o} + e^{\varepsilon_{v,i+1}(V/\psi)} \left(\frac{p_{o2}+p_{i+1}}{p_{o3}}\right)^{-\lambda/\psi}\right]$$

where

$$[10.27] \quad \varepsilon_{v,i+1} = \varepsilon_{v,i} + \frac{\kappa}{V} \ln\left(\frac{p_{o1} + p_{i+1}}{p_{o1} + p_i}\right)$$

Eqn.[10.26] with [10.27] can be used to do curve fitting for the multi-stage isotropic creep test. The parameters $\kappa/V = .0013$ and $p_{o1} =$ 10 kPa were estimated by fitting the instant test points in the first loading increment. Then try using $\lambda/V = .017$, $p_{o2} = 190$ kPa, $p_{o3} = 195$ kPa; $\psi/V = .007$, $t_o = 600$ hr. Detailed results are in Table 10.4.

Table 10.4 Curve Fitting of the Multi-Stage p Creep Test

p (kPa)	50	100	150	200	300
t (hrs)	313.5	216.5	527.5	1247.5	2159.5
ε_{vi} (%)	0	0.622	0.937	1.466	2.161
$\varepsilon_{v,i+1}$ (%)	0.233	0.690	0.978	1.495	2.211
ε_v (%)	0.622	0.937	1.466	2.161	2.908

The overall curve fitting of the laboratory data is shown in Figs.10.2,10.3. The calculated curves marched the test data well and it can be assumed that the fitting parameters have been adequately determined.

APPENDIX 10.2 Predictions of MST2 and MST10

Eqns.[10.21],[10.22] allows calculation of $(\varepsilon_v-\varepsilon_{v,iso})$ vs. t and $(\varepsilon_s-\varepsilon_{s,iso})$ vs. t in multi-stage q and p creep tests. Details for the calculation of MST2 and MST10 are in Table 10.5,10.6 respectively.

Table 10.5 Prediction of MST2, $\varepsilon_{v,iso}$ = 0.01737

q (kPa)	0	120	240	360	480	600
p (kPa)	280	280	280	280	280	280
t (hrs)	590	475	504	1006	1393	984
p_m(kPa)	280	293.31	334.98	411.11	535.36	739.68
ε_{vi}^{vp}		.01299	.01651	.01869	.02117	.02172
$(\varepsilon_v-\varepsilon_{v,iso})_i$		0	.00352	.00577	.00818	.00873
ε_{si}		0	.00118	.00281	.00647	.01341
$(\varepsilon_v-\varepsilon_{v,iso})_{i+1}$		0	.00352	.00577	.00818	.00873
$\varepsilon_{s,i+1}$		.00035	.00153	.00317	.00683	.01376
$(\varepsilon_v-\varepsilon_{v,iso})$		.00352	.00577	.00818	.00873	.00374
$(\varepsilon_s-\varepsilon_{s,iso})$		.00118	.00281	.00647	.01341	.02568

Table 10.6 Prediction of MST10, $\varepsilon_{v,iso}$ = 0.00794

q (kPa)	0	20	40	60	80	100	120	140
p (kPa)	70	76.7	83.3	90	96.7	103.3	110	116.7
t (hrs)	407	226	503	117	144	144	312	503
p_m(kPa)	70	77.83	87.50	98.83	111.46	125.14	139.91	155.58
ε_{vi}^{vp}		.00524	.00708	.00998	.01051	.01110	.01242	.01417
$(\varepsilon_v-\varepsilon_{v,iso})_i$		0	.00194	.00495	.00556	.00623	.00764	.00946
ε_{si}		0	.00027	.00097	.00120	.00152	.00231	.00357
$(\varepsilon_v-\varepsilon_{v,iso})_{i+1}$		.00010	.00204	.00504	.00565	.00717	.00867	.01062
$\varepsilon_{s,i+1}$		.00006	.00033	.00103	.00126	.00205	.00302	.00453
$(\varepsilon_v-\varepsilon_{v,iso})$		.00194	.00495	.00556	.00623	.00764	.00946	.01155
$(\varepsilon_s-\varepsilon_{s,iso})$		.00027	.00097	.00120	.00152	.00231	.00357	.00531

q (kPa)	160	180	200	240	280	320	360
p (kPa)	123.3	130	136.7	150	163.3	176.7	190
t (hrs)	1549	720	1223	719	807	1319	959
p_m(kPa)	172.02	189.32	207.38	245.67	286.89	331.13	378.51
ε_{vi}^{vp}	.01619	.01932	.02137	.02220	.02259	.02290	.02319
$(\varepsilon_v-\varepsilon_{v,iso})_i$	.01155	.01475	.01687	.01778	.01825	.01867	.01906
ε_{si}	.00531	.00852	.01107	.01234	.01330	.01456	.01691
$(\varepsilon_v-\varepsilon_{v,iso})_{i+1}$	.01286	.01630	.01693	.01787	.01835	.01876	.01915
$\varepsilon_{s,i+1}$	.00662	.01038	.01113	.01246	.01342	.01468	.01703
$(\varepsilon_v-\varepsilon_{v,iso})$	.01475	.01687	.01778	.01825	.01867	.01906	.01916
$(\varepsilon_s-\varepsilon_{s,iso})$	.00852	.01107	.01234	.01330	.01456	.01691	.01901

REFERENCES

Adachi, T. and Oka, F., 1982. Constitutive equations for normally consolidated clay based on elasto-viscoplasticity. Soil and Foundations, **22**, No.4, pp.57-70.

Azizi, F., 1987. Loi de comportement des sols raides - determination de la courbe d'etat limite de l'argile de Romainville. Doctoral Thesis, University Technologie de Compiegne, France.

Been, K. and Jefferies, M.G., 1985. A state parameter for sands. Géotechnique, **35**, pp.99-112.

Berre, T. and Iversen, K., 1972. Oedometer tests with different specimen heights on a clay exhibiting large secondary compression. Géotechnique, **22**, No.1, pp.53-70.

Bjerrum, L., 1967a. Engineering geology of Norwegian normally consolidated marine clays as related to the settlements of buildings. Géotechnique, **17**, No.2, pp.83-118.

Bjerrum, L., 1967b. Progressive failure in slopes of overconsolidated plastic clay and clay shales. J. Soil Mech. and Found. Division, ASCE, **93**, No.SN5, pp.3-49.

Borja, R.I. and Kavazanjian, E., 1985. A constitutive model for the stress-strain-time behavior of 'wet' clays. Géotechnique, **35**, No.3, pp.283-298.

Budkowska, B.B. and Fu, Q., 1989. Analysis of creep effects in frozen soils. Proc. Numerical Models in Geomechanics, Elsevier Applied Science, pp.171-178.

Burland, J.B., 1967. Deformation of soft-clay. Ph.D. thesis, Cambridge University, 1967.

Cernocky, E.P. and Krempl, E., 1979. A non-linear uniaxial integral constitutive equation incorporating rate effects, creep and relaxation. Int. J. Non-Linear Mechanics, **14**, pp.183-203.

Clausen, C.-J.F., Graham, J. and Wood, D.M., 1984. Yielding of soft clay at Mastemyr, Norway. Géotechnique, **34**, pp.581-600.

Coon, M.D. and Evans, R.J., 1971. Recoverable deformation of cohesionless soils. Journal of the Soil Mechs. and Founds. Division, ASCE, **97**, No.SM2, pp.375-391.

Crawford, C.B., 1986. State of the art: evaluation and interpretation of soil consolidation tests. Consolidation of Soils: Testing and Evaluation. ASTM STP 892, R.N. Yong and F.C. Townsend, Eds., American Society for Testing and Materials, Philadelphia, pp.378-404.

Crawford, C.B., 1988. On the importance of rate of strain in the consolidation test. Geotechnical Testing Journal, **11**, No.1 pp.60-62.

Croce, A., Burghignoli, A., Calabresi, G., Evangelista, A. and Viggiana, C., 1981. The Tower of Pisa and surrounding square: recent observation. Proc. of 10th International Conference on Soil Mechanics and Foundation Engineering, Stockholm, 15-19 June 1981, Vol.3, pp.61-70.

Crooks, J.H.A. anf Graham, J., 1976. Geotechnical properties of the Belfast estuarine deposits. Géotechnique, **26**, No.2, pp.293-315.

Darve, F., Flavigny, E. and Rojas, E., 1986. A class of incrementally non-linear constitutive relations and applications to clays. Computers and Géotechnics, **2** ,No.1, pp.43-66.

Darve, F., Gamali, H.EL, Touret, J.P., 1989. Modelling of cyclic behavior of soils on proportional and non-proportional paths. Proce. of Numerical Models in Geomechanics, Edited by S. Pietruszczak and G.N. Pande, Elsevier Applied Science.

Desai, C.S., 1980. A general basis for yield, failure and potential functions in plasticity. Int. J. Num. Anal. Meth. in Geomech., **4**, pp.361-375.

Desai, C.S., Somasundaram, S. and Frantziskonis, G., 1986. A hierarchical approach for constitutive modelling of geologic materials. Int. J. Num. Anal. Meth. in Geomech., **10**, pp.225-257.

Desai, C.S. and Zhang, D., 1987. Viscoplastic model for geologic materials with generalized flow rule. Int. J. Num. Analyt. Neth. in Geomech., **11**, No.6, pp.603-620.

Dixon, D.A. and Gray, M.N., 1985. The engineering properties of buffer materials - research at Whiteshell Nuclear Research Establishment. Proceedings of 19th Information Meeting of the Nuclear Waste Management Program, AECL Technical Report TR-350, Vol.3, pp.513-530

Dixon, D.A. and Woodcock, D.R., 1986. Physical properties and standards for testing reference buffer (1984) materials. AECL Technical Record TR352.

Domaschuk, L. and Wade, N.H., 1969. A study of bulk and shear moduli of a sand. Journal of Soil Mech. and Found.Engin., ASCE, **95**, No.SM2, 1969. pp.561-581.

Domaschuk, L. and Valliappan, P., 1975. Nonlinear settlement analysis by finite element. Journal of the Geotech. Enginn. Division, ASCE, **101**, No.GT7, pp.601-614.

Domaschuk, L., Knutsson, S., Shields, D.H. and Rahman, M.G., 1985.

Creep of frozen sand under isotropic and deviator components of stress. Journal of Energy Resources Technology, **107**, pp.199-203.

Drucker, D.C. and Prager, W., 1952. Soil mechanics and plastic analysis on limit design. Quart. Appl. Math., **10**, pp.157-165.

Duncan, J.M. and Chang, C.-Y., 1970. Nonlinear analysis of stress and strain in soils. Journal of the Soil Mechs. and Founds. Division, ASCE, **96**, No.SM5, pp.1629-1653.

Duncan, J.M., 1981. Hyperbolic stress-strain relationships. Limit Equilibrium, Plasticity and Generalized Stress-Strain in Geotechnical Engineering, Yong, R.N. and Ko, Hom-Yim, Eds., ASCE, pp.443-460.

Eringen, A.C., 1962. Nonlinear theory of continuous media. McGraw-Hill Book Co. Inc., New York.

Graham, J., Pinkney, K.V., Lew, K.V., Trainor, P.G.S., 1982. Curve-fitting and laboratory data. Canadian Geotechnical Journal, **19**, No.2, pp.201-205.

Graham, J., Crooks, J.H.A. and Bell, A.L., 1983. Time effects on the stress-strain behavior of natural soft clays. Géotechnique, **33**, No.3, pp.327-340.

Graham, J. and Houlsby, G.T., 1983. Anisotropic elasticity of a natural clay. Géotechnique, **33**, pp.165-180.

Graham, J., Gray, M.N., Sun, B.C.-C. and Dixon, D.A., 1986. Strength and volume change in a sand-bentonite buffer. Proc. of 2nd International Conference on Radioactive Waste Management, Winnipeg, Manitoba, pp.188-194.

Graham, J., Crooks, J.H.A. and Lau, S.L.-K., 1988a. Yield envelopes:

identification and geometric properties. Géotechnique, **38**, pp. 125-134.

Graham, J., Saadat, F. and Gray, M.N., 1988b. High pressure triaxial testing on the Canadian reference buffer material. Workshop on Artificial Clay Barriers for High Level Radioactive Waste Repositories, Lund, Sweden, October, 1988.

Graham, J. and Lau, S.L.K., 1988. Disturbance, storage, and stress-strain behavior in simulated underwater clay. Géotechnique, **38**, No.2, pp.279-300.

Graham, J., Saadat, F., Gray, M.N., Dixon, D.A. and Zhang, Q.-Y., 1989a. Strength and volume change behavior of a sand-bentonite mixture. Canadian Geotechnical Journal, **26**, pp.292-305.

Graham, J., Wood, D.M., Yin, J.-H. and Azizi, F., 1989b. Prediction of triaxial stress-strain behavior of Winnipeg clay using an anistropic elastic-plastic model. Proc. of 42nd Canadian Geotechnical Conference, Winnipeg, Oct.23-25. 1989, pp.155-162.

Gray, M.N., Cheung, S.C.H. and Dixon, D.A., 1984. The influences of sand content on swelling pressures and structure developed by statically compacted Na-bentonite. Atomic Energy of Canada Limited Report, AECL-7825.

Hill, R., 1950. The Mathematical Theory of Plasticity. Oxford, Clarendon Press. 355 pp.

Kabbaj, M., Oka, F., Leroueil, S. and Tavenas, F., 1986. Consolidation of natural clays and laboratory testing. Consolidation of Soils: Testing and Evaluation. ASTM STP 892, R.N. Yong and F.C. Townsend, Eds., American Society for Testing and Materials, Philadelphia, pp.378-404.

Kabbaj, M., Tavenas, F. and Leroueil, S., 1988. In situ and laboratory stress-strain relationship. Géotechnique, 38, No.1 pp.83-100.

Katona, M.G., 1984. Evaluation of viscoplastic cap model. J. of Geotechnical Engineering, **110**, No.8, pp.1106-1125.

Kérisel, J., 1985. The history of geotechnical engineering up until 1700. Proc. of 11th International Conference on Soil Mechanics and Foundation Engineering, San Francisco, 12-16 Auguat 1985, Golden Jubilee Volume, pp.1-93.

Kondner, R.L., 1963. Hyperbolic stress-strain response: cohesive soils. Journal of the Soil Mech. and Found. Engin. ASCE, **89**, No.SM1, Feb. 1963, pp.115-143.

Kondner, R.L. and Zelasko, J.S., 1963. Proc. of Second Pan-American Conference on Soil Mech. And Found. Engin., Vol.1 pp.289-333.

Ladd, C.C., Foott, R., Ishihara, K., Schlosser, F. and Poulos, H.G., 1977. Stress-deformation and strength characteristics. General report, Proc. 9th Int. Conf. Soil Mech. Fdn. Engng., Tokyo, Vol.2, pp.421-494.

Leroueil, S., Kabbaj, M., Tavenas F. and Bouchard, R., 1985. Stress-strain-strain rate relation for the compressibility of sensitive natural clays. Géotechnique, 35, No.2, pp.159-180.

Leroueil, S., 1988. Tenth Canadian Geotechnical Colloquium: recent developments in consolidation of natural clays. Canadian Geotechnical Journal, **25**, No.1, pp.85-107.

Liang, R.Y.K., Sobhanie, M. and Timmerman, D.H., 1987. A boundary surface plasticity model for the stress-strain-time behavior of clays. Constitutive Laws for Engineering Materials: Theory and Applications. Edited by C.S. Desai et al., Elsevier Science

Publishing Co., Inc. pp.699-706.

Matsui, T. and Abe, N., 1985. Elasto/viscoplastic constitutive equation of normally consolidation clays based on flow surface theory. Proc. 5th Int. Conf. Num. Meth. Geomech., Nagoya, Vol.1, pp.407-413.

Matsui, T. and Abe, N., 1986. Flow surface model of viscoplasticity for normally consolidation clays. Proc. 2nd Int. Symp. Num. Models Geomech., Ghent, pp.157-164.

Matsui, T., Abe, N. and Hayashi, K., 1989. Viscoplastic modelling of time-dependent behavior of clays. Numerical Models in Geomechnics, Edited by S. Pietruszczak and G.N. Pande, Elsevier Applied Science, pp. 100-107.

Mayne, P.W. and Klhawy, F.H., 1982. K_o-OCR-relationship in soil. Journal of the geotechnical Division, ASCE, Vol.108, No.6, pp.851-872.

Mesri, G. and Godlewski, P.M., 1977. Time-and stress-compressibility interrelationship. Journal of Geotech. Eng. Division, ASCE, **103**, No.GT5, pp.417-430.

Mesri, G. and Choi, Y.K., 1979. Strain rate behavior of Saint-Jean-Vianney clay. Discussion, Canadian Geotechnical Journal, **16**, No.4, pp.831-834.

Mesri, G. and Choi, Y.K., 1984. Time effects on the stress-strain behavior of natural soft clays. Discussion, Géotechnique, **34**, No.3, pp.439-442.

Mesri, G. and Choi, Y.K., 1985a. Settlement analysis of embankments on soft clays. J. Geotech. Engng. Div., ASCE, **111**, No.4, pp.441-464.

Mesri, G. and Choi, Y.K., 1985b. The uniqueness of end-of-primary (EOP) void ratio effective stress relationship. Proc. 11th Int. Conf. Soil Mech. Fdn. Engng., San Francisco Vol.2, pp.587-590.

Mesri, G. and Castro, A., 1987. C_α/C_c concept and K_o during secondary compression. J. Geotech. Engng. Div., ASCE, **113**, No.3, pp.230-247.

Mesri, G., 1990. Viscous-elastic-plastic modelling of one-dimensional time-dependent behaviour of clays. Discussion to be published on Canadian Geotechnical Journal, **27**.

Mitchell, J.K., 1976. Foundaments of soil behavior. John Wiley & Sons, New York, pp.422.

Mroz, Z., 1980. On hypoelasticity and plasticity approaches to constitutive modelling of inelastic behaviour of soils. Int. Journ. Numer. Anal. Methods in Geomechanics, **4**, pp.45-55.

Naghdi, P.M. and Murch, S.A., 1963. On the mechanical behavior of viscoelastic/plastic solids. J. Appl. Mech., **30**, pp.321-328.

Nayak, G.C. and Zienkiewicz, O.C., 1972. Elasto-plastic stress analysis. Generalization for various constitutive relations including strain softening. Int. J. Num. Meth. Engng., **5**, pp.113-135.

Oka, F., 1981. Prediction of time-dependent behavior of clay. Proc. of 10th International Conference on Soil Mech. and Foundation Engineering, Stockholm, Vol.1, 1981, pp.212-218.

Olszak, W. and Perzyna, P., 1966. The constitutive equations of the flow theory for a non-stationary yield condition. Proc. 11th Int. Congr. Appl. Mech., pp.545-553.

Olszak, W. and Perzyna, P., 1964. On elastic/visco-plastic soils.

Rheology and Soil Mechanics. Editors J. Kravtchenko and P.M. Sirieys, published by Springer-Verlag.

Perzyna, P., 1963. The constitutive equations for working hardening and rate sensitive plastic materials. Proc. of Vabrational Problems, Warsaw, Vol.4, No.3, pp.281-290.

Perzyna, P., 1966. Fundamental problems in viscoplasticity. Advances in Applied Mechanics, Academic Press, New York, **9**, pp.244-368.

Quigley, R.M., 1984. Quantitative mineralogy and preliminary porewater chemistry of candidate buffer and backfill materials for a nuclear fuel waste disposal vault. Atomic Energy of Canada Limited Report, AECL-7827.

Rahman, M.G., 1988. A constitutive model for creep of a frozen sand. PhD thesis, University of Manitoba, Canada.

Roscoe, K.H., Schofield, A.N. and Wroth, C.P., 1958. On the yielding of soils. Geotechniques, **8**, No.1, 1958.pp.25-53.

Roscoe, K.H., Schofield, A.N. and Thurairajah. A., 1963. Yielding of clays in states wetter than critical. Geotechnique, **13**, No.3, pp.211-240.

Roscoe, K.H. and Burland, J.B., 1968. On the generalized stress-strain behavior of 'wet clay'. Engineering Plasticity, Cambridge University Press.

Saadat, F., 1989. Constitutive modelling of the behaviour of a sand-bentonite mixture. Ph.D. thesis, University of Manitoba. 174pp. plus Tables and Figures.

Sällfors, G., 1975. Preconsolidation pressure of soft, high-plastic clays. Ph.D Thesis, Chalmers University of Technology, Gothenburg,

Sweden.

Saleeb, A.F. and Chen, W.F., 1981. Nonlinear hyperelastic (Green) constitutive models for soils: theory and calibration. Limit Equilibrium, Plasticity and Generalized Stress-Strain in Geotechnical Engineering, Yong, R.N. and Ko, Hom-Yim, Eds., ASCE, pp.492-538.

Sekiguchi, H., 1984. Theory of undrained creep rupture of normally consolidated clay based on elasto-viscoplasicity. Soils and Foundations, **24**, No.1, pp.129-147.

Skempton, A.W., 1964. Long-term stability of clay slopes. Géotechnique, **14**, No.2, pp77-102.

Suklje, L., 1969. Rheological Aspects of Soil Mechanics, published by John Wiley & Sons Lit.

Sun, Q.-X., Domaschuk, L., Shields, D.H. and Rahman, M., 1989. A viscoelastic constitutive model for creep of frozen soil. Proc. Numerical Models in Geomechanics, Elsevier Applied Science, pp.179-186.

Tavenas, F., Leroueil, S., Rochelle, P.La and Roy, M., 1978. Creep behavior of an undisturbed lightly overconsolidated clay. Can. Geotech. J., **15**, pp.402-423.

Truesdell, C., 1955. Hypo-elasticity. Journal Of Rational Mechanics and Analysis, **4**. No.1, pp.83-133.

Truesdell, C., 1965. Continuum Mechanics III — Foundations of Elasticity Theory. Gordon and Breach, Science Publishers, Ltd.

Vaid, Y.P. and Campanella, R.G., 1977. Time-dependent behavior of undisturbed clay. J. of Geotechnical Engineering, **103**, No.GT7,

pp.693-709.

Vulliet, L. and Desai, C.S., 1989. Viscoplasticity and finite elements for landslide analysis. Proc. of XII ICSMFE, Vol.2, pp.801-806, Rio deJaneiro, 1989.

Wahls, H.E., 1962. Analysis of primary and secondary consolidation. J. of the Soil Mech. and Fdn. Division, ASCE, **88**, SM6, pp.207-231.

Walker, L.K. and Raymond, G.P., 1968. The prediction of consolidation rates in a cemented clay. Canadian Geotechnical Journal, **5**, No.4, pp.192-216.

Wood, D.M. and Graham, J., 1987. Anisotropic yielding and elasticity of Winnipeg clay. Symposium on Yielding, Damage and failure of anisotropic solids. Grenoble, France. Cambridge University. Report CUED/D-SOILS/TRI99, pp.13 plus 11 figures.

Wroth, C.P. and Houlsby, G.T., 1985. Soil mechanics - property characteristics and analysis procedures, state of the art report. Proc. 11th Int. Conf. on Soil Mechs. and Founds. Eng., San Francisco, Vol.**3**, pp.1-54.

Yarechewski, D., 1988. Quality control tests for making sand-bentonite specimens for nuclear waste containment studies. B.Sc. Thesis, University of Manitoba, Winnipeg, Manitoba.

Yin, J.-H., 1984. An incremental nonlinear dilatant stress-strain model for sand. M.Sc. Thesis, Institute of Rock and Soil Mechanics, Academia Sinica, Wuhan, China.

Yin, J.-H. and Yuan, J.-X., 1985a. Incremental nonlinear models. Journal of Rock and Soil Mechs., Institute of Rock and Soil Mechanics, Academia Sinica, Wuhan, China, **6**, No.2, pp.5-14.

Yin, J.-H. and Yuan, J.-X., 1985b. A nonlinear dilatant stress-strain relationship of soils. Proc. of 1th Chinese Conf. on Shear Strength and Constitutive Relationships of Soils, Hubei, China, pp.204-211.

Yin, J.-H., Saadat, F. and Graham, J., 1988. A three modulus hypoelastic constitutive model for sand-bentonite buffer (RBM). Proc. 41st Can. Geot. Soc. Conf., Kitchener, Ontario, October 1988, pp.386-395.

Yin, J.-H. and Graham, J., 1989a. Viscous-elastic-plastic modelling of one-dimensional time-dependent behavior of clays. Can. Geotech. J., **26**, pp.199-209.

Yin, J.-H. and Graham, J. 1989b. General elastic viscous plastic constitutive relationships for 1-D straining in clays. Proc. Numerical Models in Geomechanics, Elsevier Applied Science, pp.108-117.

Yin, J.-H., Graham, J., Saadat, F. and Azizi, F., 1989. Constitutive modelling of soil behaviour using three modulus hypoelasticity. Proc. 12th Int. Conf. on Soil Mechs. and Founds. Engg. Rio de Janeiro, Brazil, August, 1989. pp.143-147.

Zienkiewicz, O.C. and Cormeau, I.C., 1974. Visco-plasticity, plasticity and creep in elastic soilds: a unified numerical solution approach. Int. J. Num. Meth. in Eng., **8**, pp.821-845.